SCUOLA INTERNAZIONALE SUPERIORE DI STUDI AVANZATI

DOCTORAL THESIS

Aspects of quantum integrability: non-equilibrium dynamics, defects and hydrodynamics

Author:
Alvise BASTIANELLO

Supervisor:
Prof. Giuseppe MUSSARDO
Dr. Andrea DE LUCA

A thesis submitted in fulfillment of the requirements for the degree of Doctor of Philosophy

in the

PhD Course in Statistical Physics

Contents

List of Publications

[1] A. Bastianello, A. De Luca, G. Mussardo, *Non relativistic limit of integrable QFT and Lieb-Liniger models*, J. Stat. Mech. (2016) 123104.

Abstract: In this paper we study a suitable limit of integrable QFT with the aim to identify continuous non-relativistic integrable models with local interactions. This limit amounts to sending to infinity the speed of light c but simultaneously adjusting the coupling constant g of the quantum field theories in such a way to keep finite the energies of the various excitations. The QFT considered here are Toda field theories and the $O(N)$ non-linear sigma model. In both cases the resulting non-relativistic integrable models consist only of Lieb–Liniger models, which are fully decoupled for the Toda theories while symmetrically coupled for the $O(N)$ model. These examples provide explicit evidence of the universality and ubiquity of the Lieb–Liniger models and, at the same time, suggest that these models may exhaust the list of possible non-relativistic integrable theories of bosonic particles with local interactions.

[2] A. Bastianello, A. De Luca, G. Mussardo, *Non relativistic limit of integrable QFT with fermionic excitations*, J. Phys. A: Math. Theor. **50** 234002 (2017).

Abstract: The aim of this paper is to investigate the non-relativistic limit of integrable quantum field theories with fermionic fields, such as the $O(N)$ Gross–Neveu model, the supersymmetric Sinh–Gordon and non-linear sigma models. The non-relativistic limit of these theories is implemented by a double scaling limit which consists of sending the speed of light c to infinity and rescaling at the same time the relevant coupling constant of the model in such a way to have finite energy excitations. For the general purpose of mapping the space of continuous non-relativistic integrable models, this paper completes and integrates the analysis done in A. Bastianello *et a*l (2016 J. Stat. Mech. 123104) on the non-relativistic limit of purely bosonic theories.

[3] A. Bastianello, L. Piroli, P. Calabrese, *Exact local correlations and full counting statistics for arbitrary states of the one-dimensional interacting Bose gas*, Phys. Rev. Lett. **120**, 190601 (2018).

Abstract: We derive exact analytic expressions for the n-body local correlations in the one-dimensional Bose gas with contact repulsive interactions (Lieb-Liniger model) in the thermodynamic limit. Our results are valid for arbitrary states of the model, including ground and thermal states, stationary states after a quantum quench, and nonequilibrium steady states arising in transport settings. Calculations for these states are explicitly presented and physical consequences are critically discussed. We also show that the n-body local correlations are directly related to the full counting statistics for the particle-number fluctuations in a short interval, for which we provide an explicit analytic result.

[4] A. Bastianello, L. Piroli, *From the sinh-Gordon field theory to the one-dimensional Bose gas: exact local correlations and full counting statistics*, arXiv:1807.06869 (2018).

Abstract: We derive exact formulas for the expectation value of local observables in a one-dimensional gas of bosons with point-wise repulsive interactions (Lieb-Liniger model). Starting from a recently conjectured expression for the expectation value of vertex operators in the sinh-Gordon field theory, we derive explicit analytic expressions for the one-point $K-$body correlation functions $\langle(\psi^\dagger)^K(\psi)^K\rangle$ in the Lieb-Liniger gas, for arbitrary integer K. These are valid for all excited states in the thermodynamic limit, including thermal states, generalized Gibbs ensembles and non-equilibrium steady states arising in transport settings. Our formulas display several physically interesting applications: most prominently, they allow us to compute the full counting statistics for the particle-number fluctuations in a short interval. Furthermore, combining our findings with the recently introduced generalized hydrodynamics, we are able to study multi-point correlation functions at the Eulerian scale in non-homogeneous settings. Our results complement previous studies in the literature and provide a full solution to the problem of computing one-point functions in the Lieb Liniger model.

[5] A. Bastianello, S. Sotiriadis, *Quasi locality of the GGE in interacting-to-free quenches in relativistic field theories*, J. Stat. Mech. (2017) 023105.

Abstract: We study the quench dynamics in continuous relativistic quantum field theory, more specifically the locality properties of the large time stationary state. After a quantum quench in a one-dimensional integrable model, the expectation values of local observables are expected to relax to a generalized Gibbs ensemble (GGE), constructed out of the conserved charges of the model. Quenching to a free bosonic theory, it has been shown that the system indeed relaxes to a GGE described by the momentum mode occupation numbers. We first address the question whether the latter can be written directly in terms of local charges and we find that, in contrast to the lattice case, this is not possible in continuous field theories. We then investigate the less stringent requirement of the existence of a sequence of truncated local GGEs that converges to the correct steady state, in the sense of the expectation values of the local observables. While we show that such a sequence indeed exists, in order to unequivocally determine the so-defined GGE, we find that information about the expectation value of the recently discovered quasi-local charges is in the end necessary, the latter being the suitable generalization of the local charges while passing from the lattice to the continuum. Lastly, we study the locality properties of the GGE and show that the latter is completely determined by the knowledge of the expectation value of a countable set of suitably defined quasi-local charges.

[6] A. Bastianello, P. Calabrese, *Spreading of entanglement and correlations after a quench with intertwined quasiparticles*, arXiv:1807.10176 (2018).

Abstract: We extend the semiclassical picture for the spreading of entanglement and correlations to quantum quenches with several species of quasiparticles that have non-trivial pair correlations in momentum space. These pair correlations are, for example, relevant in inhomogeneous lattice models with a periodically-modulated Hamiltonian parameter. We provide explicit predictions for the spreading of the entanglement entropy in the space-time scaling limit. We also predict the time evolution of one- and two-point functions of the order parameter for quenches within the ordered phase. We test all our predictions against exact numerical results for quenches in the Ising chain with a modulated transverse field and we find perfect agreement.

[7] A. Bastianello, M. Collura, S. Sotiriadis, *Quenches from bosonic Gaussian initial states to the Tonks-Girardeau limit: Stationary states and effects of a confining potential*, Phys. Rev. B 95, 174303 (2017).

Abstract: We consider the general problem of quenching an interacting Bose gas from the noninteracting regime to the strongly repulsive limit described by the Tonks-Girardeau gas with the initial state being a Gaussian ensemble in terms of the bosons. A generic multipoint correlation function in the steady state can be described fully in terms of a Fredholm-like determinant suitable both for a numerical and for an analytical study in certain limiting cases. Finally, we extend the study to the presence of a smooth confining potential showing that, in the thermodynamic limit, the time evolution of the two-point function can be mapped to a classical problem.

[8] A. Bastianello, B. Doyon, G. Watts, T. Yoshimura, *Generalized hydrodynamics of classical integrable field theory: the sinh-Gordon model*, SciPost Phys. **4**, 045 (2018) .

Abstract: Using generalized hydrodynamics (GHD), we develop the Euler hydrodynamics of classical integrable field theory. Classical field GHD is based on a known formalism for Gibbs ensembles of classical fields, that resembles the thermodynamic Bethe ansatz of quantum models, which we extend to generalized Gibbs ensembles (GGEs). In general, GHD must take into account both solitonic and radiative modes of classical fields. We observe that the quasi-particle formulation of GHD remains valid for radiative modes, even though these do not display particle-like properties in their precise dynamics. We point out that because of a UV catastrophe similar to that of black body radiation, radiative modes suffer from divergences that restrict the set of finite-average observables; this set is larger for GGEs with higher conserved charges. We concentrate on the sinh-Gordon model, which only has radiative modes, and study transport in the domain-wall initial problem as well as Euler-scale correlations in GGEs. We confirm a variety of exact GHD predictions, including those coming from hydrodynamic projection theory, by comparing with Metropolis numerical evaluations.

[9] A. Bastianello, A. De Luca, *Nonequilibrium Steady State Generated by a Moving Defect: The Supersonic Threshold*, Phys. Rev. Lett. **120**, 060602 (2018).

*Abstract:*We consider the dynamics of a system of free fermions on a 1D lattice in the presence of a defect moving at constant velocity. The defect has the form of a localized time-dependent variation of the chemical potential and induces at long times a nonequilibrium steady state (NESS), which spreads around the defect. We present a general formulation that allows recasting the time-dependent protocol in a scattering problem on a static potential. We obtain a complete characterization of the NESS. In particular, we show a strong dependence on the defect velocity and the existence of a sharp threshold when such velocity exceeds the speed of sound. Beyond this value, the NESS is not produced and, remarkably, the defect travels without significantly perturbing the system. We present an exact solution for a $\delta-$like defect traveling with an arbitrary velocity and we develop a semiclassical approximation that provides accurate results for smooth defects.

[10] A. Bastianello, A. De Luca, *Superluminal moving defects in the Ising spin chain*, Phys. Rev.

B **98**, 064304 (2018).

Abstract: Quantum excitations in lattice systems always propagate at a finite maximum velocity. We probe this mechanism by considering a defect travelling at a constant velocity in the quantum Ising spin chain in transverse field. Independently of the microscopic details of the defect, we characterize the expectation value of local observables at large times and large distances from the impurity, where a Local Quasi Stationary State (LQSS) emerges. The LQSS is strongly affected by the defect velocity: for superluminal defects, it exhibits a growing region where translational invariance is spontaneously restored. We also analyze the behavior of the friction force exerted by the many-body system on the moving defect, which reflects the energy required by the LQSS formation. Exact results are provided in the two limits of extremely narrow and very smooth impurity. Possible extensions to more general free-fermion models and interacting systems are discussed.

[11] A. Bastianello, *Lack of thermalization for integrability-breaking impurities*, arXiv:1807.00625 (2018).

Abstract: We investigate the effects of localized integrability-breaking perturbations on the large times dynamics of thermodynamic quantum and classical systems. In particular, we suddenly activate an impurity which breaks the integrability of an otherwise homogeneous system. We focus on the large times dynamics and on the thermalization properties of the impurity, which is shown to have mere perturbative effects even at infinite times, thus preventing thermalization. This is in clear contrast with homogeneous integrability-breaking terms, which display the prethermalization paradigm and are expected to eventually cause thermalization, no matter the weakness of the integrability-breaking term. Analytic quantitative results are obtained in the case where the bulk Hamiltonian is free and the impurity interacting.

Publication not discussed in the thesis:

[12] A. Bastianello, S. Sotiriadis, *Cluster expansion for ground states of local Hamiltonians*, Nucl. Phys. B **909** (2016) 1020-1078.

Abstract: A central problem in many-body quantum physics is the determination of the ground state of a thermodynamically large physical system. We construct a cluster expansion for ground states of local Hamiltonians, which naturally incorporates physical requirements inherited by locality as conditions on its cluster amplitudes. Applying a diagrammatic technique we derive the relation of these amplitudes to thermodynamic quantities and local observables. Moreover we derive a set of functional equations that determine the cluster amplitudes for a general Hamiltonian, verify the consistency with perturbation theory and discuss non-perturbative approaches. Lastly we verify the persistence of locality features of the cluster expansion under unitary evolution with a local Hamiltonian and provide applications to out-of-equilibrium problems: a simplified proof of equilibration to the GGE and a cumulant expansion for the statistics of work, for an interacting-to-free quantum quench.

Chapter 1

Introduction

Understanding the behavior of many body quantum systems is one of the most difficult and compelling challenges physicists have faced so far. Dealing with an enormous number of degrees of freedom is a necessary step towards sharpening our understanding of natural phenomena, since many-body systems are the rule rather than the exception.

It is fascinating how very simple few-body interactions can exhibit completely unexpected phenomena, when thermodynamic systems are concerned: as one of the most prominent example we can surely mention the "spontaneous symmetry breaking", which is responsible for the existence of magnets. A symmetry present in the microscopic interaction is completely destroyed by the interplay of (infinitely-)many degrees of freedom.

This simple example points out a frustrating, yet fascinating, fact: the behavior of many-body systems, either quantum or classical, is hardly extrapolated from the few-body physics. Such a difficulty triggered the need of efficiently compress the relevant information in a handful of parameters, still retaining the many-body features. This spirit is probably most successfully exploited by the renormalization group idea, where a coarse grain procedure is invoked to get rid of the astonishing amount of degrees of freedom of the original system, yet incorporating their effects in a small set of relevant quantities.

The issue of thermalization nicely fits into the landscape of compressing information: a certain system can be thought to be initialized in a perfectly well-known state, but as it evolves less and less details are relevant for its efficient description, until only a few of them (e.g. temperature, pressure,...) survive. Two main questions immediately arise: how does this mechanism of information loss take place? Which are the relevant quantities needed to describe the system at late times? Addressing these interrogatives, we should distinguish between *open* and *closed* systems, the latter being the utmost interest of this thesis.

For what it concerns open systems, i.e. coupled to an external bath assumed to be in equilibrium, the exceeding information is dissipated in the external environment. In the approximation where the system of interest is thermodynamically large, but much smaller then the external bath, the latter is unaffected during the time evolution. Conversely, the smaller system feels both dissipation and the noise feeded by the bath, which eventually enforces thermalization to take place. The mechanism is much more subtle in closed systems.

On the classical side, the thermalization issue in many-body closed systems underwent extensive investigations, especially after the famous Fermi-Pasta-Ulam-Tsingou numerical experiment in 1955 [13] (see Ref. [14] for an introduction to the problem and to more recent achievements, while in Ref. [15] a more comprehensive overview can be found). The experiment consists in numerically evolving a one-dimensional chain of anharmonic oscillators, which is randomly initialized in long-wavelength modes: due to the anharmonicity, an energy transfer towards short-wavelength modes and thermalization at late times was expected. More precisely, the experiment was initially thought to test the *ergodic hypothesis*, which states that the system passes arbitrary close to any point in the phase space with the same energy of the initial condition. However, an unexpected lack of thermalization was observed, together with a strong revival of the initial conditions and thus violating of the ergodic hypothesis.

This brings into play integrability. A classical system with N degrees of freedom is said to be Liouville-integrable if it possesses N independent integrals of motion in involution [16]: under this hypothesis, the system can be described through a set of action-variable angles, which

undergo periodic motion in the phase space. Obviously, the ergodic hypothesis does not hold for such a system. The Fermi-Pasta-Ulam-Tsingou (FPUT) model is not integrable because of the anharmonicity, but we can revert to the elegant Kolmogorov–Arnold–Moser (KAM) theory [16] (at least, as long as a finite number of degrees of freedom is involved). In particular, the KAM theory states that quasiperiodic orbits in the phase space persist under weak non-integrable perturbations of the integrable Hamiltonian. However, there is a catch: the upperbound to the perturbation strength which allows for quasi-periodic orbits exponentially vanishes in the number of the dregrees of freedom, preventing the a direct application of the KAM theory to the FPUT setup when the thermodynamic limit is concerned. The persisting revivals and lack of ergodicity were more satisfactory explained when Zabusky and Kruskal in 1965 observed that the long wavelength sector of the FPUT model is well approximated by the Korteweg-de Vries (KdV) partial differential equation [17]. KdV is an integrable differential equation and represents a new facet of integrability: since a continuum of degrees of freedom is involved, the Liouville definition cannot be applied any longer. In this case, integrability is defined through the elegant *inverse scattering method* [18], whose discussion lays beyond our purposes. Nevertheless, let us mention that a direct byproduct of the construction is the existence of infinitely many local conserved quantities (more precisely, spatial integrals of local densities), independent and in involution. These conserved quantities cause the ergodicity-breaking of the evolution, as we will extensively discuss in the strictly connected quantum case. Finally, it should be remarked that the KdV equation is nevertheless an (astonishing good) approximation of the low energy sector of the FPUT model, which is actually non integrable: indeed, on a timescale much longer than the one observed in the original experiment (see Ref. [14], in particular Ref. [19] and references therein) the non-integrability finally kicks in and the system thermalizes, confirming the original expectation.

Compared with the classical realm, closed quantum many body systems have a much shorter history: despite the first results on quantum ergodicity were obtained by Von Neumann back in 1929 [20], this research line remained essentially unexplored. Isolating a quantum system and preventing decoherence is a formidably hard task which remained an unreachable dream of experimentalists for ages, relegating the study of closed quantum systems to a mere academic question, unsuitable of any experimental check. At least, until very recently when the cold atoms' advent completely turned the tables.

The refinement of cold atoms techniques (we recommend the review Ref. [21]) allows one to isolate the system from the external environment and reach very low temperatures, thus controlling with great precision the state of the system. For example, in 1995 the Bose Einstein condensate found its first experimental realization [22–24].

After that, a succession of remarkable achievements transformed the cold atom experiments from a pioneeristic research into an extremely precise and versatile tool, where several playgrounds for theoretical physicists can be realized.

By mean of optical lattices [25] it became possible to change the effective dimensionality of the system, as well as to introduce spatially-periodic structures or traps. Moreover, great achievements concerning the fine tuning of the interaction have been made, for example by mean of Feschbach resonances [26]. From the list of the cold atoms experiment (see Ref. [27–48] for a selected sample) we cannot resist to explicitly mention the work of Kinoshita *et al.* (2006) [49], which has the same role in the quantum world that the FPUT experiment had in the classical realm, triggering the excitement of a nowadays widespread community of experimentalists and theoreticians.

The experiment consists in a one-dimensional realization of a Newton's cradle: ^{87}Rb atoms with repulsive contact interaction are cooled down in a harmonic trap, then a laser beam splits the initial cloud into two clouds of opposite momentum, that are let free to evolve (see Fig. 1.1). As the time passes, the atoms keep on colliding at the center of the trap, but no relaxation is observed, at least up to the experimentally accessible timescales: this is due to the fact that the

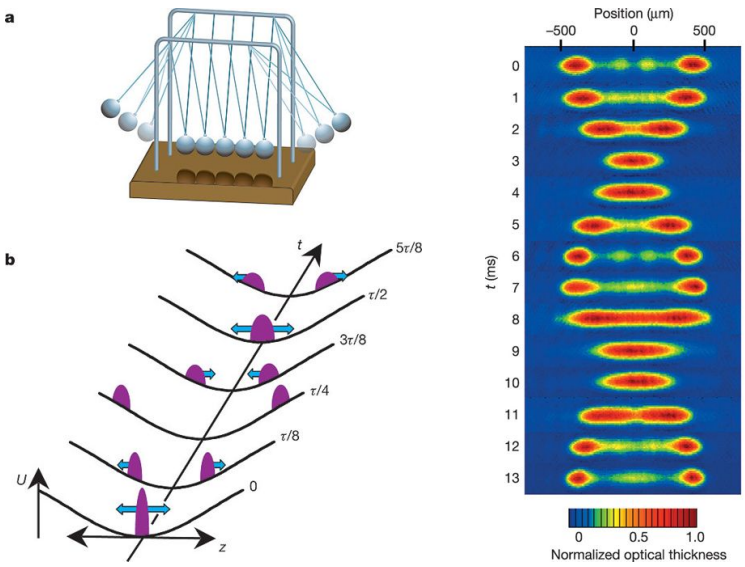

Figure 1.1: *Left panel: pictorial representation of the Newton's cradle and its quantum experimental realization. Right panel: absorption image of the colliding clouds. Even after thousands of collisions, there is no smearing of the clouds and thus no signal of equilibration. Figure taken from Ref. [49].*

colliding atoms are well described by the celebrated Lieb-Liniger (LL) model [50, 51], which will be one of the main characters of this thesis

$$H = \int \mathrm{d}x \, \frac{1}{2m} \partial_x \psi^\dagger(x) \partial_x \psi(x) + \kappa \psi^\dagger(x) \psi^\dagger(x) \psi(x) \psi(x) \,. \tag{1.1}$$

Above, the fields are quantum bosons $[\psi(x), \psi^\dagger(y)] = \delta(x-y)$. The integrability of the Lieb-Liniger model has been advocated to explain the lack of thermalization in the experiment.

While at the practical level there are no ambiguities in identifying a model as integrable, the actual, rigorous, definition of quantum integrability has been a subject of active debate until recent years [52], but a sure, definition-independent, fingerprint of integrability is the existence of infinitely many local conserved quantities, which are linearly independent and commute with each others. Integrable models, a part from free theories, are necessarily one dimensional systems: the quantum inverse scattering method [53] allows for a systematic construction of lattice integrable models, but it is confined to a single spatial dimension. For what it concerns the realm of relativistic quantum field theories, the Coleman-Mandula theorem [54] excludes the presence of infinitely many conserved charges in higher dimensions.

One dimensional many-body systems are strongly correlated, since particles moving on a line cannot avoid each others: the result is a generic failure of approximated methods which are perturbative in the interaction strength. Fortunately, alternative approximated methods, such as the Luttinger Liquid approach [55, 56], are available, but integrable models provide an outstanding opportunity of shedding light on strongly correlated one dimensional systems. Indeed, the huge number of symmetries of these models allows for several exact computations: the thermodynamics at equilibrium is nowadays a textbook topic [57], while the computation of correlation functions is still a very active research field. The importance of integrable models in our comprehension of strongly correlated systems is hardly overestimated.

A plethora of quantum integrable models exists, ranging from spin chains (e.g. the well known XXZ model [58–60]), to continuum galilean-invariant systems, such as the already mentioned Lieb-Liniger model, up to relativistic integrable field theories.

Each class of models has its own preferred route for its solution, in particular relativistic

invariance have been successfully merged with integrability in the elegant bootstrap approach [61], providing a remarkably well controlled framework to study relativistic integrable quantum field theories. Nowadays, several examples are known: the list includes purely bosonic models, as the Sinh Gordon model, or more generally Toda models [62–78], fermionic systems, as the Gross Neveu model [78], as well as supersymmetric versions of all these examples (see, for instance, Ref. [79–82]). This list increases even further if one also add to it theories with soliton excitations, as the Sine Gordon model, or various sigma models based on group manifold [78, 83, 84].

Tempted by the impressive array of results in the relativistic realm, a very natural route to analyze galilean invariant systems consists in passing through proper non relativistic (NR) limits. This the topic addressed in Chapter 2, based on Ref. [1, 2], work done in collaboration with G. Mussardo, A. De Luca, and Ref. [3], in collaboration with L. Piroli and P. Calabrese and Ref.[4] with L. Piroli. The idea of using non relativistic limits dates back to 2009 when M. Kormos, G. Mussardo and A. Trombettoni [85, 86] noticed that the Sinh Gordon (relativistic) and the Lieb Liniger (galilean) models can be connected through such a limit. Taking advantage of the results available in the Sinh Gordon model, unprecedented achievements in the Lieb Liniger model had been made. The Chapter is mainly pivoted on two main questions.

Firstly, we address which galilean invariant models can be reached through non relativisitc limits [1, 2]. Puzzled by the astonishing imbalance in the variety of the relativistic realm when compared with the galiliean case (where essentially the Lieb Liniger model and variation thereof appears to be the only integrable system with strictly local interactions), we analyzed several relativistic models and their limit. Indeed, we discovered an extremely tight bottleneck: the rich variety of particle masses, interactions and scattering matrices of relativistic models is always shrank to galilean particles (either bosons or fermions) of equal mass and pairwise interaction.

In the second part, based on Ref. [3, 4], we further deepen our knowledge of the Lieb Liniger model studying its one point correlation functions $\langle(\psi^\dagger)^K\psi^K\rangle$. Viewing the Lieb Liniger model as the non relativistic limit of the Sinh Gordon theory had a prominent role in the computation of correlation functions [85, 86], which were accessible through the non relativistic limit of the Le Clair-Mussardo expansion [87]. With the important exception of the case $K = 3$ [88], this expansion could not be resummed in a compact expression and, because of the appearance of multiple-integrals, it is not suited to be applied beyond the low density limit for $K > 3$.

By mean of other methods [89], relatively simple close expressions were obtained up to $K = 4$, leaving the correlation functions $K > 4$ still expressed in terms of multiple integral formulas and thus untractable on a practical level.

In Ref. [3, 4], taking advantage of new results obtained in the Sinh Gordon model [90, 91], we solve the long-standing problem of computing one-point functions in the Lieb Liniger model on arbitrarily excited states and for any K, in the repulsive regime $\kappa > 0$ (1.1). Our findings require the solution of a finite number of single variable, linear integral equations, which can be easily done on any laptop: in particular, the computation of the K^{th} correlator requires the solution of $2K - 1$ equations.

Furthermore, we link our findings to the full counting statistics of the number of particles in a small interval [38, 92–95], an extremely relevant quantity for experimentalists. Our findings can be used to study thermal ensembles, as well as the late time dynamics in out-of-equilibrium protocols, which will now be discussed. In particular, Chapter 3 collects four works about integrable models driven out-of-equilibrium [5–8].

A net and clear setup to probe the out-of-equilibrium properties of a closed quantum system is the celebrated *quantum quench* [96, 97]. The initially proposed setup initializes the system in a ground state of a local Hamiltonian and suddenly changes some parameters of the latter: the system is no longer described by an eigenstate of the post-quench Hamiltonian and will undergo a non trivial time evolution. As long as translationally invariant quenches are concerned, at late times the system is expected to relax in some sense to a stationary state which, for generic models

(i.e. non-integrable) is expected to be thermal. Strictly speaking, it is impossible for the system as a whole to relax to a Gibbs Ensemble: in closed quantum systems the time evolution is unitary, therefore the system remains in a pure state at any time, while a thermal density matrix is not. Despite global relaxation is obstructed, local relaxation is still possible: the system acts as its own thermodynamic bath and the details of the initial condition are progressively encoded into highly non local degrees of freedom, invisible to any local probing of the model [33].

In general, we say that a system relaxes to a density matrix $\hat{\rho}^{\infty}$ if, for any finite subsystem A of the thermodynamicalyl large system, the infinite time limit of the reduced density matrix exists

$$\lim_{t\to\infty} \hat{\rho}_A(t) = \hat{\rho}_A^{\infty}\,, \tag{1.2}$$

where $\hat{\rho}(t)$ is the time-evolved density matrix in which the system were initialized, the subscript A stands for the partial trace on the complementary of A. An equivalent statement is the requirement that all the local observables and their correlation functions relax at infinite time, being the steady state described by $\hat{\rho}^{\infty}$. As we anticipated, generic non-integrable systems are expected to reach a Gibbs Ensemble

$$\hat{\rho}^{\infty} = \frac{1}{Z} e^{-\beta H}\,, \tag{1.3}$$

where H is the post quench Hamiltonian. The effective inverse temperature β is fixed using the conservation of energy and requiring the expectation value of H to be the same on the initial state and on the stationary one

$$\mathrm{Tr}[\hat{\rho} H] = \mathrm{Tr}[\hat{\rho}^{\infty} H]\,. \tag{1.4}$$

Due to the several conserved quantities present in integrable models, the latter do not relax to a thermal ensemble, since the information of the initial state "trapped" into the conserved charges survives up to infinite times. Rather than to a thermal ensemble, integrable models relax to a Generalized Gibbs Ensemble (GGE) [98], i.e. a maximum entropy state in which the expectation value of all the relevant charges $\mathcal{Q}_j$ has been taken in account

$$\hat{\rho}^{\infty} = \frac{1}{\mathcal{Z}} e^{-\sum_j \lambda_j \mathcal{Q}_j}\,. \tag{1.5}$$

The Lagrange multipliers λ_j must be fine-tuned in such a way $\mathrm{Tr}[\hat{\rho}\mathcal{Q}_j] = \mathrm{Tr}[\hat{\rho}^{\infty}\mathcal{Q}_j]$.

Several efforts have been dedicated to test the validity of the GGE conjecture (see eg. [98–109]) which is nowadays well established (for a recent review on integrable systems out-of-equilibrium see Ref. [110]). However, understanding the minimal set of information needed in the GGE construction, i.e. which charges must be included, has been the subject of an heated debate.

For what it concerns lattice systems, a conserved charge $\mathcal{Q}$ is said to be local if it is the sum of local operators $\mathfrak{q}_j$, having the latter finite support around the lattice site j. As already mentioned, integrable systems possess infinitely many local charges and the original proposal [98] states that the GGE should be constructed with all and only the local integrals of motion. This is indeed the right recipe for free lattice models [107–109], but a failure of the original formulation of the GGE in interacting spin chains [111–114] caused a huge uproar in the community. For example, in Ref. [111] a quench in the XXZ spin chain was considered and numerical simulations with DMRG techniques [115] were compared against the GGE prediction and an ab-initio calculation of the steady state through the Quench Action method [100, 116]. While the numerical data agreed with the Quench Action, they clearly contradicted the GGE result.

This discrepancy was later attributed to the lack of completeness of the set of local charges: a new type of conserved quantity with milder locality properties was needed. These have been named quasi-local charges [117] and are sums on the lattice sites of operators with exponentially vanishing support, rather than finite as it was the case of local charges.

The introduction of quasi-local charges [118–122] in the GGE construction was proven to fully determine the steady state and to be in agreement with the Quench Action method.

On the lattice, the investigation of local charges is nowadays settled down, but the same analysis in continuum models has not reached the same level of maturity. In continuum models, local conserved charges are integral over the space of a local operator, namely a point-wise function of the fields and their space-time derivatives: as pointed out in Ref. [123, 124], this is a much more stringent locality requirement compared with the lattice counterpart. In particular, the set of strictly local charges could be not sufficient to correctly describe the post quench steady state even in free models, in contrast with the lattice case.

Section 3.1 is dedicated to this problem, discussing the work presented in Ref. [5] in collaboration with S. Sotiriadis. We carefully analyzed quenches in relativistic field theories constructed out of a single bosonic field, exploring the locality properties of the resulting GGE. In particular, while the post quench Hamiltonian has been taken as the free massive Klein-Gordon model (for the massless case see Ref. [125]), the prequench state is the ground state of an arbitrary interacting theory. The locality properties of the GGE are linked to the analytical structure of the two point correlator at initial time, the latter being non-perturbatively described by the Källen-Lehmann spectral representation [126]. As a final result of our analysis, we show that the correct GGE can be constructed out of a numerable set of quasi-local charges, whose densities have exponentially vanishing support. For what it concerns quasi-local charges in truly interacting integrable models, their construction has not been fully understood yet and, to the best of our knowledge, the only step in this direction has been made in Ref. [127].

The relatively fast, yet very intense, research that from the initial proposal of the GGE lead to the inclusion of quasilocal charges, as well as the contemporary development of the Quench Action method, contributed to a drastic perspective change in describing the GGE.

In integrable models, the Hilbert space can be spanned by a basis of common eigenvectors of all the conserved charges: each eigenstate is described by multi-particle asymptotic states [53, 61]. Due to the presence of infinitely many charges, these quasiparticles are stable (i.e. they do not decay) and undergo purely elastic two-body scatterings. In the thermodynamic limit, a coarse grained procedure can be adopted and, rather than describing the exact particle content of a state, we can use mode-occupation functions, called root densities. In the spirit of the Thermodynamic Bethe Ansatz (TBA) [57], to a GGE it is unambiguously associated a set of root densities, from which the thermodynamic of the system (and correlation functions to some extent) can be derived. Indeed, the completeness of the set of quasi-local charges has been proven showing that the correspondence Lagrange multipliers-root densities is one-to-one [122].

The quasiparticle description of integrable models has been revealed to be a precious tool not only in understanding the equilibrium thermodynamics and the long time steady states, but also the spreading of entanglement and correlation functions, as well as an efficient description of weak inhomogeneities. The work of Ref. [6] has been done in collaboration with P. Calabrese and mainly covers the spreading of entanglement entropy [128–130], which for a bipartition of the system $A \cup \bar{A}$ is defined as

$$S_A \equiv -\mathrm{Tr}\hat{\rho}_A \ln \hat{\rho}_A \,, \tag{1.6}$$

where $\hat{\rho}_A$ is the reduced density matrix of a subsystem A of a system in a pure state. Its time evolution plays a crucial role in the understanding of the non-equilibrium dynamics of isolated quantum systems. Indeed, the growth of the entanglement entropy in time has been related to the efficiency of tensor network algorithms [131–136], such as the time dependent density matrix renormalisation group.

Within the quasiparticle description, the initial state is regarded as a source of entangled quasiparticles which ballistically propagate across the system and carry entanglement. The structure of the pre-quench state in terms of the post-quench excitations is essential in dragging quantitative predictions. So far, the quasiparticle description has been always applied to

initial states where quasiparticles were independently emitted in pairs of opposite momenta: if several species were present, they were uncorrelated [107, 137–141]. In this case, the spreading of the entanglement can be quantitatively explained in terms of purely-semiclassical quantities. Very recently, another setup which lays beyond the standard quasiparticle picture was analyzed in Ref. [142], where a quantum quench in a free fermion model with several species was analyzed: particles were still created in pairs, but this time with a classical interspecies correlation. The standard quasiparticle result must be corrected, but the entanglement growth can be still described in terms of classical objects. In Ref. [6] we made a further step and consider free models with several species of excitations emitted in pairs, but with a true interspecies *quantum-correlation*. We propose a quasiparticle ansatz, where the entanglement growth is still understandable in terms of semiclassical propagating particles, but the carried entanglement cannot be interpreted as a pure classical object any longer. We test our prediction in quantum quenches in the Ising spin chain in transverse field, where a periodically modulated magnetic field allows us to produce several species of excitations at once. We found perfect agreement between our ansatz and numerical simulations. Furthermore, we provide a quasiparticle description of the time evolution of the order parameter and its correlation functions, generalizing the results of Ref. [107, 143].

A natural application of the quasiparticle picture consists in analyzing weak inhomogeneities where, in the spirit of the local density approximation, the system can be thought to locally relax to a GGE, described by a space-time dependent root density. For example, in Ref. [7] in collaboration with M. Collura and S. Sotiriadis we analyzed quantum quenches in the Lieb Liniger model from two peculiar values of the interaction, namely from the free case $\kappa = 0$ to hard core bosons $\kappa = +\infty$, i.e. the Tonks-Girardeau limit which can be mapped to free fermions [144–149]. Despite the initial and final Hamiltonians being both free, connecting the prequench modes with the post quench ones (and thus solving the quench) requires a highly non-linear mapping.

This quench protocol has already been solved in the homogeneous case choosing as initial state the non-interacting ground state (i.e. the Bose-Einstein condensate) [150]. Later, the effects of an hard wall [151] and harmonic [152] traps were included: however, the condensate is a very peculiar state. Among the flaws of this choice we can surely enlist *i)* the total absence of any space dependence in the initial correlation functions (apart from that given by the confining potential, if present); *ii)* the great dependence on the trap shape [151, 152] which makes the proper thermodynamic limit difficult to be defined. In this sense, the condensate is very pathological and therefore it is worth to investigate a different class of states which exhibit a more physical behavior: still, the initial state is required to be simple enough to allow an analytical treatment.

A good compromise that meets both requirements is given by the *gaussian* (in terms of the bosons) ensembles, for example a free thermal ensemble, with a finite correlation length. After providing the solution of such a quench in the homogeneous case, we proceed to analyze the experimentally relevant case of a confining potential.

We show how in the thermodynamic limit (which is necessary for the system to exhibit relaxation) a separation of time scales takes place: on a short time scale the system locally equilibrates to a GGE and thus can be described by a space-dependent mode density. On a larger time scale, proportional to the trap size, the system behaves as if it was a collection of classical free particles moving in an external potential: for a purely harmonic trap no relaxation is observed and the system undergoes a periodic motion. Instead, anharmonic corrections cause the system to thermalize.

Semiclassical methods in many-body quantum physics have a long and fruitful story (see eg. Ref. [153–158]), however they were essentially confined to non-interacting models. At least, this have been true until the last couple of years. In 2016 a breakthrough completely turned the tables: independently, in Ref. [159] O. Castro-Alvaredo, B. Doyon and T. Yoshimura and in Ref. [160] B. Bertini, M. Collura, J. De Nardis and M. Fagotti formulated an hydrodynamic theory

valid for interacting integrable models, now called Generalized Hydrodynamic (GHD). In the presence of weak inhomogeneities, the system is assumed to locally relax to a GGE, then GGEs at different space-times are connected invoking charge/current conservation: the result is a hydrodynamic equation for the root densities, which can be regarded as semiclassically describing a set of particles, whose effective velocities is nevertheless influenced by the interaction.

The role of the seminal work of Ref. [159, 160] is hardly overestimated and stimulated an impressive array of remarkable results. Initially used to address dishomogeneities in the initial state [159–170], it has been generalized to include small force fields [171], allowing for example a direct simulation of the Newton's cradle experiment [172]. Hydrodynamic concepts have been applied also to evaluate large-scale correlators [173–175] and to the entanglement spreading [176–178]. Corrections to hydrodynamic have been analyzed firstly in free models [179] and only very recently in truly interacting integrable models [180].

So far, we focused on the quantum world, but, as it should be clear from the very beginning of the introduction, the same questions can be reformulated in classical integrable models as well. For example, in Ref. [181] GHD has been shown to emerge in a classical gas of hard rods, i.e. hard core particles with a finite spatial extension.

Classical models do not have only solitonic (i.e. particle-like) degrees of freedom, but also radiative modes with a rather different thermodynamics: for example, one could think to the UV catastrophe of the black body radiation, whose solution led to quantum mechanics.

Quenches in classical integrable field theories and the construction of the GGE have already been considered in Ref. [182]: surprisingly, the construction of the Thermodynamic Bethe Ansatz is much more difficult in the classical realm when compared with the quantum case. However, there are several field theories which can be interpreted either quantum-mecanically or classically, for example the Sinh Gordon model: in Ref. [182] the semiclassical limit of the quantum TBA has been considered, giving access to the thermodynamics and GGE for the classical Sinh Gordon model. Furthermore, the semiclassical limit of the Le Clair-Mussardo expansion was used to study the one point functions in the classical theory. The content of Ref. [8], in collaboration with B. Doyon, G. Watts and T. Yoshimura, further extends this program considering the Generalized Hydrodynamics of classical field theories, above all the classical Sinh Gordon.

This classical study provided an unprecedented opportunity to easily test several hydrodynamic concepts: quantum systems are much harder to be numerically simulated [115], especially continuum models. On the other hand, simulations on the classical Sinh Gordon can be performed with a Metropolis-Hasting algorithm [183, 184] combined with a deterministic solution of the equations of motion. Besides generalizing the hydrodynamic to include radiative modes, we numerically benchmarked partitioning protocols and correlation functions on the eulerian scale, elucidating the limit of applicability of hydrodynamics. We performed our tests on particular observables, called vertex operators (exponential of the field defining the Sinh Gordon model), for whose expectation value we derive a closed integral equation from the semiclassical limit of the Smirnov-Negro formula [90, 91], making thus a further progress with respect to the results of Ref. [182], based on the Le Clair-Mussardo expansion.

We now set aside weakly inhomogeneous systems and rather consider the opposite limit: Chapter 4 is dedicated to out-of-equilibrium physics induced by defects, describing the work presented in Ref. [9–11]. Consider an initially homogeneous infinite system, which is assumed to be integrable, and suddenly activate a localized impurity: this is far from being an innocent operation and the effect of the impurity ballistically spread across the system, affecting it on a thermodynamic large scale (see e.g. Ref. [185, 186]). In the spirit of GHD, far from the defect the system locally equilibrates to a space-time dependent GGE which, because of the ballistic spreading, is a function of the ray $\zeta = x/t$, with x the relative distance from the defect. Such a peculiar inhomogeneous GGE has been named Local Quasi Stationary State (LQSS) [160]. As long as lattice systems are concerned, the quasiparticles possess a finite maximum velocity $v_M < \infty$, being it fundamentally due to the Lieb-Robinson bound [187]. The existence of v_M makes

natural to wonder what happens in the case of a defect suddenly activated in an homogeneous system, but then dragged at constant velocity v. In particular, can the system cope with the defect when the latter moves faster than v_M? Is an LQSS still formed and how is it affected by the velocity of the defect? Besides being a compelling question from a theoretical point of view, similar out-of-equilibrium protocols already underwent experimental investigation (see for example Ref. [47]). These questions are investigated in this chapter, based on the work done in collaboration with A. De Luca in Ref. [9, 10].

The best candidates to acquire some physical insight in this problem are *free models*, which are amenable of exact, albeit non trivial, calculations. In Ref. [9] we studied a system of hopping fermions, the defect being chosen as a localized variation of the chemical potential, while in Ref. [10] the Ising spin chain in transverse field is considered, the moving impurity being a perturbation of the magnetic field. Despite being essentially the same setup, there is a deep difference: the presence of an $U(1)$ symmetry associated with the particle-number conservation that is present in the first case, while absent in the second. This deeply affects the system response when $v > v_M$. For $v < v_M$ in both models a LQSS is formed: the out-of-equilibrium protocol can be framed in a proper time-independent scattering theory, with a parametric dependence on the defect velocity v. The LQSS is then expressed in terms of the scattering data, which can be exactly computed either in the case of a very narrow defect, or in the opposite limit of a smooth impurity, by mean of semiclassical arguments. As soon as $v > v_M$, in the hopping-fermions system the LQSS disappears and the defect does not affect the system on a thermodynamic scale anymore. In particular, the medium does not exert any friction force on the impurity (superfluidity). This is not the case of the Ising model where the LQSS persists even for $v > v_M$, albeit with peculiar differences with respect to the $v < v_M$ case. The difference in the two models is due to the $U(1)$ symmetry: the underlying scattering theory for $v \to 0^+$ has infinitely many available scattering channels (causing a rather complicated LQSS). As v is increased, the number of possible scattering channels diminishes until, for $v > v_M$ in the Ising model only two scattering channels survive. Having two available scattering channels allows for the formation of a non trivial LQSS. In the hopping fermions case instead, one of these two scattering channels is forbidden by the particle conservation and only the trivial scattering is possible, regardless the specific form of the potential: this explains the absence of LQSS and the frictionless motion.

In Ref. [11] we again consider the sudden activation of a localized defect, but the latter is kept at rest. Our intention is to investigate the late times effects of integrability-breaking impurities. In view of the remarkable difference between non-integrable and integrable models, as well as the exceptional fine tuning needed in order to realize the latter, understanding the effect of integrability-breaking perturbations is a central question, from both a theoretical and experimental point of view. In particular, what is the destiny of a system with weakly broken integrability? Homogeneous integrable-breaking perturbations have been extensively investigated and the so called "prethermalization" paradigm [188–205] has been identified. In this case the local relaxation occurs in two steps: on a short time scale the system relaxes to a GGE determined by the integrable part of the Hamiltonian, but then the non-integrable perturbation kicks in and the system slowly drifts towards a thermal state. Prethermalization has been experimentally observed [206–209]. The magnitude of the integrability breaking term changes the time scale on which the thermal state is attained [188], but relaxation to a Gibbs ensemble eventually takes place.

What it should be expected in the impurity case? The system as a whole will not thermalize: a LQSS will be surely formed, propagating from the impurity in a lightcone manner. The correct question to be posed is how the propagating density root looks like.

Based on the insight gained in the homogeneous case, any finite subsystem encompassing the defect could be expected to eventually thermalize, since integrability is broken. If this expectation was true, thermal quasiparticles should spread across the system: however, preliminary

numerical results go against this natural expectation [210].

Indeed, in Ref. [11] we studied the thermalizing properties of integrability-breaking impurities: in clear contrast with the homogeneous case, their effect is perturbative in the defect strength also at infinite time, thus preventing thermalization.

In particular, analytical computations are done in the case of a free theory in the bulk, but with an interacting defect: we build a perturbation theory in the defect strength of the emergent LQSS, which is finite at any order. For technical reasons, we consider continuum models which in the quantum case are not suited for numerical computations, however the same questions can be posed also for classical models which are most easily simulated. Perfect agreement of numerical data with the perturbative expansion is found. Our findings are framed in a simple semi-classical picture, which is expected to hold true even in the case of truly interacting integrable models, pointing out at the poor thermalizing properties of integrable-breaking impurities.

Organization of the thesis

The structure of the thesis has already been outlined while introducing the research topics, however we provide a short recap for the sake of clarity. The order in which the various topics are presented is thought to progressively build insight and get familiarity with the formalism, but each chapter is relatively independent and can be read on its own. Chapter 2 also provides a short introduction to integrable systems and their thermodynamics. Hereafter, a list of the chapters with the related papers is presented:

Chapter 2: *Non relativistic limits of integrable relativistic field theories*

- [1] A. Bastianello, A. De Luca, G. Mussardo, *Non relativistic limit of integrable QFT and Lieb-Liniger models*, J. Stat. Mech. (2016) 123104.
- [2] A. Bastianello, A. De Luca, G. Mussardo, *Non relativistic limit of integrable QFT with fermionic excitations*, J. Phys. A: Math. Theor. **50** 234002 (2017).
- [3] A. Bastianello, L. Piroli, P. Calabrese, *Exact local correlations and full counting statistics for arbitrary states of the one-dimensional interacting Bose gas*, Phys. Rev. Lett. **120**, 190601 (2018).
- [4] A. Bastianello, L. Piroli, *From the sinh-Gordon field theory to the one-dimensional Bose gas: exact local correlations and full counting statistics*, arXiv:1807.06869 (2018).

Chapter 3 *Integrable models driven out-of-equilibrium*

- [5] A. Bastianello, S. Sotiriadis, *Quasi locality of the GGE in interacting-to-free quenches in relativistic field theories*, J. Stat. Mech. (2017) 023105.
- [6] A. Bastianello, P. Calabrese, *Spreading of entanglement and correlations after a quench with intertwined quasiparticles*, arXiv:1807.10176 (2018).
- [7] A. Bastianello, M. Collura, S. Sotiriadis, *Quenches from bosonic Gaussian initial states to the Tonks-Girardeau limit: Stationary states and effects of a confining potential*, Phys. Rev. B 95, 174303 (2017).
- [8] A. Bastianello, B. Doyon, G. Watts, T. Yoshimura, *Generalized hydrodynamics of classical integrable field theory: the sinh-Gordon model*, SciPost Phys. **4**, 045 (2018) .

Chapter 4 *Impurity-induced out-of-equilibrium protocols*

- [9] A. Bastianello, A. De Luca, *Nonequilibrium Steady State Generated by a Moving Defect: The Supersonic Threshold*, Phys. Rev. Lett. **120**, 060602 (2018).
- [10] A. Bastianello, A. De Luca, *Superluminal moving defects in the Ising spin chain*, Phys. Rev. B **98**, 064304 (2018).
- [11] A. Bastianello, *Lack of thermalization for integrability-breaking impurities*, arXiv:1807.00625 (2018).

Chapter 2

Non relativistic limits of integrable relativistic field theories

This Chapter is devoted to study galilean invariant integrable models taking advantages of results available in the relativistic realm, by mean of proper non relativistic limits. We also provide a short general introduction to integrability. In particular

1. Section 2.1 provides a short summary of integrability. Following the viewpoint of the chapter, we found more natural to introduce integrability in the framework of relativistic field theories: however, several concepts are more general and do not strictly rely on relativistic invariance.

2. Section 2.2 contains the basics of the non-relativistic limits, as well as a summary of the two main characters of this chapter, namely the Lieb Liniger model (galilean) and the Sinh Gordon model (relativistic). We discuss their connection by mean of a non relativistic limit, along the line of [85, 86].

3. Section 2.3 contains the original work of Ref. [1, 2], done in collaboration with A. De Luca and G. Mussardo. We shed ligth on the striking imbalance between the set of integrable models with local interactions and relativistic invariance compared with the galilean invariant counterpart. We analyze a large number of relativistic models and discuss their non relativistic limit. Our findings show how the large variety of the relativistic world shrinks to essentially the Lieb Liniger model and its multispecies generalizations: the resulting non relativistic models are made of particles of equal mass and pairwise interaction.

4. Section 2.4 presents the work done in Ref. [3, 4] in collaboration with L. Piroli and P. Calabrese. We study the one point functions in the Lieb Liniger model, exploiting the results of Negro and Smirnov [90, 91] in the Sinh Gordon model and the non relativistic limit of the latter. Our findings provide all the one point functions in the form $\langle(\psi^\dagger)^K\psi^K\rangle$ for arbitrary K and on arbitrary thermodynamically-excited states. The one point functions are accessible through a recursive set of linear single-variable integral equations. Several applications are discussed.

2.1 Integrability in relativistic field theories

The quest of defining integrability has a long history, starting of course from the familiar definition given by Liouville in classical mechanics, where he stated that a system made of N degrees of freedom is integrable if it possesses N independent first integrals of motion in involution. Despite this transparent definition of integrable systems in classical mechanics, to define what is an integrable system in many-body quantum mechanics – and possibly reaching a classification of all such models – turns out to be a non trivial problem (see for instance [52, 69, 211, 212]). Without entering into a long and detailed examination of all pros and cons of possible alternative definitions of integrability for such quantum systems (see Ref. [52]), in the following we adopt as a guiding line the simplest and the most basic one, i.e. the request that a quantum

integrable system must have a non-trivial set of charges which commute with its Hamiltonian (this set must be infinite if we are dealing with many body systems). In particular, we demand each charge to be expressible as spatial integral of an appropriate local density.

We choose to introduce integrability through the formalism of relativistic quantum field theories, albeit several concepts are immediately transferred to galilean invariant models, lattice systems or to the classical realm. Thus, let us consider a relativistic-invariant local quantum field theory (local in the sense its dynamic is ruled by a local action).

The presence of infinitely many local charges implies stringent constraints on the structure of the Hilbert space. For example, following [78] (see Ref. [70, 71] for a more pedagogical introduction), we construct a multi-particle asymptotic state. With the notation $|A_{a_1}(\theta_1)...A_{a_n}(\theta_n)\rangle$ we label a state which contains particles of species $\{a_i\}_{i=1}^N$ and rapidity $\{\theta_i\}_{i=1}^N$, furthermore we imagine the particles to be infinitely far apart in the real space (a more satisfactory approach would involve wavepackets rather than well-defined rapidities, in order to allow for proper spatial localization of the excitations). Conventionally, the order of appearance in the state reflects the order in which the particles are arranged on the real line.

The multiparticle state can be chosen as a common eigenvector of the whole set of charges: invoking locality, a given charge $\mathcal{Q}_n$ necessarily acts additively on the the set

$$\mathcal{Q}_n|A_{a_1}(\theta_1)...A_{a_n}(\theta_n)\rangle = \left(\sum_{i=1}^{N} q_n^{a_i}(\theta_i)\right)|A_{a_1}(\theta_1)...A_{a_n}(\theta_n)\rangle \ . \tag{2.1}$$

$q_n^a(\theta)$ are called the charge eigenvalues. Because of relativistic invariance, the set of charges can be organized accordingly to their behavior under Lorentz boost

$$q_n^a(\theta) = p_n^a\, e^{s_n\theta}\,, \tag{2.2}$$

where s_n is the spin of the charge. The presence of infinitely many conserved quantities deeply affects scattering events: the scattering matrix is defined as the overlap between in-states and out states

$$S\big(\{(a_i',\theta_i')\}_{i=1}^{N'}|\{(a_i,\theta_i)\}_{i=1}^{N}\big) = \langle A_{a_1'}(\theta_1')...A_{a_{N'}'}(\theta_{N'}')|A_{a_1}(\theta_1)...A_{a_N}(\theta_N)\rangle \tag{2.3}$$

Inserting the charges $\mathcal{Q}_n$ in between the in and the out state and letting it acting once on left and then on the right, we get infinitely many constraints

$$\begin{aligned}\langle A_{a_1'}(\theta_1')...A_{a_{N'}'}(\theta_{N'}')|\mathcal{Q}_n|A_{a_1}(\theta_1)...A_{a_N}(\theta_N)\rangle = \\ = \begin{cases}\left(\sum_{i=1}^{N'} p_n^{a_i'}\, e^{s_n\theta_i'}\right)\langle A_{a_1'}(\theta_1')...A_{a_{N'}'}(\theta_{N'}')|A_{a_1}(\theta_1)...A_{a_N}(\theta_N)\rangle \\ \left(\sum_{i=1}^{N} p_n^{a_i}\, e^{s_n\theta_i}\right)\langle A_{a_1'}(\theta_1')...A_{a_{N'}'}(\theta_{N'}')|A_{a_1}(\theta_1)...A_{a_N}(\theta_N)\rangle\end{cases}\end{aligned} \ . \tag{2.4}$$

The only way to satisfy all these constraints at once for infinitely many spins is a pure elastic scattering, thus

$$N = N'\,, \qquad \theta_i' = \theta_{P(i)}\,, \qquad p_n^{a_i'} = p_n^{a_{P(i)}}\,, \tag{2.5}$$

where P is some permutation of the indexes $\{1,...,N\}$. In particular, there is no particle production. If no internal symmetry is present and the particle species can be resolved by the eigenvalues p_n^a, then the above condition further implies the conservation of the scattered species and the scattering is purely transmissive. This is achieved, for example, if particles have different masses. Indeed, the mass of a particle is nothing else than the constant p_n^a associated to the charges of spin ± 1, which are a linear combination of Hamiltonian and momentum, always present in the list of conserved charges. However, if mass degeneracy is present, reflection

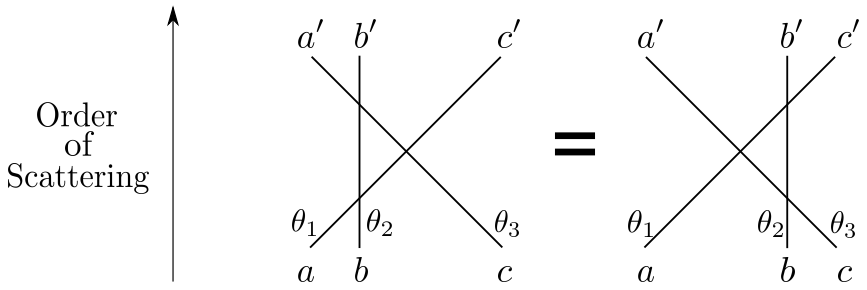

Figure 2.1: *Graphical representation of the Yang-Baxter equation* (2.9).

cannot be excluded on a general ground.

Despite being the complete elasticity of scattering events an astonishing conclusion, it is far from being the end of the story: as a matter of fact, due to the infinite number of conservation laws multiparticle scatterings factorize in two body scattering events [78]. We can suggestively write

$$|...A_a(\theta)A_b(\theta')...\rangle = \sum_{c,d} S_{a,b}^{c,d}(\theta-\theta')|...A_c(\theta')A_d(\theta)...\rangle\,, \tag{2.6}$$

where $S_{a,b}^{c,d}(\theta)$ is the two body scattering matrix. Because of Lorentz invariance, scattering amplitudes are functions only of the relative rapidity of the involved particles.

The scattering matrix cannot be an arbitrary function, but it has to satisfy proper consistency conditions, which are already embedded in the notation (2.6). For example, permuting two particles two times in (2.6) we get the so called unitarity condition

$$\sum_{c,d} S_{c,d}^{a',b'}(-\theta)S_{a,b}^{c,d}(\theta) = \delta_{a,a'}\delta_{b,b'}\,. \tag{2.7}$$

An equivalent formulation of the unitary condition is obtained taking the square of (2.6): assuming the states are normalized to 1 we get

$$\sum_{c,d} \left[S_{a',b'}^{c,d}(\theta)\right]^* S_{a,b}^{c,d}(\theta) = \delta_{a,a'}\delta_{b,b'}\,, \tag{2.8}$$

which obviously implies $\left[S_{a',b'}^{c,d}(\theta)\right]^* = S_{c,d}^{a',b'}(-\theta)$.

An extra further requirement, which trivializes in the pure transmissive case, is the Yang Baxter Equations [70, 71, 78]: this is a consistency requirement coming from the possibility of exchanging three particles in two different ways, which should nevertheless result in the same state

$$\sum_{e,f,g} S_{a,b}^{e,f}(\theta_1-\theta_2)S_{f,c}^{g,c'}(\theta_1-\theta_3)S_{e,g}^{a',b'}(\theta_2-\theta_3) = \sum_{e,f,g} S_{b,c}^{e,f}(\theta_2-\theta_3)S_{a,e}^{a',g}(\theta_1-\theta_3)S_{g,f}^{b',c'}(\theta_1-\theta_2)\,. \tag{2.9}$$

A pictorial representation is given in Fig. 2.1. So far, we have not really used relativistic invariance, outlining properties of generic (e.g. galilean invariant, lattices...) integrable systems: the only caveat is to replace the relativistic rapidity with a different parametrization.

However, relativistic invariance provides further absolutely non trivial constraints, collected altogether in the elegant Bootstrap Approach [61, 69, 70, 78, 212], which allows both for a solution and a classification of integrable field theories which possess relativistic invariance.

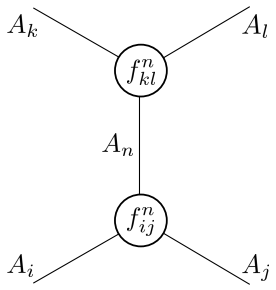

Figure 2.2: *Residue of the pole and its expression in terms of the* on-shell *coupling constants, graphical representation of Eq.* (2.13) *and* (2.14).

2.1.1 The Bootstrap Approach

The analytical properties of the scattering matrix have a clear physical interpretation [213]. For example, in generic models, branch cuts are associated with thresholds of particle production, while bound states can be interpreted as poles. This analytical control does not suffice to solve a generic field theory, but when combined with the factorizability [62–71] reveals to be extremely powerful. Here we provide a short summary on analytic properties of the S-matrix and the bootstrap approach, without any pretence of being exhaustive. For a more complete discussion, see [70, 71].

1. A distinguished property of relativistic field theories is the crossing symmetry, namely scattering amplitudes are invariant if we replace incoming particles with outgoing antiparticles (below, denoted with a bar)

$$A_a + A_b \to A_c + A_d \;\; = \;\; A_a + A_{\bar{d}} \to A_c + A_{\bar{b}} \,. \tag{2.10}$$

   Which implies

$$S^{c,d}_{a,b}(\theta) = S^{c,\bar{b}}_{a,\bar{d}}(i\pi - \theta) \,. \tag{2.11}$$

2. Scattering amplitudes are expressible in terms of the relativistic invariants of the scattering, namely the Mandelstam variables which are unaffected by the shift $\theta \to \theta + i2\pi$. Therefore, the scattering amplitude must be periodic along the imaginary direction

$$S^{c,d}_{a,b}(\theta) = S^{c,d}_{a,b}(\theta + i2\pi) \,. \tag{2.12}$$

3. The bound states correspond to the simple poles with positive residue along the imaginary segment $(0, i\pi)$ of the θ variable. Consider a S-matrix with incoming particles A_a and A_b that has a simple pole at $\theta = i\, u^n_{ab}$: in correspondence of this pole, the amplitude can be expressed as

$$S^{k,l}_{i,j}(\theta) \;\simeq\; i\, \frac{R^n}{\theta - i u^n_{ij}} \;\; , \tag{2.13}$$

   and the residue R^n is related to the *on-shell* three-particle vertex functions of the incoming particles and the bound state A_n, as shown in Fig. 2.2

$$R^n \;=\; f^n_{ij}\, f^n_{kl} \;\; . \tag{2.14}$$

   Since in the bootstrap approach the bound states are on the same footing than the asymptotic states, there is an important relation among the masses of the system: if $\theta = i u^n_{ij}$ is the

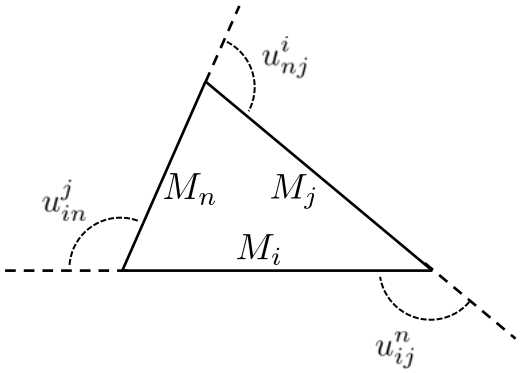

Figure 2.3: *Mass triangle, graphical representation of Eq.* (2.15) *and* (2.16)

position of the pole in the scattering of the particles A_i and A_j, the mass of the bound state is given by

$$M_n^2 = M_i^2 + M_j^2 + 2M_iM_j \cos u_{ij}^n \ . \tag{2.15}$$

Hence, the mass of the bound state is the side of a triangle made of also with the masses of the other two particles, where u_{ij}^n is one of the external angles as shown in Fig. 2.3. This figure clearly highlights the symmetric role played by the three particles. Moreover, it is easy to show that the positions of the poles in the three channels satisfy

$$u_{ij}^n + u_{in}^j + u_{jn}^i = 2\pi \ , \tag{2.16}$$

a relation that expresses a well-known properties of the external angles of a triangle.

The unitarity and crossing symmetry equations alone are not able to fix the position of the poles of these amplitudes. To achieve this goal it is necessary to make use of a dynamical condition. This is provided by the bootstrap principle [63] that posits that the bound states are on the same footing of the asymptotic states. As a consequence, the amplitudes relative to the bound states can be obtained in terms of the amplitudes of the external particles and viceversa. This translates in an additional non-linear equation that must be satisfied by the scattering amplitudes . In order to simplify our treatment, we now restrict ourselves to purely transmissive scattering, thus we simplify the notation as $S_{a,b}^{c,d}(\theta) = \delta_{b,c}\delta_{a,d}S_{a,b}(\theta)$

$$S_{i,\bar{l}}(\theta) = S_{i,j}(\theta + i\bar{u}_{jl}^k)\, S_{i,k}(\theta - i\bar{u}_{lk}^j) \ , \tag{2.17}$$

where

$$\bar{u}_{ab}^c \equiv \pi - u_{ab}^c \ . \tag{2.18}$$

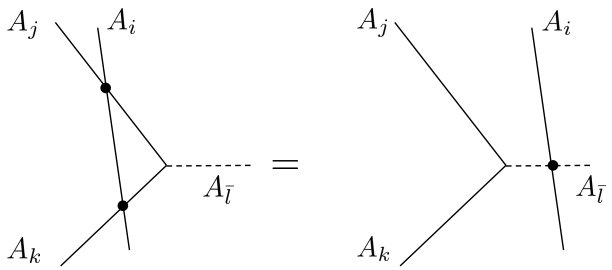

Figure 2.4: *Bootstrap equation that links the S-matrix amplitudes, where $A_{\bar{l}}$ is the bound state in the scattering process of the particles A_j and A_k (see Eq.* (2.17)*).*

This equation comes from the commutativity of the two processes shown in Fig. 2.4, obtained one from the other by the translation of the world-line of the asymptotic particle A_i. One can try then to classify the integrable QFT in terms of the set of amplitudes $S_{a,b}$ which close the bootstrap procedure, i.e. those which have a set of poles compatible with the bootstrap equation (2.17) and that can be interpreted in terms of bound states or multi-particle scattering processes of the asymptotic particles themselves. The masses of the particles are determined by the relation (2.15) while the on-shell three-coupling vertices by the residues (2.14). In practice, to implement this program, one needs to start from the amplitude that involves the lighest particle, therefore with the simplest pole structure, and then iteratively applying the bootstrap equations (2.17) and see whether this procedure consistently closes after a finite number of steps.

For the nature of this procedure, it is clear that the bootstrap will not close with a generic location of the poles: these have to be properly fine tuned in order that the iterative application of the bootstrap equations (2.17) produce meaningful new amplitudes. For instance, if there is no partial cancellation between poles and zeros of the amplitudes $S_{i,j}(\theta + i\bar{u}^k_{jl})$ and $S_{i,k}(\theta - i\bar{u}^j_{lk})$ involved in the bootstrap equation (2.17), the S-matrix amplitudes $S_{i,\bar{l}}$ will double the number of poles at each step of the iteration, so that the overall number of the poles of the S-matrix which grows multiplicatively, finally leading to inconsistencies with respect to basic requirement of QFT, such as the impossibility to have accumulation of poles in the amplitudes.

Up to now there has never been found a consistent set of purely transmissive amplitudes than do not coincide with those of the Toda Field Theories (which will be discussed in Section 2.3.2) or to theories easily related to them.

2.1.2 The thermodynamics of integrable models: the Thermodynamic Bethe Ansatz

The knowledge of the scattering matrix gives access to an astonishing amount of information. For example, from the scattering data we can exactly compute the thermodynamics following the Thermodynamic Bethe Ansatz [57], that we briefly recall. For the sake of simplicity, we assume the existence of an unique particle species with scattering matrix $S(\theta)$ (being particles of the same species indistinguishable, separate transmission and reflection does not make sense anymore). From the unitarity condition, specializing at rapidity $\theta = 0$, we get $S(0) = \pm 1$: the choice of the sign changes the natural formulation of the TBA. For definiteness, we work with the fermionic TBA, thus $S(0) = -1$ (this is the case for the Sinh Gordon model), however the bosonic and fermionic cases can be seen to be dual [214]. Models with $S(0) = -1$ are labeled as fermionic because the Pauli's exclusion principle in enforced. Indeed, specializing (2.6) to a single species and considering two particles with equal rapidities we get

$$|...A(\theta)A(\theta)...\rangle = S(0)|...A(\theta)A(\theta)...\rangle = -|...A(\theta)A(\theta)...\rangle\,. \tag{2.19}$$

This requirement removes the state from the Hilbert space, forcing $|...A(\theta)A(\theta)...\rangle = 0$. In order to obtain a thermodynamic description with a finite energy density, we should consider a finite system: introducing a finite volume causes a quantization in the possible rapidities allowed in a given state, similarly to what happens in the free systems. However, the presence of non trivial scattering among the particles leads to the Bethe-Gaudin equations [214]. Imagine a state containing particles with rapidities $\{\theta_i\}_{i=1}^N$, the system is a ring of length L with periodic boundary conditions

$$e^{iLp(\theta_i)} \prod_{j\neq i} S(\theta_i - \theta_j) = 1\,. \tag{2.20}$$

Above, $p(\theta)$ is the particle momentum. In the relativistic case we have $p(\theta) = M\sinh\theta$, but the Bethe-Gaudin equations can be written for general integrable models, provided the correct mometum and scattering matrices are employed. Pictorially (see Fig. 2.5), Eq. (2.21) can be interpreted as it follows: imagine to select the particle of rapidity θ_i and carry it around the ring

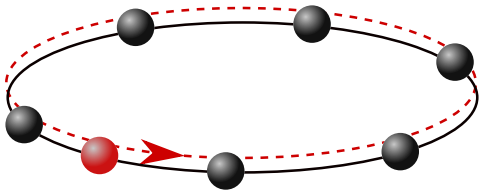

Figure 2.5: *Pictorial representation of the Bethe-Gaudin equations* (2.21)*: as periodic boundary conditions are tested moving a particle along the ring, this unavoidably interact with the others particles, explaining the* $S-$*matrix contribution of Eq.* (2.21).

until it comes back to the initial position. Doing so, it will collect a phase which receives two contributions: a term $e^{iLp(\theta_i)}$ which is the single-particle contribution, times the scattering phases with each particle present on the ring (indeed, from Eq. (2.8) we immediately get $|S(\theta)| = 1$). Equating to one the total phase, the Bethe-Gaudin equations are obtained. Notice that, if we identically set $S(\theta) = -1$ the equation trivializes in the standard free-fermion quantization rule. In the logarithmic form, the solutions to Eq. (2.21) can be parametrized in terms of a set of integers I_i

$$\frac{I_i}{L} = \frac{1}{2\pi} p(\theta_i) - \frac{1}{2\pi L} \sum_{i \neq j} i \log\left(S(\theta_i - \theta_j)\right). \tag{2.21}$$

The Pauli's exclusion principle forbids $I_i = I_j$. It should be evident that the relation between the integers and the rapidities is highly non linear and difficult to be solved. However, as long as the thermodynamic limit is concerned, we can avoid to look for an exact solution and invoke a coarse grain procedure. As $L \to \infty$, the set of allowed rapidities becomes dense and we can introduce a counting function $\rho(\theta)$, called *root density*, in such a way $L\rho(\theta)\mathrm{d}\theta$ counts how many solutions are included in the interval $[\theta, \theta + \mathrm{d}\theta]$. Sums over the states, labeled in terms of the integers I_i, become functional integrals over the possible choices of the root density. Let us proceed with a specific example, i.e. computing the thermal partition function $\mathcal{Z} = \mathrm{Tr}[e^{-\beta H}]$

$$\mathcal{Z} = \sum_{N=0}^{\infty} \frac{1}{N!} \sum_{\{I_i\}_{i=1}^N} e^{-\beta \sum_{i=1}^N E(\theta_i)} \simeq \int \mathcal{D}\rho \, e^{\mathcal{S}[\rho] - L\beta \int \mathrm{d}\theta \rho(\theta) E(\theta)}, \tag{2.22}$$

where $E(\theta) = M \cosh\theta$ is the single particle energy. Above, an entropy term $\mathcal{S}[\rho]$ must be introduced: there are many configurations of the integers I_j resulting in the same root density. In particular, we need to introduce a phase space density $\rho_t(\theta)$ (hereafter called total root density) defined as

$$\rho_t(\theta) = \frac{\partial_\theta p(\theta)}{2\pi} + \int \frac{\mathrm{d}\mu}{2\pi} \varphi(\theta - \mu)\rho(\mu). \tag{2.23}$$

Above, we defined the real function $\varphi(\theta) = -i\partial_\theta \log S(\theta)$. If $L\rho(\theta)\mathrm{d}\theta$ counts the number of rapidities in a small interval, $L\rho_t(\theta)\mathrm{d}\theta$ counts the maximum number of possible "slots" we could use in the interval $[\theta, \theta + \mathrm{d}\theta]$. The entropy term $\mathcal{S}[\rho]$ is computed simply as the (logarithm of) the number of different configurations in which we can arrange $L\rho(\theta)\mathrm{d}\theta$ elements in $L\rho_t(\theta)\mathrm{d}\theta$ available slots, respecting the Pauli's exclusion principle

$$\mathcal{S}[\rho] = L \int \mathrm{d}\theta \, \rho_t \log\rho_t - \rho\log\rho - (\rho_t - \rho)\log(\rho_t - \rho). \tag{2.24}$$

Taking now the thermodynamic limit $L \to \infty$, the path integral (2.22) localizes around the saddle point, whose solution gives the root density ρ associated with a thermal state of temperature β.

The solution can be written as an unique non-linear integral equation

$$\varepsilon(\theta) = \beta E(\theta) - \int_{-\infty}^{\infty} \frac{\mathrm{d}\mu}{2\pi} \varphi(\theta-\mu) \log\left(1+e^{-\varepsilon(\mu)}\right) . \tag{2.25}$$

where we conveniently introduced the parametrization

$$\frac{1}{e^{\varepsilon(\theta)}+1} = \frac{\rho(\theta)}{\rho_t(\theta)} . \tag{2.26}$$

Conventionally, the quantity $\rho(\theta)/\rho_t(\theta) = \vartheta(\theta)$ is called the filling function.

Solving Eq. (2.25) (in usual cases a recursion approximation scheme converges pretty fast) together with Eq. (2.23) allows one to determine the saddle point solution $\rho(\theta)$, which can be then used, for example, to compute the energy density

$$\lim_{L\to\infty} \frac{\langle H \rangle}{L} = \int \mathrm{d}\theta E(\theta)\rho(\theta) , \tag{2.27}$$

and other meaningful quantities (see the Section (2.1.3)). Albeit we worked on thermal states, the same formalism is readily adapted to include general GGEs $e^{-\sum_j \lambda_j \mathcal{Q}_j}$: it suffices to replace $\beta E(\theta)$ in Eq. (2.25) with the proper source term, given by the eigenvalues of the charges appearing in the GGE. More precisely, describing a GGE $e^{-\sum_n \lambda_n \mathcal{Q}_n}$ requires to replace $\beta E(\theta) \to \sum_n \lambda_n q_n(\theta)$ in (2.25), where $q_n(\theta)$ are the single-particle eigenvalues of the charges (2.1).

In an arbitrary GGE, it is simple to realize that the (extensive part of) the free energy (namely the logarithm of the partition function) acquires a rather simple expression in terms of the effective energy ε

$$\mathcal{F} = \lim_{L\to\infty} L^{-1} \log \mathcal{Z} = \int \frac{\mathrm{d}\theta}{2\pi} \partial_\theta p(\theta) \log(1+e^{-\varepsilon(\vartheta)}) . \tag{2.28}$$

An effect of strong correlation: the dressing of single particle eigenvalues

Eigenstates in integrable models are described by a collection of stable particles undergoing elastic scattering. In several ways they resemble free systems, for example in the construction of thermodynamics we are naturally lead to a Fermi-function distribution (2.26), usually encountered in free-fermionic systems. However, one dimensional systems are strongly correlated: indeed, the "effective energy" appearing in Eq. (2.26) feels the contribution of all the other excitations, through the integral equation Eq. (2.25).

Here we want to point out another simple situation where the correlation plays an essential role, namely the dressing of the dispersion law (and other single-particle eigenvalues). Let us consider the following problem: given a state whose Bethe Equations (2.21) are identified by a set of integers $\{I_i\}$ (which is assumed to be thermodynamically large), how does the expectation value of a given charge change if we add an extra excitation? Namely, how are the charges modified if we now consider $\{I_i\} \cup I_\ell$? The question is easily generalized to *i)* the removal of a particle and *ii)* adding/removing a finite number of particles on a thermodynamically excited background. The result of this analysis, for which the reader can see e.g. Ref. [57], is a description of the low energy sector on the top of a given state as a collection of free particles, but with a non trivial "dressing" caused by the background root distribution. This is probably best appreciated in the Quench Action paradigm [100, 116], which we will not cover here, and in the formulation of Generalized Hydrodynamic [159, 160], which will be presented in Section 3.4.

Consider then a set of integers $\{I_i\}$ and the correspondent set of rapidities $\{\theta_i\}$ determined by the Bethe Equations (2.21) at finite size. Adding a new integer I_ℓ we introduce a new rapidity θ_ℓ and rearrange the old ones $\theta_i \to \theta_i + \delta\theta_i$: the shift $\delta\theta_i$ is of order $\mathcal{O}(L^{-1})$. Focusing on the

Bethe equations for $i \neq \ell$ we can surely write

$$\frac{I_i}{L} = \frac{1}{2\pi} p(\theta_i + \delta\theta_i) - \frac{1}{2\pi L} \sum_{j\neq i, j\neq \ell} i \log\left(S(\theta_i - \theta_j + \delta\theta_i - \delta\theta_j)\right) - \frac{1}{2\pi L} \sum_{j\neq i, j\neq \ell} i \log\left(S(\theta_i - \theta_\ell + \delta\theta_i)\right). \tag{2.29}$$

Expanding the above retaining only $\mathcal{O}(L^{-1})$ corrections and using the Bethe Equations satisfied by the set $\{\theta_i\}$ we readily get

$$\delta\theta_i = \frac{1}{2\pi L \rho_t(\theta_i)} i \log\left(S(\theta_i - \theta_\ell)\right) + \frac{1}{2\pi L \rho_t(\theta_i)} \sum_{j\neq i, j\neq \ell} \varphi(\theta_i - \theta_j)\delta\theta_j + \mathcal{O}(L^{-2}). \tag{2.30}$$

We are then naturally led to the definition of the so called backflow function $F(\theta|\mu)$, which describes the shifts in the rapidities due to the insertion of new excitations

$$F(\theta|\mu) = \frac{1}{2\pi\rho_t(\theta)} i \log(S(\theta - \mu)) + \frac{1}{2\pi\rho_t(\theta)} \int \mathrm{d}\alpha\, \varphi(\theta - \alpha) F(\alpha|\mu)\rho(\alpha). \tag{2.31}$$

With the help of the backflow function, we can now analyze the change in the expectation value of a given charge $\mathcal{Q}$, defining $\Delta\langle\mathcal{Q}\rangle = \langle\{I_i\} \cup I_\ell|\mathcal{Q}|\{I_i\} \cup I_\ell\rangle - \langle\{I_i\}|\mathcal{Q}|\{I_i\}\rangle$. Let $q(\theta)$ be the single particle eigenvalue associated with the charge, then

$$\Delta\mathcal{Q} = q(\theta_\ell) + \sum_i q(\theta_i + \delta\theta_i) - \sum_i q(\theta_i) = q(\theta_\ell) + \int \mathrm{d}\mu\, \partial_\mu F(\theta_\ell|\mu)\rho(\mu)\partial_\mu q(\mu) + \mathcal{O}(L^{-1}), \tag{2.32}$$

which leads to the natural definition of dressed eigenvalues

$$q^{\mathrm{dr}}(\theta) = q(\theta) + \int \mathrm{d}\mu\, \partial_\mu F(\theta|\mu)\rho(\mu)\partial_\mu q(\mu). \tag{2.33}$$

Notice that, because of the linearity of Eq. (2.30) and (2.31), if rather than a single excitation we add a finite set $\{\theta_\ell\}_{\ell=1}^n$ of quasiparticles, then $\Delta\langle\mathcal{Q}\rangle = \sum_{\ell=1}^n q^{\mathrm{dr}}(\theta_\ell)$: a finite number of excitations over a fixed background behaves as if they were free particles, provided the single particle eigenvalues are suitably dressed (and thus become state-dependent). We close this paragraph mentioning that the derivative of a dressed quantity (i.e. $\partial_\theta q^{\mathrm{dr}}(\theta)$) satisfies a simple linear integral equation. Indeed, manipulating the definition of dressing (2.33) and the equation satisfied by the backflow function (2.31) we easily get

$$\partial_\theta q^{\mathrm{dr}}(\theta) = \partial_\theta q(\theta) + \int \frac{\mathrm{d}\mu}{2\pi} \varphi(\theta - \mu)\vartheta(\mu)\partial_\mu q^{\mathrm{dr}}(\mu), \tag{2.34}$$

where we recall the definition of the filling $\rho(\theta)/\rho_t(\theta) = \vartheta(\theta)$.

2.1.3 Correlation functions: form factors and the LeClair-Mussardo expansion

The ultimate goal in solving a quantum field theory is the computation of the correlation functions, which encode all the experimentally relevant information. The TBA alone gives access to the simplest quantities, i.e. the expectation value of the conserved charges (very recently, the expectation value of the associated current has been computed for generic systems [159, 160]).

For generic observables, additional work is needed. The form factor boostrap [61] proposes a set of axioms, similarly to the S-matrix bootstrap, which certain matrix elements of operators of interest must satisfy. More specifically, given a multi-particle state $|\theta_1, ..., \theta_n\rangle$ and a local observable $\mathcal{O}(0,0)$ placed at $x = t = 0$, the form factor $F_n^{\mathcal{O}}$ is the matrix element between the state and the vacuum

$$F_n^{\mathcal{O}}(\theta_1, ..., \theta_n) = \langle 0|\mathcal{O}(0,0)|\theta_1, ..., \theta_n\rangle. \tag{2.35}$$

More general matrix elements are obtained exploiting the crossing symmetry

$$\langle\theta_1,...,\theta_n|\mathcal{O}(0,0)|\beta_1,...,\beta_m\rangle = F^{\mathcal{O}}_{n+m}(\beta_1,...,\beta_m,\theta_1-i\pi,...,\theta_n-i\pi)\,. \tag{2.36}$$

The form factors must obey several constraints known as Watson equations [215]

$$F^{\mathcal{O}}_n(\theta_1,...,\theta_i,\theta_{i+1},...,\theta_n) = S(\theta_i-\theta_{i+1})F^{\mathcal{O}}_n(\theta_1,...,\theta_{i+1},\theta_i,...,\theta_n)\,, \tag{2.37}$$

$$F^{\mathcal{O}}_n(\theta_1+2\pi i,\theta_2,...,\theta_n) = \prod_{i=2}^{n} S(\theta_i-\theta_1)F^{\mathcal{O}}_n(\theta_1,\theta_2,...,\theta_n)\,, \tag{2.38}$$

which guarantee the consistency of the form factors under interchanges of particles. The analytical structure of the form factors can be further understood by means of physical considerations; indeed a singularity is expected whenever two rapidities differ of $i\pi$. This singularity is associated with the annihilation process of a particle and an antiparticle, as it can be seen from (2.36). In particular, such a singularity is a pole whose residue is associated with the form factors with the annihilated particles removed [61], namely

$$-i\mathrm{Res}_{\tilde\theta=\theta}F^{\mathcal{O}}_{n+2}(\tilde\theta+i\pi,\theta,\theta_1,...,\theta_n) = \left(1-\prod_{i=1}^{n}S(\theta-\theta_i)\right)F^{\mathcal{O}}_n(\theta_1,...,\theta_n)\,. \tag{2.39}$$

Similarly to the scattering matrix, further poles are associated with the bound states, providing additional constraints.

Once the bootstrap equations are solved and the form factors computed (which is an hard task), proper expansions of the correlation functions can be done. For example, the two point correlation $\langle 0|\mathcal{O}(x,t)\mathcal{O}(0,0)|0\rangle$ on the vacuum state is readily obtained inserting in the middle a decomposition of the identity in terms of the asymptotic states

$$\langle 0|\mathcal{O}(x,t)\mathcal{O}(0,0)|0\rangle = \sum_{N=0}^{\infty}\frac{1}{N!}\int\frac{\mathrm{d}^N\theta}{(2\pi)^N}\langle 0|\mathcal{O}(x,t)|\theta_1,...,\theta_n\rangle\langle\theta_1,...,\theta_n|\mathcal{O}(0,0)|0\rangle = \sum_{N=0}^{\infty}\frac{1}{N!}\int\frac{\mathrm{d}^N\theta}{(2\pi)^N}e^{it\sum_{i=1}^N E(\theta_i)+ix\sum_{i=1}^N p(\theta_i)}|F^{\mathcal{O}}_N(\theta_1,...,\theta_N)|^2\,. \tag{2.40}$$

When correlation functions on excited states are concerned, the approach is not so straightforward. For example, if we try to naively compute thermal one-point functions we find inconsistencies

$$\frac{1}{\mathcal{Z}}\mathrm{Tr}[\mathcal{O}(0,0)e^{-\beta H}] \stackrel{?}{=} \frac{1}{\mathcal{Z}}\sum_{N=0}^{\infty}\int\frac{\mathrm{d}^N\theta}{(2\pi)^N}e^{-\beta\sum_{i=1}^N E(\theta_i)}F^{\mathcal{O}}_{2N}(\theta_1,...,\theta_N,\theta_1-i\pi,...,\theta_N-i\pi)\,. \tag{2.41}$$

Due to the kinematical poles of the form factors (2.39), the above expansion is a sum of infinities and it must be properly regularized: the solution is the so-called LeClair–Mussardo series [87]

$$\frac{1}{\mathcal{Z}}\mathrm{Tr}[\mathcal{O}(0,0)e^{-\beta H}] = \sum_{N=0}^{\infty}\frac{1}{N!}\int\frac{\mathrm{d}^N\theta}{(2\pi)^N}\left(\prod_{j=1}^{N}\vartheta(\theta_j)\right)\langle\theta_N,...,\theta_1|\mathcal{O}|\theta_1,...,\theta_N\rangle_{\mathrm{c}}\,. \tag{2.42}$$

Here, the connected matrix element is defined by a careful removal of the kinematical singularities (2.39)

$$\langle\theta_k,...,\theta_1|\mathcal{O}(0,0)|\theta_1,...,\theta_k\rangle_{\mathrm{c}} = \text{finite part}\left(\lim_{\epsilon_i\to 0}F^{\mathcal{O}}_{2n}(\theta_1,...,\theta_k,\theta_k-i\pi+i\epsilon_k,...,\theta_1-i\pi+i\epsilon_1)\right)\,, \tag{2.43}$$

where the limit $\epsilon_i \to 0$ must be taken independently for each i. The filling function $\vartheta(\theta)$ is defined in terms of the root density computed from the TBA as

$$\vartheta(\theta) = \frac{\rho(\theta)}{\rho_t(\theta)} . \tag{2.44}$$

Obviously, considering GGEs rather than pure thermal states is a straightforward generalization [216]. This expansion was firstly conjectured in [87], verified on the set of the local charges in [217] and finally rigorously proven for generic states in [218]. Very recently, a generalization to two-point functions has been proposed in Ref. [219]. The LeClair-Mussardo series involves in general multiple coupled integrals that make impossible a straightforward resummation, even though in many cases its truncation to the first few terms provides quite accurate results.

2.2 The Sinh-Gordon and the Lieb Liniger models: their non relativistic connection

In this section, we introduce the Sinh-Gordon field theory and quickly sketch the solution of the Lieb Liniger model, finally we review their connection, mainly following [85, 86].

2.2.1 The Sinh-Gordon model

The Sinh-Gordon model is a quantum field theory of a real field ϕ, whose action reads

$$\mathcal{S}_{\text{ShG}} = \int \mathrm{d}x\mathrm{d}t \, \frac{1}{2c^2}(\partial_t\phi)^2 - \frac{1}{2}(\partial_x\phi)^2 - \frac{mc^4}{16\kappa}(\cosh(c^{-1}4\sqrt{\kappa}\phi) - 1) . \tag{2.45}$$

Note the unconventional choice of the notation, which has been chosen for later convenience: as a matter of fact, the desired non relativistic limit is recovered sending $c \to \infty$ and at the same time taking a small coupling limit of the interaction. The integrability of the model is well known, both at the classical [220] and at the quantum [71] level. The scattering matrix of the ShG model was firstly computed in [62] and its analysis confirmed the presence of a single excitation species (see Ref. [61] or Ref. [70] for a complete discussion). Explicitly, it reads

$$S_{\text{ShG}}(\theta) = \frac{\sinh\theta - i\,\sin(\pi\alpha)}{\sinh\theta + i\,\sin(\pi\alpha)} , \tag{2.46}$$

where the parameter α is

$$\alpha = \frac{c^{-1}16\kappa}{8\pi + c^{-1}16\kappa} . \tag{2.47}$$

From the knowledge of the scattering matrix, the thermodynamics of the model is completely fixed by the TBA, as outlined in Section 2.1.2.

Moreover, the form-factor bootstrap program of this model has been completely solved by Koubek and Mussardo [221], who obtained a closed expression for form factors of the vertex operators $e^{kc^{-1}4\sqrt{\kappa}\phi}$ for any k on arbitrary states, which reads

$$F_n^k = \langle 0|e^{kc^{-1}4\sqrt{\kappa}\phi}|\theta_1,...,\theta_n\rangle = \frac{\sin(kc\pi\alpha)}{\pi\alpha}\left(\frac{4\sin(\pi\alpha)}{N}\right)^{n/2} \det M_n(k) \prod_{i<j}^{n} \frac{F_{\min}(\theta_i-\theta_j)}{e^{\theta_i}+e^{\theta_j}} . \tag{2.48}$$

Here we introduced

$$N = \frac{1}{\cos(\pi\alpha/2)} \exp\left[-\frac{1}{\pi}\int_0^{\pi\alpha} \mathrm{d}t \frac{t}{\sin(t)}\right] , \tag{2.49}$$

$$F_{\min}(\theta) = N \exp\left[4\int_0^\infty \frac{\mathrm{d}t}{t}\frac{\sinh(t\alpha/2)\sinh(t(1-\alpha)/2)}{\sinh(t)\cosh(t/2)}\sin^2\left(\frac{t(i\pi-\theta)}{2\pi}\right)\right]. \tag{2.50}$$

Finally, the matrix $M_n(k)$ is defined as

$$[M_n(k)]_{ij} = \sigma^{(n)}_{2i-j}\frac{\sin\left[\left((i-j)c^{-1}+k\right)c\pi\alpha\right]}{\pi\alpha}, \tag{2.51}$$

where the indexes i, j run from 1 to $n-1$ and $\sigma_i^{(n)}$ are the symmetric polynomials defined as

$$\prod_{i=1}^{n}(x+e^{\theta_i}) = \sum_{k=1}^{n} x^{n-k}\sigma_k^{(n)}. \tag{2.52}$$

As a simple, but crucial, byproduct the form factors of the powers of the field ϕ^n can also be obtained, by means of a simple Taylor expansion in k of the vertex operators. Thanks to the solution of the form factor bootstrap, the LeClair-Mussardo expansion (2.42) can be used to study the one point functions: indeed, this was the route originally used to access the Lieb-Liniger one-point functions through the non relativistic limit of the Sinh Gordon model [85, 86, 88].

The LeClair-Mussardo expansion is completely general for any relativistic integrable field theory, provided the needed form factors are known. However, in the case of the Sinh Gordon model a remarkable expression, equivalent to a resummation of the LeClair-Mussardo series, has been recently proposed by Negro and Smirnov [90, 91] for a particular class of vertex operators. The formula was later simplified in Ref. [222], where it was cast into the extremely simple form

$$\frac{\langle e^{(k+1)c^{-1}4\sqrt{\kappa}\phi}\rangle}{\langle e^{kc^{-1}4\sqrt{\kappa}\phi}\rangle} = 1 + \frac{2\sin(\pi\alpha(2k+1))}{\pi}\int_{-\infty}^{\infty}\mathrm{d}\theta\,\vartheta(\theta)e^{\theta}p_k(\theta), \tag{2.53}$$

where k is a positive integer with $p_k(\theta)$ being the solution of the following integral equation

$$p_k(\theta) = e^{-\theta} + \int_{-\infty}^{\infty}\mathrm{d}\theta'\vartheta(\theta')\chi_k(\theta-\theta')p_k(\theta'), \qquad \chi_k(\theta) = \frac{i}{2\pi}\left(\frac{e^{-i2k\alpha\pi}}{\sinh(\theta+i\pi\alpha)} - \frac{e^{i2k\alpha\pi}}{\sinh(\theta-i\pi\alpha)}\right). \tag{2.54}$$

Eq. (2.53) gives us access to ratios of vertex operators, whose value can be iteratively computed. In fact, $e^{kc^{-1}4\sqrt{\kappa}\phi}$ for $k=0$ reduces to the identity operator, whose expectation value is trivially 1: expectation values $\langle e^{kc^{-1}4\sqrt{\kappa}\phi}\rangle$ are then recovered for integers k by mean of a repetitive use of Eq. (2.53). As pointed out in Ref. [90, 91, 222], arbitrary vertex operators are in principle obtainable thanks to a special symmetry of the Sinh-Gordon model.

Indeed, by mean of an accurate analysis of the LeClair-Mussardo series and using the exact form factors, it is possible to show that $e^{kc^{-1}4\sqrt{\kappa}\phi}$ is periodic in k with period α^{-1}. Thus, if α is irrational (this is not a limitation, since any number is arbitrary well approximated by an irrational one) the sequence $\{k \mod \alpha^{-1}\}_{k=1}^{\infty}$ is dense in $[0,\alpha^{-1})$ and the expectation values of all the vertex operators are in principle recovered.

2.2.2 The Lieb-Liniger model

From the experimental point of view, one of the most relevant systems is the Lieb-Liniger (LL) model [50, 51]. It describes a one-dimensional gas of point-wise interacting bosons, which can be realized in cold-atom experiments [27–32, 49]. We consider a one-dimensional gas of point-wise interacting bosons on a system of length L, described by the Hamiltonian (1.1), here reported for

convenience

$$H = \int_0^L \mathrm{d}x \frac{1}{2m} \partial_x \psi^\dagger(x) \partial_x \psi(x) + \kappa \psi^\dagger(x) \psi^\dagger(x) \psi(x) \psi(x) \,, \tag{2.55}$$

where periodic boundary conditions are assumed. Here $\psi^\dagger(x)$,$\psi(x)$ are bosonic creation and annihilation operators satisfying $\left[\psi(x), \psi^\dagger(y)\right] = \delta(x-y)$, while $\kappa > 0$ is the strength of the repulsive interaction.

The Hamiltonian (2.55) can be diagonalized by means of the Bethe ansatz [50, 51, 53]. In analogy with the free case, to each eigenstate is associated a set of real parameters $\{\lambda_j\}_{j=1}^N$, called rapidities (to be not confused with the relativistic rapidities of the previous sections), which parametrize the corresponding wave function. The latter can be written down explicitly as

$$\psi_N(x_1, \ldots, x_N) \quad = \quad \sum_P A(P) \prod_{j=1}^N e^{i\lambda_{P_j} x_j} \,, \qquad x_1 \leq x_2 \leq \ldots \leq x_N \,, \tag{2.56}$$

where the sum is over all the permutations of the $\{\lambda_j\}_{j=1}^N$ and the symmetric extension is assumed for a different ordering of the coordinates $\{x_j\}_{j=1}^N$. The coefficients $A(P)$ are not independent: changing permutation we are rearranging the order of the rapidities in the wavefunction (2.56). Thus, in strict analogy to the asymptotic state notation used in the relativistic case, the coefficients $A(P)$ for different P are connected through scattering matrixes. Denoting with $\Pi_{j,j+1}$ the permutation exchanging the rapidities at positions j and $j+1$, we have

$$A(P) = S_{\mathrm{LL}}(\lambda_{P_j} - \lambda_{P_{j+1}}) A(\Pi_{j,j+1} P) \,, \tag{2.57}$$

where $S_{\mathrm{LL}}(\lambda)$ is the Lieb Liniger scattering matrix

$$S_{\mathrm{LL}}(\lambda) = \frac{\lambda - 2im\kappa}{\lambda + 2im\kappa} \,. \tag{2.58}$$

The role of $S_{\mathrm{LL}}(\lambda)$ as a scattering matrix is further elucidated imposing periodic boundary conditions on the wavefunction (2.56). In this case, Bethe Gaudin equations formally identical to the relativistic case are obtained

$$e^{i\lambda_j L} \prod_{k \neq j}^N S_{\mathrm{LL}}\left(\lambda_j - \lambda_k\right) = 1 \,. \tag{2.59}$$

Given a solution to the system (2.59), the momentum and energy of the corresponding eigenstate are immediately obtained as

$$P(\{\lambda_j\}) = \sum_{j=1}^N p(\lambda_j) \,, \qquad \mathcal{E}(\{\lambda_j\}) = \sum_{j=1}^N E(\lambda_j) \,, \tag{2.60}$$

where $p(\lambda) = \lambda$ and $E(\lambda) = \lambda^2/(2m)$ are the single-particle momentum and energy respectively. In addition to energy and momentum, it is possible to show that the Lieb-Liniger Hamiltonian displays an infinite set of local conserved operators $\{Q_i\}$ [223], as it should be because of its integrability.

2.2.3 The non-relativistic limit

We now finally review the non-relativistic limit of the Sinh-Gordon model [85, 86]. The correspondence between the Sinh Gordon and the Lieb-Liniger models can be established by looking at the corresponding scattering matrices. Comparing the relativistic momentum $p(\theta) =$

$Mc\sinh\theta$ of the sinh-Gordon with the galilean momentum of the Lieb Liniger model $p(\lambda)=\lambda$, for $c\to\infty$ it is natural to set $\theta\sim\lambda/mc$ (where we recall $\lim_{\rm NR} M=m$ [224]). Using this correspondence, it is immediate to realize (we attach labels "ShG" and "LL" to distinguish quantities, respectively, in the Sinh Gordon and Lieb Liniger models if confusion can arise)

$$\lim_{c\to\infty} S_{\rm ShG}(c^{-1}m^{-1}\lambda)=S_{\rm LL}(\lambda). \tag{2.61}$$

The limit is immediately extended to the whole thermodynamics through the Bethe equations. In particular, the relation between the Sinh Gordon root density $\rho^{\rm ShG}$ and the Lieb-Liniger one $\rho^{\rm LL}$ can be easily understood looking at the total excitation density. In particular, requiring

$$D=\int_{-\infty}^{\infty}{\rm d}\theta\,\rho^{\rm ShG}(\theta)=\int_{-\infty}^{\infty}{\rm d}\lambda\,c^{-1}m^{-1}\rho^{\rm ShG}(c^{-1}m^{-1}\lambda)\,, \tag{2.62}$$

one is led to the natural identification

$$\rho^{\rm LL}(\lambda)=c^{-1}m^{-1}\rho^{\rm ShG}(c^{-1}m^{-1}\lambda)\,. \tag{2.63}$$

This scaling guarantees that the Bethe equations for the ShG model become those of the LL gas, provided the total root distribution is rescaled in the same way, namely

$$\rho_t^{\rm LL}(\lambda)=c^{-1}m^{-1}\rho_t^{\rm ShG}(c^{-1}m^{-1}\lambda)\,. \tag{2.64}$$

In particular, this implies the filling function of the ShG field theory reduces, at the leading order, to the filling function in the LL model $\vartheta^{\rm ShG}(c^{-1}m^{-1}\lambda)=\vartheta^{\rm LL}(\lambda)$.

The non-relativistic limit is more involved at the level of correlation functions. Consider now the action of the ShG model obtained from the action (2.45). In the non relativistic limit, we can consider the power expansion of the interaction and neglect all terms beyond ϕ^4 that will finally disappear taking $c\to\infty$

$$\mathcal{S}_{\rm ShG}=\int{\rm d}x{\rm d}t\,\frac{1}{2c^2}:(\partial_t\phi)^2:-\frac{1}{2}:(\partial_x\phi)^2:-\frac{m^2c^2}{2}:\phi^2:-\frac{16}{4!}m^2\kappa:\phi^4:+\mathcal{O}(c^{-2}) \tag{2.65}$$

where :: means that the expression must be normal ordered with respect to the free modes of the field. The power expansion of the action generates a $c-$divergent mass term and a finite quartic interaction, plus further interactions negligible in the NR limit. In order to extract from ϕ the proper NR fields we split it in two parts associated with positive and negative frequencies

$$\phi(t,x)=\frac{1}{\sqrt{2m}}\left(e^{imc^2t}\psi^\dagger(t,x)+e^{-imc^2t}\psi(t,x)\right)\ . \tag{2.66}$$

The exponential factors take care of the fast oscillating behavior induced by the m^2c^2 term of the Lagrangian (2.65), while in the NR limit the smooth dynamics of the theory is encoded into the ψ fields. From the Lagrangian we get the field Π conjugated to ϕ

$$\Pi(t,x)\ =\ \frac{1}{c^2}\partial_t\phi(t,x)\ =\ i\sqrt{\frac{m}{2}}\left(e^{imc^2t}\psi^\dagger(t,x)-e^{-imc^2t}\psi(t,x)\right)+\mathcal{O}(c^{-2}) \tag{2.67}$$

where we used that ψ and all its derivatives are supposed to be non singular in the NR limit. Imposing the canonical equal time commutation rules $[\phi(t,x),\Pi(t,y)]=i\delta(x-y)$, it is easy to show that in the NR limit the ψ fields behave as canonical non relativistic bosonic fields:

$$[\psi(t,x),\psi(t,y)]=0,\qquad [\psi(t,x),\psi^\dagger(t,y)]\ =\ \delta(x-y)\ . \tag{2.68}$$

Note that with this definition of the relativistic fields, the normal ordering of the action with respect to the free modes of ϕ is completely equivalent to the normal ordering with respect the $\psi^\dagger$ fields, that must appear always on the left of the ψ fields. Substituting now (2.66) in (2.65) we obtain a cancellation of the mass term

$$\begin{aligned}\mathcal{S}_{\text{ShG}} = \int \mathrm{d}x\mathrm{d}t\, \frac{i}{2} : \left(e^{imc^2t}\partial_t\psi^\dagger + e^{-imc^2t}\partial_t\psi\right)\left(e^{imc^2t}\psi^\dagger - e^{-imc^2t}\psi\right) : + \\ -\frac{1}{4m} : \left(e^{imc^2t}\partial_x\psi^\dagger + e^{-imc^2t}\partial_x\psi\right)^2 : -\frac{1}{3!}\kappa : \left(e^{imc^2t}\psi^\dagger + e^{-imc^2t}\psi\right)^4 : + \mathcal{O}(c^{-2})\,. \quad (2.69)\end{aligned}$$

However the limiting procedure has not been completed yet: indeed we have to expand the above expression and retain only the terms in which the oscillating phases are absent. Expanding the expression in (2.69), we find a sum of terms as

$$\int \mathrm{d}x\mathrm{d}t\; e^{imc^2nt}\mathcal{O}(t,x)\;\;, \quad (2.70)$$

where $\mathcal{O}(t,x)$ are fields made of products of ψ and $\psi^\dagger$ operators (therefore smooth for $c\to\infty$) and n an integer. It is not correct to naively state that $e^{imc^2nt}\mathcal{O}(t,x) \xrightarrow{c\to\infty} 0$ for $n\neq 0$, but this is true once we consider time integrations over an infinitesimal (but not zero) time interval Δt

$$\int_{t_0}^{t_0+\Delta t}\mathrm{d}t\; e^{imnc^2t}\mathcal{O}(t,x) \simeq \mathcal{O}(t_0,x)\int_{t_0}^{t_0+\Delta t}\mathrm{d}t\; e^{imnc^2t} = \mathcal{O}(t_0,x)e^{imnc^2t_0}\frac{e^{imc^2n\Delta t}-1}{imc^2} \sim c^{-2}\,. \quad (2.71)$$

Above, $n\neq 0$ and Δt is kept fixed in the $c\to\infty$ limit, but it is considered to be small enough to approximate $\mathcal{O}(t,x)\simeq\mathcal{O}(t_0,x)$ in the whole integration domain. Thus, the correspondence between the relativistic fields and the non relativistic ones is readily written as

$$\lim_{\text{NR}} : \phi^{2K+1} := 0, \qquad \lim_{\text{NR}} : \phi^{2K} := \binom{2K}{K}\frac{1}{(2m)^K}(\psi^\dagger)^K(\psi)^K\,. \quad (2.72)$$

Precisely, the corresponcence holds in a weak sense inside correlation functions. The NR limit of (2.69) can be extracted neglecting all the fast oscillating phases and the resulting action

$$\lim_{\text{NR}}\mathcal{S}_{\text{ShG}} = \int \mathrm{d}x\mathrm{d}t\,\frac{i}{2}\left(\partial_t\psi^\dagger\psi - \psi^\dagger\partial_t\psi\right) - \frac{1}{2m}\partial_x\psi^\dagger\partial_x\psi - \kappa\psi^\dagger\psi^\dagger\psi\psi\;\;. \quad (2.73)$$

The final expression of the action we got in the non-relativistic limit can be readily recognized as the one that can be derived from the Hamiltonian of the Lieb-Liniger model. This value of the coupling constant we got from the limit of the action is consistent with that of the scattering matrix.

2.3 The zoo of relativistic integrable models and the non relativistic bottleneck

The stage of relativistic integrable models displays an impressive number of different characters, thus it is very tempting to explore galilean invariant integrable systems through non relativistic limits. For example, just mentioning the models we will study in this section, the list is rather long: besides the already mentioned Sinh-Gordon model [62, 221, 225], we will explore the Bullough-Dodd model [62, 226–228] or, more generally, the Toda Field Theories [62–64, 66–77], but also the vectorial $O(N)$ non-linear sigma model [78]. The list grows even longer allowing for fermionic excitation, such as in the supersymmetric Sinh-Gordon model (SShG) [229, 230], the $O(N)$ Gross-Neveu model (GN) [78, 231, 232] and the supersymmetric non-linear sigma model

(SNLS) [79–82, 233, 234]. Compared to this extraordinary richness of relativistic examples, the paucity of non-relativistic integrable models (NRIM) with interactions strictly local and galilean invariant is rather dazzling, their list being essentially given by the Lieb-Liniger model. The fact that the Lieb-Liniger model is, under certain general conditions discussed below, probably the only non-trivial example of NRIM may not be accidental and the aim of this section is indeed to argue about the universal ubiquity of this model. Let's also add that the only other known NRIM are, to the best of our knowledge, variations of the same theme, i.e. systems made of coupled Lieb Liniger models relative to different species of particles [235, 236].

This section is dedicated to pinpoint NRIM making use of the richness of the relativistic ones, describing the work presented in Ref. [1, 2]. Namely, we have explored the possibility of identifying NRIM in terms of the non-relativistic limit of known integrable QFT (IQFT). Let us comment more precisely the terms of the problem: given the relativistic invariance and the locality of the starting QFT, the Hamiltonian of the non relativistic model will belong to the general class

$$H = \int \mathrm{d}x \left(\sum_{k=1}^{r} \frac{1}{2m_k} \partial_x \psi_k^\dagger \partial_x \psi_k \right) + V\left(\{\psi_k^\dagger, \psi_l\} \right) , \tag{2.74}$$

where $V(\{\psi_k^\dagger, \psi_l\})$ is a *local* potential term, function of the complex fields $\psi_k^\dagger$ and ψ_l, but not of their derivatives (m_k is the mass of these fields). Depending on the relativistic model from which we start, we can end up with either galilean bosons or fermions (or a mixture of them).

These considerations help in clarifying that the non-relativistic integrable models we are looking for are those entirely defined by the local potential term $V(\{\psi_k^\dagger, \psi_l\})$.

We anticipate that in all the cases we analyzed, the non relativistic limit always projects on Hamiltonians of the type (2.74) with only two body interactions, namely multispecies generalizations (integrable by construction) of the single species Lieb Liniger model (1.1), already known in literature by other means. A posteriori, this fact can be explained as it follows. Assuming that the potential V can be expanded in series and, requiring particle-number conservation, we have (sum on the repeated indices)

$$V(\{\psi_k^\dagger, \psi_l\}) = \mu_{a,b} \psi_a^\dagger \psi_b + \frac{1}{2!} \mu_{a,b,c,d} \psi_a^\dagger \psi_b^\dagger \psi_c \psi_d + \frac{1}{3!} \mu_{a,b,c,d,e,f} \psi_a^\dagger \psi_b^\dagger \psi_c^\dagger \psi_d \psi_e \psi_f \cdots \tag{2.75}$$

The first quadratic term must necessarily be diagonal on the species $\mu_{a,b} \propto \delta_{a,b}$, otherwise a single particle of a given species would not be stable. Once we set $\sum_{a,b} \mu_{a,b} \psi_a^\dagger \psi_b = \sum_a \mu_a \psi_a^\dagger \psi_a$, the latter is a chemical potential term that does not affect the dynamics and can be thus removed. So, it remains to discuss the presence of quartic and higher order interactions. Notice that, in non-relativistic models, particle production is forbidden even for virtual processes, therefore an n-body local interaction terms (where $n > 2$) in the non relativistic Hamiltonian would represent a genuine higher-body interaction, involving n-particles simultaneously present at the same position. It is hard to imagine how these processes can be compatible at least with Yang-Baxter integrability, since they would spoil the possibility of factorising an n-body scattering process into a sequence of 2-body interactions. This seems to suggest that the interaction in NRIM is restricted to the quartic order only, the freedom being restricted on how different species are coupled together.

In view of the large number of models analyzed, we omit a detailed discussion of each of them. Therefore, we discuss in detail the non relativistic limit of bosonic models, namely the Bullogh Dodd, the Toda theories (the first giving a single species Lieb Liniger model, the second multispecies, but decoupled, Lieb Liniger models) and the $O(N)$ symmetric model. As we are going to see, new techniques compared with those of the previous section are needed in order to correctly study the non relativistic limit, which rather than from a direct analysis of the action must be extracted from the Heisenberg equation of motion (Bullogh-Dodd and Toda) or from the

Feynman diagrams coming from the large$-N$ expansion of the $O(N)$ model. After these models will have been studied in details, we present the non relativistic limit of theories with fermionic interactions: since the techniques are closely related to those of the bosonic models, we avoid to present a detailed derivation (but the reader can refer to Ref. [2]). For the sake of completeness, we mention two further non relativistic limits which have been studied in literature, but are not presented in this thesis, namely the Sine Gordon model which goes to the attractive Lieb Liniger model [237] and the Thirring model, which is fermion based and dual to the Sine Gordon and goes to a fermionic galilean system dual to the attractive Lieb Liniger [238].

2.3.1 The Bullough-Dodd model and its non relativistic limit

The simplest integrable relativistic field theory after the Sinh-Gordon model is the Bullogh-Dodd (BD) model [62, 226–228]. This integrable model is described by a relativistic Lagrangian with only one real field

$$\mathcal{L}_{\text{BD}} = \frac{1}{2}\partial_\mu\phi\partial^\mu\phi - \frac{m^2c^4}{6g^2}\left(:e^{2gc^{-1}\phi}: + :2e^{-gc^{-1}\phi}: -3\right) \quad . \tag{2.76}$$

Similarly to the sinh-Gordon case, a non trivial limit is attained taking the weak coupling limit of the interaction: the c^{-1} factor in the exponential has been inserted for this purpose. The Bullogh-Dodd, together with the Sinh Gordon and the Sine Gordon models, is the only integrable QFT whose action is written in terms of a single bosonic field [71]. This integrable field theory is described by only one stable particle whose scattering matrix is [62]

$$S_{\text{BD}} = f_{\frac{2}{3}}(\theta) f_{-\frac{\alpha}{3}}(\theta) f_{\frac{\alpha-2}{3}}(\theta) \ , \tag{2.77}$$

where

$$\alpha = \frac{c^{-1}g^2}{2\pi}\frac{1}{1+\frac{c^{-1}g^2}{4\pi}} , \qquad f_x(\theta) = \frac{\sinh\theta + i\sin\pi x}{\sinh\theta - i\sin\pi x} \tag{2.78}$$

Looking at the $c \to \infty$ of the scattering matrix obtained thorough the correspondence $\theta \simeq \lambda/(mc)$, there is no doubt we will eventually reach again the Lieb Liniger model

$$\lim_{\text{NR}} S_{\text{BD}} = \frac{\lambda - i\frac{g^2}{6}m}{\lambda + i\frac{g^2}{6}m} \tag{2.79}$$

that matches the Lieb Liniger scattering matrix provided we choose $\kappa = g^2/12$ in the Lieb Liniger Hamiltonian (1.1). This result strongly suggests the LL model is also the NR limit of the BD model, but in order to prove it, we must consider also the NR limit of the dynamics. Differently from the ShG case, the NR limit of the dynamics obtained from the action gives an incorrect result and the proper limit must be taken from the equations of motion, as we are going to show explicitly.

Incorrect NR limit got from the action

If we blindly follow the steps that brought us from the relativistic ShG action to the non relativistic LL action, we will see that this gives rise to an inconsistent result with the limit of the scattering matrix obtained above. Indeed, after we split the field once again in its modes as in

(2.66), following the previous strategy we expand the BD action and retain only the non vanishing terms in the $c \to \infty$ limit

$$\mathcal{S}_{\rm BD} \;=\; \int \mathrm{d}x\mathrm{d}t \;:\frac{1}{2c^2}(\partial_t\phi)^2: -\frac{1}{2}:(\partial_x\phi)^2: -\frac{m^2c^2}{2}:\phi^2: -cm^2\frac{g}{6}:\phi^3: -m^2\frac{g^2}{8}:\phi^4: +\mathcal{O}(c^{-1})\,. \tag{2.80}$$

A new cubic term is present in this expression, in contrast to the ShG case (2.65). Moreover this term is divergent when $c \to \infty$. On the other hand, though, if we plug the expansion (2.66) of the field in the above action, the cubic term seems to not contribute at all, since always gives oscillating terms

$$c\int_{t_0}^{t_0+\Delta t}\mathrm{d}t:\left(e^{imc^2t}\psi^\dagger + e^{-imc^2t}\psi\right)^3: \sim c^{-1}\,. \tag{2.81}$$

Therefore, it is tempting to neglect the cubic term in (2.80). Proceeding in this way, the NR limit of the BD action gives

$$\lim_{\rm NR}\mathcal{S}_{\rm BD} = \int \mathrm{d}x\mathrm{d}t\;\frac{i}{2}\left(\partial_t\psi^\dagger\psi - \psi^\dagger\partial_t\psi\right) - \frac{1}{2m}\partial_x\psi^\dagger\partial_x\psi - \frac{3}{16}g^2\psi^\dagger\psi^\dagger\psi\psi\;. \tag{2.82}$$

Even though we can recognize in the above a NR action associated with a LL model, the value of the coupling is not the correct one to match with the NR limit of the scattering matrix (2.79), where the coupling appearing in the LL model (1.1) turns out to be $\kappa = g^2/12$. This discrepancy is due to a subtle role of the cubic term of the action (2.80): its effect cannot be neglected and renormalizes the density-density interaction of the LL model, as we now explain.

Correct NR limit got from the equation of motion

In light of the discrepancy found between the NR limit of the scattering matrix and the action, we now proceed more carefully and consider the NR limit employing directly Heisenberg equation of motion we can get form the Bullogh Dodd Lagrangian. We will see that, in this picture, the role of the cubic term in (2.80) is correctly taken in account and the NR limit of the dynamics matches with that of the scattering matrix

$$\frac{1}{c^2}\partial_t^2\phi \;=\; \partial_x^2\phi - \frac{m^2c^3}{3g}:\left(e^{2gc^{-1}\phi} - e^{-gc^{-1}\phi}\right):\,. \tag{2.83}$$

We now power expand the equation of motion keeping only those terms that do not vanish in the $c \to \infty$ limit

$$\frac{1}{c^2}\partial_t^2\phi = \partial_x^2\phi - m^2c^2\phi - cm^2\frac{g}{2}:\phi^2: -m^2\frac{g^2}{2}:\phi^3:\,. \tag{2.84}$$

Inserting the mode decomposition (2.66), we recast the above in an integral equation where we integrate in a small time window Δt

$$\begin{aligned} i\psi^\dagger(t_0+\Delta t) = i\psi^\dagger(t_0) + \epsilon\int_{t_0}^{t_0+\Delta t}\mathrm{d}t\;\Big[&e^{-i2mc^2(t-t_0)}i\partial_t\psi + \frac{1}{2m}\partial_x^2\left(\psi^\dagger + e^{-i2mc^2(t-t_0)}\psi\right) + \\ &-\frac{cg\sqrt{m}e^{-imc^2(t-t_0)}}{4\sqrt{2}}:\left(e^{imc^2(t-t_0)}\psi^\dagger + e^{-imc^2(t-t_0)}\psi\right)^2: + \\ &-\frac{g^2e^{-imc^2(t-t_0)}}{8}:\left(e^{imc^2(t-t_0)}\psi^\dagger + e^{-imc^2(t-t_0)}\psi\right)^3:\Big] \end{aligned} \tag{2.85}$$

The parameter ϵ has been introduced to efficiently keep track of the recursive solution of the above integral equation, that we now study, and at the end of the computations will be set $\epsilon = 1$.

In particular, the following general structure will emerge

$$i\psi^\dagger(t_0+\Delta) = i\psi^\dagger(t_0) + \sum_{n>j} \epsilon^n \Delta t^{n-j} \sum_{a=0}^{n} c^{a-2j} \mathcal{O}_{n,j,a}(t_0)\,. \tag{2.86}$$

The operators $\mathcal{O}_{n,j,a}(t_0)$ are normal ordered functions of $\psi(t_0)$ and $\psi^\dagger(t_0)$ which can contain fast oscillating phases, but the power law behavior in c has been made explicit in (2.86). The index a counts how many times the $c-$divergent cubic term is used in the iterative solution up to order n. As the scattering matrix admits a well-defined NR limit, we expect that also this expression will be well-behaved. Based on the power counting, one must have then that $\mathcal{O}_{n,j,a} = 0$ whenever $a - 2j > 0$ (such a claim can be checked). After having ideally solved recursively the equation of motion, we can take $c \to \infty$ (at fixed Δt) and obtain

$$i\psi^\dagger(t_0+\Delta t) = i\psi^\dagger(t_0) + \sum_{n\geq 2j; n\geq 1} \epsilon^n \Delta t^{n-j} \mathcal{O}_{n,j,2j}(t_0)\,, \tag{2.87}$$

At this stage, after we took the NR limit, we take a derivative with respect to the Δt parameter and compute the resulting expression at $\Delta t = 0$

$$i\partial_t \psi^\dagger(t_0) \;= \epsilon \mathcal{O}_{1,0,0}(t_0) + \epsilon^2 \mathcal{O}_{2,1,2}(t_0) \;\; . \tag{2.88}$$

In this way, we obtain the desired equation of motion, since the expression must be valid for any t_0. Above, the term $\mathcal{O}_{1,0,0}$ is what we would have got from the naive limit of the Lagrangian, while $\mathcal{O}_{2,1,2}$ is a contribution due to the cubic term which appears at the second order in the iterative solution.

Indeed, a rather lengthy, but straightforward, computation of (2.85) up to the second iteration shows that there are no c-divergent terms (as it should be) and the presence of a new term linear in Δt at the second iterative solution, due to the cubic term in the action. We leave the technical computations to Appendix 2.A where we derive the final NR Hamiltonian from the equation of motion

$$H = \int \mathrm{d}x \; \frac{\partial_x \psi^\dagger \partial_x \psi}{2m} + \frac{g^2}{12} \psi^\dagger \psi^\dagger \psi \psi \;\; . \tag{2.89}$$

This Hamiltonian is indeed the one of the Lieb Liniger model (1.1) with the choice $\kappa = g^2/12$, consistently to what we got from the NR limit of the scattering matrix in the BD model.

Therefore, we can conclude that the NR limit of the BD theory is once again the LL model, as for the ShG case. We are now going to show that the same happens for all other Toda Field Theories which, in the NR limit, end up to be a set of decoupled LL models.

2.3.2 The Toda Field Theories

We now briefly recall some basic properties and formulas of the Toda Field Theories and subsequently take the non relativistic limit: an exhaustive review of these models is beyond our present program and we limit ourselves to the most relevant information.

The Toda Field Theories associated to a Lie algebra G of rank r are lagrangian models involving r bosonic fields which is convenient to collect altogether in a vector $\phi = (\phi_1, \ldots, \phi_r)$. The Lagrangian density of these models are given by $\left(\partial_0 = \frac{1}{c}\partial_t\,,\;\; \partial_1 = \partial_x\right)$

$$\mathcal{L} \;=\; \frac{1}{2}\,(\partial_\mu \phi)\cdot(\partial^\mu \phi) - \frac{c^4 m^2}{g^2} \sum_{i=1}^{r+1} q_i [\exp(c^{-1} g \alpha_i \cdot \phi) - 1] \;\; , \tag{2.90}$$

where m^2 and g are real parameters while $\{\alpha_i\}_{i=1}^r$ is the set of the simple roots of G. In the perspective of considering the NR limit, we make explicit the speed of light. At the classical level

the equations of motion of these theories admit a Lax pair formulation and therefore there is an infinite hierarchy of conserved charges responsible for the classical integrability of the models for all Lie algebras. In the following we mainly focus our attention on the simply-laced algebras A_n, D_n and E_n, i.e. those with simple roots of the same length, here taken to be $\sqrt{2}$. The Toda Field Theories based on the non-simply laced algebras can be defined, at least at the classical level, by the so-called *folding* procedure, which consists of an identification of the roots using the symmetry properties of the Dynkin diagrams. The quantum properties of the non-simply laced models requires however a separate discussion and, for this reason, we refer the reader to the Ref. [74–77] for all details on this particular issue. From now on, as said above, we focus only on the simply-laced models.

The set of the integer numbers $\{q_i\}$ presented in eq. (2.90) is different for each algebra and it is related to the definition of the *maximal root* of the algebra, given by

$$\alpha_{r+1} \;=\; -\sum_{i=1}^{r} q_i\,\alpha_i \;\;. \tag{2.91}$$

The extended set of roots, obtained by adding the maximal root, form the Dynkin diagram of the *affine Lie algebras*. For these systems, posing $q_{r+1} = 1$, we have

$$\sum_{i=1}^{r+1} q_i \alpha_i = 0, \qquad \sum_{i=1}^{r+1} q_i = h \;\;, \tag{2.92}$$

where, for the simply-laced algebras, h coincides with the Coxeter number of G. At the level of perturbation theory, the Taylor expansion of the Lagrangian provides a quadratic term plus an infinite number of interaction vertexes:

$$\mathcal{L} = \frac{1}{2}\sum_{a=1}^{r} \partial_\mu \phi^a \partial^\mu \phi^a - \sum_{j=2}^{\infty} \frac{mc^{4-j} g^{j-2}}{j!} \sum_{a_1,\ldots,a_j} C^{(j)}_{a_1,\ldots,a_j} \phi^{a_1} \ldots \phi^{a_j} \,. \tag{2.93}$$

It is easy to see that the massive nature of these field theories comes from the last exponential term in (2.90), the one with the maximal root. Indeed, expanding in series of g the Lagrangian density, it is for the presence of this term that we have a well-defined minimum of the Lagrangian, with the classical values of the masses of the various particles A_a obtained diagonalising the quadratic terms of the Lagrangian

$$M^2_{ab} \;= m^2 C^{(2)}_{ab} \;= m^2 \sum_{i=1}^{r+1} q_i \alpha^a_i \alpha^b_i \;\;. \tag{2.94}$$

In the basis of the eigenvectors, $C^{(2)}_{ab} \;= \mu^2_a \delta_{ab}$. It is simple to see that the mass spectrum is degenerate if the group of the automorphisms of the Dynkin diagram is non trivial.

For the simply-laced algebra, there is a remarkable result concerning the mass spectrum [64, 65]: collecting the mass values into a r-dimensional vector

$$\mathbf{m} \;=\; (m_1, m_2, \cdots m_r) \;\;,$$

it can be proven that this vector is the Perron-Frobenius eigenvectors of the $(r \times r)$ incidence matrix $\mathcal{I}$ of the algebra G, defined by

$$\mathcal{I} \;=\; 2\mathbf{1} - \mathcal{C} \;\;, \tag{2.95}$$

where $\mathcal{C}_{ij} = 2\alpha_i \cdot \alpha_j / \alpha_j^2$ is the Cartan matrix of the algebra G.

After the quadratic term - responsible for the mass spectrum of the theories – the next perturbative term of the Lagrangian theories (2.90) consists of the three-particle coupling constants (in the adimensional units)

$$C^{(3)}_{abc} = \sum_i q_i \alpha^a_i \alpha^b_i \alpha^c_i \ . \tag{2.96}$$

As discussed in [64–68], on the basis in which the mass term is diagonal $C^{(2)}_{ab} = \mu_a^2 \delta_{ab}$, these three-coupling constants $C^{(3)}_{abc}$ have an interesting geometrical interpretation, since it is possible to prove that they vanish if it is impossible to draw a triangle with sides made of μ_a, μ_b, and μ_c whose internal angles are rational fraction of π, a natural consequence of the fact that the masses are expressed by algebraic numbers. Moreover, when they are different from zero, the quantities $C^{(3)}_{abc}$ are proportional to the area $\mathcal{A}^{abc}$ of the aforementioned mass triangle and, for the simply-laced algebras, we have

$$\left| C^{(3)}_{abc} \right| = \frac{4}{\sqrt{h}} \mathcal{A}^{abc} \ . \tag{2.97}$$

Obviously the non-vanishing values of $C^{(3)}_{abc}$ indicate the possible scattering processes in which enter the particles and their bound states, see Fig. 2.2. The three-coupling constants are very important quantities because, for the renormalization properties of the simply-laced models, their exact S-matrix can be written down requiring tree-level consistency with the classical mass spectra and the non-zero $C^{(3)}_{abc}$ responsible for the one-particle exchanges.

All the perturbative divergences of Lagrangian theories as (2.90) come from the tadpole diagrams, that can be eliminated by defining the normal ordering. This appears, though, to introduce into the theories an infinite set of counterterms which do not necessarily preserve the form of the Lagrangian (2.90) which only depends on two parameters, m and g. However, for exponential terms, their normal ordering only induces a multiplicative change in them, and therefore for the Lagrangian (2.90) only a renormalization of the mass scale m^2 (below, Λ is an UV cutoff)

$$m^2 \ \to \ m^2 \left(\frac{\Lambda^2}{m^2} \right)^{\frac{g^2 c - 2}{4\pi}} \ . \tag{2.98}$$

Hence, for the Toda Field Theories the infinities are renormalised only in terms of the mass scale, while the coupling constant g is not affected. In $(1+1)$ dimensions there are however also the *finite* corrections induced by the loop diagrams. For the Toda Field Theories based on the simply-laced algebras, it is pretty remarkable that they do not alter the mass ratios [64–68] as well as the inherent integrable structure of the theory that emerges from the tree level diagrams. It is for this reason that one can write down the S-matrix of these simply-laced Toda Field Theories which have their physical poles fixed by the fusion angles given by the classical value of the masses and the non-zero three-coupling constants $C^{(3)}_{abc}$.

The exact two-body S-matrix of various simply-laced Toda Field Theories has been computed and compared with the lowest order perturbation theory in several papers [62, 64–73]. There is, however, a remarkable integral representation formula that encodes, at once, all S-matrix amplitudes relative to the scattering of the particles A_a and A_b of a generic simply-laced Toda Field Theory: the formula reads [72, 73]

$$S_{ab}(\theta) \ = \ \exp\left[\int_0^\infty \frac{\mathrm{d}t}{it} \left(8 \sinh\left(\frac{Bt}{2}\right) \sinh\left(\frac{\pi t}{h} - \frac{Bt}{2}\right) \left(2\cosh\frac{\pi t}{h} - \mathcal{I} \right)^{-1}_{ab} - 2\delta_{ab} \right) \sin(\theta t) \right] . \tag{2.99}$$

and employs the incidence matrix $\mathcal{I}$ of the algebra, see eq. (2.95), the Coxeter exponent h and the function B of the coupling constant g given by

$$B = \frac{1}{4h}\frac{c^{-1}g^2}{1+c^{-1}g^2/8\pi} \ , \tag{2.100}$$

where in this formula we have already conveniently inserted the speed of light c.

Non-relativistic limit of the Toda Field Theories

Rather than approaching the non relativistic limit of the Toda models from their S-matrix, we rather prefer looking firstly to the action. In particular, the NR limit of the dynamics can be worked out for all the Toda theories at once through a simple generalization of what has been done in Section 2.3.1 for the Bullogh Dodd model, i.e. passing through the equations of motion. Here we present only the main steps of the procedure. We consider the Heisenberg equation of motion for the fields ϕ^a, in the basis in which the mass term is diagonal

$$\frac{1}{c^2}\partial_t^2\phi^a = \partial_x^2\phi^a - m^2c^2\mu_a^2\phi^a - m^2\sum_{j=2}^{\infty}\frac{g^{(j-1)}c^{3-j}}{j!}C^{(j+1)}_{a,a_1,\dots,a_j} : \phi^{a_1}\dots\phi^{a_j} : \ . \tag{2.101}$$

The equations of motion are readily derived from the expansion of the Lagrangian (2.93), where we renormalized the mass parameter (2.98) through the normal ordering. Next, we split all the fields in modes

$$\phi^a(t,x) = \frac{1}{\sqrt{2m_a}}\left(e^{im_ac^2t}\psi_a^\dagger(t,x) + e^{-im_ac^2t}\psi_a(t,x)\right) \ , \tag{2.102}$$

where $m_a = m\mu_a$. By mean of canonical commutation rules for the fields ϕ^a and their conjugate momenta, we find that in the NR limit the fields ψ_a are independent NR bosonic species

$$[\psi_a(x),\psi_b(y)] = 0 \quad , \quad [\psi_a(x),\psi_b^\dagger(y)] = \delta_{a,b}\delta(x-y) \ . \tag{2.103}$$

Proceeding now as in Section 2.3.1, first we neglect all the terms that will be suppressed in the limit $c\to\infty$, arriving in this way to the simplified equation of motion

$$\frac{1}{c^2}\partial_t^2\phi^a = \partial_x^2\phi^a - m^2c^2\mu_a^2\phi^a - m^2\frac{cg}{2}C^{(3)}_{a,a_1,a_2} : \phi^{a_1}\phi^{a_2} : -m^2\frac{g^2}{3!}C^{(4)}_{a,a_1,\dots,a_j} : \phi^{a_1}\phi^{a_2}\phi^{a_3} : \ . \tag{2.104}$$

Notice the presence, as it was already the case for the BD model, of a c divergent term for the three-couplings. Inserting in eq. (2.104) the NR fields ψ_a and converting this equation in an integral equation analogue to eq. (2.85), we can essentially repeat the same analysis with the same conclusion, namely that the three-couplings $C^{(3)}$ contributes to the NR limit through a two steps process.

Of course, for the case of general Toda Field Theories, the presence of different masses implies extra technicalities: for example the absence of a c divergent term in the iterative solution of (2.104) is not completely obvious. Consider the first order iterative solution of (2.104): the possible troublesome term comes from the time integration related to $C^{(3)}$:

$$c\int_{t_0}^{t_0+\Delta t}\mathrm{d}t\ e^{i(-m_a\pm_1m_{a_1}\pm_2m_{a_2})c^2(t-t_0)}\ C^{(3)}_{a,a_1,a_2}\psi_{a_1}^{\pm_1}(t_0)\psi_{a_2}^{\pm_2}(t_0) \tag{2.105}$$

where we adopted the convention $\psi^+ = \psi^\dagger$ and $\psi^- = \psi$. Such a term is c divergent if and only if we have mass degeneracy $m_a = \pm_1 m_{a_1} \pm_2 m_{a_2}$, but this – we know – is impossible in the Toda theories. As we already mentioned, the three body coupling is proportional to the area of a triangle whose sides are the masses of the involved particles [64–68]. The mass degeneracy is

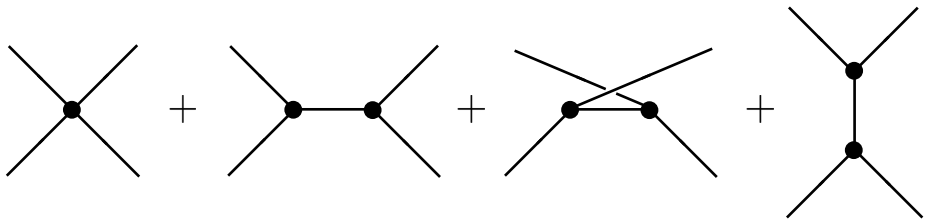

Figure 2.6: *Representation of the coupling $\mathcal{M}$ of Eq.* (2.107) *through Feynman graphs.*

incompatible with any of such triangles, therefore if by chance the kinematics condition $m_a = \pm_1 m_{a_1} \pm_2 m_{a_2}$ is satisfied, the relative coupling is zero and (2.105) is never divergent in the limit $c \to \infty$.

After long, but straightforward, calculations we can compute the second step in the iterative solution of the equations of motion and then extract the $\sim \Delta t$ term, exactly as in the BD model. The resulting NR equation of motion can be written as:

$$i\partial_t \psi_a^\dagger = \frac{1}{2m_a}\partial_x^2 \psi_a^\dagger - \frac{g^2}{24} \sum_{a_1,a_2,a_3,\pm_1,\pm_2,\pm_3} \frac{1}{\sqrt{\mu_a \mu_{a_1} \mu_{a_2} \mu_{a_3}}} \left[\mathcal{M}^{\pm_1,\pm_2\pm_3}_{a,a_1,a_2,a_3}\ \psi^{\pm_1}_{a_1}\psi^{\pm_2}_{a_2}\psi^{\pm_3}_{a_3}\right]_{\mu_a \pm_1 \mu_{a_1} \pm_2 \mu_{a_2} \pm_3 \mu_{a_3}=0} \tag{2.106}$$

Above $[...]_{...}$ means we are summing only those terms that satisfy the zero mass condition and the coupling $\mathcal{M}$ is a pure geometric quantity:

$$\mathcal{M}^{\pm_1,\pm_2,\pm_3}_{a,a_1,a_2,a_3} = C^{(4)}_{a,a_1,a_2,a_3} + \sum_b \left[\frac{C^{(3)}_{a,a_3,b} C^{(3)}_{b,a_1,a_2}}{(\mp_1 \mu_{a_1} \mp_2 \mu_{a_2})^2 - \mu_b^2} + \frac{C^{(3)}_{a,a_1,b} C^{(3)}_{b,a_2,a_3}}{(\mp_2 \mu_{a_2} \mp_3 \mu_{a_3})^2 - \mu_b^2} + \frac{C^{(3)}_{a,a_2,b} C^{(3)}_{b,a_3,a_1}}{(\mp_3 \mu_{a_3} \mp_1 \mu_{a_1})^2 - \mu_b^2} \right] \tag{2.107}$$

Equation (2.106) is still quite complicated, but it can be immediately simplified if $\mathcal{M}$ is recognised to be a scattering amplitude. Notice, indeed, that (2.107) coincides with the sum of the tree level scattering amplitudes of Fig. 2.6, these graphs computed at zero rapidity and in adimensional units, where the particle a is outgoing and the particles a_j are outgoing/ingoing depending on the sign $\pm_j$, as the zero mass condition in (2.107) suggests. This feature is already present in the Bullogh Dodd model, as discussed in Appendix 2.A. For the integrability of the Toda Field Theories, scattering events do not change the ingoing and outgoing particles and therefore most of the $\mathcal{M}$ amplitudes are indeed zero. Imposing separately the particle number conservation of each species, we arrive to the final NR equations of motion relative to a density-density interaction:

$$i\partial_t \psi_a^\dagger = \frac{1}{2m_a}\partial_x^2 \psi_a^\dagger - \frac{g^2}{8} \sum_{a,a'} \frac{\Lambda_{a,a'}}{\mu_a \mu_{a'}}\ \psi_a^\dagger \psi_{a'}^\dagger \psi_{a'} \tag{2.108}$$

$$\Lambda_{a,a'} = C^{(4)}_{a,a,a',a'} + \sum_b \left[\frac{[C^{(3)}_{a,a',b}]^2}{(\mu_{a'} - \mu_a)^2 - \mu_b^2} + \frac{[C^{(3)}_{a,a',b}]^2}{(\mu_a + \mu_{a'})^2 - \mu_b^2} - \frac{C^{(3)}_{a,a,b} C^{(3)}_{b,a',a'}}{\mu_b^2} \right] \tag{2.109}$$

The NR Hamiltonian associated with these equations of motion, from which (2.108) can be derived, is readily written as

$$H = \int \mathrm{d}x \left[\sum_a \frac{\partial_x \psi_a^\dagger \partial_x \psi_a}{2m_a} + \frac{g^2}{16} \sum_{a,a'} \frac{\Lambda_{a,a'}}{\mu_a \mu_{a'}} \psi_a^\dagger \psi_{a'}^\dagger \psi_a \psi_{a'} \right] . \tag{2.110}$$

Hence, it seems that the NR limit of the Toda Field Theories consists of a set of bosons of different species, coupled together through a density-density interaction. It remains though to check whether some of the couplings $\Lambda_{a,a'}$ vanish. Since in the Toda Field Theories the scattering is purely transmissive, such a feature must be also true in the NR limit. However, an inter-species density-density interaction such as in the Hamiltonian (2.110) is never purely transmissive and therefore, to be consistent with the scattering of the Toda theories, different species must be necessarily decoupled $\Lambda_{a,a'} \propto \delta_{a,a'}$. This can be explicitly checked in the A_n and D_n series, since in Ref. [239] the tree level scattering amplitude has been calculated: specialising the result of this paper to the zero rapidity case, one can check that the coupling constants in (2.110) are indeed diagonal $\Lambda_{a,a'} \propto \delta_{a,a'}$. In [68] the tree level diagonal scattering amplitude at zero rapidity has been computed for all simply-laced Toda Field Theories and this leads to the expression

$$\Lambda_{a,a'} = \frac{2\mu_a^2}{h}\delta_{a,a'} \ . \tag{2.111}$$

With this extra piece of information, we finally arrive to the conclusion that the Hamiltonian coming from the NR limit of the Toda Field Theories consists of a set of r decoupled Lieb-Liniger models, all with the same interaction but different masses

$$H = \int \mathrm{d}x \sum_a \left[\frac{\partial_x \psi_a^\dagger \partial_x \psi_a}{2m_a} + \frac{g^2}{8h} \psi_a^\dagger \psi_a^\dagger \psi_a \psi_a \right] \ . \tag{2.112}$$

The non relativisic limit of the S-matrix

We have just seen how, from a direct analysis of the action, the non relativistic limit of the Toda field theories consists in a set of decoupled Lieb Liniger models. This conclusion can be reached in full generality from the scattering matrix, for all simply-laced Toda Field theories, employing the general expression (2.99) of the S-matrix amplitudes and taking its NR limit. For $c \to \infty$ the relative rapidity is approximatively $\theta \sim \frac{v}{c}$ with v the relative velocity of the two particles: in order to make manifest the NR limit, in the integral of eq. (2.99) we can make the change of variable $\tau = c^{-1}t$, so that

$$S_{ab}(\theta) = \exp\left[\int_0^\infty \frac{d\tau}{i\tau} \left(8 \sinh\left(\frac{Bc\tau}{2}\right) \sinh\left(\frac{\pi c\tau}{h} - \frac{Bc\tau}{2}\right) \left(2\cosh\frac{\pi c\tau}{h} - \mathcal{I}\right)^{-1}_{ab} - 2\delta_{ab} \right) \sin(v\tau) \right] \tag{2.113}$$

In the limit $c \to \infty$, we have that $Bc \to \frac{g^2}{4h}$. On the other hand, in the limit $c \to \infty$ the matrix $T_{ab} \equiv \left(2\cosh\frac{\pi c\tau}{h} - \mathcal{I}\right)^{-1}_{ab}$ becomes purely diagonal

$$T_{ab} \simeq \delta_{ab}\, e^{-\frac{\pi c\tau}{h}} \quad , \quad c \to \infty \tag{2.114}$$

and thus the NR limit of the scattering amplitudes becomes diagonal as well

$$S_{ab}(\theta) \to \exp\left[i2\delta_{ab} \int_0^\infty \frac{d\tau}{\tau} e^{-\frac{g^2}{4h}\tau} \sin(v\tau) \right] = \exp\left[\delta_{ab} \ln\left(\frac{\frac{g^2}{4h} + iv}{\frac{g^2}{4h} - iv} \right) \right] \ , \tag{2.115}$$

where the position of the branch cut of the logarithm is fixed along the negative real semiaxis. Thus different particles are decoupled in the NR limit (their scattering matrix is simply 1) and only the scattering of identical particles survives

$$S_{aa} \to \frac{\lambda - i2m_a\frac{g^2}{8h}}{\lambda + i2m_a\frac{g^2}{8h}} \ . \tag{2.116}$$

The above parametrization of the NR scattering matrix is written in terms of the relative non relativistic rapidity, which coincides with the relative momentum, for an easier comparison with the LL scattering matrix: the above scattering describes a collision of two particles of mass m_a and coupling $g^2/8h$, consistently with the result from the equations of motion.

2.3.3 $O(N)$ non-linear sigma model and coupled Lieb-Liniger models

As we showed in the previous section, the remarkable richness of Toda field theories is essentially lost in the NR limit, which consists in a trivial set of decoupled Lieb Liniger models. Such a conclusion has indeed a deep reason: it results from a conspiracy between the purely transmissive scattering of Toda theories and the density-density form of the interaction term, which seems to be ubiquitous in all the NR limit. This kind of interaction will always induce a non-vanishing reflection coefficient. Moreover, it is generically true that whenever two species of particles can be distinguished using the conserved quantities of the theory, integrability imposes a purely transmissive scattering. Therefore, the only consistent possibility in such case is that different species end up decoupled in the NR limit.

The most promising way-out to this dungeon is to have an additional symmetry, so that different species have the same eigenvalues under the conserved charges of non zero spin. This in particular requires mass degeneracy among the particles. The simplest candidate that fulfills all these requirements is the $O(N)$ non-linear sigma model, that is to say a integrable relativistic field theory [78] based on N constrained bosonic fields

$$S = \int \mathrm{d}x\mathrm{d}t \sum_j^N \frac{1}{2}\partial_\mu \phi_j \partial^\mu \phi_j \quad , \quad \sum_j^N \phi_j^2 = \omega N \ . \tag{2.117}$$

The presence of the constraint makes the model interacting and massive, the mass of the particles (identical for all the species) depends on the parameter ω in eq. (2.117), which has to be properly renormalized to absorb UV divergences. Equivalent formulations of the model rescale the fields in such a way the constraint is normalized to one $\sum_j \phi_j^2 = 1$, then ωN appears as a coupling constant in front of the action. The scattering matrix of the model is [83]

$$\begin{aligned} A_i(\theta_1)A_j(\theta_2) = \delta_{i,j}\mathcal{S}^1(\theta_1-\theta_2)\sum_{k=1}^N A_k(\theta_2)A_k(\theta_1) + \\ \mathcal{S}^2(\theta_1-\theta_2)A_j(\theta_2)A_i(\theta_1) + \mathcal{S}^3(\theta_1-\theta_2)A_i(\theta_2)A_j(\theta_1) \end{aligned} \tag{2.118}$$

where

$$\mathcal{S}^3(\theta) = -\frac{1}{N-2}\frac{i2\pi}{\theta}\mathcal{S}^2(\theta), \qquad \mathcal{S}^1(\theta) = -\frac{1}{N-2}\frac{i2\pi}{i\pi-\theta}\mathcal{S}^2(\theta) \tag{2.119}$$

$$\mathcal{S}^2(\theta) = U(\theta)U(i\pi-\theta), \qquad U(\theta) = \frac{\Gamma\left(\frac{1}{N-2} - i\frac{\theta}{2\pi}\right)\Gamma\left(\frac{1}{2} - i\frac{\theta}{2\pi}\right)}{\Gamma\left(\frac{1}{2} + \frac{1}{N-2} - i\frac{\theta}{2\pi}\right)\Gamma\left(-i\frac{\theta}{2\pi}\right)} \tag{2.120}$$

The presence of the constraint (2.117) makes the NR limit of this theory much more difficult to be performed when compared to the previous cases, in particular we cannot proceed through the equation of motion any longer, rather we must rely on the path integral. For the sake of clarity, let us first present and comment the results, leaving the technicalities for later.

From the scattering matrix analysis, it is simple to understand that a sensible NR limit can only be obtained in the combined limit $c \to \infty$ and $N \to \infty$, but keeping Nc^{-1} constant. The NR limit of the scattering matrix is compatible with that of multiple species NR bosonic Hamiltonian

at the integrable point (Yang Gaudin model) [235, 236]

$$H = \sum_j \frac{\partial_x \psi_j^\dagger \partial_x \psi_j}{2m} + \kappa \sum_{jj'} \psi_j^\dagger \psi_{j'}^\dagger \psi_j \psi_{j'} \quad . \tag{2.121}$$

Matching the scattering matrices requires $\kappa = \pi c N^{-1}$, a quantity that must be finite in the NR limit. The mass of the NR model can be written as a complicated function of the renormalized ω coupling of (2.117), but more conveniently we can use m as the free parameter and rather consider ω to be determined from m.

We will indeed confirm that the Hamiltonian (2.121) is the Hamiltonian coming from the NR of the $O(N)$ model. This will be achieved at the level of correlation functions in the Fourier space, with the ground state of the non linear sigma model sent to the vacuum state of the NR model (thus, the state with zero particles). The correlators of the relativistic theory are mapped in those of the NR model provided we identify the NR fields splitting the relativistic ones in positive and negative frequencies

$$\begin{aligned} \psi_j(k^0, k^1) &= \sqrt{2m}\, \phi_j(k^0 - mc^2, k^1)\, \Theta(mc^2 - k^0)\,, \\ \psi_j^\dagger(-k^0, -k^1) &= \sqrt{2m}\, \phi_j(k^0 + mc^2, k^1)\, \Theta(mc^2 + k^0)\,, \end{aligned} \tag{2.122}$$

where Θ is the Heaviside Theta function. Thus, at the level of correlation functions we have

$$\langle \prod_i \frac{\psi_{j_i}(k_i^0, k_i^1)}{\sqrt{2m}} \prod_{i'} \frac{\psi_{j_{i'}}^\dagger(q_{i'}^0, q_{i'}^1)}{\sqrt{2m}} \rangle = \lim_{\text{NR}} \left[\langle \prod_i \phi_{j_i}(k_i^0 - mc^2, k_i^1) \prod_{i'} \phi_{j_{i'}}(-q_{i'}^0 + mc^2, -q_{i'}^1) \rangle \right] \quad , \tag{2.123}$$

The correspondence between the correlation functions will be found through an analysis of the Feynman graphs in the Fourier space: the NR limit of the Feynman graphs of the sigma model reduces to the Feynman diagrams of (2.121). It must be said that the relation in Fourier transform between the ϕ_j and ψ_j fields is in perfect agreement with the usual splitting of the relativistic field (2.66). In order to see this we can write ϕ_j in the coordinate space:

$$\phi_j(t, x) = \int \frac{\mathrm{d}^2 k}{(2\pi)^2} e^{ik^0 t - ik^1 x} \phi_j(k^0, k^1) = \frac{1}{\sqrt{2m}} \left[e^{imc^2 t} \psi_j^\dagger(t, x) + e^{-imc^2 t} \psi_j(t, x) \right] \quad . \tag{2.124}$$

These results will be soon discussed in more details. For the time being, let us notice an interesting property of the Hamiltonian (2.121) got in the NR limit. For the $O(N)$ sigma model, its NR limit requires Nc^{-1} to be constant, therefore necessarily $N \to \infty$ and then the Hamiltonian (2.121) in principle describes an *infinite* set of different bosonic species. The requirement of dealing with infinite species is of course rather unphysical, but we can easily circumvent this issue with the simple observation that the Hamiltonian (2.121) separately conserves the number of particles of each different species. Therefore, we can simply project on states with a *finite* number of different particle species. If we pose a bound to the possible indexes we plug in the correlation functions, for example we impose all the indexes $j_i, j_{i'}$ that appear in (2.123) to be comprised from 1 to n, then we are describing the NR model with n different species, since all the particles associated with fields $\psi_{j>n}$ are absent by construction. In this way from the non linear sigma model we can extract, in the NR limit, Yang Gaudin models with a finite and arbitrary number of different species: in particular we can even get the single species LL model, just posing to zero the density of all other particles.

Non relativistic limit of the scattering matrix

The NR limit of the scattering matrix of the non linear sigma model can be easily studied. Considering the relativistic scattering amplitudes (2.119-2.120) it is immediate to understand that the only sensible way to take the NR limit is keeping Nc^{-1} constant while $c \to \infty$. In this case we easily obtain (as usual $\theta \simeq \lambda/(mc)$)

$$\mathcal{S}^1 \xrightarrow{\text{NR}} 0, \qquad \mathcal{S}^2 \xrightarrow{\text{NR}} \frac{\lambda}{\lambda + i2\pi mcN^{-1}}, \qquad \mathcal{S}^3 \xrightarrow{\text{NR}} -\frac{i2\pi mcN^{-1}}{\lambda + i2\pi mcN^{-1}} \tag{2.125}$$

Therefore we obtain the following non relativistic scattering

$$A_{j'}(\lambda_1)A_j(\lambda_2) = \frac{\lambda_1 - \lambda_2}{\lambda_1 - \lambda_2 + i2\pi mcN^{-1}} A_j(\lambda_2)A_{j'}(\lambda_1) + \frac{-i2\pi mcN^{-1}}{\lambda_1 - \lambda_2 + i2\pi mcN^{-1}} A_{j'}(\lambda_2)A_j(\lambda_1) \tag{2.126}$$

This NR scattering is exactly the same of the Yang Gaudin model (2.121) and strongly suggests the latter as the correct NR limit of the non linear sigma model. However, the mapping of the scattering matrix alone is not enough to safely reach this conclusion, in particular the scattering matrices cannot fix the mapping between the correlation functions of the two models: in order to do this, we analyse the NR limit of the dynamics.

As we have already anticipated, the NR limit at the level of the dynamics will be performed at the level of Feynman diagrams. The Feynman diagrams of the Yang Gaudin model (2.121) provide a power expansion in terms of the coupling $\kappa = \pi N^{-1} c$, thus it is natural to compare such an expansion with the large N expansion of the non linear sigma model that produces a power series in $1/N$, then of course we must study the NR limit of the latter. In this perspective, we firstly proceed in reviewing the Feynman rules for the NR bosons, then the large N expansion of the non linear sigma model. Finally we see how, in the NR limit, the diagrams of the sigma model become those of the Yang Gaudin model. However, the NR mapping is complicated because of the subtle issue of the renormalization that the sigma model must undergo before taking the proper limit. In particular, the model requires mass and field strength renormalization [240]: since any order in $1/N$ introduces new divergent counterterms, we are in principle forced to verify the mapping order by order. Because of this issue we verify the NR mapping in the two cases, i.e. at the tree level where no renormalization is needed and at $\mathcal{O}(N^{-1})$, where a non trivial renormalization must be introduced. However we feel confident that this non trivial check, joint with the mapping of the exact (non perturbative) scattering matrix, is enough to identify the bosonic Yang Gaudin model as the NR limit of the non linear sigma model.

Feynman diagrams of the multi-species interacting bosons

The Feynman graphs of the NR model (2.121) are easily constructed in terms of a free (retarded) NR propagator G_{NR} and an interaction vertex involving four fields. Since G_{NR} connects a creation field $\psi_j^\dagger$ with an annihilation one ψ_j, we must distinguish graphically the two sides of the propagator. Therefore, we represent it with an arrow that flows from $\psi_j^\dagger$ towards ψ_j (Fig. 2.7). In the Fourier space we denote the NR propagator as $\tilde{G}_{\text{NR}}$ and its value is (the momentum flow is chosen in agreement with the direction of the arrow):

$$\tilde{G}_{\text{NR}}(k^0, k^1) = \frac{-i}{k^0 + \frac{(k^1)^2}{2m} - i\epsilon} \tag{2.127}$$

Since the interaction vertex conserves the number of particles, it must have an equal number of incoming and outgoing arrows (Fig. 2.7) and its value is simply $-i\kappa$. The fact that the fields in the interaction of (2.121) are normal ordered prevents any self interaction of the vertex. It must

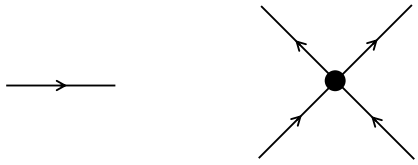

Figure 2.7: *Diagrammatic representation of the propagator and interaction vertex of the Yang Gaudin model.*

be said that in the Feynman diagrams we should also keep track of the different species, thus is principle we should attach a label on each arrow: the propagators can connect only $\psi_j^\dagger$ with the same species ψ_j. The interaction conserves separately the number of each species, thus if the incoming arrows are associated with (j, j') species, even the outgoing arrows are labeled (j, j').

Large N expansion of the non linear sigma model

We now review the large N expansion for the non linear sigma model [240, 241]. The first step consists in representing the constraint that appears in the action (2.117) by mean of an auxiliary field Λ and an integral representation of the functional Dirac delta:

$$\delta\left(\sum_j \phi_j^2 - \omega N\right) = \int \mathcal{D}\Lambda \; e^{-i\int \mathrm{d}x\mathrm{d}t \; \frac{\Lambda}{2}\left(\sum_j \phi_j^2 - \omega N\right)} \quad . \tag{2.128}$$

This representation of the constraint leads naturally to define an *auxiliary action* with unconstrained bosons and a ghost field

$$\mathcal{S}_{\text{aux}} = \int \mathrm{d}x\mathrm{d}t \; \sum_j \frac{1}{2}\partial_\mu \phi_j \partial^\mu \phi_j - \frac{\Lambda}{2}\left(\sum_j \phi_j^2 - N\omega\right) \quad . \tag{2.129}$$

Correlation functions in the non linear sigma model can be equivalently computed with the constrained action (2.117) or with the above unconstrained one at the price of introducing an extra field in the path integral: the second formulation naturally leads to the large N expansion. Since the action is quadratic in terms of the bosonic fields, in principle we could perform exactly the path integral over ϕ_j and reduce ourselves to a path integral for the single field Λ, however such an operation makes less transparent the construction of the Feynman rules, so we proceed along another direction. Notice that the ghost field plays the role of an effective space-time dependent mass for the bosonic field: knowing in advance that the bosons become massive because of the constraint, we shift the ghost field $\Lambda \to \Lambda + m^2c^2$. This operation does not affect the correlation functions of the bosonic fields, but has the advantage of making explicit a constant mass term for the bosons (we discard in the action an inessential additive constant):

$$\mathcal{S}_{\text{aux}} = \int \mathrm{d}x\mathrm{d}t \; \sum_j \frac{1}{2}\left(\partial_\mu \phi_j \partial^\mu \phi_j - m^2c^2\phi_j^2\right) - \frac{\Lambda}{2}\left(\sum_j \phi_j^2 - N\omega\right) \quad . \tag{2.130}$$

For the time being the mass m is a free parameter that will be fixed soon. It is convenient to perform the path integral over the ϕ_j fields through Feynman diagrams, using the massive action to generate the free propagators. The path integral over the ghost field is left for a second moment and at this stage the latter behaves as a classical current coupled with the ϕ_j fields. In these Feynman graphs we represent free propagators as continuous lines, the ghost field is a dotted line and, as it is clear from (2.130), it interacts with two bosonic fields of the same species, but (for the moment) it does not propagate. These Feynman diagrams have two kinds of external

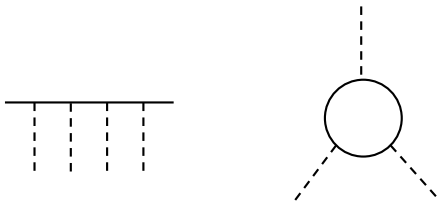

Figure 2.8: *In the Feynman diagrams that describe the path integral in ϕ_j at fixed ghost field there are two classes of connected diagrams. The graphs involving external continuous legs (left) and the graphs in which only the external legs of the ghost field appear (right).*

legs: continuous external legs represent the ϕ_j fields we are considering in the actual correlators to be computed, then of course we have dotted external legs representing the "external source" Λ. Therefore the (connected) Feynman diagrams are naturally organized in two classes: those with external continuous legs and those that have only dotted external legs, as described in Fig. 2.8. With these Feynman diagrams we describe the integration over the ϕ_j fields, but in order to compute the correlators we should also integrate over the ghost field Λ

$$\langle ... \rangle = \int \mathcal{D}\Lambda \; e^{i \int \mathrm{d}x\mathrm{d}t \; \frac{N\omega}{2}\Lambda} \quad \sum [\text{Feynman diagrams}] \; , \tag{2.131}$$

where the Feynman diagrams are of course Λ dependent because of the dotted external legs.

Clearly it is impossible to compute exactly the path integral and we must rely on perturbation theory, but in order to do so we need, as a starting point, a gaussian action for the ghost field to generate a Λ propagator: we are going to extract it from the sum of the Feynman diagrams. Among the various connected Feynman diagrams with only dotted external legs (thus associated with only the auxiliary field as "external current"), we are interested in the graphs with two dotted legs drawn in Fig. 2.9. Since this graph has only two dotted external lines, it is quadratic in the ghost field: we label as $\mathcal{G}$ both this graph and its value. We now use the fact that the sum of the Feynman diagrams can be riexponentiated in terms of the connected diagrams [126] to write the sum in (2.131) as

$$\sum [\text{Feynman graphs}] = \sum [\text{Feynman graphs without } \mathcal{G}] \, e^{\mathcal{G}} \; . \tag{2.132}$$

Thus Eq. (2.131) can be written as

$$\langle ... \rangle = \int \mathcal{D}\Lambda \; e^{i \int \mathrm{d}x\mathrm{d}t \; \frac{N\omega}{2}\Lambda + \mathcal{G}} \quad \sum [\text{Feynman graphs without } \mathcal{G}] \; . \tag{2.133}$$

We can now use the graph $\mathcal{G}$, quadratic in the ghost field, to define a propagator for Λ

$$\langle \Lambda(k^\mu)\Lambda(q^\mu)\rangle_0 = (2\pi)^2 \delta\left(k^\mu + q^\mu\right) \Gamma\left(k^\mu k_\mu\right) \; , \tag{2.134}$$

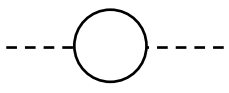

Figure 2.9: *The connected diagram that contributes to the gaussian part of the effective action in the large N limit.*

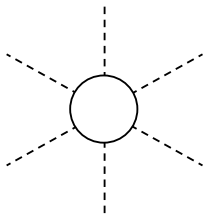

Figure 2.10: *The integration over the internal loops of continuous lines gives a N factor.*

where Γ^{-1} is simply the value of the loop diagram in Fig. 2.9:

$$\Gamma^{-1}\left(k^\mu k_\mu\right) = -\frac{N}{2}\int \frac{\mathrm{d}^2 q}{(2\pi)^2}\frac{1}{q^\mu q_\mu - m^2c^2 + i\epsilon_1}\frac{1}{\left(k^\mu - q^\mu\right)\left(k_\mu - q_\mu\right) - m^2c^2 + i\epsilon_2}\,, \tag{2.135}$$

where we should independently take $\epsilon_{1,2} \to 0$. The factor N comes from the summation over all the species of particles in the internal loop and the contractions are done with the Minkowski metric with restored c:

$$\eta_{\mu\nu} = \begin{pmatrix} \frac{1}{c^2} & 0 \\ 0 & -1 \end{pmatrix}\,. \tag{2.136}$$

This integral can be done exactly and it is computed in Appendix 2.B, where we get

$$\Gamma\left(k^\mu k_\mu\right) = i4\pi c N^{-1} m^2 \sqrt{\left(\frac{k_\mu k^\mu}{m^2c^2} - 4\right)\frac{k_\mu k^\mu}{m^2c^2}}\left(\log\left[\frac{\sqrt{4 - \frac{k_\mu k^\mu}{m^2c^2}} + \sqrt{-\frac{k_\mu k^\mu}{m^2c^2}}}{\sqrt{4 - \frac{k_\mu k^\mu}{m^2c^2}} - \sqrt{-\frac{k_\mu k^\mu}{m^2c^2}}}\right]\right)^{-1}\,. \tag{2.137}$$

Thanks to this propagator we can now perturbatively compute the path integral in the ghost field and find the final Feynman rules to compute the correlators of the bosonic fields ϕ_j. In particular, the new Feynman diagrams are constructed from the old ones simply letting the auxiliary field (dotted line) to propagate, thus the final Feynman diagrams can be constructed out of these different objects:

1. Massive bosonic standard propagators (continuous lines).
2. The propagators of the ghost field (dashed lines).
3. The interaction vertexes that can be read from the the auxiliary action (2.130). One vertex couples a dotted line with two continuous lines, instead the interaction proportional to ω involves a single dotted line and no continuous lines.
4. Since we are interested in the correlators of the physical fields, the dotted lines appear only as internal propagators in the Feynman diagrams.
5. An extra recipe is needed: since we used the graphs of Fig. 2.9 to construct the propagator of the ghost field, these should not enter in the final Feynman graphs (their contribution has already been resummed in the dotted propagator), thus we should remove them by hand from the Feynman diagrams.

In terms of these Feynman diagrams we can readily exploit the large N limit as it follows. N divergent contributions to the Feynman graphs come from closed loops of continuous lines (namely the internal loops of Fig. 2.10 with an arbitrary number of departing dotted legs). Each closed loop gives an N factor coming from the sum of the internal continuous propagators over the different indexes of ϕ_j. On the other hand the Γ (2.137) propagator carries a factor $1/N$,

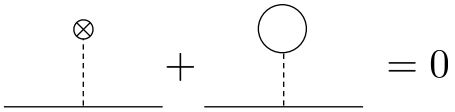

Figure 2.11: *Cancellation of N divergent graphs.*

therefore any dotted line counts as $1/N$. Actually it is useful to split the factor $\frac{1}{N} = \frac{1}{\sqrt{N}}\frac{1}{\sqrt{N}}$ and attach each of these factors $\frac{1}{\sqrt{N}}$ at the edges of the dotted lines. With this convention for the power counting, an internal loop with n departing dotted lines contributes as $N^{1-n/2}$, therefore the only loops that are not suppressed in N are those with $n = 1$ and $n = 2$. However, notice that the loops with two legs ($n = 2$) are excluded by the point 5 of the Feynman rules. We are left with the more dangerous loops with only a departing dotted line, but now we take advantage of the fact that the mass m has not been fixed yet: tuning m properly we can ask the interaction proportional to ω to cancel the one loop diagrams, as shown in Fig. 2.11.

This requirement is immediately translated in a mass equation that ties together the coupling ω with the mass m

$$\omega - \int \frac{\mathrm{d}^2 k}{(2\pi)^2} \frac{i}{k_\mu k^\mu - m^2 c^2 + i\epsilon} = 0 \ . \tag{2.138}$$

After we impose this mass equation, ω explicitly disappears from all the Feynman diagrams and it contributes only through the mass m.

Notice we can read this equation backward: once we gave the value of m (that is the physical parameter), from the equation we read the positive (infinite) value ω must attain. Now the Feynman diagrams describe a proper large N expansion through the insertion of a progressive number of internal dotted propagators: at the zeroth order of the expansion we get free bosons of mass m.

In particular, we can conveniently think the propagators of the ghost field to define an effective vertex for the ϕ_j fields, as depicted in Fig. 2.12. As a matter of fact, since the dotted lines are never external legs, they can only appear coupled to the continuous lines as in Fig. 2.12: we can regard such a graph as an effective (non local) vertex of four fields mediated by the ghost field. Pursuing this interpretation we can write the following effective action (below $\Gamma(x^\mu)$ is the Γ propagator written in the coordinate space by mean of a simple Fourier transform):

$$\mathcal{S}_{\text{eff}} = \mathcal{S}_{\text{free}} + \int \mathrm{d}^2 x \mathrm{d}^2 y \ \frac{i}{8} \sum_{jj'} \phi_j^2(x^\mu)\phi_{j'}^2(y^\mu)\Gamma(x^\mu - y^\mu) \, . \tag{2.139}$$

Where $\mathcal{S}_{\text{free}}$ is the massive free action for the bosonic fields ϕ_j. However, this expression is not enough to reproduce the Feynman diagrams of the large N expansion; this is due to the selection rules on the Feynman diagrams. The correct expansion, matching the original one in (2.131), is recovered adding the following extra rules for the Feynman diagrams extracted from (2.139):

1. The mass equation prevents the appearance of closed loops as those of Fig. 2.11. This exclusion is not implemented in the above effective action.

2. The large N expansion prevents the appearance of closed loops which would correspond to Fig. 2.9. Indeed, this diagram was already taken into account in (2.132) to give the propagator (2.134) to the field Λ.

Until now we dealt with the bare action, but the large N expansion of the non linear sigma model presents UV divergences that must be properly renormalized [240]. The renormalization

affects the mass (we can equivalently renormalize the coupling ω due to the mass transmutation) and requires the insertion of a field strength counterterm. In particular, the latter amounts to the addition in the effective action (2.139) of a term proportional to $\sum_j \partial_\mu \phi_j \partial^\mu \phi_j$.

NR limit of the Feynman diagrams

Armed with the large N expansion of the non linear sigma model we can finally study the NR mapping of the dynamics through the correlation functions. The first step is to show that the free propagator of the putative NR fields defined in (2.122) reduces to the NR propagators, as it should be. The check is immediate: applying the definition (2.122) we have

$$\langle \psi_j(k^0,k^1)\psi_{j'}(q^0,q^1)\rangle_0 = 2m\Theta(mc^2-k^0)\Theta(mc^2-q^0)\langle \phi_j(k^0-mc^2,k^1)\phi_{j'}(q^0-mc^2,q^1)\rangle_0 \,. \quad (2.140)$$

Above, the expectation value is taken on the vacuum and propagating the fields in absence of interactions. Then noticing that the relativistic correlator gives an energy conservation law $\delta(k^0+q^0-2mc^2)$ we discover that the above is identically zero, because of the product of the Θ functions with the δ over the energies

$$\Theta(mc^2-k^0)\Theta(mc^2-q^0)\delta(k^0+q^0-2mc^2) = \Theta(mc^2-k^0)\Theta(k^0-mc^2)\delta(k^0+q^0-2mc^2) = 0 \ . \quad (2.141)$$

We now consider $\langle \psi^\dagger \psi\rangle_0$, with the same passages and making explicit the propagator of the relativistic field we get

$$\langle \psi_j^\dagger(k^0,k^1)\psi_{j'}(q^0,q^1)\rangle_0 = (2\pi)^2\delta_{jj'}\delta\left(k^\mu-q^\mu\right)\Theta(mc^2-k^0)\frac{i2m}{\frac{1}{c^2}(k^0-mc^2)^2-(k^1)^2-m^2c^2+i\epsilon} \ . \quad (2.142)$$

Then we use the following splitting of the propagator (the identity holds apart from an inessential rescaling of the vanishing regulator ϵ)

$$\frac{i}{k_\mu k^\mu - m^2c^2+i\epsilon} = \frac{c}{2\sqrt{(k^1)^2+m^2c^2}}\left[\frac{-i}{k^0+c\sqrt{(k^1)^2+m^2c^2}-i\epsilon}+\frac{-i}{-k^0+c\sqrt{(k^1)^2+m^2c^2}-i\epsilon}\right] , \quad (2.143)$$

then the NR limit of (2.142) easily follows:

$$\lim_{\rm NR}\langle \psi_j^\dagger(k^0,k^1)\psi_{j'}(q^0,q^1)\rangle_0 = (2\pi)^2\delta_{jj'}\delta\left(k^\mu-q^\mu\right)\frac{-i}{k^0+\frac{(k^1)^2}{2m}-i\epsilon} \ . \quad (2.144)$$

The above expression is in agreement with the NR propagator (2.127), therefore the free part of the effective action (2.139) correctly reproduces the NR propagators, after the NR limit has been taken. We now proceed to test the NR mapping at tree level in the effective action (2.139): since at the tree level the Feynman graphs do not contain any free momentum to be integrated, the NR limit is easily taken. In particular, the additional rule 2) presented below Eq. (2.139),

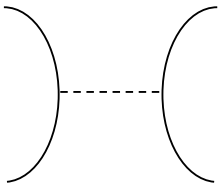

Figure 2.12: *Four field vertex mediated by the ghost field.*

can be safely ignored at the tree level, as it only concerns loops. First of all we insert the mode splitting (2.124) in the interaction of the effective action (2.139), in this way we obtain several vertexes for the non relativistic fields with oscillating phases. Now, notice that the NR limit of the propagators forces all the momenta (even those of internal propagators) to attain NR values, therefore the only interaction vertexes relevant at tree level are those such that all the NR fields of the vertex can attain NR values at the same time. The oscillating phases in the coordinate space mean momentum shifts in the Fourier space: this fact, joint with the overall energy conservation, leads to the conclusion that only the number conserving vertexes (i.e. those of the form $\psi^\dagger\psi^\dagger\psi\psi$) are relevant for the NR limit. However, in principle two possible indexes structures for the vertex are allowed, i.e.

$$\int \mathrm{d}^2x\mathrm{d}^2y\ \frac{i}{2(2m)^2}\sum_{jj'}\psi_j^\dagger(x^\mu)\psi_j(x^\mu)\psi_{j'}^\dagger(y^\mu)\psi_{j'}(y^\mu)\Gamma(x^\mu-y^\mu) \tag{2.145}$$

and

$$\int \mathrm{d}^2x\mathrm{d}^2y\ \frac{i}{4(2m)^2}\sum_{jj'}\psi_j^\dagger(x^\mu)\psi_j^\dagger(x^\mu)\psi_{j'}(y^\mu)\psi_{j'}(y^\mu)\Gamma(x^\mu-y^\mu)e^{i2mc^2(x^0-y^0)}\ . \tag{2.146}$$

Notice that the indexes structure of the vertex in the NR model is the same as the first of the above (i.e. the number of each particle species is separately conserved), on the other hand the Yang Gaudin model does not have an interaction analogue to the second term, that instead allows for tunneling among different species. In fact, among the two vertexes only the first matters in the NR limit. In order to see this, we Fourier transform the vertexes. Eq. (2.145) becomes

$$\int \frac{\mathrm{d}^8k}{(2\pi)^6}\delta\left(k_1^\mu+k_3^\mu-k_2^\mu-k_4^\mu\right)\ \frac{i}{2(2m)^2}\sum_{jj'}\psi_j^\dagger(k_1^\mu)\psi_j(k_2^\mu)\psi_{j'}^\dagger(k_3^\mu)\psi_{j'}(k_4^\mu)\ \Gamma((k_1-k_2)^\mu(k_1-k_2)_\mu)\ . \tag{2.147}$$

In the NR limit, as we already said, the momenta in the fields are constrained to attain NR values, thus the NR limit of this interaction vertex simply amounts to take the NR limit of Γ at fixed momenta $k_1^\mu-k_2^\mu$. Using the explicit expression (2.137) we get

$$\lim_{\mathrm{NR}}\frac{i}{2(2m)^2}\Gamma((k_1-k_2)^\mu(k_1-k_2)_\mu)=-\pi cN^{-1}\ , \tag{2.148}$$

thus the NR limit of (2.147) exactly fits the NR interaction vertex, apart from an i factor. The latter comes from the fact that in the path integral it enters i times the effective action, thus in the Feynman diagrams (2.148) acquires the extra i needed to match the NR vertex. It remains to show that in the NR limit the vertex (2.146) vanishes: moving in the Fourier space we get an expression similar to (2.147), but the extra phases factor shift the momentum in Γ of $2mc^2$. Thus the relevant vertex in the NR limit is

$$\lim_{\mathrm{NR}}\ \Gamma\left(\frac{1}{c^2}(k_1^0+k_2^0-2mc^2)^2-(k_1^1+k_2^1)^2\right)=0\ , \tag{2.149}$$

as it can be immediately checked from the explicit expression for Γ (2.137). This last step concludes the desired mapping: the Feynman diagrams at tree level of the effective action (2.139) are sent to the tree level Feynman graphs of the Yang Gaudin model.

This remarkably simple picture get more involved beyond the tree level because of the following reasons:

1. The relativistic effective vertex is not normal ordered, differently from the NR vertex. The

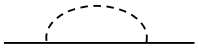

Figure 2.13: *This relativistic graph does not have a NR counterpart, due to the normal ordering in the interaction of the Yang Gaudin model.*

unwanted graphs excluded by the normal ordering are obtained making two of the external legs of the effective vertex (Fig. 2.12) to autointeract. One autointeraction has already been eliminated by the mass equation (Fig. 2.11), thus we are left with the "unwanted" graph of Fig. 2.13 that appears at the $\mathcal{O}(N^{-1})$ expansion of the theory and is of course absent at the tree level. Since Fig. 2.13 has two legs it is natural to ask ourselves if this graph can be completely removed by a mass (or equivalently the coupling ω) or of the field strength renormalization. In the relativistic theory an exact cancellation seems to be impossible, because the graph of Fig. 2.13 has a non trivial momentum dependence. Despite these difficulties it could be that in the NR limit this cancellation occurs: in fact, we are going to explicitly show this fact at $\mathcal{O}(N^{-1})$ of the expansion.

2. The relativistic diagrams obey to an extra "selection rule" that is irrelevant as long we remain at tree level, but as soon as we allow for loops we must forcefully exclude the loop diagrams of Fig. 2.9: such a rule is not present in the NR diagrams. However, this is not expected to be relevant in the NR limit: at tree level we showed that only the effective vertex (2.145) is relevant in the NR limit. Assume this is true beyond tree level and compute the NR counterpart of the internal loop of Fig. 2.9. Its value is

$$-N\int\frac{\mathrm{d}^2q}{(2\pi)^2}\frac{-i}{q^0+\frac{(q^1)^2}{2m}-i\epsilon_1}\frac{-i}{q^0-k^0+\frac{(q^1-k^1)^2}{2m}-i\epsilon_2}\ , \tag{2.150}$$

where k is the momentum injected in the loop. Notice that the above integral is zero because we are free to deform the integral in q^0 in the lower complex plane without embracing any singularity. Therefore, the selection rule we should forcefully impose in the relativistic theory is already naturally implemented in the NR model.

3. The correct procedure to take the NR limit is not on the propagators and vertexes, but on the diagrams themselves. In principle we should consider a whole diagram and take its NR limit, showing it reduces to a diagram of the NR model. While at the tree level such a procedure is completely equivalent to take the limit of the building blocks of the diagrams (propagators and interaction vertexes), this is no longer true beyond the tree level because of the presence of UV divergent integrals. In fact, the relativistic theory must be properly renormalized before taking the NR limit. This is the major obstacle in providing a mapping of the whole set of the Feynman diagrams, since at any order new counterterms are introduced and the theory must be renormalized from scratch.

To get convinced that these issues do not spoil the NR limit we test the simplest example where the model must be renormalized. Thus we change perspective and instead of considering the Feynman diagrams at tree level, we focus on the $\mathcal{O}(N^{-1})$ diagrams depicted in Fig. 2.14 (here diagrams are not meant to be building blocks for larger diagrams: the external legs are indeed the external legs of the whole Feynman diagram).

At the zeroth order the mass equation makes the (c) and (d) graphs to cancel each other, but the graph (b) (that is $\sim \mathcal{O}(N^{-1})$) is actually divergent and forces us to modify the mass equation, as well as to introduce a field renormalization counterterm. Of course, the NR limit of the $\mathcal{O}(N^{-1})$ correlators must reduce to the first order expansion in the coupling $\lambda = \pi c N^{-1}$

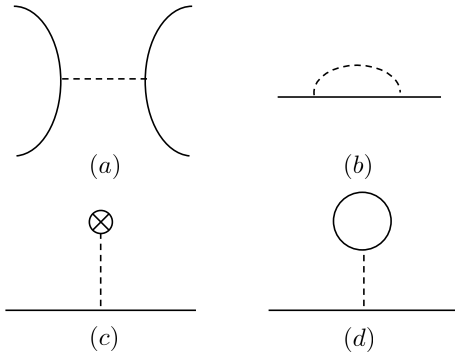

Figure 2.14: *Graphs relevant at $\mathcal{O}(N^{-1})$.*

of the Yang Gaudin model: thus among the graphs of Fig. 2.14 only the four leg vertex (a) must survive in the NR limit. Actually, the fact that the (a) graph reproduces in the NR limit the correct 4 leg NR graph it is exactly what we showed at tree level (indeed, (a) is a tree-like Feynman diagram). Therefore, it remains to check if the graphs (b), (c) and (d) (or rather their sum) vanish in the NR limit. These three graphs contribute to the two point correlator $\langle\phi(k^\mu)\phi(q^\mu)\rangle$. Leaving out the δ over the momenta, the three graphs contribute as:

$$(b) = -\int \frac{\mathrm{d}^2 p}{(2\pi)^2} \frac{i}{(p^\mu - k^\mu)(p_\mu - k_\mu) - m^2c^2 + i\epsilon} \Gamma(p_\mu p^\mu) \ , \tag{2.151}$$

$$(c) = \frac{N}{2}\omega \int \frac{\mathrm{d}^2 p}{(2\pi)^2} \Gamma(p_\mu p^\mu), \qquad (d) = -\frac{N}{2}\left[\int \frac{\mathrm{d}^2 p}{(2\pi)^2} \Gamma(p_\mu p^\mu)\right] \int \frac{\mathrm{d}^2 k}{(2\pi)^2} \frac{i}{k_\mu k^\mu - m^2c^2 + i\epsilon} \ . \tag{2.152}$$

Since for large momenta the Γ propagators diverges as $\sim p^\mu p_\mu$ (with logarithmic corrections), the (b) graph is UV divergent and first of all we should extract its divergent part. In the graph (b) we perform a Wick rotation $p^\mu \to \bar{p}^\mu = (-ip^0, p^1)$ and $k^\mu \to \bar{k}^\mu = (-ik^0, k^1)$, then we rewrite it as

$$\begin{aligned}(b) = &\int \frac{\mathrm{d}^2 p}{(2\pi)^2} \frac{\Gamma(-\bar{p}_\mu \bar{p}^\mu)}{(\bar{p}^\mu \bar{p}_\mu + m^2c^2)} + \int \frac{\mathrm{d}^2 p}{(2\pi)^2} \left[\frac{-\bar{k}^\mu \bar{k}_\mu}{(\bar{p}^\mu \bar{p}_\mu + m^2c^2)^2} + \frac{4(\bar{p}_\mu \bar{k}^\mu)^2}{(\bar{p}_\mu \bar{p}^\mu + m^2c^2)^3}\right] \Gamma(-\bar{p}_\mu \bar{p}^\mu) + \\ &+ \int \frac{\mathrm{d}^2 p}{(2\pi)^2} \left[\frac{1}{(\bar{p}^\mu - \bar{k}^\mu)(\bar{p}_\mu - \bar{k}_\mu) + m^2c^2} - \frac{1}{(p^\mu p_\mu + m^2c^2)} + \frac{k^\mu k_\mu}{(\bar{p}^\mu \bar{p}_\mu + m^2c^2)^2} + \right. \\ &\left. - \frac{4(\bar{p}_\mu \bar{k}^\mu)^2}{(\bar{p}_\mu \bar{p}^\mu + m^2c^2)^3}\right] \Gamma(-\bar{p}_\mu \bar{p}^\mu) \ , \end{aligned} \tag{2.153}$$

where the contractions are performed through the Euclidean metric

$$\eta^E_{\mu\nu} = \begin{pmatrix} \frac{1}{c^2} & 0 \\ 0 & 1 \end{pmatrix} \ . \tag{2.154}$$

The third integral of Eq. (2.153) is UV finite, differently from the first and second integrals that provide, respectively, a mass and a field strength renormalization. As a matter of fact,

thanks to the symmetries of the integration domain, the second integral can be rewritten as

$$\int \frac{\mathrm{d}^2 p}{(2\pi)^2}\left[\frac{-\bar{k}^\mu \bar{k}_\mu}{(\bar{p}^\mu \bar{p}_\mu + m^2c^2)^2} + \frac{4(\bar{p}_\mu \bar{k}^\mu)^2}{(\bar{p}_\mu \bar{p}^\mu + m^2c^2)^3}\right]\Gamma(-\bar{p}_\mu \bar{p}^\mu) = \\ = k_\mu k^\mu \int \frac{\mathrm{d}^2 p}{(2\pi)^2}\left[\frac{1}{(\bar{p}^\mu \bar{p}_\mu + m^2c^2)^2} + \frac{2\bar{p}_\mu \bar{p}^\mu}{(\bar{p}_\mu \bar{p}^\mu + m^2c^2)^3}\right]\Gamma(-\bar{p}_\mu \bar{p}^\mu) \ , \tag{2.155}$$

i.e. exactly in the form of the field strength counterterm discussed below Eq. (2.139). The first UV divergent integral in Eq. (2.153) can be absorbed, rather than in a mass renormalization, in a renormalization of the coupling ω modifying the mass equation from Eq. (2.138) to

$$(c) + (d) + \int \frac{\mathrm{d}^2 p}{(2\pi)^2}\frac{1}{(\bar{p}^\mu \bar{p}_\mu + m^2c^2)}\Gamma(-\bar{p}_\mu \bar{p}^\mu) = 0 \ . \tag{2.156}$$

Compared with the mass equation (2.138), ω is shifted by a $\mathcal{O}(N^{-1})$ UV divergent term. Now that the $\mathcal{O}(N^{-1})$ has been made finite by the renormalization, we can take the NR limit of the finite part of the (b) graph, that vanishes in the NR limit. Thus we conclude that, after the proper renormalization, the NR limit of the $\mathcal{O}(N^{-1})$ order consists in a free non relativistic propagator and a four field correlator that matches the first perturbative order of the Yang Gaudin model, as it should be.

2.3.4 The Super Sinh Gordon and its non relativistic limit

The Super Sinh Gordon (SShG) model is a IQFT based on a real bosonic field ϕ and on a Majorana spinor χ, coupled in a supersymmetric way [229, 230]

$$\mathcal{S}_{\mathrm{SShG}} = \int \mathrm{d}x\mathrm{d}t \ \frac{1}{2}\partial_\mu \phi \partial^\mu \phi + \frac{1}{2}\bar{\chi}\left(i\partial\!\!\!/ - mc\cosh\left(c^{-1}2\sqrt{\kappa}\phi\right)\right)\chi - \frac{m^2c^4}{16\kappa}\left(\cosh(c^{-1}4\sqrt{\kappa}\phi) - 1\right) . \tag{2.157}$$

If in the above action the fermionic field is ignored, one recovers the action of the Sinh Gordon model, so that SShG is the natural supersymmetric extension of the purely bosonic case. Consistently, in the NR limit the SShG model reduces to the supersymmetric extension of the Lieb Liniger model, namely the Yang-Gaudin model with a fermionic and a bosonic species [242–245]. This model consists in two species of NR particles coupled through a density-density interaction

$$H = \int \mathrm{d}x \ \frac{\partial_x \psi^\dagger \partial_x \psi}{2m} + \frac{\partial_x \Psi^\dagger \partial_x \Psi}{2m} + \kappa \psi^\dagger \psi^\dagger \psi \psi + 2\kappa \psi^\dagger \psi \Psi^\dagger \Psi \, , \tag{2.158}$$

where ψ and Ψ are standard NR bosonic and fermionic fields respectively.

The SShG model, besides being integrable, is also supersymmetric. Nowadays SUSY is a widespread topic of theoretical physics, originally born in the framework of high energy physics in $3+1$ dimensions [54, 246]. However its presence is now widely spread to many different fields. For example, in the context of $1+1$ dimensional systems, it appears as a key tool to identify interesting classes of universality [247–249] as well as to constraint scattering amplitudes in IQFT out of criticality [80] or to avoid confinement of topological excitations [250].

On a general ground, supersymmetric models possess an equal number of bosonic and fermionic excitations: supersymmetry exchanges ones with the others. SUSY, as other continuous symmetries, can be described as a sequence of infinitesimal transformations induced by the proper generators, i.e. the supercharges. However, while many continuous symmetries are usually implemented by generators which satisfy a Lie Algebra (and therefore the symmetry group is a Lie Group), in SUSY the situation is different: the supercharges, together with the

Hamiltonian and the momentum, form instead a graded Lie Algebra [251], in which the role of anticommutators (rather than only commutators) is fundamental.

We briefly discuss these aspects on the simple class of SUSY invariant actions which the SShG belongs to, in such a way to prepare the ground for the subsequent discussion. In particular, the SShG action is an example of a wide class of QFT with $\mathcal{N} = 1$ supersymmetry [252] (i.e. with a pair of conserved supercharges)

$$\mathcal{S}_{\text{SUSY}} = \int \mathrm{d}x\mathrm{d}t\, \frac{1}{2}\partial_\mu\phi\partial^\mu\phi + \frac{1}{2}\bar{\chi}i\partial\!\!\!/\chi - \frac{1}{2}(W'[\phi])^2 - \frac{1}{2}\bar{\chi}\chi W''[\phi]\,, \tag{2.159}$$

where ϕ is a bosonic real field and χ is majorana spinor which, with the following choice of the γ matrices

$$\gamma^0 = c\begin{pmatrix} 0 & -i \\ i & 0 \end{pmatrix}, \qquad \gamma^1 = \begin{pmatrix} 0 & i \\ i & 0 \end{pmatrix}, \qquad \bar{\chi} = \chi^\dagger\gamma^0 c^{-1}\,, \tag{2.160}$$

can be chosen to have real components

$$\chi = \begin{pmatrix} \chi^+ \\ \chi^- \end{pmatrix}, \qquad \chi^\pm \text{ real fields } . \tag{2.161}$$

In Eq. (2.159) $W[\phi]$ is an analytic potential. It is immediate to see that, if in the above action we choose $W[\phi] = \frac{4mc^3}{16\kappa}\cosh(c^{-1}4\sqrt{\kappa}\phi/2)$, the SShG action (2.157) is readily recovered. In the perspective of taking the NR limit, we restore c in the definition of the Minkowski metric

$$\eta^{\mu\nu} = \begin{pmatrix} c^{-2} & 0 \\ 0 & -1 \end{pmatrix} . \tag{2.162}$$

Supersymmetric actions, even more general than the one given above and with larger supersymmetries, can be efficiently generated with the method of superfields. An extensive discussion of the beautiful and elegant superspace formalism is beyond our current purposes, that is focused on the integrability aspects rather than on the supersymmetric ones. However, the interested reader can refer to [252, 253] for a clear and complete discussion of the subject.

Actions in the form (2.159) have two conserved Hermitian supercharges [254], which are linear in the fermionic fields

$$Q_\pm = \frac{1}{c}\int \mathrm{d}x\, \left(\frac{1}{c}\partial_t\phi \pm \partial_x\phi\right)\chi^\mp \mp W'(\phi)\chi^\pm \ . \tag{2.163}$$

Their relevant commutators/anticommutators are easily computed

$$\{Q_\pm, Q_\pm\} = \frac{2}{c}H \pm 2P, \qquad \{Q_+, Q_-\} = 0, \qquad [H, Q_\pm] = 0, \qquad [P, Q_\pm] = 0\ , \tag{2.164}$$

where H and P are, respectively, the Hamiltonian and the momentum generator, i.e. H, P, $Q_\pm$ form the $\mathcal{N} = 1$ superalgebra with zero central charge [252]. An additional comment is due: the absence of the central charge, i.e. the fact the $\{Q_+, Q_-\}$ vanishes, is true if the potential $W[\phi]$ does not sustain solitonic excitations. In fact, if topologically charged excitations are instead allowed, the aforementioned anticommutator does not vanish and it is equal to the topological charge [254]. Here, since we are ultimately interested in the SShG model, we are in the simpler situation in which topological excitations are absent, thus we have to consider the algebra given in Eq. (2.164).

SUSY can be equivalently implemented in terms of infinitesimal transformations generated by the supercharges

$$\delta_\pm\phi = [Q_\pm, \phi] = -i\chi^\mp, \quad \delta_\pm\chi^\mp = \{Q_\pm, \chi^\mp\} = \frac{1}{c}\partial_t\phi \pm \partial_x\phi, \quad \delta_\pm\chi^\pm = \{Q_\pm, \chi^\pm\} = \mp W'[\phi] \ , \tag{2.165}$$

and it is easy to check that such an infinitesimal transformation is indeed a symmetry for the action, $\delta S_{\text{SUSY}} = 0$.

The presence of SUSY in the SShG plays a key role in the determination of the exact scattering matrix of the system, since this new symmetry provides extra constraints on the scattering matrix, that must be added to those coming from the unitarity and Yang Baxter conditions. In the SShG model bound states and topological excitations are absent and the particle content of the model is the same as the one guessed from perturbation theory, i.e. a bosonic and fermionic species of degenerated mass. Of course, perturbative effects dress the bare mass that appears in the action, but supersymmetry ensures the equality of the two renormalized masses. Consider now a bosonic and a fermionic single particle states $|b(\theta)\rangle$ and $|f(\theta)\rangle$, the action of the supercharges $Q_\pm$ on these states can be readily worked out imposing they send a boson into a fermion

$$Q_\pm |b(\theta)\rangle \propto |f(\theta)\rangle \,, \qquad Q_\pm |f(\theta)\rangle \propto |b(\theta)\rangle \ , \tag{2.166}$$

while the correct prefactors follow as soon as we impose the superalgebra (2.164), leading to [80]

$$Q_+ |b(\theta)\rangle = e^{i\pi/4}\sqrt{Mc}\, e^{\theta/2} |f(\theta)\rangle \,, \qquad Q_- |b(\theta)\rangle = ie^{i\pi/4}\sqrt{Mc}\, e^{-\theta/2} |f(\theta)\rangle \ , \tag{2.167}$$

$$Q_+ |f(\theta)\rangle = e^{-i\pi/4}\sqrt{Mc}\, e^{\theta/2} |b(\theta)\rangle \,, \qquad Q_- |f(\theta)\rangle = -ie^{-i\pi/4}\sqrt{Mc}\, e^{-\theta/2} |b(\theta)\rangle \ , \tag{2.168}$$

where M is the renormalized mass of the model. It must be said that in the above transformations there is a certain amount of freedom, since we can redefine the phases in the fermionic and bosonic states as we wish: the choice of $e^{i\pi/4}$ has been made to match the usual mode splitting of perturbation theory. The action of the supercharges over one-particle states naturally generalizes to multiparticle states: since the charges are local, they act additively on the multiparticle states. However, because of their fermionic nature, we get an extra minus sign each time we move across a fermionic particle

$$Q_\pm^{(n)} = Q_\pm^{(1)} \otimes 1 \otimes 1 \otimes ... + Q_F \otimes Q_\pm^{(1)} \otimes 1 \otimes ... + Q_F \otimes Q_F \otimes Q_\pm^{(1)} \otimes ... \ , \tag{2.169}$$

where $Q_\pm^{(n)}$ is the supercharge acting on the n particles Hilbert space (obtained as tensor product of the one particle spaces), $Q_\pm^{(1)}$ is the supercharge acting on the one particle states and

$$Q_F |b(\theta)\rangle = |b(\theta)\rangle \,, \qquad Q_F |f(\theta)\rangle = - |f(\theta)\rangle \tag{2.170}$$

is the fermion parity operator.

Because of supersymmetry, the scattering matrix is strongly constrained [80]. In particular the scattering matrix of SShG has been computed in [81, 233] and a convenient basis to choose is $\{|bb\rangle, |ff\rangle, |bf\rangle, |fb\rangle\}$

$$S_{\text{SShG}}(\theta) = Y(\theta) \begin{pmatrix} 1 - \frac{2i\sin\alpha\pi}{\sinh\theta} & -\frac{i\sin\alpha\pi}{\cosh\frac{\theta}{2}} & 0 & 0 \\ -\frac{i\sin\alpha\pi}{\cosh\frac{\theta}{2}} & -1 - \frac{2i\sin\alpha\pi}{\sinh\theta} & 0 & 0 \\ 0 & 0 & -\frac{i\sin\alpha\pi}{\sinh\frac{\theta}{2}} & 1 \\ 0 & 0 & 1 & -\frac{i\sin\alpha\pi}{\sinh\frac{\theta}{2}} \end{pmatrix} \ , \tag{2.171}$$

$$Y(\theta) = \frac{\sinh(\theta/2)}{\sinh(\theta/2) + i\sin(\alpha\pi)} \exp\left[i \int_0^\infty \frac{\mathrm{d}t}{t} \frac{\sinh(t(1-\alpha))\sinh(t\alpha)}{\cosh t \cosh^2(t/2)} \sin(t\theta/\pi) \right] \quad . \tag{2.172}$$

The parameter α is linked to the bare coupling of the action as

$$\alpha = \frac{c^{-1}16\kappa}{16\pi + c^{-1}16\kappa} \quad . \tag{2.173}$$

The scattering matrix exhausts the basic information we need in order to take the NR limit of SShG, but we should first at least mention the generalities of its NR counterpart, presented in Eq. (2.158). As we already mentioned, this NR model is integrable and its particle content consists in a bosonic species and a fermionic one, as it is clear from the Hamiltonian: since the interaction is repulsive, bound states are absent. Besides being integrable, the model is also supersymmetric. However, the supersymmetry in this NR model is slightly different from its relativistic counterpart: with the same notation used in Eq. (2.158) we define the non-hermitian NR supercharge q

$$q = \int \mathrm{d}x \, \Psi^\dagger \psi \quad . \tag{2.174}$$

As it is clear, q is a fermionic operation that simply replaces a boson with a fermion at the same position, the Hermitian conjugate $q^\dagger$ does the opposite operation. A simple calculation shows that both q and $q^\dagger$ are indeed symmetries for the Hamiltonian (2.158). Unlike the relativistic case, the algebra of $q, q^\dagger$ no longer involves the Hamiltonian and the momentum, but rather the total number of particles

$$\{q, q\} = 0, \qquad \{q^\dagger, q\} = \int \mathrm{d}x \left(\Psi^\dagger \Psi + \psi^\dagger \psi \right) \quad . \tag{2.175}$$

On the one particle asymptotic states the action of the supercharge is far easy, because if a boson is present it replaces it with a fermion, otherwise it annihilates the state

$$q\,|b(k)\rangle = |f(k)\rangle\,, \qquad q\,|f(k)\rangle = 0 \ , \tag{2.176}$$

while $q^\dagger$ exchanges the role of the fermion and of the boson. On multiparticle states, the non relativistic supercharges q and $q^\dagger$ act as their relativistic cousins, i.e. as (2.169). The two-body scattering matrix of the NR model is far simpler to be derived with respect to the SShG case, since the two-body eigenfunctions (and even the many-body one through the coordinate Bethe Ansatz) can be explicitly found [242, 244] and from them we read the scattering matrix. In the same basis we used for the relativistic scattering matrix, but using the non relativistic rapidities, it states

$$S(\lambda) = \begin{pmatrix} \frac{\lambda - i2m\kappa}{\lambda + i2m\kappa} & 0 & 0 & 0 \\ 0 & -1 & 0 & 0 \\ 0 & 0 & \frac{-i2m\kappa}{\lambda + i2m\kappa} & \frac{\lambda}{\lambda + i2m\kappa} \\ 0 & 0 & \frac{\lambda}{\lambda + i2m\kappa} & \frac{-i2m\kappa}{\lambda + i2m\kappa} \end{pmatrix} . \tag{2.177}$$

Taking the NR limit

After this basic introduction to the SShG model and to its NR counterpart, we proceed now in taking the NR limit and show that one model is sent into the other. As usual, the identification is twofold: we firstly analyze the NR limit of the exact scattering matrix and recognize the latter to match with that of the NR model (2.158). This simple calculation indicates the correct path for

obtaining the limit: while c is sent to infinite we should simultaneously take the small coupling limit. Indeed, this is implicit in the parametrization we chose for the interaction. Indeed, it is immediate to find the NR scattering matrix (2.177) as the limit of the relativistic scattering matrix (2.171), provided as usual $\theta \simeq \lambda/(mc)$.

Besides the scattering matrix, we can obtain the NR limit of the supercharges analyzing their action on the one-particle states (2.167), (2.168) and (2.176). In particular, we can identify

$$\lim_{\text{NR}} \frac{e^{-i\pi/4}Q_+ + ie^{-i\pi/4}Q_-}{2\sqrt{mc}} = q \ . \tag{2.178}$$

Of course, besides the limit of the scattering matrix, understanding the mapping at the level of the dynamics is highly desirable. The most direct way to get the NR limit is to proceed from the (normal ordered) equations of motion of the model, but the preliminary step is to correctly identify the NR fields starting from the relativistic ones. For what it concerns the bosons, we can reside to the same mode-splitting (2.66) and an analogue operation must be done for the fermionic fields. The correct splitting is

$$\chi^+(t,x) = -\sqrt{\frac{c}{2}}\left(e^{imc^2t}e^{i\pi/4}\Psi^\dagger(t,x) + e^{-imc^2t}e^{-i\pi/4}\Psi(t,x)\right) \ , \tag{2.179}$$

$$\chi^-(t,x) = i\sqrt{\frac{c}{2}}\left(e^{imc^2t}e^{i\pi/4}\Psi^\dagger(t,x) - e^{-imc^2t}e^{-i\pi/4}\Psi(t,x)\right) \ . \tag{2.180}$$

It is an immediate check to verify that the canonical anti-commutation rules for the Majorana fermions

$$\{\chi^\pm(t,x),\chi^\pm(t,y)\} = c\,\delta(x-y), \qquad \{\chi^\pm(t,x),\chi^\mp(t,y)\} = 0 \ , \tag{2.181}$$

ensure that Ψ and $\Psi^\dagger$ obeys the NR anticommutation rules.

In order to extract the NR dynamics of the ψ and Ψ fields we proceed through the Heisenberg equations of motion, normal ordered with respect to the NR field (that are directly associated to the mode expansion of the free part of the relativistic action)

$$\left(i\gamma^\nu\partial_\nu - mc \ :\cosh(c^{-1}2\sqrt{\kappa}\phi):\right)\chi = 0 \ , \tag{2.182}$$

$$\partial_\mu\partial^\mu\phi = -:\left(\frac{mc^2}{4\sqrt{\kappa}}\right)^2 c^{-1}4\sqrt{\kappa}\sinh(c^{-1}4\sqrt{\kappa}\phi): -\sqrt{\kappa}m:\sinh(c^{-1}2\sqrt{\kappa}\phi)\bar{\chi}\chi: \ . \tag{2.183}$$

As a matter of fact, rather than Eq. (2.182), it is much more convenient to consider a second order differential equation, applying $\left(-i\gamma^\mu\partial_\mu - mc\cosh(c^{-1}2\sqrt{\kappa}\phi)\right)$

$$\left(\partial_\mu\partial^\mu + m^2c^2:\cosh^2(c^{-1}2\sqrt{\kappa}\phi):+:i2m\sqrt{\kappa}\sinh(c^{-1}2\sqrt{\kappa}\phi)\gamma^\mu\partial_\mu\phi:\right)\chi = 0 \ . \tag{2.184}$$

This has the nice property of being diagonal in the fermionic field. We can now easily take the NR limit plugging in the above equations the mode expansion, then taking $c \to \infty$. For $c \to \infty$ the potentials in the equation of motion can be Taylor expanded: the oscillating terms of the mode expansion take care of the m^2c^2 divergent terms that appear Taylor expanding the above equations of motion. After this cancellation, we are left with finite quantities and oscillating terms. Matching then the fast oscillating phases finally leads to the desired NR equation of motion, similarly to what we did for the Bullogh-Dodd and the Toda models: here we do not repeat the same calculations, but just report the result

$$i\partial_t\Psi^\dagger = \frac{\partial_x^2\Psi^\dagger}{2m} - 2\kappa\psi^\dagger\psi\Psi^\dagger, \qquad i\partial_t\psi^\dagger = \frac{\partial_x^2\psi^\dagger}{2m} - 2\kappa\psi^\dagger\psi^\dagger\psi - 2\kappa\psi^\dagger\Psi^\dagger\Psi \ . \tag{2.185}$$

These equations of motion are exactly those that can be derived from the NR Hamiltonian (2.158), consistently with what we already knew from the scattering matrix. With the NR limit of the dynamics, we conclude the identification of Eq. (2.158) as the proper NR limit of the SShG model.

2.3.5 The Gross Neveu model and its non relativistic limit

The Gross Neveu (GN) model is a purely fermionic IQFT [78, 231, 232] which is based on N majorana spinors $\chi_i(x,t)$, $i = 1, 2, \dots N$ and with action

$$\mathcal{S}_{\text{GN}} = \int \mathrm{d}x\mathrm{d}t \sum_{j=1}^{N} \frac{1}{2}\bar{\chi}_j i\partial\!\!\!/ \chi_j + \frac{\beta}{N}\left(\sum_{j=1}^{N}\bar{\chi}_j\chi_j\right)^2 . \tag{2.186}$$

Similarly to the $\mathcal{O}(N)$ non linear sigma model of Section 2.3.3, the proper NR limit is attained $c, N \to \infty$ but c/N finite and the GN model reduces to a multicomponent Lieb Liniger model with fermionic particles [235, 236]

$$H^{\text{NR}}_{\text{GN}} = \int dx \left[\sum_j \frac{\partial_x \Psi_j^\dagger \partial_x \Psi_j}{2m} - \kappa \sum_{j,j'} \Psi_j^\dagger \Psi_{j'}^\dagger \Psi_{j'} \Psi_j\right] , \tag{2.187}$$

where Ψ_j are independent non relativistic fermionic fields. In the above summations, we discarded the upper bound of the indexes on purpose: in the NR limit, the GN model describes at once all the possible numbers of different species, as it happened in the $\mathcal{O}(N)$ non linear sigma model.

Despite the absence of an explicit mass term in the action, a mass is dynamically generated and therefore the fermions χ_i are effectively massive [231]. For this reason, the use of naïve perturbation theory is problematic. In order to control the qualitative and quantitative features of the GN model is instead better to use the large N expansion techniques, by means of which we are able to recognise GN as an asymptotically free theory with a certain number of bound states [231, 255]. In addition to these features, the GN model has also been identified to be integrable [232], and the scattering matrix of the elementary particles [78] is

$$S^{cd}_{ab}(\theta) = \delta^b_a \delta^d_c S^{(1)}(\theta) + \delta^d_a \delta^c_b S^{(2)}(\theta) + \delta^c_a \delta^d_b S^{(3)}(\theta) , \tag{2.188}$$

where the amplitudes

$$S^{(3)}(\theta) = -\frac{1}{N-2}\frac{i2\pi}{\theta}S^2(\theta), \qquad S^{(1)}(\theta) = -\frac{1}{N-2}\frac{i2\pi}{i\pi-\theta}S^2(\theta), \qquad S^{(2)}(\theta) = U(\theta)U(i\pi-\theta) \tag{2.189}$$

are parameterised in terms of Γ functions

$$U(\theta) = \frac{\Gamma\left(-\frac{1}{N-2} - i\frac{\theta}{2\pi}\right)\Gamma\left(\frac{1}{2} - i\frac{\theta}{2\pi}\right)}{\Gamma\left(\frac{1}{2} - \frac{1}{N-2} - i\frac{\theta}{2\pi}\right)\Gamma\left(-i\frac{\theta}{2\pi}\right)} . \tag{2.190}$$

Note that the scattering amplitudes above are completely independent from the coupling constant β of the GN model: as a matter of fact, due to the mass transmutation, the coupling of the four-fermions interaction in the GN action enters in all the physical quantities simply through the renormalised mass m, that can be equivalently used to parameterise the theory [78, 231, 255]. Similarly to the $\mathcal{O}(N)$ non linear sigma model analyzed in Section 2.3.3, a non trivial non-relativistic limit is attained letting $c, N \to \infty$, but N/c constant. At the level of dynamics, the limit can be properly studied by mean of the large N expansion in a similar fashion: we avoid

to repeat such a similar computation (but the reader can refer to Ref. [2]) and directly study the limit of the scattering matrix (as usual $\theta \simeq \lambda/(mc)$)

$$\lim_{\rm NR} S_{ab}^{cd} = \delta_a^d \delta_b^c \frac{\lambda}{\lambda - i2\pi mcN^{-1}} + \delta_a^c \delta_b^d \frac{-i2\pi mcN^{-1}}{\lambda - i2\pi mcN^{-1}} \ , \tag{2.191}$$

This scattering matrix is in perfect agreement with that of the candidate NR model in Eq. (2.187), provided we choose $\kappa = \pi c N^{-1}$, that is kept constant in the NR limit. Note that the presence of bound states in the GN model is reflected in the attractive interaction in (2.187).

2.3.6 The SUSY Non Linear Sigma model and its non relativistic limit

The last model we consider is the supersymmetric non-linear sigma model (SNLS) [79, 234], that is integrable and supersymmetric. Its action contains an equal number of real bosonic fields and majorana spinors

$$\mathcal{S}_{\rm SNLS} = \int {\rm d}x{\rm d}t \ \sum_j \frac{1}{2}\partial_\mu \phi_j \partial^\mu \phi_j + \frac{1}{2}\sum_j \bar{\chi}_j i\partial\!\!\!/ \chi_j + \frac{\beta}{N}\left(\sum_j \bar{\chi}_j \chi_j\right)^2 \ , \tag{2.192}$$

subjected to the constraints

$$\sum_j \phi_j^2 = \frac{N}{8}\beta^{-1}, \qquad \sum_j \phi_j \chi_j = 0 \ . \tag{2.193}$$

As it is clear from its action, the SNLS lies in between the Gross-Neveu model and the non-linear sigma model. Indeed, the non-relativistic limit reflects this fact, with the corresponding Hamiltonian given by

$$H^{\rm NR}_{\rm SNLS} = \int {\rm d}x \ \sum_j \frac{\partial_x \psi_j^\dagger \partial_x \psi_j}{2m} + \sum_j \frac{\partial_x \Psi_j^\dagger \partial_x \Psi_j}{2m} + \kappa \sum_{j,j'} \left(\psi_j^\dagger \psi_{j'}^\dagger \psi_{j'} \psi_j - \Psi_j^\dagger \Psi_{j'}^\dagger \Psi_{j'} \Psi_j + 2\psi_j^\dagger \Psi_{j'}^\dagger \psi_{j'} \Psi_j\right) \ , \tag{2.194}$$

where ψ_i and Ψ_i are bosonic and fermionic fields respectively. This model is a supersymmetric mixture equally suspended between the NR limit of the GN model and the NR limit of the non-linear sigma model. The above non relativistic model belongs to a wider class of supersymmetric integrable models presented in [256].

Similarly to both its non-supersymmetric partners, its NR limit emerges once more from its large N expansion, which will not reported here (see Ref. [2]). We rather revert to the limit of the scattering matrix, that is most compactly expressed in a rotated basis [79]: starting from the bosonic and fermionic asymptotic states, we define the following states (without loss of generality, we can sit in the center of mass frame)

$$|S^{ab}\rangle = \frac{1}{\sqrt{\cosh\theta}}\left[\cosh\left(\frac{\theta}{2}\right)|b^a(\theta)b^b(-\theta)\rangle + \sinh\left(\frac{\theta}{2}\right)|f^a(\theta)f^b(-\theta)\rangle\right] \ , \tag{2.195}$$

$$|T^{ab}\rangle = \frac{1}{\sqrt{\cosh\theta}}\left[-\sinh\left(\frac{\theta}{2}\right)|b^a(\theta)b^b(-\theta)\rangle + \cosh\left(\frac{\theta}{2}\right)|f^a(\theta)f^b(-\theta)\rangle\right] \ , \tag{2.196}$$

$$|U^{ab}\rangle = \frac{1}{\sqrt{2}}\left[|b^a(\theta)f^b(-\theta)\rangle + |f^a(\theta)b^b(-\theta)\rangle\right], \qquad |V^{ab}\rangle = \frac{1}{\sqrt{2}}\left[|b^a(\theta)f^b(-\theta)\rangle - |f^a(\theta)b^b(-\theta)\rangle\right] \ . \tag{2.197}$$

The SUSY invariant scattering matrix is diagonal on each set of states

$$\langle S^{cd}_{\rm out}|S^{ab}_{\rm in}\rangle = \langle U^{cd}_{\rm out}|U^{ab}_{\rm in}\rangle = S_1(2\theta)\delta^{ac}\delta^{bd} + S_2(2\theta)\delta^{ab}\delta^{cd} + S_3(2\theta)\delta^{ad}\delta^{bc} \ , \tag{2.198}$$

$$\langle T^{cd}_{\text{out}}|T^{ab}_{\text{in}}\rangle = \langle V^{cd}_{\text{out}}|V^{ab}_{\text{in}}\rangle = \mathcal{T}_1(2\theta)\delta^{ac}\delta^{bd} + \mathcal{T}_2(2\theta)\delta^{ab}\delta^{cd} + \mathcal{T}_3(2\theta)\delta^{ad}\delta^{bc} \ , \tag{2.199}$$

with the following scattering amplitudes [79]

$$S_1(\theta) = \left(1 - \frac{i\sin\left(\frac{\pi}{N-2}\right)}{\sinh\left(\frac{\theta}{2}\right)}\right) S(\theta), \qquad S_2(\theta) = -\frac{2\pi i}{N-2}\frac{S_1(\theta)}{i\pi-\theta}, \qquad S_3(\theta) = -\frac{2\pi i}{N-2}\frac{S_1(\theta)}{\theta} \ , \tag{2.200}$$

$$\mathcal{T}_1(\theta) = \left(1 + \frac{i\sin\left(\frac{\pi}{N-2}\right)}{\sinh\left(\frac{\theta}{2}\right)}\right) S(\theta), \qquad \mathcal{T}_2(\theta) = -\frac{2\pi i}{N-2}\frac{\mathcal{T}_1(\theta)}{i\pi-\theta}, \qquad \mathcal{T}_3(\theta) = -\frac{2\pi i}{N-2}\frac{\mathcal{T}_1(\theta)}{\theta} \ . \tag{2.201}$$

Above we have $S(\theta) = R_1(\theta)R_1(i\pi-\theta)R_2(\theta)R_2(i\pi-\theta)$ and:

$$R_1(\theta) = \frac{\Gamma\left(\frac{1}{N-2} - \frac{i\theta}{2\pi}\right)\Gamma\left(\frac{1}{2} - \frac{i\theta}{2\pi}\right)}{\Gamma\left(-\frac{i\theta}{2\pi}\right)\Gamma\left(\frac{1}{2} + \frac{1}{N-2} - \frac{i\theta}{2\pi}\right)} \ , \tag{2.202}$$

$$R_2(\theta) = \frac{\Gamma\left(-\frac{i\theta}{2\pi}\right)}{\Gamma\left(\frac{1}{2} - \frac{i\theta}{2\pi}\right)}\prod_{l=1}^{\infty}\frac{\Gamma\left(\frac{1}{N-2} - \frac{i\theta}{2\pi} + l\right)\Gamma\left(-\frac{1}{N-2} - \frac{i\theta}{2\pi} + l - 1\right)\Gamma^2\left(-\frac{i\theta}{2\pi} + l - \frac{1}{2}\right)}{\Gamma\left(\frac{1}{N-2} - \frac{i\theta}{2\pi} + l + \frac{1}{2}\right)\Gamma\left(-\frac{1}{N-2} - \frac{i\theta}{2\pi} + l - \frac{1}{2}\right)\Gamma^2\left(-\frac{i\theta}{2\pi} + l - 1\right)} \ . \tag{2.203}$$

The two supercharges $Q_\pm$ act on the asymptotic states as those of the SShG, sending a fermion f^a in a boson b^a and vice versa: supersymmetry sends $|S\rangle$ states in $|U\rangle$ states (and the opposite) and $|T\rangle$ states in $|V\rangle$ states, but the two pairs are not mixed. This is indeed the reason why the scattering amplitudes of these states are pairwise equal.

Despite the complicated appearance, the NR limit is rather simple to be extracted and leads to a simple result. First of all, notice that in the NR limit the rotated basis reduces to

$$\lim_{\text{NR}}|S^{ab}\rangle = |s^{ab}\rangle = |b^a(\lambda)b^b(-\lambda)\rangle \, , \quad \lim_{\text{NR}}|U^{ab}\rangle = |u^{ab}\rangle = \frac{1}{\sqrt{2}}\left[|b^a(\lambda)f^b(-\lambda)\rangle + |f^a(\lambda)b^b(-\lambda)\rangle\right] \ , \tag{2.204}$$

$$\lim_{\text{NR}}|T^{ab}\rangle = |t^{ab}\rangle = |f^a(\lambda)f^b(-\lambda)\rangle \, , \quad \lim_{\text{NR}}|V^{ab}\rangle = |v^{ab}\rangle = \frac{1}{\sqrt{2}}\left[|b^a(\lambda)f^b(-\lambda)\rangle - |f^a(\lambda)b^b(-\lambda)\rangle\right] \ . \tag{2.205}$$

Letting $c \to \infty$ and $N \to \infty$, but with N/c constant, the simple result is

$$\langle s^{cd}_{\text{out}}|s^{ab}_{\text{in}}\rangle = \langle u^{cd}_{\text{out}}|u^{ab}_{\text{in}}\rangle = \frac{2\lambda}{2\lambda + i2\pi mcN^{-1}}\delta^{ac}\delta^{bd} - \frac{i2\pi mcN^{-1}}{2\lambda + i2\pi mcN^{-1}}\delta^{ad}\delta^{bc} \, , \tag{2.206}$$

$$\langle t^{cd}_{\text{out}}|t^{ab}_{\text{in}}\rangle = \langle v^{cd}_{\text{out}}|v^{ab}_{\text{in}}\rangle = \frac{2\lambda}{2\lambda - i2\pi mcN^{-1}}\delta^{ac}\delta^{bd} - \frac{i2\pi mcN^{-1}}{2\lambda - i2\pi mcN^{-1}}\delta^{ad}\delta^{bc} \, . \tag{2.207}$$

In the two lines above we can easily recognise the scattering matrix of a repulsive multicomponent Lieb-Liniger bosonic gas and that of an attractive multicomponent Lieb Liniger based on fermions [235], and it is consistent with the Hamiltonian (2.194).

2.3.7 Concluding remarks

In this section we studied galilean integrable systems by mean of proper non relativistic limits of integrable QFTs. The interest is twofold: firstly, the great imbalance in the richness of IQFTs and galilean integrable systems with local interaction needed to be investigated. Indeed, we testified an incredible loss of details passing from the relativistic to the non relativistic realm: very complicated relativistic scattering matrices reduce, in the non relativistic limit, to a few basic ingredients, which are attributable to a Lieb Liniger-like interaction. In particular, we analyzed

several bosonic models. Firstly, we addressed the Bullogh Dodd model, whose limit is still a single species Lieb Liniger model. Then, we revert to the simply-laced Toda Field Theories and the $O(N)$ non-linear sigma model, finding that in the first case we end up in a *decoupled* set of Lieb-Liniger models of different masses, while in the second case in a symmetrically *coupled* set of Lieb-Liniger models, all with the same mass and repulsive interaction. We subsequently include also fermions in our analysis, exploring the non relativistic limit of the supersymmetric Sinh Gordon model, of the Gross Neveu model and the supersymmetric $O(N)$ sigma model: again, mixtures of bosons and fermions with contact pairwise interactions have been found. Among the latter, the resulting non relativistic limit of the SUSY sigma model allows for tunneling among the several species. As already mentioned at the beginning of the section (see Eq. (2.75) and the discussion below), this lack of variety is due to a combination of *i)* strictly local interactions and *ii)* integrability. Indeed, while in relativistic models virtual processes are allowed, any term in the Taylor expansion of the local interaction in galilean invariant models is associated with actual scattering processes: the factorization of many-body scattering matrices into two-body amplitudes forcefully allows only pairwise interactions in the local potential.

The second motivation for our analysis resides in the possibility of using the techniques proper of the relativistic realm in addressing the non relativistic models. Indeed, this idea already led to great achievements in computing correlation functions in the Lieb Liniger model, seen as the non relativistic limit of the Sinh Gordon. In principle, passing through the relativistic model we analyzed, we could study the multi-species generalizations of the Lieb Liniger model, which are experimentally relevant.

However, a great obstruction in fulfilling such a program is the great difficulty in computing the relativistic form factors beyond the few-particle sector: this is unavoidable aiming to a complete study of galilean systems. An important exception is the Sinh Gordon model, where all the needed form factors are known [221] and this gave access to the Lieb Liniger model through the LeClair-Mussardo expansion [85, 86]. Actually, the very recent results in the Sinh Gordon model proposed by Smirnov and Negro (see Section 2.2.1) allow for an even better understanding of the Lieb Liniger model: this is the topic of the next section.

2.4 One point correlation functions in the Lieb Liniger model

Correlation functions encode all of the information which can be experimentally extracted from a many-body quantum system and thus their computation is of primary interest. At the same time, the problem of their computation is extremely complicated from the theoretical point of view, restricting us, in general, to rely uniquely on perturbative or purely numerical methods. In this respect, the exact methods that can be built taking advantage of integrability offer an unique chance to explore strongly correlated systems. The computation of correlation functions constitute a remarkable challenge, which has attracted a constant theoretical effort over the past fifty years [53, 257–259]. Classical studies have in particular focused on ground-state and thermal correlations, and joint efforts have led to spectacular results, for example in the case of prototypical interacting spin models such as the well-known Heisenberg chain [260–278].

For what it concerns the Lieb Liniger model, several results have already been obtained in the ground-state [279–290] and at thermal equilibrium [291–300], the problem of computing its experimentally measurable correlation functions [28, 30–32, 301–303] for generic macrostates of the system still challenges the community. Until recently, even the simplest one-point functions appeared to be an open issue in the case of generic excited states. Even more urgent is the question on the *full counting statistics* of local observables, most prominently for the particle-number fluctuations. Indeed, the latter provides fundamental information on the quantum fluctuations of the system, and can also be probed experimentally [38, 92–94, 301, 302]. Yet, no theoretical prediction for this quantity, not even approximate, was available in the existing literature for the

Lieb-Liniger model. More generally, the full counting statistics of local observables in and out of equilibrium have been considered in many studies [304–319], even though analytical results in integrable systems have been provided only in a handful of cases [320–326].

In this perspective, recognizing the Lieb Liniger model as the non relativistic limit of the Sinh Gordon model Ref. [85, 86] has been an important breakthrough. In turn, one-point functions in this relativistic field theory can be obtained by means of the LeClair-Mussardo series [87], which was exploited in Ref. [85, 86] to derive explicit formulas in the Lieb-Liniger gas for the one point functions $\langle(\psi^\dagger)^K(\psi)^K\rangle$. The ideas introduced in [85, 86] led to exact closed expressions for the experimentally relevant pair and three-body correlations [88], by mean of a brute force resummation of the LeClair-Mussardo expansion. Importantly, these results hold for arbitrary excited states, since the LeClair-Mussardo series itself was proven to be valid in general and not only for ground and thermal states [218].

The findings of [85, 86] were later recovered and generalized by Pozsgay in Ref. [89]. By exploiting a scaling limit of the XXZ Heisenberg chain to the Lieb-Linger gas [327, 328], exact multiple-integral formulas were obtained for the generic K-body one-point function.

A natural question is whether or not similar formulas could be derived for the other models analyzed so far: sadly, the computation of form factors is incredibly difficult. While computing few-body form factors in relativistic integrable field theories already represent a remarkable achievement, the story is different in the non relativistic world, where few-body form factors can be computed thanks to the explicit wavefunction given by the coordinate Bethe Ansatz [53]. In practice, the NR limits are useful in computing one point correlation functions only if form factors are known for multi-particles excited states: to the best of our knowledge, such a difficult quest has been achieved only in the Sinh Gordon case [221].

However, the already mentioned results on the correlation functions in the Sinh Gordon are not the end of the story. Indeed, despite their conceptual importance, multiple-integral representations are not suitable for numerical evaluation: compact, single integral expressions where reached for $K = 2, 3, 4$, leaving the case $K > 4$ intractable at a practical level.

In this Section, following Ref. [3, 4], we make a step forward and provide general closed formulas for the K-body one-point functions in the Lieb-Liniger model which are sufficiently simple to be easily evaluated numerically. Their form differs from the one found in [89], and only involves simple integrals. Our strategy follows the method introduced in [85, 86]: however, while the starting point of [85, 86] was provided by the LeClair-Mussardo series, we consider the alternative Negro-Smirnov formula presented in Section 2.2.1. In particular, in addition to the analysis of correlations in thermal and GGE states, we also discuss the implications of our findings for the full counting statistics of the number of particles in a small interval. Finally, we mention that within the framework of the recently introduced Generalized Hydrodynamics (GHD) [159, 160] our result allows for an efficient computation of correlation functions on an Eulerian scale [174, 175] (see also discussion in Section 3.4). We do not report such a calculation here, but the reader can refer to Ref. [4]. For the sake of clarity, we first collect the results and then present their derivation.

2.4.1 Summary of the results

Our main result is a general formula for the thermodynamic limit of one-point functions in the Lieb-Liniger model

$$\langle(\psi^\dagger(x))^K\psi^K(x)\rangle = (K!)^2\,(m\kappa)^K \sum_{\sum_j jn_j=K}\prod_j\left[\frac{1}{n_j!}\left(\frac{\mathcal{B}_j}{2\pi m\kappa}\right)^{n_j}\right]. \tag{2.208}$$

Above, with $\langle ...\rangle$ we indicate the expectation value over a GGE identified by the root density ρ. The sum is taken over all the possible integers $n_j \geq 1$ such that the constraint $\sum_{j=1}^{\infty} jn_j = K$ is

satisfied; the coefficients $\mathcal{B}_j$ are defined as

$$\mathcal{B}_j = \frac{1}{j}\int_{-\infty}^{+\infty} \mathrm{d}\lambda\, \vartheta(\lambda) b_{2j-1}(\lambda)\,, \tag{2.209}$$

where the functions $b_j(\lambda)$ satisfy the following set of integral equations

$$b_{2n}(\lambda) = \int_{-\infty}^{+\infty} \frac{\mathrm{d}\mu}{2\pi}\, \vartheta(\mu)\left\{\varphi(\lambda-\mu)[b_{2n}(\mu) - b_{2n-2}(\mu)] + \Gamma(\lambda-\mu)[2b_{2n-1}(\mu) - b_{2n-3}(\mu)]\right\}\,, \tag{2.210}$$

$$b_{2n+1}(\lambda) = \delta_{n,0} + \int_{-\infty}^{+\infty} \frac{\mathrm{d}\mu}{2\pi}\, \vartheta(\mu)\left\{\Gamma(\lambda-\mu) b_{2n}(\mu) + \varphi(\lambda-\mu)[b_{2n+1}(\mu) - b_{2n-1}(\mu)]\right\}, \tag{2.211}$$

with the convention $b_{j\leq 0}(\lambda) = 0$ and

$$\varphi(\lambda) = \frac{4m\kappa}{\lambda^2 + (2m\kappa)^2}\,, \qquad \Gamma(\lambda) = \frac{2\lambda}{\lambda^2 + (2m\kappa)^2}\,. \tag{2.212}$$

Notice that $\varphi(\lambda)$ is the same kernel entering in the TBA equations of Section 2.1.2, namely $\varphi(\lambda) = -i\partial_\lambda \log S(\lambda)$ with $S(\lambda)$ the Lieb-Liniger scattering matrix (2.58). Eq. (2.208) is most easily encoded in the following generating function

$$1 + \sum_{n=1}^{\infty} X^n \frac{\langle (\psi^\dagger)^n (\psi)^n\rangle}{(n!)^2 (m\kappa)^n} = \exp\left(\frac{1}{2\pi m\kappa}\sum_{n=1}^{\infty} X^n \mathcal{B}_n\right)\,, \tag{2.213}$$

where we omitted the spatial dependence of the bosonic fields. Comparison between the Taylor expansion in X on both sides gives (2.208).

We note the hierarchical structure of the integral equations above. Indeed, each equation is a linear integral equation for a given unknown function $b_i(\lambda)$, where $b_{j<i}(\lambda)$ only contribute as source terms. In this perspective, obtaining the functions $b_{j\leq 2K-1}(\lambda)$ (and thus the K^{th} one point function in the Lieb Liniger gas), boils down to solving recursively $2K-1$ linear integral equations. The latter can be easily solved for example by a simple iterative scheme.

It is useful to compare our formulas with existing results in the literature. As we previously discussed, efficient integral formulas were already known for $\mathcal{O}_K$ with $K = 2, 3, 4$ [88, 89]. These are also expressed in terms of the solution to simple integral equations, but their form differs from the one we found. It is non-trivial to see the equivalence between the two, which is most easily established numerically. In this respect, we extensively tested that our formulas give the same results of those of [88, 89] for $K = 2, 3, 4$ and different macrostates. Furthermore, it is possible to show the equivalence by means of a perturbative analytical expansion in the filling function $\vartheta(\lambda)$ (see Ref. [4]). For higher K and before our result, we could reside either on the LeClair-Mussardo expansion [87], or on the multiple integral representation derived in [89], the latter being equivalent to a resummation of the whole LeClair-Mussardo series. However, the presence of multiple integrals makes the computation of these expressions unfeasible on a practical level.

In summary, not only our formulas provide an exact representation of the one-point correlations in arbitrary macrostates, but are also entirely expressed in terms of simple integrals of the solution to linear integral equations. This makes them particularly convenient for numerical evaluation, providing a full solution to the problem of computing one-point functions in the Lieb-Liniger model.

2.4.2 One-point functions in the Lieb-Liniger model

The Lieb Liniger correlation functions are recovered from those of the Sinh Gordon model (see Section 2.2.3), once the proper normal ordering is considered. For the sake of convenience, we recall Eq. (2.72) which reads

$$\lim_{\rm NR} : \phi^{2K+1} := 0, \qquad \lim_{\rm NR} : \phi^{2K} := \binom{2K}{K} \frac{1}{(2m)^K} (\psi^\dagger)^K (\psi)^K . \tag{2.214}$$

The normal ordering procedure requires further comments. Inserting the mode expansion (2.66) into ϕ^{2K} and using the commutation relations to obtain a normal ordered expression, we obtain two types of terms: the first one is $(\psi^\dagger)^K(\psi)^K$; the second consists of products of fields $(\psi^\dagger)^n(\psi)^n$ with $n < K$, coupled to UV-singular terms coming from equal point commutators $\delta(0)$. Of course, the output of the LeClair-Mussardo series (as well as of the Negro-Smirnov formula) refers to the renormalized fields, where UV-divergent quantities have been removed. However, it remains true that all the normal ordered fields $: \phi^{2n} :$ with $n \leq K$ contribute to the expectation value of ϕ^{2K}. In order to obtain the Lieb-Liniger one point functions from the ShG formulas presented in the previous section, the decomposition of ϕ^{2K} in normal ordered fields must be performed explicitly.

A consistent derivation is performed assuming a linear mixing between normal ordered and non-normal ordered fields [85, 86]

$$: \phi^{2K} := \phi^{2K} - \sum_{n=1}^{K-1} \left(\frac{\kappa}{4}\right)^{(K-j)} \mathcal{N}_n^K \phi^{2n} . \tag{2.215}$$

Here the coefficients $\mathcal{N}_j^K$ can be fixed as it follows. The field ϕ^{2K} usually has non trivial matrix elements in each particle sector, namely $\langle 0|\phi^{2K}|\theta_1, ..., \theta_{n'}\rangle \neq 0$. Instead, $: \phi^{2K} :$ is required to have trivial matrix element between the vacuum and the whole $n < 2K$ particle sector

$$\langle 0| : \phi^{2K} : |\theta_1, ..., \theta_n\rangle = 0, \qquad \forall\, n < 2K . \tag{2.216}$$

Imposing this condition and employing the exact form factors of the powers of the fields, one can derive the mixing coefficients $\mathcal{N}_n^K$. In the following, we refer to the form factors of the Sinh Gordon model reviewed in Section 2.2.1. Being ultimately interested in the implications for the Lieb-Liniger model, we will work under the assumption of the NR limit $c \to \infty$, which allows us to simplify our calculations: for example, the normalization constant N entering in the expression of the form factors (2.49) simply becomes 1. The symmetric polynomials $\sigma_k^{(n)}$ (2.52) hugely simplify as well, leading to the compact result [237]

$$\det M_n(k) \to \left(\frac{\sin(2k\kappa)}{c^{-1}2\kappa}\right)^{n-1} \det\left[\binom{n}{2i-j}\right] = \left(\frac{\sin(2k\kappa)}{c^{-1}2\kappa}\right)^{n-1} 2^{n(n-1)/2}, \tag{2.217}$$

where the matrix M has been defined in Eq. (2.51). Furthermore, we obtain

$$F_{\min}\left(c^{-1}m^{-1}\lambda\right) \to \frac{\lambda}{\lambda + i2m\kappa}, \tag{2.218}$$

where $F_{\min}(\theta)$ is defined in (2.50) . Putting these terms together we obtain the non-relativistic limit of the form factor of the vertex operators $e^{kc^{-1}4\sqrt{\kappa}\phi}$ on n particle states (2.48), which reads

$$F_n^k \to c^{n/2} 2^{n(n-1)/2} \left(\frac{\sin(2k\kappa)}{\sqrt{2\kappa}}\right)^n \prod_{i<j}^{n} \frac{\lambda_i - \lambda_j}{\lambda_i - \lambda_j + i2m\kappa} . \tag{2.219}$$

The form factors of the powers of the fields can be simply obtained by means of a Taylor expansion in k of the form factors of the exponential fields. Imposing (2.216) on (2.215) immediately leads to the following constraint

$$\sum_{j=1}^{K-1} \mathcal{M}_{a,j}\mathcal{N}_j^K = \mathcal{M}_{a,K}\,, \qquad a \in \{1,...,K-1\}, \qquad \text{with } \mathcal{M}_{n,n'} = \partial_x^{2n'} \sin^{2n}(x)\Big|_{x=0}. \tag{2.220}$$

Remarkably, in the NR limit the normal ordering expression can be explicitly solved and the fields ϕ^{2K} expressed in terms of the normal ordered ones

$$\phi^{2K} = \sum_{j=1}^{K} \frac{\mathcal{M}_{j,K}}{(2j)!} \left(\frac{\kappa}{4}\right)^{K-j} :\phi^{2j}: \,. \tag{2.221}$$

The normal ordering procedure acquires a very simple form when applied to the vertex operators. Indeed, we have

$$\lim_{\rm NR}\langle e^{4q\sqrt{\kappa}\phi}\rangle = 1+\sum_{j=1}^{\infty}\frac{(4q\sqrt{\kappa})^{2j}}{(2j)!}\lim_{\rm NR}\langle\phi^{2j}\rangle = 1+\sum_{n=1}^{\infty}\left(\sum_{j=n}^{\infty}\frac{(4q\sqrt{\kappa})^{2j}}{(2j)!}\mathcal{M}_{n,j}\left(\frac{\kappa}{4}\right)^{j}\right)\left(\frac{\kappa}{4}\right)^{-n}\lim_{\rm NR}\langle:\phi^{2n}:\rangle\,. \tag{2.222}$$

Here q is kept constant in the NR limit (the choice of such a normalization will soon be clear) and we made use of Eq. (2.221). Now, notice that

$$\sum_{j=n}^{\infty}\frac{(4q\sqrt{\kappa})^{2j}}{(2j)!}\left(\frac{\kappa}{4}\right)^{j}\mathcal{M}_{n,j} = \frac{1}{(2n)!}\sum_{j=n}^{\infty}\frac{(4q\sqrt{\kappa})^{2j}}{(2j)!}\left(\frac{\kappa}{4}\right)^{j}\partial_x^{2j}\sin^{2n}(x)\Big|_{x=0} = \frac{\sin^{2n}(2q\kappa)}{(2n)!}\,, \tag{2.223}$$

which allows us to rewrite the NR limit of the vertex operator in the simple form

$$\lim_{\rm NR}\langle e^{4q\sqrt{\kappa}\phi}\rangle = \lim_{\rm NR}\left\langle :e^{\frac{2}{\sqrt{\kappa}}\sin(2q\kappa)\phi}:\right\rangle = 1+\sum_{n=1}^{\infty}\frac{\sin^{2n}(2q\kappa)}{(2n)!}\left(\frac{\kappa}{4}\right)^{-n}\lim_{\rm NR}\langle:\phi^{2n}:\rangle\,. \tag{2.224}$$

By means of Eq. (2.72), we can finally establish the following relation between the NR limit of vertex operators and the one point functions in the Lieb-Liniger model

$$\lim_{\rm NR}\langle e^{4q\sqrt{\kappa}\phi}\rangle = 1+\sum_{n=1}^{\infty}\Big(1-\cos(4q\kappa)\Big)^{n}\frac{\langle(\psi^\dagger)^n(\psi)^n\rangle}{(n!)^2(\kappa m)^n}\,. \tag{2.225}$$

With this last compact result, we now revert to the non relativistic limit of the Negro-Smirnov formula (2.53): a limit $c\to\infty$ with k fixed of the l.h.s. leads to a trivial result. We will then follow the approach consisting in rescaling $k\to q=ck$ and subsequently take $c\to\infty$, while keeping q fixed. In this case, at first order in c^{-1} we obtain

$$\frac{\langle e^{(q+c^{-1})4\sqrt{\kappa}\phi}\rangle}{\langle e^{q4\sqrt{\kappa}\phi}\rangle} = 1+c^{-1}4\sqrt{\kappa}\lim_{c\to\infty}\left[\frac{\langle\phi e^{4q\sqrt{\kappa}\phi}\rangle}{\langle e^{4q\sqrt{\kappa}\phi}\rangle}\right]+...= 1+c^{-1}\partial_q\lim_{c\to\infty}\partial_q\log\langle e^{4q\sqrt{\kappa}\phi}\rangle+...\,, \tag{2.226}$$

where the neglected terms are higher order in the c^{-1} expansion. Note that the zeroth-order term is naturally canceled out by the r.h.s. of (2.53) and the Negro-Smirnov formula reduces to (we recall that the non relativistic limit of the filling function in the Sinh-Gordon goes to the filling in the Lieb Liniger model, which we still call ϑ for the sake of simplicity)

$$\partial_q\lim_{\rm NR}\log\langle e^{4q\sqrt{\kappa}\phi}\rangle = \frac{2}{m\pi}\int_{-\infty}^{\infty}{\rm d}\lambda\,\vartheta(\lambda)p_q^{\rm LL}(\lambda)\,, \tag{2.227}$$

where we defined

$$p_q^{\rm LL}(\lambda) = \lim_{c\to\infty}\left[\sin(4q\kappa)p_{cq}(c^{-1}m^{-1}\lambda)\right], \tag{2.228}$$

where the function $p_k(\theta)$ was defined in Eq. (2.54). From the NR limit of the integral equation satisfied by $p_k(\theta)$, we easily obtain an integral equation for $p_q^{\rm LL}(\lambda)$

$$p_q^{\rm LL}(\lambda) = \sin(4q\kappa) + \int_{-\infty}^{\infty} {\rm d}\mu\, \vartheta(\mu)\chi_q^{\rm LL}(\lambda-\mu)p_q^{\rm LL}(\mu), \qquad \chi_q^{\rm LL}(\lambda) = \frac{i}{2\pi}\left(\frac{e^{-iq4\kappa}}{\lambda+i2m\kappa} - \frac{e^{iq4\kappa}}{\lambda-i2m\kappa}\right). \tag{2.229}$$

Thanks to the fact that $\langle e^{4q\phi\sqrt{\kappa}}\rangle = 1$ for $q=0$, we can explicitly integrate eq. (2.227) and obtain an expression for the NR limit of the vertex operator

$$\lim_{\rm NR}\langle e^{4q\sqrt{\kappa}\phi}\rangle = \exp\left[\frac{2}{m\pi}\int_{-\infty}^{\infty}{\rm d}\lambda\,\vartheta(\lambda)\int_0^q {\rm d}q'\, p_{q'}^{\rm LL}(\lambda)\right]. \tag{2.230}$$

Looking at Eq. (2.225), we can immediately understand that a convenient expansion of the above relation in terms of the trigonometric functions $\sin(4\kappa q)$ and $\cos(4\kappa q)$ will ultimately allow us to reach the one point functions in the LL model. In this perspective, we rewrite the kernel $\chi_q^{\rm LL}(\lambda)$ as

$$\chi_q^{\rm LL}(\lambda) = \frac{1}{2\pi}\left[\cos(q4\kappa)\varphi(\lambda) + \sin(q4\kappa)\Gamma(\lambda)\right], \tag{2.231}$$

where φ and Γ have been defined in Eq. (2.212). As it should be clear, an iterative solution to Eq. (2.229) will naturally provide a power expansion in terms of the trigonometric functions $\sin(4q\kappa)$ and $\cos(4q\kappa)$. However, it is convenient to consider a different form of series expansion, and define the functions $A_j(\lambda)$ and $B_j(\lambda)$ as the coefficients of the series

$$\int_0^q {\rm d}q'\, p_{q'}^{\rm LL} = \frac{1}{4\kappa}\sum_{j=0}^{\infty}\sin(q\kappa 4)(1-\cos(4\kappa q))^j A_j(\lambda) + \frac{1}{4\kappa}\sum_{j=1}^{\infty}(1-\cos(4q\kappa))^j B_j(\lambda). \tag{2.232}$$

For the moment, the functions $A_j(\lambda)$ and $B_j(\lambda)$ need to be determined. The form of this series is completely general and describes an arbitrary power series in terms of the trigonometric functions $\sin(4\kappa q)$ and $\cos(4\kappa q)$. Taking the derivative with respect to q of both sides of this equation we get

$$p_q^{\rm LL}(\lambda) = \sum_{j=0}^{\infty}(1-\cos(4q\kappa))^j b_{2j}(\lambda) + \sin(q4\kappa)(1-\cos(4q\kappa))^j b_{2j+1}(\lambda), \tag{2.233}$$

where

$$b_{2j}(\lambda) = (2j+1)A_j(\lambda) - jA_{j-1}(\lambda), \qquad b_{2j+1}(\lambda) = (j+1)B_{j+1}(\lambda). \tag{2.234}$$

The set of integral equations satisfied by $b_j(\lambda)$ are readily obtained using Eq. (2.233) in the integral equation (2.229). The derivation is long but straightforward, and leads to the set of integral equations (2.210) and (2.211). Defining

$$\mathcal{A}_j = \int_{-\infty}^{\infty}{\rm d}\lambda\,\vartheta(\lambda)A_j(\lambda), \tag{2.235}$$

$$\mathcal{B}_j = \int_{-\infty}^{\infty}{\rm d}\lambda\,\vartheta(\lambda)B_j(\lambda), \tag{2.236}$$

and combining Eq. (2.225) with Eq. (2.230) we finally get

$$1+\sum_{n=1}^{\infty}\Big(1-\cos(4q\kappa)\Big)^n\frac{\langle(\psi^\dagger)^n(\psi)^n\rangle}{(n!)^2(m\kappa)^n}= \\ \exp\left(\frac{1}{2\pi m\kappa}\sum_{j=0}^{\infty}\sin(q\kappa 4)(1-\cos(4\kappa q))^j\mathcal{A}_j+\frac{1}{2\pi m\kappa}\sum_{j=1}^{\infty}(1-\cos(4q\kappa))^j\mathcal{B}_j\right). \quad (2.237)$$

For consistency, we must have $\mathcal{A}_j=0$. This can be seen analytically (see Ref. [4]) as well as numerically to high precision for different filling functions $\vartheta(\lambda)$. Setting $\mathcal{A}_j=0$ and replacing $X=1-\cos(4q\kappa)$, we finally obtain (2.213), and hence our main result Eq. (2.208).

2.4.3 Applications

In this section we present several applications of our main result (2.208). In particular, after explicitly evaluating one-point functions for different macrostates, we discuss in detail the connection between the one point correlation functions and the full counting statistics of the particle number. Finally, we combine our result with the recently introduced generalized hydrodynamics [159, 160] to analyze inhomogeneous out-of-equilibrium protocols. Our results can also be used to obtain correlation functions at the Eulerian scale [174, 175], but we do not report here the discussion which can be found in Ref. [4].

Thermal states and out-of-equilibrium protocols

In order to show the versatility of our formula (2.208), we report its explicit evaluation for different macrostates. In Fig. 2.15 we report explicit values of the correlations for thermal states $\rho=e^{-\beta H}/\mathrm{tr}[e^{-\beta H}]$ as a function of the interaction (subfigure (a)) and of the temperature (subfigure (b)). As a point of principle, we evaluated our formulas up to $n=8$ for a wide range of the parameters, showing that they are extremely suitable for numerical evaluation. Note that the correlators $g_n=\langle(\psi^\dagger)^n\psi^n\rangle/(\langle\psi^\dagger\psi\rangle)^n$ are only a function of the rescaled parameters $\gamma=\kappa/\langle\psi^\dagger\psi\rangle$ and $\tau=\beta^{-1}(\langle\psi^\dagger\psi\rangle)^{-2}$. As a non-trivial check of our formulas we see that the limit $\lim_{\gamma\to 0}g_n(\gamma)=n!$ is recovered from our numerical results [89].

As another example, we evaluated our formulas in two other physical situations. The first one is an interaction quench where the initial state is the ground state of the non-interacting Hamiltonian [113]; at large time the system reaches a steady state whose rapidity distribution functions were computed analytically in [113], allowing us to obtain the corresponding local correlators. The latter are reported in subfigure (c) of Fig. 2.15. Note in particular the different limiting behavior $\lim_{\gamma\to 0}g_n(\gamma)=1$. The second physical situation is obtained by considering two halves of an infinite system which are prepared in two thermal states $\rho=e^{-\beta_{L/R}H}/\mathrm{tr}[e^{-\beta_{L/R}H}]$ with $\beta_L=1$, $\beta_L=2$ and suddenly joined together. At large time t and distances x from the junction, time- and space-dependent quasi-stationary states will emerge [159, 160]. In particular, a local relaxation to a GGE will occur for each "ray" $\zeta=x/t$, so that local observable will display non-trivial profiles as a function of ζ [159, 160]. We refer to Section 3.4 for more details, while here we simply report in subfigure (d) of Fig. 2.15 an example of profiles for $\beta_L=0.25$ and $\beta_R=0.5$. Fig. 2.15 shows unambiguously the great versatility of our formulas, which can be easily evaluated for very different physical situations.

The full counting statistics

As one of the most interesting applications of our formulas, the knowledge of the expectation values of the one point functions $\langle(\psi^\dagger)^K(\psi)^K\rangle$ gives us access to the full counting statistics [38, 92–94] of the number of particles within a small interval, as we show in this section. Given

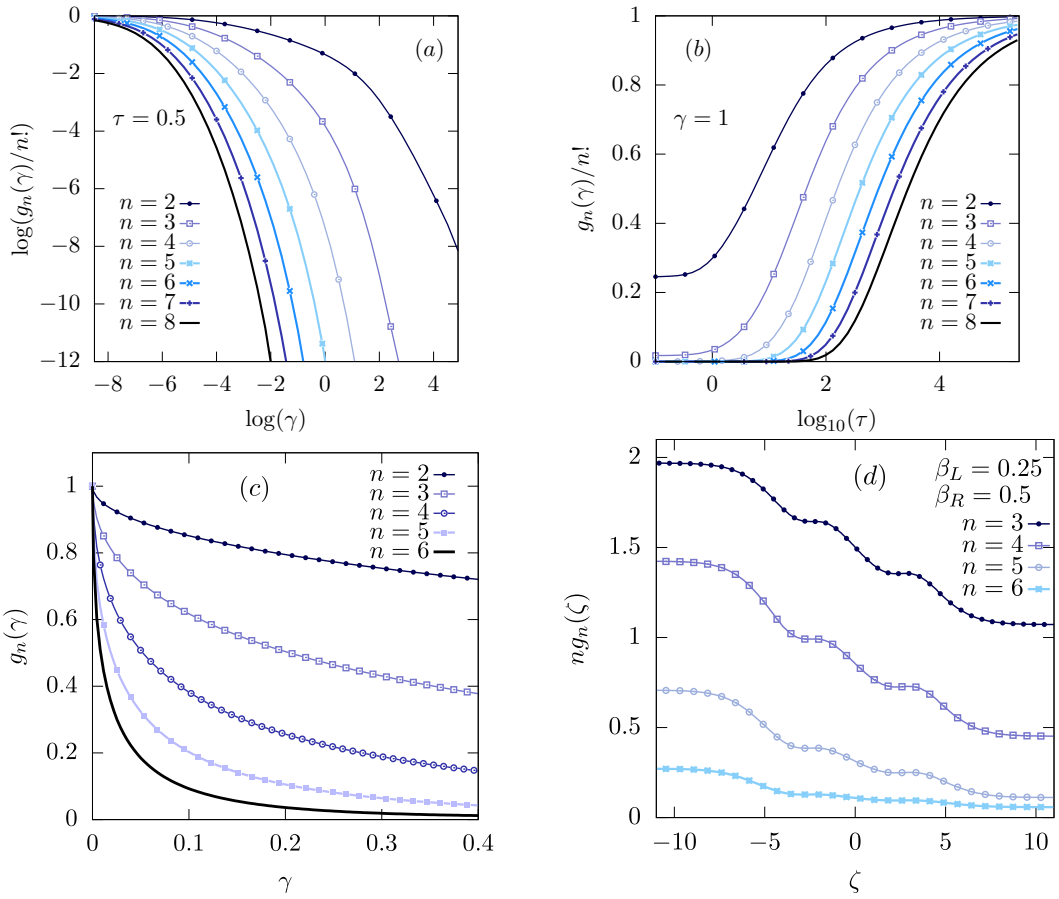

Figure 2.15: *Sunfigures* (a)*-*(b)*: the plots show the correlators* g_n *computed using Eq.* (2.208) *for thermal states* $\rho = e^{-\beta H}/\mathrm{tr}[e^{-\beta H}]$*. Subfigures* (a) *and* (b) *show the correlators as a function of the interaction* γ *and the normalized temperature* τ *respectively (cf. the main text). Subfigures* (c)*-*(d)*: local correlators on non-thermal states. Subfigure* (c)*: the plot shows the correlators* g_n *computed using Eq.* (2.208) *on the steady state reached at long times after an interaction quench where the initial state is the ground state of the non-interacting Hamiltonian [113]. Subfigure* (d)*: Profiles of* $g_n(\zeta)$ *for the partitioning protocols studied in Refs. [159, 160], cf. the main text. The two halves of the infinite systems, which are joined together at* $t = 0$ *are prepared in thermals states with inverse temperatures* $\beta_L = 0.25$*,* $\beta_R = 0.5$*. The interaction coupling is fixed to be* $\kappa = 1$*. Fig. taken from Ref. [4].*

an interval of width Δ, the mean number of particles we can measure in it is simply $\Delta\langle\psi^\dagger\psi\rangle$. However, the number of particles is a stocastic variable subjected to statistical fluctuations, and a full description of the quantum system should include the whole probability distribution of the latter, not only its mean value.

We define $\hat{N}_\Delta$ the operator which counts the number of particles within a small interval of length Δ. In second quantization, it reads

$$\hat{N}_\Delta = \int_0^\Delta \mathrm{d}x\, \psi^\dagger(x)\psi(x)\,. \tag{2.238}$$

Its spectrum include all and only positive integers, being its eigenvalues the number of particles. For this reason, we have the spectral decomposition

$$\hat{N}_\Delta = \sum_{n=0}^{\infty} n\hat{P}_n\,, \tag{2.239}$$

where $\hat{P}_n$ is the projector on the space of fixed number n of particles. Therefore, the probability of finding n particles in the interval n for a given macrostate is the expectation value $P_\Delta(n) = \langle \hat{P}_n \rangle$, which is the object we aim to compute. In this respect, our main result is

$$\lim_{\Delta \to 0} \frac{P_\Delta(n)}{\Delta^n} = \frac{\langle (\psi^\dagger)^n (\psi)^n \rangle}{n!}\,, \tag{2.240}$$

which will be derived in the following. First, it is convenient to look at the generating function $\chi(\gamma) = \langle e^{i\gamma \hat{N}_\Delta} \rangle$. Indeed, $P_\Delta(n)$ is readily recovered from its Fourier transform

$$\int_{-\infty}^{\infty} \frac{\mathrm{d}\gamma}{2\pi}\, e^{-i\gamma n'} \left\langle e^{i\gamma \hat{N}_\Delta} \right\rangle = \int_{-\infty}^{\infty} \frac{\mathrm{d}\gamma}{2\pi} \left\langle \sum_{n=0}^{\infty} e^{i\gamma(n-n')} P_n \right\rangle = \delta(n-n') P_\Delta(n)\,. \tag{2.241}$$

It is useful to express $\chi(\gamma)$ in terms of normal ordered correlation functions. This can be achieved thanks to the following identity

$$\exp\left[i\gamma \int_0^\Delta \mathrm{d}x\, \psi^\dagger(x)\psi(x) \right] =: \exp\left[\left(e^{i\gamma} - 1\right) \int_0^\Delta \mathrm{d}x\, \psi^\dagger(x)\psi(x) \right] :\,, \tag{2.242}$$

whose derivation is not hard, but it involves several passages and it is left to Ref. [4] (see also Ref. [7, 150]). Making use of a power expansion of the normal ordered exponential, we obtain

$$\begin{aligned} \int \frac{\mathrm{d}\gamma}{2\pi}\, e^{-i\gamma n} \left\langle e^{i\gamma \int_0^\Delta \mathrm{d}x\, \psi^\dagger(x)\psi(x)} \right\rangle &= \sum_{j=0}^{\infty} \frac{1}{j!} \int \frac{\mathrm{d}\gamma}{2\pi} e^{-in\gamma} \left(e^{i\gamma} - 1\right)^j \langle : \left(\int_0^\Delta \mathrm{d}x\, \psi^\dagger(x)\psi(x) \right)^j : \rangle = \\ &= \sum_{j=0}^{\infty} \frac{1}{j!} \sum_{m=0}^{j} \binom{j}{m} (-1)^{j-m} \left[\int \frac{\mathrm{d}\gamma}{2\pi}\, e^{i\gamma(m-n)} \right] \langle : \left(\int_0^\Delta \mathrm{d}x\, \psi^\dagger(x)\psi(x) \right)^j : \rangle\,. \end{aligned} \tag{2.243}$$

In each term of the series expansion, the integration in γ provides Dirac δs that constrain the support on integers values. Through a proper reorganization of the sum, we arrive at the final result

$$P_\Delta(n) = \frac{1}{n!} \left[\sum_{j=0}^{\infty} \frac{(-1)^j}{j!} \left\langle : \left(\int_0^\Delta \mathrm{d}x\, \psi^\dagger(x)\psi(x) \right)^{j+n} : \right\rangle \right]\,. \tag{2.244}$$

As it is clear, the one point functions do not determine the full counting statistics for arbitrary Δ and the whole multi-point correlators are needed. Nevertheless, in the $\Delta \to 0$ limit we can invoke the continuity of the correlators and extract the leading orders. We finally obtain

$$P_\Delta(n) = \frac{1}{n!} \Delta^n \Big(\langle (\psi^\dagger(0))^n (\psi(0))^n \rangle + \mathcal{O}(\Delta) \Big)\,, \tag{2.245}$$

from which Eq. (2.240) immediately follows. The approximation which led from Eq. (2.244) to Eq. (2.245) is clearly valid if we can truncate the series, which requires the interval to be small if compared with the density $\Delta \ll D^{-1}$; furthermore, we assumed that the correlation functions are approximately constant on a range Δ. This last condition can be estimated as $\Delta \ll \sqrt{\langle \psi^\dagger \psi \rangle / \langle \partial_x \psi^\dagger \partial_x \psi \rangle}$.

From the evaluation of Eq. (2.240), it is clear that different macrostates display very different full counting statistics for the particle fluctuations. In particular, the latter provides a lot of information of a given macrostate. For the sake of presentation, we report in Fig. 2.16 the probabilities $P_\Delta(n)$ for different thermal states up to $n = 8$.

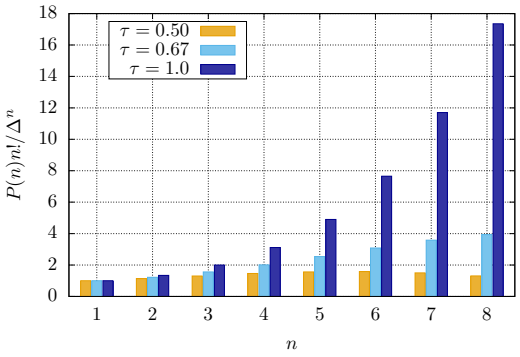

Figure 2.16: *Rescaled probability distribution for the particle number within an interval of length Δ. The plot shows results for different thermal states. The rescaled interaction is set to $\gamma = 0.1$. Fig. taken from Ref.[4].*

2.4.4 Concluding remarks

In this section we have derived analytic expressions for the n-body local correlation functions for arbitrary macrostates in the Lieb-Liniger model, by exploiting the non-relativistic limit of the ShG field theory. We present a full survey of their physical applications, which include a computation of the full counting statistics for particle-number fluctuations. We have shown that our formulas are extremely convenient for explicit numerical computations, by presenting their evaluation for several physically interesting macrostates, including thermal states, GGEs and non-equilibrium steady states arising in transport problems. Furthermore, by building upon recent results within the framework of GHD, efficient formulas for the computation of multi-point correlations at the Eulerian scale can be provided (see Ref. [4]). Complementing previous studies in the literature, our results provide a full solution to the problem of computing one-point functions in the Lieb-Liniger model.

For what it concerns the study of correlation functions through non relativistic limits, several important directions remain to be investigated. On the one hand, an interesting generalization of the LeClair-Mussardo series for non-local observables was derived in [219], and it is natural to wonder whether an appropriate non-relativistic limit could be performed to obtain analogous results also for the Lieb-Liniger gas. These would be extremely relevant in connection with cold-atom experiments. On the other hand, it is natural to wonder if results similar to the Negro-Smirnov formula can be obtained also in other models whose non relativistic limit is known.

In particular, the most natural question pertains the Sine-Gordon field theory, which is mapped onto the attractive one-dimensional Bose gas [237]. Indeed, the techniques which eventually led to the Negro-Smirnov formula in the ShG model were originally introduced in the Sine-Gordon model [329, 330]. However, in the Sine-Gordon case only zero-temperature results were achieved so far [331].

2.A Non relativistic limit of the dynamics of the Bullogh-Dodd model

In this Appendix the technical passages to extract the NR limit of the equation of motion for the Bullogh Dodd model are presented. We recall the relativistic equation of motion (2.84) in which we already dropped the unessential terms

$$\frac{1}{c^2}\partial_t^2\phi = \partial_x^2\phi - m^2c^2\phi - cm^2\frac{g}{2} : \phi^2 : -m^2\frac{g^2}{2} : \phi^3 : . \tag{2.246}$$

Actually, it is more instructive to keep arbitrary the interaction couplings and consider:

$$\frac{1}{c^2}\partial_t^2\phi = \partial_x^2\phi - m^2c^2\phi - c\frac{v_3}{2} : \phi^2 : -\frac{v_4}{3!} : \phi^3 : . \tag{2.247}$$

Notice that this equation of motion can be thought to be derived from the relativistic Lagrangian

$$\mathcal{L} = \frac{1}{2}\partial_\mu\phi\partial^\mu\phi - \frac{m^2c^2}{2}\phi^2 - c\frac{v_3}{3!} : \phi^3 : -\frac{v_4}{4!} : \phi^4 : . \tag{2.248}$$

Splitting now the field in its modes (2.66) , from the equation of motion (2.247) we write the integral equation for the NR modes:

$$\begin{aligned} i\psi^\dagger(t_0+\Delta t) = i\psi^\dagger(t_0) + \int_{t_0}^{t_0+\Delta t} \mathrm{d}t \ \Big[& e^{-i2mc^2(t-t_0)} i\partial_t\psi + \frac{1}{2m}\partial_x^2\left(\psi^\dagger + e^{-i2mc^2(t-t_0)}\psi\right) + \\ & -c\frac{v_3 e^{-imc^2(t-t_0)}}{4m\sqrt{2m}} : \left(e^{imc^2(t-t_0)}\psi^\dagger + e^{-imc^2(t-t_0)}\psi\right)^2 : \\ & -\frac{v_4 e^{-imc^2(t-t_0)}}{3!(2m)^2} : \left(e^{imc^2(t-t_0)}\psi^\dagger + e^{-imc^2(t-t_0)}\psi\right)^3 : \Big] . \end{aligned} \tag{2.249}$$

From these equations we want to extract, after having taken the NR limit, the $\mathcal{O}(\Delta t)$ term and then get from it the NR equation of motion. Thanks to the power counting argument (2.86) we know that in order to do this we need to solve (2.249) iteratively up to the second iteration. Moreover, as we discussed after (2.86), at the second iterative solution the only terms that do not give a vanishing contribution are those of the first iterative solution associated with v_3. In this perspective, we compute the first iterative solution keeping only the important terms:

$$\begin{aligned} \Big[i\psi^\dagger(t_0+\Delta t)\Big]_{\text{first iteration}} = i\psi^\dagger + \frac{\Delta t}{2m}\partial_x^2\psi^\dagger - \frac{\Delta t v_4}{8m^2}\psi^\dagger\psi^\dagger\psi - \frac{v_3 c^{-1}}{4m\sqrt{2m}}\Bigg[& \frac{e^{ic^2m\Delta t}-1}{im}\psi^\dagger\psi^\dagger + \\ & +2\frac{e^{-ic^2m\Delta t}-1}{-im}\psi^\dagger\psi + \frac{e^{-3ic^2m\Delta t}-1}{-3im}\psi\psi\Bigg] + ... \end{aligned} \tag{2.250}$$

where the fields on the right are all computed at time t_0. Now we should take the above and plug it in (2.249) to get the second iterative solution: this is a tedious but simple calculation. At this point let $c \to \infty$ and drop all the vanishing terms (in particular the linear terms in v_3 of the first iteration vanish, but the crucial point is to drop them only after we have computed the second iteration). Keeping only the non vanishing terms of order $\mathcal{O}(\Delta t)$, the result of this operation is:

$$\Big[i\psi^\dagger(t_0+\Delta t)\Big]_{\text{second order}} = i\psi^\dagger + \frac{\Delta t}{2m}\partial_x^2\psi^\dagger - \frac{\Delta t v_4}{8m^2}\psi^\dagger\psi^\dagger\psi + \Delta t\frac{5}{3}\frac{v_3^2}{8m^4}\psi^\dagger\psi^\dagger\psi + ... \tag{2.251}$$

Because of the power counting (2.85) the second order solution is enough to extract the NR limit. Deriving in Δt we find the NR equation of motion

$$i\partial_t\psi^\dagger = \frac{1}{2m}\partial_x^2\psi^\dagger - \frac{1}{8m^2}\left(v_4 - \frac{5}{3}\frac{v_3^2}{m^2}\right)\psi^\dagger\psi^\dagger\psi \tag{2.252}$$

and from this the non relativistic Hamiltonian

$$H = \int dx \ \frac{\partial_x\psi^\dagger\partial_x\psi}{2m} + \frac{1}{16m^2}\left(v_4 - \frac{5}{3}\frac{v_3^2}{m^2}\right)\psi^\dagger\psi^\dagger\psi\psi\,. \tag{2.253}$$

Notice that we can give a physical meaning to the coupling $v_4 - \frac{5}{3m^2}v_3^2$, since it can be associated with a scattering amplitude. In particular, it is equal to the two body scattering amplitude at tree level of the Lagrangian (2.248) with $c = 1$ and at zero rapidity, moreover a similar interpretation of the NR coupling is also present in the more complicated NR limit of the Toda theories (Fig. 2.6). This equality can be traced back to the fact that the iterative solution of the equation of motion (2.247) can be indeed represented through tree level Feynman diagrams. Of course, plugging in the above the coefficients v_3 and v_4 in order to match (2.246) and (2.247), we get the NR limit of the Bullogh Dodd model (2.89).

2.B The Γ propagator

We compute the Γ propagator defined by eq. (2.135), i.e.

$$\Gamma^{-1}\left(k^\mu k_\mu\right) = -\frac{N}{2}\int \frac{\mathrm{d}^2 q}{(2\pi)^2}\frac{1}{q^\mu q_\mu - m^2c^2 + i\epsilon_1}\frac{1}{\left(k^\mu - q^\mu\right)\left(k_\mu - q_\mu\right) - m^2c^2 + i\epsilon_2}\,, \tag{2.254}$$

where the limits $\epsilon_1 \to 0^+$ and $\epsilon_2 \to 0^+$ must be independently taken. First of all we perform a Wick rotation going in the Euclidean space $\bar{q}^\mu = (-iq_0, q_1)$, in this perspective we also consider the Euclidean version of the k momentum $\bar{k}^\mu = (-ik_0, k_1)$

$$\begin{aligned}&\int \frac{\mathrm{d}^2 q}{(2\pi)^2}\frac{1}{q^\mu q_\mu - m^2c^2 + i\epsilon_1}\frac{1}{\left(k^\mu - q^\mu\right)\left(k_\mu - q_\mu\right) - m^2c^2 + i\epsilon_2} \to \\ &\to i\int \frac{\mathrm{d}^2 q}{(2\pi)^2}\frac{1}{\left[\bar{q}^\mu \bar{q}_\mu + m^2c^2\right]\left[\left(\bar{k}^\mu - \bar{q}^\mu\right)\left(\bar{k}_\mu - \bar{q}_\mu\right) + m^2c^2\right]}\,,\end{aligned} \tag{2.255}$$

where the contractions are performed with the euclidean metric

$$\eta^E_{\mu\nu} = \begin{pmatrix} \frac{1}{c^2} & 0 \\ 0 & 1 \end{pmatrix}\,. \tag{2.256}$$

The next step is to move in adimensional units and shift $\bar{q}_0 \to c^2 m\bar{q}_0$ and $\bar{q}_1 \to cm\bar{q}_1$, we also introduce the adimensional euclidean vector s^μ in such a way $\bar{k}^\mu = (c^2 m s^0, cms^1)$:

$$\frac{i}{cm^2}\int \frac{\mathrm{d}^2 q}{(2\pi)^2}\frac{1}{\left[\mathbf{q}^2 + 1\right]\left[(\mathbf{s} - \mathbf{q})^2 + 1\right]}\,. \tag{2.257}$$

After the rescaling, the scalar products are done with the standard euclidean metric and thus we use the standard notation $\mathbf{q}$ to indicate vectorial quantities. Using the Feynman's trick

$$\frac{1}{AB} = \int_0^1 \mathrm{d}x\,\frac{1}{\left[xA + (1-x)B\right]^2} \tag{2.258}$$

we rewrite the integral as

$$\frac{i}{cm^2}\int_0^1 \mathrm{d}x\int \frac{\mathrm{d}^2 q}{(2\pi)^2}\frac{1}{\left[\mathbf{q}^2 - (1-x)2\mathbf{sq} + 1 + (1-x)\mathbf{s}^2\right]^2}\,. \tag{2.259}$$

The last passages amount to shift the momentum $\mathbf{q}$ in order to make the integral symmetric under rotations, at this point the integration in $\mathbf{q}$ becomes trivial. The x integration can be done

as well and we get

$$\frac{1}{2\pi}\frac{i}{cm^2}\frac{1}{\sqrt{(4+\mathbf{s}^2)\mathbf{s}^2}}\log\left[\frac{\sqrt{4+\mathbf{s}^2}+\sqrt{\mathbf{s}^2}}{\sqrt{4+\mathbf{s}^2}-\sqrt{\mathbf{s}^2}}\right] \quad . \tag{2.260}$$

Tracking back the euclidean rotation and the rescaling we have $\mathbf{s}^2 = -\frac{k_\mu k^\mu}{m^2c^2}$ in the standard Minkowski metric, then Γ can be finally written as

$$\Gamma\left(k^\mu k_\mu\right) = i4\pi c N^{-1} m^2 \sqrt{\left(\frac{k_\mu k^\mu}{m^2c^2}-4\right)\frac{k_\mu k^\mu}{m^2c^2}}\left(\log\left[\frac{\sqrt{4-\frac{k_\mu k^\mu}{m^2c^2}}+\sqrt{-\frac{k_\mu k^\mu}{m^2c^2}}}{\sqrt{4-\frac{k_\mu k^\mu}{m^2c^2}}-\sqrt{-\frac{k_\mu k^\mu}{m^2c^2}}}\right]\right)^{-1} \quad . \tag{2.261}$$

Chapter 3

Integrable models driven out-of-equilibrium

This chapter is dedicated to various aspects of out-of-equilibrium physics of integrable models. In particular, it is organized into four sections:

1. Section 3.1 is dedicated to homogeneous out-of-equilibrium protocols and to the description of the steady state, presenting the work of Ref. [5], done in collaboration with S. Sotiriadis. In particular, we investigated the locality properties of the GGE in interacting-to-free quenches in continuum models. As we discussed in the introduction, the GGE was originally proposed to be constructed out of the local conserved charges [98]: while this simple recipe has been experienced to be correct in free lattice models, quasilocal charges need to be added in the description of truly interacting integrable models. However, the locality properties of the GGE in continuous systems are far less investigated. In Ref. [123] has been pointed out how the notion of local charges in continuum systems is much more stringent compared with the lattice counterpart, and this could lead to a failure of the local charges to describe the steady state even in free systems. As we show in Ref. [5], this is indeed the case: we carefully analyze interacting-to-free quenches in a bosonic relativistic model. Relativistic invariance gave us non perturbative control on the steady state correlation functions, which cannot be described by only the local charges. We show that a correct description of the GGE can be obtained in terms of a countable set of suitably defined quasi-local charges.

2. Section 3.2 is dedicated to the entanglement growth in homogeneous quenches. Indeed, the (scaling part of the) entanglement growth can be described through the creation of locally entangled excitations, that subsequently carry around the entanglement [137]. We present the work of Ref. [6], in collaboration with P. Calabrese: in free systems, we generalize the commonly assumed pair structure of the initial state to include several, quantum correlated, species of excitations. The entanglement growth can be still understood in terms of ballistically propagating excitations, but the interspecies quantum correlation affects the entanglement weight carried by each particle, which has a purely quantum nature (in the single pair case, the entanglement weight allows instead a classical interpretaion). Our ansatz is tested on the Ising spin chain in a periodically modulated tranverse field, which allows the desired multi-species structure of the post quench state. We also provide a quasiparticle descritpion for the growth of the order parameter and its correlators, thus generalizing the findings of Ref. [107, 143].

3. Section 3.3 is pivoted on Ref. [7], in collaboration with M. Collura and S. Sotiriadis, and illustrates the first truly inhomogeneous quench of this thesis. We consider a quantum quench in the Lieb Liniger model (1.1) between two extreme situations, i.e. from the free case $\kappa = 0$ to the infinitely repulsive regime $\kappa = +\infty$, known as Tonks Girardeau limit [144–149]. In each of these two limits the model is free, thus feasible of exact computations.

   This problem has already been addressed choosing as initial state the non interacting ground state, i.e. the Bose Einstein condensate (BEC) [150], with later generalizations including a trap [151, 152]. However, the choice of the BEC has several drawbacks, which

prevent a straightforward definition of the thermodynamic limit when a trapping potential is concerned. Therefore, we considered quenches from gaussian states, above all thermal states of non interacting bosons ($\kappa = 0$). This choice allows us to straightforwardly analyze a (thermodynamically large) trap, studying its late time effects: in particular, we testify the emergence of a semiclassical picture, where the quantum gas can be efficiently described in terms of a collection of non-interacting classical particles.

4. In Section 3.4 we finally address inhomogeneous quenches in truly interacting integrable models. Thanks to the recent breakthrough of Ref. [159, 160] , a Generalized Hydrodynamic (GHD) description of integrable models allows to supplement the semiclassical picture of ballistically traveling particles with the non-trivial scattering data. Albeit most of investigations focus on the quantum world, the same concepts can be transferred to classical integrable models as well. Indeed, in this section we present the work of Ref. [8], in collaboration with B. Doyon, G. Watts and T. Yoshimura, where we study GHD for classical integrable field theories, with particular focus on the classical Sinh Gordon model. Classical systems offer a great opportunity to test hydrodynamic concepts, especially in continuous models whose quantum counterpart is difficult to be numerically simulated. In contrast, in the classical case a simple Metropolis-Hasting algorithm [183, 184] allows to test a great variety of predictions, e.g. partitioning protocols and correlation functions.

3.1 Quasilocality of the GGE for interacting-to-free quenches in continuum models

As we anticipated in the introduction, integrable systems behave very differently from non-integrable ones when driven out-of-equilibrium. In particular, let us consider an homogeneous quantum quench [96, 97]: from an initial, translational invariant given initial state, we let the system to evolve by mean of a local Hamiltonian, assumed to be integrable. Due to the conserved charges of the integrable model, relaxation to the GGE [98] density matrix $\hat{\rho}$ is attained

$$\hat{\rho} = \frac{1}{\mathcal{Z}} e^{-\sum_j \lambda_j \mathcal{Q}_j} \tag{3.1}$$

with $\mathcal{Q}_j$ the relevant conserved charges. The Lagrange multipliers λ_j must be fixed in such a way that the expectation value of the charges on the steady state coincides with that on the initial state. However, as we anticipated, which are the relevant charges that must be used is an absolutely non-trivial issue, neither is the "convergence" of the above expression when infinitely many charges are considered.

In its original formulation, the GGE is constructed only out of local charges and early works [107–109] confirmed the correctness of this picture in free systems (i.e. the simplest example of integrable models) on a lattice. In the case of interacting lattice systems, the inclusion of quasilocal charges (sum of operators with exponentially vanishing support) is needed [111–114, 117–122]. For what it concerns free homogeneous systems, the Hamiltonian can be diagonalized in the Fourier space and the GGE acquires a simple form when expressed in terms of the modes. For definiteness, let us assume $\eta(k), \eta^\dagger(k)$ are annihilation/creation modes that diagonalize the free Hamiltonian (only one particle species is assumed)

$$H_{\text{free}} = \int \mathrm{d}k\, E(k)\eta^\dagger(k)\eta(k) + \text{const.} \tag{3.2}$$

and the GGE density matrix is written as a thermal state, with a momentum-dependent temperature

$$\hat{\rho}^M = \frac{1}{\mathcal{Z}} e^{-\int \mathrm{d}k\, \lambda(k) E(k)\eta^\dagger(k)\eta(k)}\,. \tag{3.3}$$

Above, we attached a label "M" in order to distinguish the "momentum formulation of the GGE" from other definitions, which will be later introduced.

Relaxation in free models is simply described by Eq. (3.3) and this holds true in discrete and continuum models as well [332, 333]. However, while in lattice models the equivalence of Eq. (3.3) with a GGE constructed out of local charges has been established (and we will see an explicit example), the same correspondence has been taken for granted in continuum systems for a long time. In Ref. [123] (see also Ref. [124]) the equivalence of the GGE constructed on the modes (3.3) with that built on the local charges has been questioned for the first time. Let us stress again that, following the common definition, local charges in continuum models can be written as spatial integration of local operators, i.e. point-wise functions of the fields and their derivatives. However, cleverly exploiting the continuum limit of a lattice system, in Ref. [123] it was shown that local charges of the lattice model can result, after the continuum limit has been taken, in charges in the continuum which are not strictly local under the usual definition. Indeed, in close relation with the lattice systems, charges expressed as spatial integration of finite-support operators can be produced.

This makes natural wondering if *i)* the inclusion of only local charges in the GGE (3.1) is sufficient to reproduce the GGE in the momentum space (3.3) and *ii)* if it is not the case and the GGE cannot be written in the form of Eq. (3.1), if the knowledge of the expectation values of the local charges is at least enough to fix the GGE in its momentum formulation (3.3), namely to determine the root density.

This Section conveys the work of Ref. [5] (in collaboration with S. Sotiriadis) and further investigates these questions, carefully addressing the locality properties of the GGE in interacting-to-free quantum quenches. In order to be more precise, let us introduce a few definitions.

1. We define the momentum GGE (MGGE) as the GGE constructed in terms of the modes, i.e. we assume the existence of a function $\lambda(k)$ and use it to construct the density matrix (3.3). The value of $\lambda(k)$ is fixed matching the expectation value of $\eta^\dagger(k)\eta(k)$ on the GGE with that on the initial state.

2. We define the local GGE (LGEE) as that coming from the original definition: the GGE is constructed out of only local charges. Moreover, the existence of a set of Lagrange multipliers $\{\lambda_i\}$ is assumed such that

   (a) The series $\sum_{j=0}^{\infty}\lambda_j\mathcal{Q}_j^{\mathrm{L}}$ is a "well defined operator", where $\{\mathcal{Q}_j^{\mathrm{L}}\}_j$ is the set of all the local charges. By mean of well defined operator, we mean the result of the infinite summation must not depend on the limiting procedure, for example changing the order of the sum should not affect the final result.

   (b) For any local operator (and their correlators) the steady state expectation value is described by the LGGE density matrix $\hat{\rho}^{\mathrm{L}} = e^{-\sum_{j=0}^{\infty}\lambda_j\mathcal{Q}_j^{\mathrm{L}}}/\mathcal{Z}$.

3. We define the truncated local GGE (TGGE) by mean of a limiting procedure. Firstly, we order the local charges in terms of their locality (size of the support on the lattice, order of the highest derivative in the continuum) from the more local to the less local. Then, we say the TGGE is realized if:

   (a) Define the truncated GGE density matrix $\hat{\rho}_N^{\mathrm{T}} = e^{-\sum_{j=0}^{N}\lambda_j^{(N)}\mathcal{Q}_j}/\mathcal{Z}$. The set $\{\lambda_j^{(N)}\}_{j=0}^{N}$ is fixed in such a way the expectation value of the first N charges computed on the truncated GGE coincides with the expectation value on the initial state: this request will be discussed later on, since the expectation value of local charges is often UV singular in the continuum. The superscript (N) on the Lagrange multipliers makes explicit that we keep in account the possibility that their choice depends on N.

(b) For any local observable $\mathcal{O}(t,x)$, the expectation value obtained with the truncated GGE converges to the correct steady state for $N \to \infty$

$$\lim_{t\to\infty} \langle \mathcal{O}(t,x) \rangle = \lim_{N\to\infty} \mathrm{Tr}\left[\hat{\rho}_N^{\mathrm{T}} \mathcal{O}(t,x)\right] . \tag{3.4}$$

4. Finally, we define the quasilocal GGE (QGGE) to be constructed out of a numerable set of quasilocal charges $\{\mathcal{Q}_n^{\mathrm{Q}}\}_{n=0}^{\infty}$ and an associated set of Lagrange multipliers $\{\lambda_n\}_{n=0}^{\infty}$ such that:

   (a) The operator $\sum_{n=0}^{\infty} \lambda_n \mathcal{Q}_n^{\mathrm{Q}}$ is well defined, independently from the limiting procedure needed to define the series.

   (b) The set of Lagrange multipliers is completely fixed by the expectation value of the quasilocal charges $\{\mathcal{Q}_n^{\mathrm{Q}}\}_{n=0}^{\infty}$.

Taking as granted the MGGE to be trustful for quenches towards free models, we investigate if, for a general class of interacting-to-free quenches, the MGGE can be rephrased in one of the other definitions. More specifically, we consider a relativistic model described by a single real bosonic field ϕ and quench from the ground state of a generic interaction ruled by the Lagrangian

$$\mathcal{L} = \int \mathrm{d}x \, \frac{1}{2} \partial_\mu \phi \partial^\mu \phi - V(\phi) \tag{3.5}$$

to the free massive point (Klein-Gordon model)

$$\mathcal{L}_{\mathrm{KG}} = \int \mathrm{d}x \, \frac{1}{2} \partial_\mu \phi \partial^\mu \phi - \frac{m^2}{2} \phi^2 . \tag{3.6}$$

We now summarize our findings. We show that the LGGE formulation is not correct and quantify the discrepancy from correlation functions computed with a LGGE and the true correlation functions in the steady state. The situation is less critical if the TGGE is considered: a sequence of Lagrange multipliers $\{\lambda_n^{(N)}\}_{n=1}^{N}$ such that Eq. (3.4) holds true can be found (and we explicitly construct it), but it cannot be fixed in terms of the expectation value of (suitably regularized) local charges. Therefore, even the formulation of the truncated GGE is not correct. Finally, we revert to the QGGE showing it is indeed the right procedure.

Our analysis of the continuous model is performed in parallel with a natural lattice discretization, in order to highlights the differences between the two cases (on the lattice, LGGE and TGGE are indeed correct).

In particular:

1. Section 3.1.1 analyzes the LGGE in the simple example of a free-to-free quench (i.e. $V(\phi) = M^2\phi^2/2$ in Eq. (3.5)), which is amenable of a full analytical computation.

2. Section 3.1.2 approaches the same problem, but assuming a generic interaction in the pre-quench action. We perform such an analysis taking advantage of the non-perturbative Källen-Lehmann spectral representation of the initial state [126].

3. Section 3.1.3 analyzes the TGGE formulation.

4. Finally, Section 3.1.4 shows that the correct GGE formulation in the continuum case necessarily needs quasilocal charges.

3.1.1 Mass quench in the Klein-Gordon field theory

In this and in the following section we describe the class of quenches we choose to consider and address the issue about the validity of the LGGE.

To demonstrate our argument in the simplest possible example, in this section we consider a quantum quench of the mass parameter in the Klein-Gordon field theory. This quench has been studied in [96] and the steady state is known in the momentum-space form (3.3) so that we can directly test its consistency with LGGE. We study in parallel the equivalent quench in the lattice version of the model, which is nothing but a system of coupled harmonic oscillators. As we will see, the discrepancy between the LGGE and the exact steady state is absent in the lattice version, meaning that the problem arises only in the continuum limit.

We consider the Klein-Gordon model in one spatial dimension (3.6), the local charges are quadratic in the fields [105]:

$$\mathcal{Q}^L_{2n} = \frac{(-1)^n}{2}\int \mathrm{d}x\ \partial_t\phi\partial_x^{2n}\partial_t\phi + \phi\left[\partial_x^{2n}(-\partial_x^2+m^2)\right]\phi = \int \mathrm{d}k\ k^{2n}E(k)\eta^\dagger(k)\eta(k)\ , \tag{3.7}$$

$$\mathcal{Q}^L_{2n+1} = (-1)^n\int \mathrm{d}x\ \partial_t\phi\partial_x^{2n+1}\phi = \int \mathrm{d}k\ k^{2n+1}\eta^\dagger(k)\eta(k)\ . \tag{3.8}$$

The system is initialized in the ground state of the model with mass M and then at initial time the mass parameter is abruptly changed to m. The Hamiltonian of the system is readily written as:

$$H = \int \mathrm{d}x\ \frac{1}{2}\Pi^2 + \frac{1}{2}(\partial_x\phi)^2 + \frac{1}{2}m^2\phi^2 = \int \mathrm{d}k\ E(k)\eta^\dagger(k)\eta(k) + \text{const.} \tag{3.9}$$

In standard notation: $\Pi = \partial_t\phi$ is the field conjugate to ϕ and $\eta(k)^\dagger, \eta(k)$ are the creation and annihilation operators with standard bosonic commutation rules $[\eta(k), \eta^\dagger(q)] = \delta(k-q)$.

The above Hamiltonian admits an obvious lattice discretization in terms of coupled harmonic oscillators:

$$H^{\text{lat}} = \sum_j \frac{1}{2}\Pi_j^2 + \frac{1}{2\Delta^2}(\phi_{j+1}-\phi_j)^2 + \frac{m^2}{2}\phi_j^2 = \int_{-\pi/\Delta}^{\pi/\Delta} \mathrm{d}k\ E^{\text{lat}}(k)\eta^\dagger(k)\eta(k) + \text{const.}\ . \tag{3.10}$$

In the lattice model the momentum space is constrained to the first Brillouin zone $(-\pi/\Delta, \pi/\Delta)$ where Δ is the lattice spacing. The dispersion relation in the two cases is:

$$E(k) = \sqrt{k^2+m^2} \qquad E^{\text{lat}}(k) = \sqrt{2\Delta^{-2}(1-\cos(k\Delta))+m^2}\ . \tag{3.11}$$

As shown in [96] the relation between the pre-quench creation and annihilation operators $\eta_0(k), \eta_0^\dagger(k)$ and the post-quench ones $\eta(k), \eta^\dagger(k)$ is a Bogoliubov transformation

$$\eta(k) = \frac{1}{2}\left(\sqrt{\frac{E(k)}{E_0(k)}} + \sqrt{\frac{E_0(k)}{E(k)}}\right)\eta_0(k) + \frac{1}{2}\left(\sqrt{\frac{E(k)}{E_0(k)}} - \sqrt{\frac{E_0(k)}{E(k)}}\right)\eta_0^\dagger(-k)\ , \tag{3.12}$$

where the index "0" denotes the pre-quench dispersion relation that corresponds to mass M. The initial state expectation value of the conserved momentum-mode occupation number operators $\eta^\dagger(k)\eta(k)$ is therefore

$$\langle\eta^\dagger(k)\eta(q)\rangle_0 = \delta(k-q)\vartheta(k) = \delta(k-q)\frac{1}{4}\frac{(E(k)-E_0(k))^2}{E_0(k)E(k)}\,. \tag{3.13}$$

Above, $\vartheta(k)$ is the excitation density, which is nothing else that the filling of the TBA (Section 2.1.2) when we restrict to free models.

Using (3.13) we can immediately understand that a straightforward application of the LGGE

recipe is problematic. As a matter of fact the computation of the Lagrange multipliers associated with the local charges passes through the expectation values of the latter, but the defining integrals (3.7-3.8) are UV divergent, since $\vartheta(k) \sim |k|^{-4}$ for large k.

We postpone the discussion about the delicate issue of regularizing the local charges to Section 3.1.3, since in the current formulation of the LGGE we find an obstacle at a more fundamental level. Indeed, before asking how we could fix the Lagrange multipliers, we should understand if they actually exist, i.e. if $\vartheta(k)$ is compatible with a LGGE.

As a matter of facts, we will show that, without explicitly deriving the Lagrange multipliers, the LGGE form imposes strong analyticity constraints that are sufficient in order to compare it with the exact one as given by the MGGE and to obtain information about the large distance behaviour of correlators. From this comparison we can easily see that the LGGE is not equivalent with the exact steady state which is given by the MGGE. The excitation density in the MGGE $\vartheta^{\mathrm{M}}(k)$ is:

$$\vartheta^{\mathrm{M}}(k) = \frac{1}{e^{\lambda(k)E(k)} - 1} \ . \tag{3.14}$$

Imposing $\vartheta(k) = \vartheta^{\mathrm{M}}(k)$ we compute the Lagrange multipliers or "effective temperature" $\lambda(k)$

$$\lambda(k) = \frac{1}{E(k)} \log \left(\frac{E_0(k) + E(k)}{E_0(k) - E(k)} \right)^2 \ . \tag{3.15}$$

We note that $\lambda(k)$ is an even function of k as it should be, since the initial state is parity invariant. The LGGE is constructed using an infinite sum of the local charges. Due to parity invariance only the even charges $\mathcal{Q}^L_{2n}$ defined in (3.7) enter in this construction. Writing this sum in momentum space we have

$$\sum_{n=0}^{\infty} \lambda_n \mathcal{Q}^L_{2n} = \int \mathrm{d}k \left(\sum_{n=0}^{\infty} \lambda_n k^{2n} \right) E(k) \eta^\dagger(k) \eta(k) + \text{constant} \tag{3.16}$$

so that, comparing the LGGE with the MGGE, we identify the LGGE prediction for the effective temperature $\lambda^{\mathrm{L}}(k)$ with the power series

$$\lambda^{\mathrm{L}}(k) = \sum_{n=0}^{\infty} \lambda_n k^{2n} \ . \tag{3.17}$$

We conclude that the momentum-dependent effective temperature for a LGGE is necessarily defined through a power series, regardless of the actual values of the Lagrange multipliers λ_n. Accordingly with the definition of LGGE, it must be stressed that (3.17) does not state that the effective temperature is Taylor-expandable around $k = 0$, but that it coincides with the series itself: if the latter has a finite convergence radius R_{conv} and diverges beyond it, then the effective temperature becomes infinite as well. Conversely, in order for the exact steady state, which is given by the MGGE, to be equivalent to a LGGE, $\lambda(k)$ must be a power series in terms of k^2. More importantly, in order for the LGGE to be correct, this power series must be such that the excitation density computed through the LGGE converges to the actual value for any real momentum, since otherwise it would lead to incorrect predictions for the values of local observables, as we will show next. While it is true that the correct effective temperature $\lambda(k)$ (3.15) can be Taylor expanded around zero, the radius of convergence R_{conv} of this series is $R_{conv} = \min\{m, M\}$, because this is the distance from the origin of the closest of the branch-cut singularities of (3.15), which are located at $k = \pm im$ and $k = \pm iM$ in the complex plane. This means that the correct effective temperature (3.15) cannot be described through an unique power series valid for any real momentum. This discrepancy is well captured by the two point correlator in the steady

state $\langle\phi(x,t)\phi(y,t)\rangle_{t\to\infty}$, which in terms of the root density is written as

$$\langle\phi(x)\phi(y)\rangle_{t\to\infty} = \langle\phi(x)\phi(y)\rangle_{\rm MGGE} = \int \frac{\mathrm{d}k}{2\pi}\frac{e^{ik(x-y)}}{2\sqrt{k^2+m^2}}(2\vartheta(k)+1)\ . \tag{3.18}$$

In particular, the non-analyticity point of the excitation density $\vartheta(k)$ that is closer to the real axis determines the long-distance decay of the two-point correlator. As a result, using either $\vartheta(k)$ or $\vartheta^{\rm L}(k)$ in the above, results in a difference in the long-distance asymptotic behavior of the two-point correlator.

We postpone a detailed comparison between the predictions of LGGE and MGGE on the two-point correlator to Section 3.1.2, where we discuss the general case of an arbitrary pre-quench theory, but it is worth anticipating the results. In particular, the discrepancy is more evident when the pre-quench mass M is chosen smaller than the post-quench one, $M < m$. Due to the branch cut at $k = \pm iM$ in the excitation density (3.13), the leading asymptotics behavior of the two point correlator (3.18) is an exponential decay $\sim e^{-M|x-y|}$ with multiplicative algebraic corrections. In contrast, a LGGE would predict asymptotes $\sim e^{-m|x-y|}$, if the radius of convergence of (3.17) is infinite (and a non-exponential decay, otherwise), which is different from the correct one. The detailed derivation of these asymptotes, as well as the discussion of the opposite case $m < M$ and of a finite convergence radius for (3.17) can be found in Section 3.1.2.

We now study the lattice system (3.10): the local charges are a simple discretization of the continuum case and as before only the even charges are needed.

$$(\mathcal{Q}^L_{2n})^{\rm lat} = \frac{1}{2}\sum_j \Pi_{n+j}\Pi_j + \phi_{n+j}\left(m^2\phi_j + \frac{2\phi_j-\phi_{j+1}-\phi_{j-1}}{\Delta^2}\right) = \int_{-\pi/\Delta}^{\pi/\Delta}\mathrm{d}k\ \cos(k\Delta n)E^{\rm lat}(k)\eta^\dagger(k)\eta(k)\,. \tag{3.19}$$

Therefore, a LGGE on the lattice can be written in the momentum space as:

$$\sum_{n=0}^{\infty}\lambda_n^{\rm lat}(\mathcal{Q}^L_{2n})^{\rm lat} = \int_{-\pi/\Delta}^{\pi/\Delta}\mathrm{d}k\left(\sum_{n=0}^{\infty}\lambda_n^{\rm lat}\cos(k\Delta n)\right)E^{\rm lat}(k)\eta^\dagger(k)\eta(k) + \text{const.}\ . \tag{3.20}$$

In marked contrast to the continuum case, in the lattice we reach the conclusion that in order for the LGGE to be equivalent to the MGGE the effective temperature $\lambda(k)$ must be a *Fourier series* of k instead of a power series. The correct effective temperature is still given by (3.15) with $E_0(k)$ and $E(k)$ replaced by the lattice dispersion relation. We notice that, since the effective temperature is a smooth function of k over all the Brillouin zone for any $\Delta \neq 0$, it possesses an *absolutely convergent* Fourier series [334]. This means that, unlike the continuum case, in the lattice the definition of the LGGE is equivalent to the correct MGGE, since the latter can be expressed as the exponential of a sum of local charges unambiguously determined by the Lagrange multipliers.

Comparing these two models we can have a better understanding of the continuum limit. Heuristically to pass from the lattice to the continuum we would make the correspondence $\phi_j \leftrightarrow \phi(\Delta j)$, then Taylor expand the field when its position is shifted by a finite number of sites $\phi_{j+1} = \phi(\Delta j) + \Delta\partial_x\phi(\Delta j) + ...$ and find the continuum local charges as linear combinations of those on the lattice. As already pointed out in [123], this is not the only way to take the continuum limit: we can consider a combined limit for $(\mathcal{Q}^L_{2n})^{\rm lattice}$, letting $\Delta \to 0$ but keeping $n\Delta = y$ constant,

thus naturally finding the bosonic analogue of the set of quasilocal charges introduced in [123].

$$\mathcal{Q}^{\mathrm{Q}}(y) = \frac{1}{2}\int \mathrm{d}x\ \partial_t\phi(x+y)\partial_t\phi(x) + \phi(x+y)(-\partial_x^2+m^2)\phi(x) = \int \mathrm{d}k\ \cos(ky)E(k)\eta^\dagger(k)\eta(k) + \text{const.}\,. \quad (3.21)$$

We write only the even charges, but of course a similar operation can be performed on the odd ones. It is straightforward to verify from scratch that the quasilocal charges $\mathcal{Q}^{\mathrm{Q}}(y)$ are indeed integrals of motion of the continuum model. Moreover they are complete in the sense that they are sufficient in order to describe the MGGE

$$\int \mathrm{d}k\ \lambda(k)E(k)\eta^\dagger(k)\eta(k) = \int \mathrm{d}y\ \mathcal{K}(y)\mathcal{Q}^{\mathrm{Q}}(y), \qquad \text{with}\ \ \mathcal{K}(y) = \int \mathrm{d}k\,\lambda(k)\cos(ky) \quad (3.22)$$

and the Fourier transform of $\lambda(k)$ given by (3.15) is well defined. It must be said that using the whole set of charges $\{\mathcal{Q}^{\mathrm{Q}}(y)\}_{y\in\mathbb{R}}$ to fix the GGE is unfeasible on a practical level, since we should measure a non-countable infinite set of observables (since $y \in \mathbb{R}$). This issue will be addressed later in Section 3.1.4, where we show that the set $\{\mathcal{Q}^{\mathrm{Q}}(y)\}_{y\in\mathbb{R}}$ is overcomplete and the GGE is described by a countable infinite set of suitably defined quasilocal charges. Of course, for a quench protocol that breaks parity invariance we must use also the odd charges.

Apart from demonstrating that local charges are insufficient to describe the steady state of the mass quench and that quasilocal charges are instead complete, it is useful to quantify how much nonlocal the GGE is, i.e. how far from local the kernel $\mathcal{K}(y)$ must be in order to describe the correct steady state as given by the MGGE for the mass quench. Obviously considering an arbitrary kernel $\mathcal{K}(y)$ in (3.22) allows for quite nonlocal features, e.g. in the extreme case of a constant kernel points that are infinitely far away would be coupled. Understanding how fast $\mathcal{K}$ decays is important from the viewpoint of a truncation of the GGE [109], when we are interested only on observables within a finite subsystem: in practice, we cannot measure experimentally an infinite number of charges, therefore knowing in advance whether or not the contribution of $\mathcal{Q}^{\mathrm{Q}}(y)$ is negligible would be very helpful.

Using the parity invariance of the effective temperature, $\mathcal{K}(y)$ can be computed as:

$$\mathcal{K}(y) = \int \mathrm{d}k\,\lambda(k)e^{iky}\ , \quad (3.23)$$

so that the large distance behavior of $\mathcal{K}(y)$ can be readily estimated from the non-analyticity points of $\lambda(k)$ in the complex plane. Since $\mathcal{K}(y)$ is symmetric in its argument we can suppose $y > 0$, then we can move the integration path in the upper complex plane, integrating around the non-analyticity points and branch-cuts. The non-analyticity point closest to the real axis determines the leading behavior of $\mathcal{K}$ at large distances. In particular, if this point has imaginary part ξ, then $\mathcal{K}$ is exponentially damped $\mathcal{K}(y) \sim e^{-\xi|y|}$, in general with extra non-exponential corrections. From the expression of the effective temperature (3.15) with the relativistic dispersion relation, we see that the first non-analyticity point is a branch-cut singularity at k equal to the smallest mass among m and M, therefore:

$$\mathcal{K}(y) \sim e^{-|y|\min(m,M)}\ . \quad (3.24)$$

In particular, the larger the masses are, the closer the MGGE or the equivalent QGGE is to a LGGE, since only quasilocal charges with a smaller spread are needed.

Apart from the long distance behavior, we can also easily characterize $\mathcal{K}(y)$ at short distances, showing that it is logarithmically divergent. At large momenta $\lambda(k)$ is slowly decaying:

$$\lambda(k) = \frac{1}{|k|}\log\left(\frac{16k^4}{(m^2-M^2)^2}\right) + \mathcal{O}\left(\frac{\log|k|}{|k|^3}\right) \quad . \tag{3.25}$$

From this expansion, after simple calculations, we can extract the singular behavior of $\mathcal{K}$ at zero:

$$\mathcal{K}(y) \simeq 8\left[\frac{1}{2}(\log y)^2 + (\gamma + \log r)\log y\right] + \text{const.}, \qquad y \to 0 \ , \tag{3.26}$$

where γ is the Euler-Mascheroni constant and

$$r = \frac{1}{2}\sqrt{|m^2 - M^2|} \ . \tag{3.27}$$

Notice that the leading divergence in (3.26) is *universal* and does not depend on the particular mass shift, provided the latter is not zero.

In the next section we will extend these results to the more general case of an interacting-to-free quench: we show that the LGGE is never sufficient to correctly describe the steady state in continuous field theories, we explain how we can see the discrepancy in correlations of local fields and finally we quantify the non-locality properties of the quasilocal charges that are required for the correct description.

3.1.2 Failure of the LGGE in interacting-to-free quenches

In the previous section we showed how the LGGE is not sufficient to correctly describe the steady state of a mass (free-to-free) quench, but actually we can reach the same conclusion in the more general case of any interacting-to-free quench. We now consider a single bosonic field in one dimension with an arbitrary pre-quench interacting theory:

$$\mathcal{L}_{t<0} = \int \mathrm{d}x\ \frac{1}{2}\left(\partial_\mu\phi\partial^\mu\phi - m^2\phi^2\right) - V(\phi) \quad \xrightarrow{t=0} \quad \mathcal{L}_{t>0} = \int \mathrm{d}x\ \frac{1}{2}\left(\partial_\mu\phi\partial^\mu\phi - m^2\phi^2\right) \ . \tag{3.28}$$

Interacting to free quenches in field theories have already been studied [332, 333] and it has been shown that, whenever the post-quench Lagrangian is massive ($m \neq 0$) and the initial state satisfies the cluster property, we have equilibration of local observables to the gaussian MGGE. Here we assume exponential clustering, although the above result is expected to hold even for weaker clustering, as long as equilibration takes place [333]. If the post-quench theory is massless ($m = 0$) the situation is more complicated and the system relaxes to a non gaussian ensemble [125].

Hereafter, we will focus only on the massive post-quench case. This quench protocol is parity invariant, therefore we can consider only even charges in the construction of the GGE: in the previous section we showed how LGGE implies analyticity constraints on the effective temperature $\lambda(k)$. Our strategy is to check whether or not these constraints are consistent with $\vartheta(k) = \vartheta^{\mathrm{L}}(k)$. In the mass quench $\vartheta(k)$ was known explicitly thanks to the fact that the pre-quench theory was free. In this more general case we cannot perform this task explicitly, nevertheless the knowledge of the analytic properties of $\vartheta(k)$ will be sufficient for our purposes and we can obtain such information using the *Källén-Lehmann spectral representation* for the correlators of ϕ and $\partial_t\phi$ [126].

This representation is exact (not perturbative) and relies only on relativistic invariance, providing an integral representation for the two point correlators of the fields ϕ and $\partial_t\phi$ on the

Figure 3.1: *Representation of the points and domains where the spectral function $\sigma(\mu^2)$ is nonzero, in the simplest case of only one particle of mass M. The spectral function presents a $\delta-$like singularity in correspondence with the one particle state M^2, then multiple thresholds in correspondence with multiparticle states, therefore starting at $\mu^2 = n^2M^2$ with $n = 2, 3, 4, \dots$.*

initial state, in terms of a *spectral density* σ:

$$\langle\tilde{\phi}(k)\tilde{\phi}(q)\rangle_0 = \frac{\delta(k+q)}{2}\int_0^\infty \mathrm{d}\mu^2 \frac{\sigma(\mu^2)}{\sqrt{k^2+\mu^2}}\,, \quad \langle\tilde{\Pi}(k)\tilde{\Pi}(-k)\rangle_0 = \frac{\delta(k+q)}{2}\int_0^\infty \mathrm{d}\mu^2\sigma(\mu^2)\sqrt{k^2+\mu^2}\ . \tag{3.29}$$

The spectral density is real and positive. It exhibits $\delta-$like singularities in correspondence with the masses of the particles of the pre-quench theory and it has thresholds in correspondence with multiparticle states (Fig. 3.1).

$$\sigma(\mu^2) = \sum_{j=1}^{n} Z_j\delta(\mu^2 - M_j^2) + \Theta(\mu^2 - 4M_1^2)\tau(\mu^2)\ . \tag{3.30}$$

Above, M_j are the unknown masses of the particles of the pre-quench theory and they are supposed to be ordered $M_1 < .. < M_n$, Z_j are the field renormalization parameters and they are positive quantities. The continuous threshold starts from the minimal energy of a two particle state, that is $2M_1$. In Eq. (3.30), Θ is a Heaviside step-function and other thresholds are hidden in the function τ in correspondence with multiparticle states of higher mass particles. It is useful to mention [126] that the spectral density is normalized to 1:

$$\int_0^\infty \mathrm{d}\mu^2\ \sigma(\mu^2) = 1\ . \tag{3.31}$$

Using the parity invariance of $\vartheta(k)$ and (3.29) we get:

$$\vartheta(k) = \frac{1}{4}\int \mathrm{d}\mu^2\ \sigma(\mu^2)\frac{\left(E(k) - \sqrt{k^2+\mu^2}\right)^2}{E(k)\sqrt{k^2+\mu^2}}\ . \tag{3.32}$$

It must be stressed that the use of the Källén-Lehmann spectral decomposition allows us to go beyond perturbation theory and in particular to compare the LGGE and MGGE *directly in the renormalized theory*, that is after the UV divergent constants (masses, field strengths etc.) have been correctly regularized in the limit of infinite UV cut-off. Nevertheless notice that from (3.32) and (3.30), the expectation values of the local charges still remain UV divergent, as it happens also in the free case of Section 3.1.1, meaning that local charges are not renormalisable by means of standard Renormalization Group theory. This issue is absent in the expectation values of the quasilocal charges which are instead UV finite, exactly as in the mass quench studied in the previous section. Therefore the same problems in the computation of the LGGE's Lagrange multipliers are still present in this more general quench.

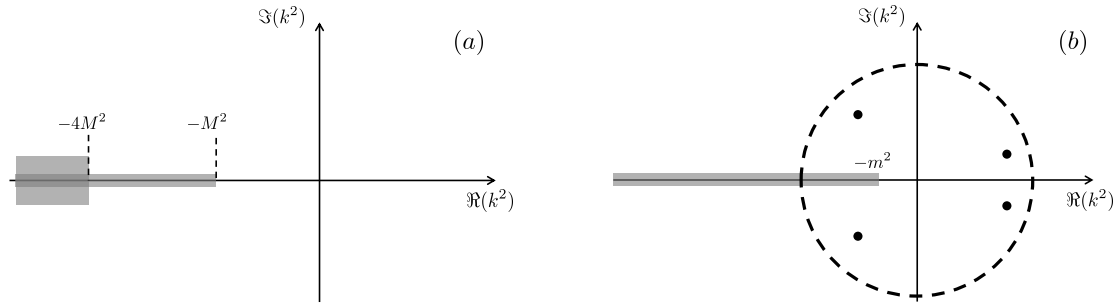

Figure 3.2: *Subfigure (a): Singularities of $F(k)$ as a function of k^2 in the complex plane. For simplicity we assume a pre-quench theory with only one type of particle whose mass is M. branch-cuts are located on the negative real axis at $k^2 = -(nM)^2$ with $n \in \{1, 2, 3...\}$ corresponding to single or multi-particle excitations that are present in the ground state of the pre-quench theory. Only the branch-cut at $k^2 = -M^2$ is a divergent square root singularity, while the others are non-divergent.*
Subfigure (b): Singularities of $F^L(k)$. Inside the disk of radius R_{conv} (depicted by the dashed circle) i.e. the radius of convergence of the series $\lambda^L(k)$, there is always a branch-cut (thick gray line) along the negative real axis starting from $k^2 = -m^2$. Possible additional poles (black dots) are located at the zeros of equation (3.37). These are the only allowed non-analyticities of $F^L(k)$.

Instead of considering the excitation density, it is more convenient to study the analytic behavior of a slightly different quantity:

$$F(k) \equiv E(k)[2\vartheta(k) + 1] \ . \tag{3.33}$$

Besides allowing a more straightforward comparison between the MGGE and LGGE analyticity predictions, we will see that this quantity is related to the Fourier transform of the two-point field correlator and different analytic behaviors of LGGE and MGGE will be translated into differences in the large distance behavior of the two point correlator. We define $F^{\mathrm{L}}(k)$ by mean of the replacement $\vartheta^{\mathrm{L}}(k) \to \vartheta(k)$ in Eq. (3.33): of course, $\vartheta(k) = \vartheta^{\mathrm{L}}(k)$ is equivalent to $F(k) = F^{\mathrm{L}}(k)$. In the following we will show that this equality is in fact impossible. The expressions of the two quantities above can be derived from (3.14) and (3.32) and using the canonical commutation rules:

$$F(k) = \frac{1}{2}\int_0^\infty \mathrm{d}\mu^2 \, \sigma(\mu^2)\frac{2k^2 + m^2 + \mu^2}{\sqrt{k^2 + \mu^2}} \ , \tag{3.34}$$

$$F^{\mathrm{L}}(k) = E(k)\left(1 + \frac{2}{e^{\lambda^{\mathrm{L}}(k)E(k)} - 1}\right) \ . \tag{3.35}$$

Above, $\lambda^{\mathrm{L}}(k)$ is the effective temperature in the momentum space which is associated to a LGGE, having thus the already discussed analytic properties. Now we can easily study the analytic behavior of $F(k)$ and then compare it with that of $F^{\mathrm{L}}(k)$:

1. The analytic structure of $F(k)$ can be immediately seen from the properties of the spectral density σ of the pre-quench ground state: we have branch-cut singularities at k equal to the particle masses of the pre-quench theory and also branch-cuts at the thresholds of multiparticle states, as depicted in Fig. 3.2(a). Notice that all non analyticities in $F(k)$ are determined by the physical properties of the pre-quench theory. From (3.34) $F(k)$ behaves for large momenta as:

$$F(k) = E(k)\left(1 + \frac{1}{k^4}\frac{1}{4}\int \mathrm{d}\mu^2 \sigma(\mu^2)(m^2 - \mu^2)^2 + \mathcal{O}(1/k^6)\right) \ . \tag{3.36}$$

2. To understand the analytic structure of $F^{\mathrm{L}}(k)$ on the other hand, we use (3.35) and the fact that, as explained in Section 3.1.1, $\lambda^{\mathrm{L}}(k)$ must be an analytic function of k^2 within the radius of convergence R_{conv} of the series (3.17): $\lambda^{\mathrm{L}}(k) = \sum_{n=0}^{\infty} \lambda_n k^{2n}$. Based on this fact and due to the presence of $E(k) = \sqrt{k^2 + m^2}$, $F^{\mathrm{L}}(k)$ exhibits a branch-cut starting at $k^2 = -m^2$. This branch cut is a non-divergent singularity, unless $\lambda^{\mathrm{L}}(\pm im) = 0$. Note that there is no choice of analytic function $\lambda^{\mathrm{L}}(k)$ for which this branch-cut would be removed. Other possible non-analyticity points are located at the zeros of the denominator of (3.35), i.e. the solutions of the equation:

$$\lambda^{\mathrm{L}}(k)E(k) = 2ji\pi\,, \qquad j \in \mathbb{Z}\ . \tag{3.37}$$

Notice that $E(k)$ is analytic everywhere except at $k = \pm im$. Apart from these points, for any fixed j the corresponding solution $\tilde{k}_j$ is the zero of an analytic function and so it must be an isolated zero. This means that the singularities of $F^{\mathrm{L}}(k)$ coming from zeros of (3.37) are poles of some finite order.

These poles and the branch-cut at $k^2 = -m^2$ are the only non-analyticity points of $F^{\mathrm{L}}(k)$ compatible with the locality requirement for the charges included in a LGGE, as depicted in Fig. 3.2(b). Notice that changing $\lambda^{\mathrm{L}}(k)$ but keeping it analytic can only affect the position and possibly the order of the poles, but it can neither introduce extra branch-cut singularities, nor remove the branch-cut placed at $k^2 = -m^2$. Note that in order for λ^{L} to describe a physical correlator it must be real for real momenta. Indeed $\langle\phi(x)\phi(y)\rangle_{\mathrm{LGGE}}$ must be real which in combination with parity invariance means that its Fourier transform must be real and therefore λ^{L} too. This implies that all Lagrange multipliers λ_n must be real. Outside of the radius of convergence R_{conv} the series either diverges to $\pm\infty$ or does not exist at all. In the second case it is impossible to define (3.35), therefore the only sensible cases are $\lambda^{\mathrm{L}}(k) \to \pm\infty$ for $|k| \geq R_{conv}$. Then $F^{\mathrm{L}}(k) = \pm E(k)$ and so neither of these two cases can match with the correct asymptotic behavior (3.36).

It is now clear that a quench protocol like (3.28) is incompatible with the LGGE, due to the incompatibility in the analytic structure of $\lambda(k)$.

So far we studied the GGE in the momentum space, but the GGE predictions are meant to be tested on local observables: it is important to understand if the discrepancy we observe for quantities in momentum space has any noticeable consequences in coordinate space. To this end we study the two point correlator comparing the LGGE prediction $\langle\phi(x)\phi(y)\rangle_{\mathrm{LGGE}}$ with the exact large time result $\langle\phi(x)\phi(y)\rangle_{t\to\infty} = \langle\phi(x)\phi(y)\rangle_{\mathrm{MGGE}}$. We can easily compute the two expressions for $\langle\phi(x)\phi(y)\rangle$ as:

$$\langle\phi(x)\phi(y)\rangle_{t\to\infty} = \langle\phi(x)\phi(y)\rangle_{\mathrm{MGGE}} = \int \frac{\mathrm{d}k}{2\pi} \frac{e^{ik(x-y)}}{2(k^2+m^2)} F(k)\ , \tag{3.38}$$

$$\langle\phi(x)\phi(y)\rangle_{\mathrm{LGGE}} = \int \frac{\mathrm{d}k}{2\pi} \frac{e^{ik(x-y)}}{2(k^2+m^2)} F^{\mathrm{L}}(k)\ . \tag{3.39}$$

Having already showed that there is no way for F and F^{L} to be equal, we conclude that they cannot give equal two point correlators. This is particularly evident at large distances, where we can easily compare the two predictions showing that they give qualitatively different results. Since the correlator is symmetric under exchange of x and y we can assume $x > y$ without loss of generality. Thanks to the algebraic decay of $F(k)$ (3.36), we can compute (3.38) and (3.39) deforming the integration path in the upper complex k-plane, going around any non-analyticities of the integrand that are crossed. The different analytic structure between $F(k)$ and $F^{\mathrm{L}}(k)$ means different path deformations. Fig. 3.3(a) shows the non-analyticities and corresponding path

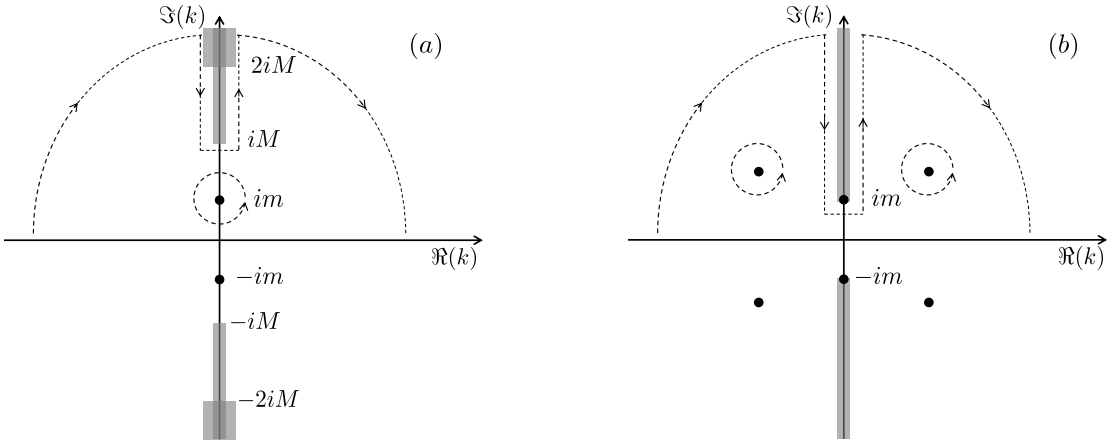

Figure 3.3: *Subfigure (a): deformation of the integration path for the calculation of (3.39) for the exact large time limit or equivalently the MGGE expectation value. For simplicity we consider the case of a single type of particle of mass M in the pre-quench theory. Branch-cuts start at $k = \pm inM$ for $n \in \{1, 2, ..\}$. First order poles are located at $k = \pm im$, due to the factor $(k^2 + m^2)^{-1}$ in (3.39).*
Subfigure (b): deformation of the integration path for the calculation of (3.39) for a LGGE expectation value: two branch-cuts are present starting from $k = \pm im$. The integrand diverges at the branch-cut points due to the presence of the extra factor of $(k^2 + m^2)^{-1}$ in (3.39). Moreover poles determined by the solutions of (3.37) may be present symmetrically located with respect to the origin, since (3.37) is even in k.

deformation for (3.38) using the Källén-Lehmann spectral decomposition, while Fig. 3.3(b) corresponds to the LGGE. For the moment we assume that the radius of convergence R_{conv} of λ^{L} is infinite. We will later discuss the case of finite R_{conv}. To proceed to the calculation of the long distance behavior, we distinguish between two cases: when the post-quench mass m is larger or smaller than the pre-quench mass M.

1. **Pre-quench mass smaller than post-quench mass,** $M < m$:

   In this case, the correct long distance behavior which is given by the MGGE (Fig. 3.3(a)) is determined by the branch-cut singularity at $k = iM$. Thanks to (3.34), we know that this is a square root singularity and the long distance behavior can be readily derived:

   $$\langle \phi(x)\phi(y)\rangle_{\mathrm{MGGE}} = \frac{Z}{4\sqrt{2M\pi}} \frac{e^{-M|x-y|}}{\sqrt{|x-y|}} + \dots , \qquad \text{for } |x-y| \to \infty \ , \tag{3.40}$$

   where Z is the positive field-strength renormalization constant associated with the $\delta-$ singularity of σ at $\mu^2 = M^2$ (3.30). On the other hand, the prediction of a LGGE (Fig. 3.3(b)) cannot be matched with this asymptotic behavior: the branch-cut at $k = im$ results in an exponentially decaying factor $e^{-m|x-y|}$ that is incorrect compared to (3.40). The only way in which we could capture the correct exponential behavior of (3.40) would be to choose the effective temperature in such a way that a first order pole appears at $k = iM$, but even then such a pole would give a plain exponential decay and it would never capture the algebraically decaying factor $1/\sqrt{|x-y|}$ of (3.40).

2. **Pre-quench mass larger than post-quench mass**, $m < M$:

   In this case the leading behavior of the exact two point correlator (Fig. 3.3(a)) is not given by the branch-cut, but by the pole at $k = im$. Instead, the branch-cut at $k = iM$ gives

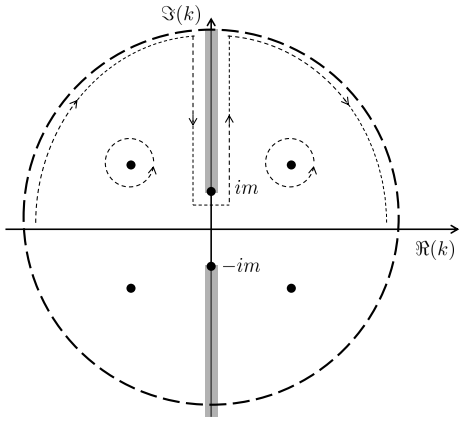

Figure 3.4: *Deformation of the integration path in the complex plane for the computation of the two point correlator with a LGGE (see Eq.* (3.43) *and discussion below), in the case in which the effective temperature has a finite radius of convergence (dashed black line). The interagtion path is constrained in the disk of convergence of the effective temperature.*

subleading corrections:

$$\langle\phi(x)\phi(y)\rangle_{\text{MGGE}} = Ae^{-m|x-y|} + \frac{Z}{4\sqrt{2M\pi}}\frac{e^{-M|x-y|}}{\sqrt{|x-y|}} + ... \qquad |x-y| \to \infty \ , \tag{3.41}$$

where the constant A is:

$$A = \frac{1}{8m}\int \mathrm{d}\mu^2 \sigma(\mu^2)\sqrt{\mu^2 - m^2} \ . \tag{3.42}$$

Consider now the long distance behavior predicted by a LGGE (Fig. 3.3(b)): this time the branch-cut is in the right position to give the exponentially decaying factor $e^{-m|x-y|}$, but it would not be a pure exponential decay, since we are dealing with a branch-cut and not with a pole. Even if we adjusted the effective temperature to obtain the correct leading behavior, the subleading term will not be exponentially damped $e^{-M|x-y|}$ as predicted by the correct computation (3.41). In this case the LGGE fails to catch the correct subleading behavior of the two point correlator at large distances.

Now we consider what happens in the presence of a finite radius of convergence R_{conv}. As explained earlier, for real k outside of the convergence disk i.e. $|k| > R_{conv}$ the only meaningful possibilities are $\lambda^{\text{L}}(k) = \pm\infty$. In this case the two point correlator is:

$$\langle\phi(x)\phi(y)\rangle_{\text{LGGE}} = \int_{-R_{conv}}^{+R_{conv}} \frac{\mathrm{d}k}{2\pi}\frac{e^{ik(x-y)}}{2(k^2+m^2)}\Big(F^{\text{L}}(k) \mp E(k)\Big) \pm \int_{-\infty}^{+\infty}\frac{\mathrm{d}k}{2\pi}\frac{e^{ik(x-y)}}{2\sqrt{k^2+m^2}} \ . \tag{3.43}$$

The second term, in the large distance limit is exponentially damped $\sim e^{-m|x-y|}$. Consider instead the first term: λ^{L} is well defined and analytic in the whole interval, therefore we can consider the analytic continuation of the integrand to the whole complex plane. In particular, $F^{\text{L}}(k)$ is analytic in the whole disk of radius R_{conv}: the large distance behavior of the first term can be computed deforming the integration path in the complex plane, enclosing the non-analyticity points, but in contrast to the previous analysis the integration path is constrained inside the disk (Fig. 3.4). The leading behavior of the two point correlator is no more exponentially damped: differently from before, we cannot lift the integration path from the real axis and we are forced to touch it at the edges of the disk, therefore the end points of the integration contour give a contribution that decays slower than exponentially. Actually, if the radius of convergence is taken

very large, it could happen that the magnitude of the contributions given by the edges of the integration path is very small, in particular vanishing in the limit $R_{\text{conv}} \to \infty$. In this perspective, to compute the asymptotic decay of the two point correlator we should rather look at the non analyticity points inside the disk and therefore we come back to the previous discussion. Overall we conclude that the LGGE fails not only quantitatively, but also qualitatively, to predict the correct asymptotic behavior for the long distance correlator.

3.1.3 The truncated local GGE

So far we analysed the validity of the LGGE definition, now we discuss instead the truncated version TGGE. The content of this section is organized in two distinct steps. Firstly we address the question if there exists at least one sequence of TGGE such that (3.4) is satisfied: this question is well posed independently from the issue of fixing the Lagrange multipliers. The second relevant question is which kind of information is needed in order to fix unambiguously the sequence of truncated GGE, i.e. which are the properties of the charges whose expectation value must be known in advance in order to pursue the construction.

While we find a positive answer to the first question through an explicit construction of a suitable sequence of TGGEs, the second issue is delicate: due to the fact that the expectation values of the local charges are always UV divergent as shown in the previous section, the latter need a proper regularisation. In the literature this problem has been dealt with by regularising the initial state by means of a sharp or exponential UV cutoff. In this case all ultra-local charges acquire finite values and it is easy to see from (3.7) and (3.18) that the correlation function can be expressed directly in terms of them as a short-distance Taylor expansion. However such a regularisation would modify the initial state in a physically relevant way by introducing an explicit energy scale measurable through the values of physical observables. In fact it is impossible to determine a suitable UV cutoff that would consistently and uniquely reproduce the short distance observables in the original initial state [335]. As we have already pointed out, in equilibrium quantum field theory any UV cutoff has already been consistently removed by the standard renormalisation group procedure and physical observables are independent of them. Thus any additional cutoff would require a new renormalisation scheme and a redefinition of the quench protocol. For these reasons, a GGE that does not invoke any additional cutoff on the field theory is desirable.

To circumvent the problem of UV divergences of the charges, we consider the expectation values of the quasi-local charges $\langle \mathcal{Q}^{\mathrm{Q}}(y) \rangle$. On a qualitative level, the local charges $\mathcal{Q}^{\mathrm{L}}_{2n}$ test the system pointwise and are nothing but derivatives of the quasilocal charges $\mathcal{Q}^{\mathrm{Q}}(y)$ (3.21) computed at $y = 0$. Therefore, instead of computing pointwise information, we can consider a small interval and address the following question: given an interval $0 \leq y \leq \epsilon$, is the knowledge of $\langle \mathcal{Q}^{\mathrm{Q}}(y) \rangle$ sufficient in order to determine the GGE? This question can be seen as a natural regularisation of the local charges that attempts to preserve their locality as much as possible: if $\langle \mathcal{Q}^{\mathrm{Q}}(y) \rangle$ was regular at $y = 0$ (more specifically Taylor expandable) its knowledge in a finite small interval $0 \leq y \leq \epsilon$ would have been equivalent to the knowledge of its Taylor coefficients, i.e. the expectation value of the local charges. However, as we are going to show, the information contained in any finite interval is simply insufficient to fix the TGGE, i.e. we ultimately need the knowledge of the expectation value of quasi-local charges at arbitrarily large distances. In particular, this means that any regularisation of the local charges that would be able to fix the GGE, would be essentially equivalent to quasi-local charges with an arbitrary range, consistently with the regularised version of the local charges used in [124].

After this short summary, we start constructing the required sequence of TGGE: as we have already seen, the use of local charges in the construction of the GGE is encoded in the effective temperature that must be an even power series in momentum. Of course, in the case of a truncated LGGE the series is finite and we obtain a polynomial. In particular, a TGGE with N

charges is associated with a polynomial of degree N in the variable k^2

$$\vartheta_N^{\mathrm{T}}(k) = \frac{1}{e^{\lambda_N^{\mathrm{T}}(k)E(k)} - 1}, \qquad \lambda_N^{\mathrm{T}}(k) = \sum_{n=0}^{N} \lambda_n^{(N)} k^{2n} \ . \tag{3.44}$$

Based on our knowledge about the correctness of the MGGE, the convergence of the truncated local GGE is translated into the existence of a sequence of polynomials $\lambda_N^{\mathrm{T}}(k)$ such that

$$\int \frac{\mathrm{d}k}{2\pi} \frac{e^{ik(x-y)}}{2\sqrt{k^2+m^2}} (2\vartheta(k)+1) = \lim_{N\to\infty} \int \frac{\mathrm{d}k}{2\pi} \frac{e^{ik(x-y)}}{2\sqrt{k^2+m^2}} (2\vartheta_N^{\mathrm{T}}(k)+1) \ , \tag{3.45}$$

As already anticipated, we now show that such a sequence indeed exists by means of an explicit construction. As a preliminary step, we introduce the polynomials $q_N(k)$ defined as

$$q_N(k) = \frac{1}{\Lambda_N} \sqrt{\frac{N}{2\pi}} \left(1 - \left(\frac{k}{2\Lambda_N} \right)^2 \right)^{2N} \ . \tag{3.46}$$

Above, Λ_N is a $N-$dependent parameter with dimensions of energy, on which we will comment further in a while. The polynomials q_N possess some features important for what follows: first of all they are always positive $q_N(k) \geq 0$ for any real momentum. More importantly, consider their asymptotic behaviour for large N in the region $|k| < 2\Lambda_N$: if Λ_N is chosen in such a way that $N/\Lambda_N^2 \to \infty$, then

$$q_N(k) \simeq \frac{1}{\Lambda_N} \sqrt{\frac{N}{2\pi}} e^{-2N\left(\frac{k}{2\Lambda_N}\right)^2} \ . \tag{3.47}$$

and the above gaussian is more and more peaked in the $N \to \infty$ limit, until we obtain a Dirac δ-function centered at $k = 0$. Moreover, if we choose Λ_N in such a way that it diverges in the $N \to \infty$ limit, but at the same time $N/\Lambda_N^2 \to \infty$, the polynomials $q_N(k)$ tend to a δ-function over an increasing interval of momenta from $-\Lambda_N$ to $+\Lambda_N$. For example, we can require $\Lambda_N \propto N^{1/3}$: the proportionality constant has the dimension of a momentum, but its actual value is completely irrelevant in the following discussion.

From the polynomials $q_N(k)$ and the correct value of the effective temperature $\lambda(k)$, we construct now the effective temperatures for our truncated LGGEs

$$\lambda_{2N}^{\mathrm{T}}(k) = \int_{-\Lambda_N}^{\Lambda_N} \mathrm{d}p \ \lambda(p) q_N(k-p) + C \left(\frac{k}{\Lambda_N} \right)^{2N} \ , \tag{3.48}$$

where C is a positive constant with the dimension of an inverse energy, but its actual value is completely irrelevant. Since q_N are even polynomials of order $4N$, the $\lambda_{2N}^{\mathrm{T}}(k)$ defined above is an even polynomial of the same order as well, thus it can be interpreted as the effective temperature associated with a TGGE constructed out of the first $2N$ even local charges. It should be clarified that by this it is not meant that the TGGE constructed in this way gives correctly the values of the first $2N$ local charges, which is not literally possible due to their UV divergences. Instead, this ensemble should be considered simply as an element of a sequence of TGGEs designed to converge to the correct steady state.

Notice also that, being the effective temperature λ and the polynomials q_N both positive functions, the $\lambda_{2N}^{\mathrm{T}}$ polynomial we defined is strictly positive as well: this is important to avoid a negative or singular excitation density when (3.48) is plugged in (3.45). Consider now the behavior of $\lambda_{2N}^{\mathrm{T}}(k)$ in the large N limit: for any $|k| < \Lambda_N$ we get that $\lambda_{2N}^{\mathrm{T}}(k)$ approaches the correct effective temperature $\lambda(k)$. This can be easily seen from the fact that for $|k| < \Lambda_N$ the argument of $q_N(k-p)$ is always in the region where q_N mimics the delta function, since $|k-p| < 2\Lambda_N$ over all the integration domain. In the same region, the additional term in (3.48) does

not matter, because for $|k| < \Lambda_N$ it gives an exponentially vanishing contribution. Since Λ_N is chosen to be divergent in N, $\lambda^{\mathrm{T}}_{2N}(k)$ approaches the correct value $\lambda(k)$ on an interval of an increasing, divergent, length.

However, when $\lambda^{\mathrm{T}}_{2N}$ is used in the integral (3.45), its argument is not constrained to the interval $|k| < \Lambda_N$, but rather runs over the whole real axis. In particular, the integral over the domain $|k| > \Lambda_N$ (where $\lambda^{\mathrm{T}}_{2N}(k)$ is completely different from $\lambda(k)$) must be guaranteed to give a vanishing contribution when $N \to \infty$: this holds true thanks to the presence of the additional term in (3.48). Indeed, being the integral of (3.48) a positive quantity, we have

$$\lambda^{\mathrm{T}}_{2N}(k) \geq C \left(\frac{k}{\Lambda_N} \right)^{2N} . \tag{3.49}$$

Therefore, for $|k| > \Lambda_N$ the polynomial $\lambda^{\mathrm{T}}_{2N}(k)$ is more and more divergent in k when N is sent to infinity, providing an effective cut off in the consequent excitation density (3.45)

$$\vartheta^{\mathrm{T}}_{2N}(k) \simeq \vartheta(k)\Theta(\Lambda_N^2 - k^2) , \qquad N \gg 1 , \tag{3.50}$$

where Θ is the Heaviside Theta function. This finally guarantees that

$$\lim_{N\to\infty} \int \frac{\mathrm{d}k}{2\pi} \frac{e^{ik(x-y)}}{\sqrt{k^2+m^2}} \vartheta^{\mathrm{T}}_{2N}(k) = \lim_{N\to\infty} \int_{-\Lambda_N}^{\Lambda_N} \frac{\mathrm{d}k}{2\pi} \frac{e^{ik(x-y)}}{\sqrt{k^2+m^2}} \vartheta(k) = \int_{-\infty}^{+\infty} \frac{\mathrm{d}k}{2\pi} \frac{e^{ik(x-y)}}{\sqrt{k^2+m^2}} \vartheta(k) . \tag{3.51}$$

The above identity guarantees the convergence of the correlation function that corresponds to the above constructed sequence of TGGEs to the correct value (3.45).

Notice that even though Λ_N behaves as an effective cut off, it is introduced through the GGE construction and there is no need to impose any additional external cut off on the field theory itself, thus the above construction is fully compatible with standard RG applied on the initial state.

Even though the required sequence of truncated LGGEs has been constructed, it must be stressed that the previous construction is strongly based on the exact effective temperature $\lambda(k)$, that is ultimately in one-to-one correspondence with the excitation density. Thus, as we anticipated, we now investigate the amount of information needed to fix unambiguously the sequence of truncated GGEs. In particular, we show that the knowledge of the expectation value $\langle \mathcal{Q}^{\mathrm{Q}}(y) \rangle$ for $0 \leq y \leq \epsilon$ is insufficient for any finite ϵ.

The proof of this fact is simple: directly from the definition of the quasi-local charges, the expectation value (normalized on the system size L) on the initial state is

$$L^{-1} \langle \mathcal{Q}^{\mathrm{Q}}(y) \rangle = \int \frac{\mathrm{d}k}{2\pi} \cos(ky) E(k) \vartheta(k) . \tag{3.52}$$

As we see, the expectation value of the quasi-local charges is linked to the excitation density by means of a simple Fourier transform. Of course, the Fourier transform is invertible only if we are allowed to span the whole axis. Thus, the information on the quasi local charges with $0 \leq y \leq \epsilon$ is not enough to unambiguously fix the excitation density. Let then $\vartheta'(k)$ be another excitation density such as

$$\vartheta(k) - \vartheta'(k) = \frac{1}{E(k)} \int_{|\tau|>\epsilon} \mathrm{d}\tau \, \cos(\tau k) a(\tau) , \tag{3.53}$$

where $a(\tau)$ is any reasonable function, such that both $\vartheta(k)$ and $\vartheta'(k)$ are positive functions for any k (this is needed because any physical relevant excitation density is a positive real function) and such that both give a finite excitation energy. Both $\vartheta(k)$ and $\vartheta'(k)$ are parity invariant $k \to -k$

and when plugged in (3.52) they give exactly the same result for $0 \leq y \leq \epsilon$, however different excitation densities means different correlators.

Previously we showed how we can construct a sequence of truncated LGGE that reproduces the expectation value of correlators of a given excitation density: therefore, we can construct two sequences of TGGE, one converging to $\vartheta(k)$ and the other to $\vartheta'(k)$, that give different predictions for the local observables despite having the same expectation value of the quasi-local charges over the selected interval.

Thus, we can conclude that the information contained in an interval of finite length ϵ is not enough to fix the GGE: we are in principle forced to consider $\epsilon \to \infty$, i.e. quasi local charges with arbitrary spread.

3.1.4 Quasi locality of the GGE

In the previous sections we carefully analyzed the LGGE and TGGE definitions: albeit we found that a proper sequence of TGGE converging to the correct MGGE can be actually found, we also showed that the quasilocal charges of (in general) arbitrary extension (3.21) are actually needed to fix the GGE. In this perspective, it is more natural to construct the ensemble directly in terms of the quasilocal charges. First, as we did for the mass quench, we want to verify that the MGGE can indeed be expressed as a QGGE. Second, we study the locality properties of the ensemble encoded in the kernel $\mathcal{K}(y)$ (3.22). Lastly, we characterize the amount of information needed to unambiguously fix the QGGE: despite the continuous nature of the set of quasilocal charges, we show that only a countable set of information is actually needed.

To verify that quasilocal charges correctly describe the exact steady state i.e. the MGGE, we should verify that it is possible to compute the Fourier transform of the effective temperature. Using the Källen-Lehman spectral decomposition (3.32) we see that $\lambda(k)$ has no singularities for real k and moreover it is easy to see that $\sigma(k)$ decays algebraically for large momenta. We therefore have that for large momenta

$$\lambda(k) \simeq \frac{1}{|k|} \log\left(\frac{k^4}{r^4}\right) + \mathcal{O}\left(\frac{\log|k|}{|k|^3}\right), \qquad r = \left[\frac{1}{16}\int \mathrm{d}\mu^2\, \sigma(\mu^2)(m^2-\mu^2)^2\right]^{\frac{1}{4}} . \tag{3.54}$$

This guarantees that the effective temperature has a proper Fourier transform and therefore $\mathcal{K}(y)$ is well defined (3.23) for any $y \neq 0$, but it has the same logarithmic divergence in $y = 0$ as in the free mass quench, once we substitute in (3.26) the new definition of r. We can now study the decaying properties of $\mathcal{K}$: exactly as we did for the mass quench in Section 3.1.1, the non-analyticity point of $\lambda(k)$ closest to the real axis rules the large distance behavior of $\mathcal{K}$. From (3.14) we can express $\lambda(k)$ in terms of $\vartheta(k)$:

$$\lambda(k) = \frac{1}{E(k)} \log\left(1 + \frac{1}{\vartheta(k)}\right) . \tag{3.55}$$

Using (3.32) and (3.55), we can readily see that $\lambda(k)$ acquires the non-analyticities of the spectral density, but additional logarithmic branch-cuts may appear too. However, it is possible to show that in the strip $|\Im(k)| < \min(m, M)$ (where M is the minimum among the pre quench masses) there are no logarithmic branch cuts. Since there is surely a branch cut at $k = i\min(m, M)$ due to the presence of the square roots, this information is enough to extract the long distance behavior of $\mathcal{K}(y)$:

$$\mathcal{K}(y) \sim e^{-\min(m,M)|y|} , \tag{3.56}$$

where we neglect non exponential corrections. The inverse masses of the pre-quench and post-quench theory provide the minimum length scale required for an effective truncation of the

quasilocal charges that should be included in the QGGE. Retaining quasi-local charges up to the minimum mass scale is expected to give a good description of the two point correlator, nevertheless any truncation would fail to exactly capture its asymptotic behavior.

In order to show the absence of logarithmic branch cuts in the strip $|\Im(k)| < \min(m, M)$ we can argue as follows: we choose the logarithmic branch cut of $\log z$ to start from 0 and to reach $-\infty$ along the real axis, therefore the branch cut is crossed every time the $\Re(z) \leq 0$ and $\Im(z)$ changes its sign. As a first step we can find regions in the complex plane such that the imaginary part of the analytical continuation of the excitation density is different from zero: in these regions there is no logarithmic branch cut. Looking at (3.55), this is possible if and only if $\Im\vartheta(k) \neq 0$. Thanks to (3.32) we have

$$\Im\vartheta(k) = \frac{1}{2}\int \mathrm{d}\mu^2\, \sigma(\mu^2)\, \Im\left[f\left(\frac{2}{|m^2-\mu^2|}\left[k^2 + \frac{m^2+\mu^2}{2}\right]\right)\right] \ , \tag{3.57}$$

where the complex function $f(z)$ is defined to be

$$f(z) = \frac{z}{\sqrt{z+1}\sqrt{z-1}} \ . \tag{3.58}$$

Since the spectral density is real and strictly positive, a non vanishing imaginary part of the excitation density is guaranteed as soon as the imaginary part of the integrand has a constant sign for all values of μ in the support of σ. The imaginary part of $f(z)$ has a constant sign in each quadrant of the complex plane and this allows us to identify regions where the imaginary part of the excitation density is not zero. For example the first quadrant $\Re(z) > 0, \Im(z) > 0$ in terms of the complex momentum k is identified as:

$$\Re(k)^2 - \Im(k)^2 + \frac{m^2+\mu^2}{2} > 0, \qquad \Re(k)\Im(k) > 0 \ . \tag{3.59}$$

Solving the first inequality with respect to the imaginary part and requiring the inequality to be satisfied for any μ in the support of the spectral density we find a region in the complex plane of the momentum such that the imaginary part of the excitation density is never zero. Considering also the inequalities coming from the other quadrants we have:

$$\Im\vartheta(k) \neq 0 \ \ \forall\, k \in A, \qquad A = \left\{ |\Im(k)| < \sqrt{\Re(k)^2 + \frac{m^2+M^2}{2}} \text{ and } \Im(k)\Re(k) \neq 0 \right\} \ . \tag{3.60}$$

Because of this condition, if logarithmic branch cuts are present in the strip $|\Im(k)| < \min(m, M)$ they must be located along the imaginary axis. Looking at the expression for the effective temperature (3.32) it is evident that the integrand along this axis and within the strip $|\Im(k)| < \min(m, M)$ is always real and strictly positive. Since logarithmic branch cuts occur only when the real part of the excitation density $\vartheta(k)$ is negative, we conclude that there is no logarithmic branch cut in the strip.

We finally address the problem of quantifying the amount of information needed in order to determine the GGE. Recalling the expression (3.52) that links the excitation density with the expectation value of the local charges, we understand that the two are linked through a simple Fourier transform. Knowing $\langle \mathcal{Q}^{\mathrm{Q}}(y) \rangle$ for each y we can certainly invert the Fourier transform (3.52) and obtain the excitation density, which completely fixes the effective temperature and thus the GGE, as already pointed out in [123]. However, we are going to show that a continuous amount of information is not really needed and we can restrict ourselves to a countable set of suitably defined quasi-local charges. Consider the function $E(k)\vartheta(k)$, whose Fourier transform is the expectation value of the quasi-local charges (3.21): as it is clear from the Källén-Lehmann spectral decomposition, this is a positive, bounded, continuous function of k. Moreover, in all

the quenches we considered so far and in any meaningful quench, the total energy density is finite

$$\int \mathrm{d}k\, E(k)\vartheta(k) < \infty \ . \tag{3.61}$$

The above statement, combined with the fact that $E(k)\vartheta(k)$ is positive and bounded, implies that $E(k)\vartheta(k)$ is square-integrable

$$\int \mathrm{d}k\, |E(k)\vartheta(k)|^2 < \infty \ . \tag{3.62}$$

Therefore, $E(k)\vartheta(k)$ as well as its Fourier transform, belongs to the Hilbert space of the square-integrable functions, that is a well-known separable Hilbert space, i.e. it possesses a countable orthonormal basis that, without loss of generality, can be chosen to be real. In what follows we can use essentially any basis we prefer, but as a concrete example we choose the eigenfunctions of the harmonic oscillator

$$f_n(y) = \frac{(\omega/\pi)^{1/4}}{\sqrt{2^n n!}} e^{-\frac{\omega}{2}y^2} H_n(\sqrt{\omega}y) \tag{3.63}$$

where in the above ω is a parameter inserted for dimensional reasons, but its actual value does not affect the subsequent discussion, while $H_n(y)$ are the Hermite polynomials. Then, it is true that we can expand $\langle \mathcal{Q}^{\mathrm{Q}}(y)\rangle$ in terms of these eigenfunctions. Since $\langle \mathcal{Q}^{\mathrm{Q}}(y)\rangle$ is even, only the even functions f_n will enter in its expansion

$$\langle \mathcal{Q}^{\mathrm{Q}}(y)\rangle = \sum_{n=0}^{\infty} c_{2n}\, f_{2n}(y), \qquad c_{2n} = \int \mathrm{d}y\, f_{2n}(y)\, \langle \mathcal{Q}^{\mathrm{Q}}(y)\rangle \ . \tag{3.64}$$

Therefore the knowledge of the c_{2n} constants determines $\langle \mathcal{Q}^{\mathrm{Q}}(y)\rangle$ and then, through Fourier transform, we can fix $E(k)\vartheta(k)$: these equalities hold in the sense of the L^2 norm, but this determines an unique continuous function $\vartheta(k)$. The excitation density of course fixes the effective temperature and thus the QGGE.

Therefore, the QGGE is in one-to-one correspondence with the set of the c_{2n} coefficients, but the latter can be easily seen to be the expectation value of properly defined quasi-local charges:

$$c_{2n} = \langle \mathcal{Q}^{\mathrm{Q}}_{2n}\rangle\,, \qquad \mathcal{I}^{\mathrm{Q}}_{2n} = \int \mathrm{d}y\, f_{2n}(y)\mathcal{Q}^{\mathrm{Q}}(y) \ . \tag{3.65}$$

The charges $\mathcal{Q}^{\mathrm{Q}}_{2n}$ are clearly quasi-local: the coupling among different points is given by the kernel f_{2n} that, because of our choice (3.63), is damped by a gaussian kernel. Thus, we conclude that the knowledge of the expectation value of the countable set of quasi-local charges $\mathcal{Q}^{\mathrm{Q}}_{2n}$ unambiguously fixes the GGE.

3.1.5 Concluding remarks

In this section we carefully analyzed the locality properties of the GGE describing the steady state after interacting-to-free homogeneous quenches in relativistic continuum models. As was pointed out in Ref. [123], in free continuum models the GGE constructed out of only local charges can fail even for free systems, in contrast with the lattice-based models.

Indeed, we showed that it is the case and the local charges (i.e. spatial integral of local densities) cannot correctly describe the GGE, the discrepancy being clearly visible in the large distance asymptotics of two point correlators. On the contrary, quasilocal charges (i.e. spatial integrals of operators with vanishing support) are needed: more specifically, we show that the correct GGE can be constructed out of a numerable set of suitably defined conserved charges.

3.2 Spreading of entanglement after a quench with intertwined quasiparticles

The central object of this Section is the entanglement entropy (1.6) [128–130] , whose definition we recall for the sake of convenience

$$S_A \equiv -\mathrm{Tr}\hat{\rho}_A \ln \hat{\rho}_A, \tag{3.66}$$

where $\hat{\rho}_A \equiv \mathrm{Tr}_{\bar{A}}|\psi\rangle\langle\psi|$ is the reduced density matrix of a subsystem A (having $\bar{A}$ as complement) of a system in a pure state $|\psi\rangle$. Its growth is responsible of the efficiency of tensor network algorithms such as DMRG [131–136]. Furthermore, the extensive value (in subsystem size) reached by the entanglement entropy at long time has been understood as the thermodynamic entropy of the ensemble describing stationary local properties of the system [139–141, 336–343].

The quasiparticle description frames the entanglement growth in a simple semiclassical picture, which nevertheless provides the (scaling part of the) time evolution of the entanglement. In this perspective, the initial state is regarded as a source of entangled quasiparticles which ballistically propagate across the system and carry entanglement. Understanding the structure of the correlations between the emitted quasiparticles is fundamental in dragging quantitative predictions. For example, in Ref. [138] the XY spin-chain has been considered

$$H_{XY} = -\sum_{j=1}^{N}\left[\frac{1+\gamma}{4}\sigma_j^x\sigma_{j+1}^x + \frac{1-\gamma}{4}\sigma_j^y\sigma_{j+1}^y + \frac{h}{2}\sigma_j^z\right], \tag{3.67}$$

and quenched in the magnetic field $h^{t<0} \to h$, starting from the ground state at $h^{t<0}$. The XY model is diagonalised in terms of spinless fermions through a Jordan-Wigner transformation: in the thermodynamic limit $N \to \infty$ the momentum is continuous, thus the fermions obey $\{\eta(k), \eta^\dagger(q)\} = \delta(k-q)$, and

$$H_{XY} = \int_{-\pi}^{\pi} \mathrm{d}k\, E(k)\eta^\dagger(k)\eta(k) + \text{const.}. \tag{3.68}$$

The prequench ground state, identified with the vacuum of the prequench modes $|0_{h^{t<0}}\rangle$, is readily written in terms of the post quench vacuum $|0_h\rangle$ in the form of a squeezed state

$$|0_{h^{t<0}}\rangle \propto \exp\left[-\int_0^{\pi} \mathrm{d}k\, \mathcal{K}(k)\eta^\dagger(k)\eta^\dagger(-k)\right]|0_h\rangle\,, \tag{3.69}$$

with $\mathcal{K}$ a non trivial function of h and $h^{t<0}$, its specific form being irrelevant for our purposes. Squeezed states are common in quenches in free theories, due to the fact that the pre and post quench modes are usually connected through a Bogoliubov rotation. The form of Eq. (3.69) is rather appealing: the quench modes are excited in pairs of opposite momenta, distinct pairs being created independently. In this case, the entanglement growth is well described by the following quasiparticle picture [137].

The initial state is regarded as a source of quasiparticles, homogeneously distributed in space. After the quench, each particle ballistically propagates with velocity $v(k) = \partial_k E(k)$. Pairs originated at different positions or with different momentum are unentangled, only particles belonging to the same pair of momentum $(k, -k)$ and originated in the same position are entangled. Given the partition of the system $A \cup \bar{A}$ and considered a time t, only pairs such that one quasiparticle belongs to A and the other to $\bar{A}$ contribute to the entanglement, being their contribution additive. In the case where A is chosen to be an interval of length ℓ, the entanglement

entropy, in the space-time scaling limit $t, \ell \to \infty$ with t/ℓ fixed, has the following scaling form

$$S_A(t) = 2t \int_{2|v(k)|t<\ell} \frac{\mathrm{d}k}{2\pi} |v(k)| s(k) + \ell \int_{2|v(k)|t\geq\ell} \frac{\mathrm{d}k}{2\pi} s(k)\,, \tag{3.70}$$

where $s(k)$ is the contribution to the entanglement associated with each pair. In the standard homogeneous situation, the weight $s(k)$ can be fixed by requiring that for $t \to \infty$ the entanglement entropy density matches the thermodynamic one of the post quench steady state [139–141]

$$s(k) = -\vartheta(k) \log \vartheta(k) - \big[1 - \vartheta(k)\big] \log \big[1 - \vartheta(k)\big], \tag{3.71}$$

being $\vartheta(k) = |\mathcal{K}(k)|^2/(1 + |\mathcal{K}(k)|^2)$ the density of excitations of momentum k, i.e. $\langle \eta^\dagger(k)\eta(q)\rangle = \delta(k-q)\vartheta(k)$. The generalisation to several, *uncorrelated*, particle species is obvious, one has just to sum over the contributions of each independent species. This is a simple further step which allows us to describe quenches in truly interacting models where several particle species may be present. Indeed, in Ref. [139] quenches in the XXZ spin-chain have been considered, and the quasiparticle picture (3.70) (through a suitable dressing of the velocity $v(k)$ and the weight $s(k)$) has been found to be correct. Interestingly, also Eq. (3.71) has a very simple semiclassical interpretation. Indeed, focussing on a given momentum k, $s(k)$ is just the entropy (i.e. the logarithm of the number of equivalent microstates) of a mode which is occupied with probability $\vartheta(k)$ and empty with probability $1 - \vartheta(k)$.

The main physical feature for the entanglement evolution captured by Eq. (3.70) is the so-called light-cone spreading, i.e. a linear increase at short time followed by saturation to an extensive value in ℓ. Indeed, if a maximum velocity v_{max} for the quasiparticles exists, then since $|v(k)| \leq v_{\mathrm{max}}$, the second term vanishes when $2v_{\mathrm{max}}t < \ell$, and the first integral is over all positive momenta, so that $S_A(t)$ is strictly proportional to t. On the other hand as $t \to \infty$, the first term is negligible and $S_A(\infty)$ is proportional to ℓ. Actually, analytical, numerical and experimental results [339–342, 344–350] suggest that such a light-cone spreading is more generically valid that what suggested by the quasiparticle picture.

At this point, it must be clear that the physical assumptions behind the validity of Eq. (3.70) for the entanglement evolution is that quasiparticles must be produced *uniformly in space and in uncorrelated pairs of opposite momenta*. Given the large success of Eq. (3.70) in describing the entanglement evolution in the scaling regime, a lot of recent activity has been devoted to understand how Eq. (3.70) gets modified when some of these assumptions are weakened. For example, the quasiparticle picture has been extended to large-scale inhomogeneous setups [176] in which the initial state is regarded as a *non uniform* source of quasiparticles which ballistically propagate for $t > 0$. While the final expression (3.70) is slightly modified in order to keep in account the initial inhomogeneity, the core of the result is still Eq. (3.71), where $\vartheta(k)$ is promoted to have a weak spatial dependence and the semiclassical interpretation of the entanglement weight still holds true.

Another setup in which the semiclassical interpretation can be applied, but which lays outside the usual framework of uncorrelated pairs, has been studied in Ref. [142] in a free-fermion model. In that case, the homogeneous initial state was populated with excitations of n different species, with a constraint on the sum of the excitation densities $\sum_{i=1}^n \vartheta_i(k) = 1$ which ultimately introduces non trivial correlations. However, this constraint is classical in nature and it does not spoil the semiclassical interpretation of the entanglement entropy. As a matter of facts, the constraint changes the form of Eq. (3.71), which nevertheless can still be viewed as the entropy of fermions obeying the extra condition. In particular, the entanglement growth is fully determined in terms of the excitation densities $\{\vartheta_i(k)\}_{i=1}^n$ and of the velocities of each species $\{v_i(k)\}_{i=1}^n$ with no other information required.

In this section we investigate those situations where the initial state is populated by several

quasiparticle species, which are non trivially *quantum-correlated*. The presence of true quantum correlation among the excitations forces us to dismiss the simple entanglement weight (3.71) together with its classical interpretation. However, despite this lack of classicality, the quasiparticle paradigm will still hold true and the entanglement growth (in the scaling limit) is fully determined in terms of ballistically-propagating localised excitations.

In particular, we are interested in free Hamiltonians possessing n species of excitations (assumed to be fermionic for concreteness)

$$H = \sum_{i=1}^{n} \int_{-B}^{B} \mathrm{d}k \, E_i(k) \eta_i^\dagger(k) \eta_i(k) \, . \tag{3.72}$$

Each mode has its own group velocity $v_i(k) = \partial_k E_i(k)$ and we assume the existence of a single Brillouin zone $[-B, B]$. The initial state $|\Psi\rangle$ is taken to be a non trivial generalisation of the single species squeezed state (3.69), i.e.

$$|\Psi\rangle \propto \exp\left[- \int_0^B \mathrm{d}k \sum_{i=1,j=1}^{n} \mathcal{M}_{i,j}(k) \, \eta_i^\dagger(k) \eta_j^\dagger(-k) \right] |0\rangle \, , \tag{3.73}$$

where $|0\rangle$ is the vacuum $\eta_i(k)|0\rangle = 0$. This class of states is gaussian, i.e. the knowledge of all the correlation functions can be reduced, by mean of a repeated use of the Wick Theorem, to the two-point correlators

$$\langle \eta_i^\dagger(k) \eta_j(q) \rangle = \delta(k-q) \, \mathcal{C}^{(1)}_{i,j}(k), \qquad \langle \eta_i^\dagger(k) \eta_j^\dagger(q) \rangle = \delta(k+q) \, \mathcal{C}^{(2)}_{i,j}(k) \, , \tag{3.74}$$

where the correlation matrices $\mathcal{C}^{(1)}(k)$, $\mathcal{C}^{(2)}(k)$ have dimension $n \times n$ and are functions of $\mathcal{M}(k)$, the specific relation being inessential for our purposes. The contact point with the previous literature can be made in the case where $\mathcal{C}^{(1)}(k)$ and $\mathcal{C}^{(2)}(k)$ are diagonal on the particle species. States in the form (3.73) are not rare, making our generalisation more than a mere academic question. For example, we can reside to suitable inhomogeneous quenches in free models in order to realise states such as (3.73), as we explain thereafter.

Our quasiparticle ansatz will be formulated in full generality without looking at a precise model, however we ultimately rely on the periodically-modulated inhomogeneous Ising chain as a convenient benchmark

$$H = -\frac{1}{2} \sum_{j=1}^{N} \left[\sigma_j^x \sigma_{j+1}^x + h_j \sigma_j^z \right] , \tag{3.75}$$

where we require h_j to be periodic with period n

$$h_j = h_{j+n} \, . \tag{3.76}$$

The periodicity of the magnetic field effectively splits the original lattice into n sublattices coupled in a non trivial way, each one with lattice spacing n so that the Hamiltonian (3.75) can be then diagonalised in terms of n particle species $\{\eta_i(k)\}_{i=1}^n$. Starting in the ground state for a given set of magnetic fields and quenching towards different $\{h_j\}_{j=1}^n$ creates initial states in the form (3.73). Of course, in the scaling region where the quasiparticle description holds true, the lengthscale of the inhomogeneity is negligible: such a quench can be regarded as being homogeneous with several species of quasiparticles.

This section is organised as it follows: in Section 3.2.1 we present a general discussion of our quasiparticle ansatz for states in the form (3.73). In Section 3.2.3 we benchmark our predictions in the inhomogeneous Ising model, providing the details of its solution. In Section 3.2.4 we provide a quasiparticle description for the time evolution of the correlators of the order parameter

in the inhomogeneous Ising model, thus generalising the results of Ref. [107, 143].

3.2.1 The quasiparticle prediction for the entanglement entropy spreading

In this section we present our result for the time evolution of the entanglement entropy. Of course, being a quasiparticle prediction, its derivation is not rigorous, but relies on reasonable physical arguments and on the experience gained from the existing literature. Our arguments are somehow related to those of Ref. [176], where the standard quasiparticle picture for a single species and pair excitations has been extended to weakly inhomogeneous non-equilibrium protocols. For definiteness, we focus on a a bipartition $A \cup \bar{A}$ where A is an interval of length ℓ. Following the standard quasiparticle picture, we regard the initial state as a source of excitations such that *i)* quasiparticles generated at different spatial points are not entangled, *ii)* quasiparticles associated with pairs of different momentum are not entangled. As usual [137, 176], we further assume the contribution to the entanglement of unentangled pairs to be additive

$$S_A(t) = \int_{-\infty}^{\infty} \mathrm{d}x \int_0^B \frac{\mathrm{d}k}{2\pi} s_A(x,k,t)\,. \tag{3.77}$$

Here, $s_A(x,k,t)$ is the contribution to the entanglement at time t given by the quasiparticles originated at $t=0$ in position x and with momentum $\pm k$ (the momentum integration in (3.77) runs on positive values in order to avoid double counting). The difficulty, as well as the main result of our investigation, is finding the correct ansatz for $s_A(x,k,t)$: we propose to construct $s_A(x,k,t)$ out of suitable finite-dimensional ancillary Hilbert spaces and partitions thereof. To each position x and momentum k we associate a Hilbert space constructed as a Fock space starting from a vacuum $|0^{x,k}\rangle$, acting with $2n$ fermions $\{f_j^{x,k}, [f_i^{x,k}]^\dagger\} = \delta_{i,j}$; such a Hilbert space has dimension 2^{2n}. We recall that n is the number of different species of quasiparticles. We have in mind the following, suggestive, correspondence

$$f_i^{x,k} \longleftrightarrow \eta_i(k)\,, \qquad\qquad f_{i+n}^{x,k} \longleftrightarrow \eta_i(-k)\,. \tag{3.78}$$

In order to make clearer and precise such a statement, we consider a state in the ancillary Hilbert space encoded in a density matrix $\hat{\rho}^{x,k}$ such that: *i)* it is gaussian in the fermions $f_i^{x,k}$ (i.e. the Wick Theorem holds true); *ii)* its correlators are the same of the corresponding modes. More specifically, let us organise the $\eta_i(k)$ modes and the fermions $f_i^{x,k}$ in single vectors as

$$\Gamma(k) = \begin{pmatrix} \eta_1(k) \\ \dots \\ \eta_n(k) \\ \eta_1(-k) \\ \dots \\ \eta_n(-k) \\ \eta_1^\dagger(k) \\ \dots \\ \eta_n^\dagger(k) \\ \eta_1^\dagger(-k) \\ \dots \\ \eta_n^\dagger(-k) \end{pmatrix}, \qquad\qquad \mathcal{F}_{x,k} = \begin{pmatrix} f_1^{x,k} \\ \dots \\ f_{2n}^{x,k} \\ [f_1^{x,k}]^\dagger \\ \dots \\ [f_{2n}^{x,k}]^\dagger \end{pmatrix}. \tag{3.79}$$

We then consider the correlation functions $\langle \Gamma(k)\Gamma^\dagger(q)\rangle$ and $\langle \mathcal{F}_{x,k}\mathcal{F}_{x,k}^\dagger\rangle_{\hat{\rho}^{x,k}}$, where the first expectation value is taken with respect to the state in Eq. (3.73), while the second on the ancillary Hilbert space on the density matrix $\hat{\rho}^{x,k}$ which is defined in such a way to satisfy (we recall that

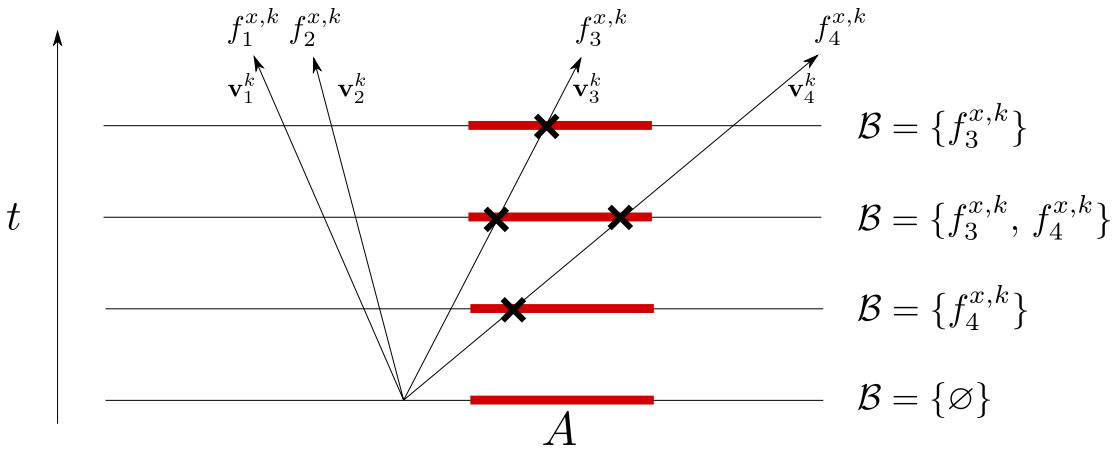

Figure 3.5: *Quasiparticles which contribute to the entanglement entropy at time t. We consider a bipartition of the system $A \cup \bar{A}$ where A is a single interval (red thick line). We show the ballistic evolution of some pairs of quasiparticles with momentum k and originated in position x. Each fermion $f_i^{x,k}$ propagates with its own velocity $\mathbf{v}_i^k$. At a given time t, the initial set of fermions is divided into two subsets $\mathcal{B}$ and $\bar{\mathcal{B}}$, where in $\mathcal{B}$ appear those fermions which are carried in A by the ballistic evolution. Figure taken from Ref. [6].*

momenta are positive)

$$\langle \Gamma(k)\Gamma^\dagger(q)\rangle = \delta(k-q)\mathcal{C}(k), \qquad \mathcal{C}(k) = \langle \mathcal{F}_{x,k}\mathcal{F}_{x,k}^\dagger\rangle_{\hat{\rho}^{x,k}}\,. \tag{3.80}$$

We finally impose $\langle f_i^{x,k}\rangle_{\hat{\rho}^{x,k}} = 0$. Given that the density matrix $\hat{\rho}^{x,k}$ is Gaussian, having established its one- and two-point functions completely fixes the density matrix itself. The matrix $\mathcal{C}(k)$ has dimension $4n \times 4n$ and may be written in terms of the correlation matrices $\mathcal{C}^{(1)}(k)$ and $\mathcal{C}^{(2)}(k)$ in (3.74) as

$$\mathcal{C}(k) = \left(\begin{array}{c|c|c|c} \mathrm{Id} - \mathcal{C}^{(1)}(k) & 0 & 0 & [\mathcal{C}^{(2)}(-k)]^\dagger \\ \hline 0 & \mathrm{Id} - \mathcal{C}^{(1)}(-k) & [\mathcal{C}^{(2)}(k)]^\dagger & 0 \\ \hline 0 & \mathcal{C}^{(2)}(k) & \mathcal{C}^{(1)}(k) & 0 \\ \hline \mathcal{C}^{(2)}(-k) & 0 & 0 & \mathcal{C}^{(1)}(-k) \end{array}\right). \tag{3.81}$$

In particular, thanks to the block structure

$$\mathcal{C}(k) = \left(\begin{array}{c|c} \mathrm{Id} - M & N \\ \hline N^\dagger & M \end{array}\right), \tag{3.82}$$

with M and N being $2n \times 2n$ matrices (and $M = M^\dagger$), it is always possible to define a density matrix $\hat{\rho}^{x,k}$ such that Eq. (3.80) holds true.

This picture semiclassically describes the initial conditions. Now we consider the time evolution: to each ancillary fermion we associate a velocity through the correspondence (3.78)

$$f_i^{x,k} \to \mathbf{v}_i^k = v_i^k(k), \qquad f_{i+n}^{x,k} \to \mathbf{v}_{i+n}^k = v_i^k(-k)\,. \tag{3.83}$$

Then, at a given time t, we introduce a bipartition of the ancillary Hilbert space $\mathcal{B} \cup \bar{\mathcal{B}}$ accordingly to the following rule (see also Fig. 3.5)

$$i \in \mathcal{B} \qquad \Longleftrightarrow \qquad x + t\mathbf{v}_i^k \in A\,. \tag{3.84}$$

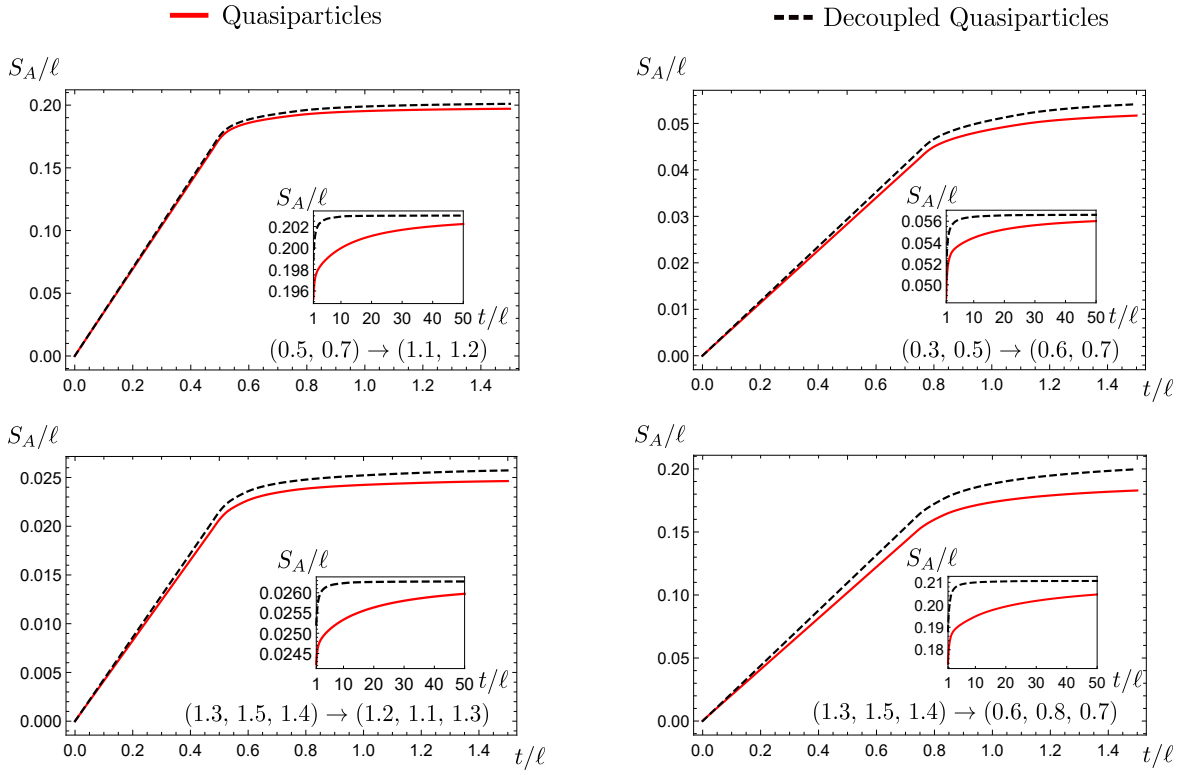

Figure 3.6: *Entanglement entropy evolution for various quenches* $\{h_i^{t<0}\}_{i=1}^n \to \{h_i\}_{i=1}^n$ *in the inhomogeneous Ising model (further details in Section 3.2.3), for a bipartition* $A \cup \bar{A}$*, where* A *is a finite interval of length* ℓ*. In each panel we plot the rescaled entanglement entropy* S_A/ℓ *as a function of the rescaled time* t/ℓ *and compare our ansatz (continuous red line) with a naive application of the uncorrelated quasiparticle formula* (3.70) *(black dashed line), finding sizeable differences. At infinite time, the two predictions approach the same (thermodynamic) value as it should be (see insets). Figure taken from Ref. [6].*

We set $s_A(x,k,t)$ as the entanglement entropy of such a bipartition, i.e. we construct the reduced density matrix $\hat{\rho}_{\mathcal{B}}^{x,k} = \mathrm{Tr}_{\bar{\mathcal{B}}}[\hat{\rho}^{x,k}]$ and pose

$$s_A(x,k,t) = -\mathrm{Tr}_{\mathcal{B}}\left[\hat{\rho}_{\mathcal{B}}^{x,k} \log(\hat{\rho}_{\mathcal{B}}^{x,k})\right] . \tag{3.85}$$

Notice that, without explicitly computing $\hat{\rho}_{\mathcal{B}}^{x,k}$, we can take advantage of the gaussianity of the reduced density matrix and express the Von Neumann entropy in terms of the correlation matrix [351–353]. In particular, let $\mathcal{C}^{\mathcal{B}}(k)$ be the correlation matrix extracted from $\mathcal{C}(k)$ in (3.81) retaining only those degrees of freedom in the $\mathcal{B}$ subspace, then it holds

$$s_A(x,k,t) = -\mathrm{Tr}\Big[\mathcal{C}^{\mathcal{B}}(k) \log \mathcal{C}^{\mathcal{B}}(k)\Big] . \tag{3.86}$$

For the equivalence between Eqs. (3.85) and (3.86) see Ref. [6, 351–353]. Notice that the traces in Eqs. (3.85) and (3.86) are on very different spaces.

In analogy to Eq. (3.70), we can explicitly perform the integration over x in the case when A is an interval of length ℓ. For simplicity, we assume that the quasiparticles are ordered in such a way that $\mathbf{v}_i^k > \mathbf{v}_j^k$ if $i < j$. This does not imply a loss of generality, since when it is not the case we can always, at fixed momentum, reorder the quasiparticles in such a way this requirement holds true, at the price that the needed reordering is momentum-dependent. Under these assumptions

we have

$$S_A(t) = -\int_0^B \frac{\mathrm{d}k}{2\pi} \sum_{i=1}^{2n} \sum_{j=1}^{i} \max\left[0, \min[-t\mathbf{v}_{i+1}^k, \ell - t\mathbf{v}_j^k] - \max[-t\mathbf{v}_i^k, \ell - t\mathbf{v}_{j-1}^k]\right] \mathrm{Tr}\left[\mathcal{C}^{\mathcal{B}_{j,i}} \log \mathcal{C}^{\mathcal{B}_{j,i}}\right] , \tag{3.87}$$

where we conventionally set $\mathbf{v}_0^k = \infty$ and $\mathbf{v}_{2n+1}^k = -\infty$. The set of indexes $\mathcal{B}_{j,i}$ that must be extracted from the two-point correlation matrix is

$$\mathcal{B}_{j,i} = (j, j+1, ..., i) \cup (j+n, j+n+1, ..., i+n) . \tag{3.88}$$

The prediction to the entanglement growth provided by our ansatz quantitatively differs from the case where correlations are ignored (i.e., Eq. (3.70) extended to several species). This is clearly shown in Fig. 3.6, where we provide a few explicit examples anticipating our analysis of the Ising model of Section 3.2.3. Notice that although the two curves for correlated and uncorrelated pairs are quantitatively different, the light-cone spreading of entanglement still occurs even in the presence of correlations, as manifested by an initial linear increase followed by saturation to an extensive value in ℓ (which must be the same in the two cases). Yet, the growth rate of the entanglement for $2v_{\max}t < \ell$ is different.

A very important physical feature of the new prediction (3.87) is that it cannot be rewritten only in terms of the mode populations $\vartheta_i(k)$ and velocities $v_i(k)$, but the correlations in the initial state must be taken into account. Thus, contrarily to the standard uncorrelated case [139], the knowledge of the stationary state is not enough to fix the entire time dependence of the entanglement entropy.

3.2.2 Consistency checks

Given that our prediction (3.86) for the time evolution of the entanglement entropy is after all just a well thought conjecture, its validity must be ultimately tested against ab-initio calculations (either exact or numerical simulations). However, we can perform some non-trivial consistency checks comparing with the already well-established literature. First, we remark that, since the initial state (3.73) is pure, the density matrix associated with the ancillary Hilbert space $\hat{\rho}^{x,k}$ corresponds to a pure state as well, i.e. $\hat{\rho}^{x,k} = |\Psi^{x,k}\rangle\langle\Psi^{x,k}|$, for a certain state $|\Psi^{x,k}\rangle$. This automatically guarantees the following properties.

1. The entanglement entropy $S_A(t)$ must be symmetric under exchange $A \leftrightarrow \bar{A}$. In Eq. (3.85) this follows from the fact that exchanging A with $\bar{A}$ is equivalent to $\mathcal{B} \leftrightarrow \bar{\mathcal{B}}$ and that for any set of pairs with weight $s_A(x,k,t)$ Eq. (3.85) is symmetric under this operation.

2. Consider a given set of pairs and their weight $s_A(x,k,t)$: if all the particles at time t belong to the same set (either A or $\bar{A}$), we must have $s_A(x,k,t) = 0$. This is immediately guaranteed by the fact that $\mathrm{Tr}\left[\hat{\rho}^{x,k} \log \hat{\rho}^{x,k}\right] = 0$, being $\hat{\rho}^{x,k}$ associated with a pure state.

3. If only one particle species is present, then we must recover the standard quasiparticle prediction [137]. In the single species case, $\mathcal{C}^{(1)}(k)$ and $\mathcal{C}^{(2)}(k)$ are simple numbers, moreover $\mathcal{C}^{(1)}(k)$ is, by definition, the density of excitations $\mathcal{C}^{(1)}(k) = \vartheta(k)$. Thus the block matrix $\mathcal{C}(k)$ (3.81) specialised to a single species case reads

$$\mathcal{C}(k) = \begin{pmatrix} 1-\vartheta(k) & 0 & 0 & [\mathcal{C}^{(2)}(-k)]^\dagger \\ 0 & 1-\vartheta(-k) & [\mathcal{C}^{(2)}(k)]^\dagger & 0 \\ 0 & \mathcal{C}^{(2)}(k) & \vartheta(k) & 0 \\ \mathcal{C}^{(2)}(-k) & 0 & 0 & \vartheta(-k) \end{pmatrix} . \tag{3.89}$$

When the quasiparticle of momentum k is in A, while the companion at momentum $-k$ belongs to $\bar{A}$, the reduced correlation matrix is

$$\mathcal{C}^{\mathcal{B}} = \begin{pmatrix} 1-\vartheta(k) & 0 \\ 0 & \vartheta(k) \end{pmatrix} . \tag{3.90}$$

Thus, from Eq. (3.86) we get

$$s_A(x,k,t) = [-\vartheta(k)\log\vartheta(k) - (1-\vartheta(k))\log(1-\vartheta(k))]\Big|_{\substack{x+v_k t\in A \\ x+v_{-k}t\in\bar{A}}} , \tag{3.91}$$

which coincides with the single species weight Eq. (3.71). Then, in the case where we are interested in a single interval, Eq. (3.70) is readily recovered from Eq. (3.87).

4. In the case of several particle species, but *uncorrelated* (i.e. $\mathcal{C}^{(1)}(k)$ and $\mathcal{C}^{(2)}(k)$ are diagonal), the generalisation of Eq. (3.70) to many species is readily obtained, as a straightforward extension of the single-species case.

5. At infinite time and choosing A to be a finite interval, we must recover the Von Neumann entropy constructed on the late time steady state, i.e. it must hold true

$$\lim_{t\to\infty} S_A(t) = \ell \sum_i \int_{-B}^{B} \frac{\mathrm{d}k}{2\pi} s_i(k) , \tag{3.92}$$

where

$$s_i(k) = -\vartheta_i(k)\log\vartheta_i(k) - \big[1-\vartheta_i(k)\big]\log\big[1-\vartheta_i(k)\big] . \tag{3.93}$$

This property is simply proven: for a very large time, looking at a set of pairs originated in (x,k), at most one quasiparticle belongs to A [354]. The distance between two quasiparticles associated with fermions $f_i^{x,k}$ and $f_j^{x,k}$ is $t|\mathbf{v}_i^k - \mathbf{v}_j^k|$, thus if $t > \ell/|\mathbf{v}_i^k - \mathbf{v}_j^k|$ they cannot both belong to A (under the assumption of absence of velocity degeneracies). Therefore, if only the fermion $f_i^{x,k}$ belongs to A, constructing the reduced correlation matrix we find exactly Eq. (3.90) with $\vartheta(k) \to \vartheta_i(k)$. Thus, $s_A(x,k,t)$ reduces to Eq. (3.93). Considering the spatial integration in Eq. (3.77) we simply get a prefactor ℓ and Eq. (3.92) immediately follows.

3.2.3 The inhomogeneous Ising model

We now discuss the solution of the inhomogeneous Ising model (3.75) which provides a benchmark for our ansatz. We introduce fermionic degrees of freedom $\{d_j, d_{j'}^\dagger\} = \delta_{j,j'}$ through a Jordan Wigner transformation

$$d_j = e^{i\pi\sum_{l=1}^{j-1}\sigma_l^+\sigma_l^-}\sigma_j^+ , \qquad \sigma_j^\pm = (\sigma_j^x \pm i\sigma_j^y)/2 . \tag{3.94}$$

In fermionic variables, the Ising Hamiltonian (3.75) can be rewritten as

$$H = \sum_{j=1}^{N}\left[-\frac{1}{2}\left(d_j^\dagger d_{j+1}^\dagger + d_j^\dagger d_{j+1} + \text{h.c.}\right) + h_j d_j^\dagger d_j\right] + \text{boundary terms.} \tag{3.95}$$

Hereafter, we are interested in the thermodynamic limit $N\to\infty$ so that the boundary terms do not play any role and can be discarded. In order to diagonalise the Hamiltonian, it is convenient

to move to Fourier space and define

$$d_j = \int_0^{2\pi} \frac{\mathrm{d}k}{\sqrt{2\pi}} e^{ikj} \alpha(k)\,, \tag{3.96}$$

where $\{\alpha(k), \alpha^\dagger(q)\} = \delta(k-q)$. In Fourier space, the Hamiltonian reads

$$H = -\int_0^{2\pi} \mathrm{d}k \frac{1}{2}\Big(e^{ik}\alpha^\dagger(k)\alpha(k) + e^{ik}\alpha^\dagger(k)\alpha^\dagger(2\pi-k) + \text{h.c.}\Big) + \int_0^{2\pi} \mathrm{d}k\mathrm{d}q\, \delta(e^{in(q-k)}-1)\tilde{h}(q-k)\alpha^\dagger(k)\alpha(q)\,, \tag{3.97}$$

where we exploited the periodicity of h_j and defined

$$\tilde{h}(k) = \sum_{j=0}^{n-1} h_j e^{ikj}\,. \tag{3.98}$$

In the Hamiltonian (3.97), the periodic field h_j couples the modes accordingly to the "roots of unity rule". Now, we introduce several fermionic species splitting the Brillouin zone; in the momentum basis, we define $\beta_i(k)$ fermions as

$$\beta_i(k) = \alpha(k + (i-1)2\pi/n), \qquad i = 1 \dots n. \tag{3.99}$$

The momentum k of the $\beta_i(k)$ fermions runs on the reduced Brillouin zone $k \in [0, 2\pi/n)$ and they satisfy standard anticommutation rules $\{\beta_i(k), \beta_j^\dagger(q)\} = \delta_{i,j}\delta(k-q)$. In terms of these fermions, the Hamiltonian becomes

$$H = \int_0^{2\pi/n} \mathrm{d}k \Bigg[-\frac{1}{2}\sum_{j=1}^{n}\Big(e^{ik+(j-1)2\pi/n}\beta_j(k)^\dagger\beta_j(k) + e^{ik+(j-1)2\pi/n}\beta_j(k)^\dagger\beta_{n-j}^\dagger(2\pi/n-k) + \text{h.c.}\Big) + \sum_{i,j=1}^{n}\frac{1}{n}\tilde{h}((j-i)2\pi/n)\beta_i^\dagger(k)\beta_j(k)\Bigg]. \tag{3.100}$$

We get a more compact notation organising the $\beta_i(k)$ fermions in an unique vector as,

$$B^\dagger(k) = \Big(\beta_1^\dagger(k),\, \beta_2^\dagger(k),\, ...,\, \beta_n^\dagger(k),\, \beta_1(2\pi/n-k),\, \beta_2(2\pi/n-k),\, ...,\, \beta_n(2\pi/n-k)\Big) \tag{3.101}$$

and writing the Hamiltonian as

$$H = \int_0^{\pi/n} \mathrm{d}k\, B^\dagger(k)\mathcal{H}^h(k)B(k)\,. \tag{3.102}$$

The matrix $\mathcal{H}^h(k)$ can be written as

$$\mathcal{H}^h(k) = T(k) + \mathfrak{h}\,, \qquad T(k) = \left(\begin{array}{c|c} T_d(k) & T_{od}(k) \\ \hline T_{od}^\dagger(k) & -T_d(2\pi-k) \end{array}\right), \qquad \mathfrak{h} = \left(\begin{array}{c|c} \mathfrak{h}_d & 0 \\ \hline 0 & -\mathfrak{h}_d^* \end{array}\right), \tag{3.103}$$

where the matrix elements of the $n \times n$ blocks are

$$[T_d(q)]_{a,b} = -\delta_{a,b} \cos\left(q + 2\pi \frac{a}{n}\right), \tag{3.104}$$

$$[T_{od}(q)]_{a,b} = -i\delta_{n-1-a,b} \sin\left(q + 2\pi \frac{a}{n}\right), \tag{3.105}$$

$$[\mathfrak{h}_d]_{a,b} = \frac{1}{n}\tilde{h}\Big(\frac{2\pi}{n}(b-a)\Big). \tag{3.106}$$

The desired modes are identified through the diagonalisation of $\mathcal{H}^h(k)$. Indeed, given the block form of $\mathcal{H}^h(k)$, it always exists an unitary transformation $U^h(k)$ such that

$$[U^h(k)]^\dagger \mathcal{H}^h(k) U^h(k) = \left(\begin{array}{c|c} \mathcal{E}^h(k) & 0 \\ \hline 0 & -\mathcal{E}^h(k) \end{array}\right). \tag{3.107}$$

Here $\mathcal{E}^h(k)$ are positive defined diagonal matrices, which are the energies of the modes

$$[\mathcal{E}^h(k)]_{i,j} = \delta_{i,j} E_i(k). \tag{3.108}$$

The modes $\eta_i(k)$ are then identified as the solution of the linear equation

$$B(k) = U^h(k) G^h(k), \tag{3.109}$$

where $G^h(k)$ is defined as

$$\big[G^h(k)\big]^\dagger = \Big(\eta_1^\dagger(k),\, \eta_2^\dagger(k),\, ...,\, \eta_n^\dagger(k),\, \eta_1(-k),\, \eta_2(-k),\, ...,\, \eta_n(-k)\Big). \tag{3.110}$$

With this definition, we made the Brillouin zone symmetric around zero.

Having diagonalised the Hamiltonian for arbitrary magnetic field, we can now consider a quench changing the magnetic field from $\{h_j^{t<0}\}_{j=1}^n$ to $\{h_j\}_{j=1}^n$. Then the pre and post quench modes are connected through a proper Bogoliubov transformation. In particular, from Eq. (3.109) we have

$$U^{h^{t<0}}(k) G^{h^{t<0}}(k) = B(k) = U^h(k) G^h(k) \quad \Longrightarrow \quad G^{h^{t<0}}(k) = \Big[\big(U^{h^{t<0}}(k)\big)^\dagger U^h(k)\Big] G^h(k). \tag{3.111}$$

We finally need to show that the initial state (i.e. the ground state $\{h_j^{t<0}\}_{j=1}^n$), when expressed in the post quench modes for a magnetic field $\{h_j\}_{j=1}^n$, is of the form in Eq. (3.73). The initial state is the vacuum for the prequench modes, therefore, using Eq. (3.111), we can readily write the set of equations

$$\left(\sum_{j=1}^n \mathcal{U}_{i,j}(k)\eta_j(k) + \sum_{j=1}^n \mathcal{U}_{i,j+n}(k)\eta_j^\dagger(-k)\right)|0_{h^{t<0}}\rangle = 0, \qquad \forall i \in \{1, ..., n\}, \tag{3.112}$$

where for compactness we set

$$\mathcal{U}_{i,j}(k) = \Big[\big(U^{h^{t<0}}(k)\big)^\dagger U^h(k)\Big]_{i,j}. \tag{3.113}$$

It is then straightforward to realise that $|0_{h^{t<0}}\rangle$ can be written in the form Eq. (3.73), i.e.

$$|0_{h^{t<0}}\rangle \propto \exp\left[-\int_0^{\pi/n} \mathrm{d}k \sum_{i=1,j=1}^n \mathcal{M}_{i,j}(k)\, \eta_i^\dagger(k)\eta_j^\dagger(-k)\right]|0_h\rangle, \tag{3.114}$$

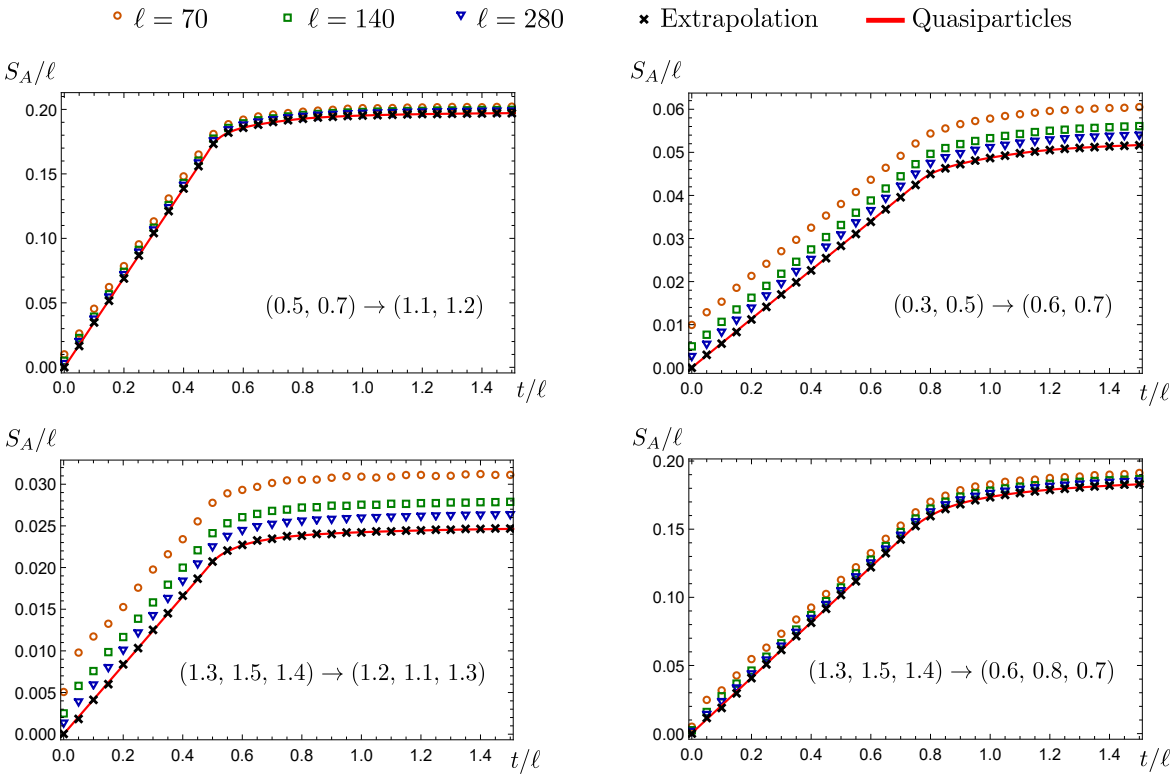

Figure 3.7: *Entanglement entropy evolution for various quenches* $\{h_i^{t<0}\}_{i=1}^n \to \{h_i\}_{i=1}^n$ *in the inhomogeneous Ising model. We consider a bipartition* $A \cup \bar{A}$ *where* $A = [1, \ell]$. *In each panel we plot the rescaled entanglement entropy* S_A/ℓ *as a function of the rescaled time* t/ℓ. *When the finite* ℓ *data are extrapolated to* $\ell \to \infty$, *as explained in the text, the agreement with the quasiparticle prediction is perfect. Figure taken from Ref. [6].*

provided the matrix $\mathcal{M}_{i,j}(k)$ satisfies the equation

$$\sum_{j=1}^{n} \mathcal{U}_{i,j}(k)\mathcal{M}_{j,i'}(k) = \mathcal{U}_{i,i'+n}(k), \qquad \forall i \in \{1, ..., n\}\,. \tag{3.115}$$

We can then conclude that quenches in the inhomogeneous Ising spin chain (3.75) fall within the framework of our ansatz for the entanglement spreading, which can now be tested. As we saw, finding the energies of the modes $E_i(k)$ and the $t = 0$ correlations of the post quench modes boils down to diagonalising finite-dimensional matrices; even though pushing further the analytical calculations can be cumbersome (especially if several species are involved), this last step can be quickly carried out numerically.

In Fig. 3.7 we test the ansatz against direct exact numerical calculations in the Ising model for various choices of the pre and post quench magnetic fields. Numerical calculations have been carried out on a lattice of 1200 sites with periodic boundary conditions, by mean of a direct solution of the free fermion model. We consider time t and subsystem sizes ℓ such that the finite size of the entire system does not play a role. We focus on a bipartition where A is a finite interval of length ℓ. The figure shows that as ℓ becomes larger, the numerical results clearly approach the quasiparticles ansatz. In order to provide a stronger evidence for the correctness of our conjecture we provide an extrapolation to $\ell \to \infty$. In this perspective, we assume a regular expansion in powers of ℓ^{-1}

$$\frac{S_A(t/\ell)}{\ell} = s_A^{\mathrm{QP}}(t/\ell) + \frac{1}{\ell} s_A^1(\ell, t) + ... \tag{3.116}$$

where $s_A^{\rm QP}$ is the quasiparticle prediction. Performing a fit of our data with the above form at order $\mathcal{O}(\ell^{-1})$, we obtain the extrapolation that are represented as crosses in the figure. It is evident that these extrapolations perfectly match the quasiparticle ansatz for all the considered quenches.

3.2.4 Time evolution of the order parameter correlations

Although the main focus of Ref. [6] is the entanglement entropy, the quasiparticle picture may provide useful information even for other quantities, primarily the order parameter $\langle\sigma_j^x\rangle$ and its two-point correlation [96, 97]. For the quantum quench in the homogeneous Ising model, it has been shown that the quasiparticle prediction is qualitatively and quantitatively correct only for quenches within the ordered phase[107, 143, 355]. For quenches from the ordered phase to the paramagnetic one, the quasiparticle picture can be heuristically adapted to provide correct results [107, 143]. Instead in the case of quenches starting from the paramagnetic phase, it is still not known whether it is possible to use these ideas to have an exact ansatz; anyhow a discussion of this issue is beyond our current scope, see Ref. [107, 143]. Consequently, in this section we limit ourselves to extend the quasiparticle picture for the order parameter correlations to initial states with correlated quasiparticles for quenches *within the ferromagnetic phase* and to test the prediction in the inhomogeneous Ising chain (3.75).

Correlation functions of the order parameter are non local objects when expressed in the fermionic basis

$$\langle\sigma_j^x\sigma_{j'}^x\rangle = \left\langle (d_j^\dagger + d_j) e^{-i\pi\sum_{l=j+1}^{j'-1} d_l^\dagger d_l} (d_{j'}^\dagger + d_{j'}) \right\rangle . \tag{3.117}$$

Although the computation of the correlator (and its time evolution) ultimately boils down to an extensive use of the Wick theorem and evaluating determinants, the large number of the involved degrees of freedom makes the calculation very complicated. In Ref. [107, 143] a first-principle calculation was carried out in the homogeneous Ising model, resulting in a scaling behaviour that can be interpreted a posteriori in terms of quasiparticles. While in principle possible, we do not try to generalise the complicated methods of Ref. [107, 143], but, inspired by the resulting expression, we directly attempt a quasiparticle ansatz which is then numerically verified. A posteriori, we will see that our ansatz fails to describe those situations where $\langle\sigma_j^x\rangle = 0$ on the initial state, as expected on the basis of the results for the homogeneous case [107, 143].

Inspired by Ref. [107, 143], we conjecture the following ansatz for the logarithm of the two-point correlator

$$\log|\langle\sigma_j^x\sigma_{j'}^x\rangle| = \int_{-\infty}^{\infty} \mathrm{d}x \int_0^B \frac{\mathrm{d}k}{2\pi} \log(p_A(x,k,t)) + \ldots \tag{3.118}$$

where A is the interval of extrema j and j', the quantity $p_A(x,k,t)$ is discussed hereafter. An explicit space integration may eventually lead to a formula similar to the entropy one in Eq. (3.87).

Our ansatz, relies on the following assumptions, similar to those used in the entanglement entropy case: *i)* quasiparticles generated at different spatial points or belonging to pairs of different momenta are uncorrelated; *ii)* the large distance behaviour of the correlator Eq. (3.117) is ultimately determined by the string

$$e^{-i\pi\sum_{l=j+1}^{j'} d_l^\dagger d_l} = \prod_{l=j+1}^{j'} (1 - 2d_l^\dagger d_l) . \tag{3.119}$$

(In passing: most likely *ii)* is the hypothesis that is failing for quenches from the disordered phase.) Consider then a semiclassical computation of $\langle e^{-i\pi\sum_{l=j+1}^{j'} d_l^\dagger d_l}\rangle$: since pairs originated at different positions or having different momentum are uncorrelated, the expectation value

should factorise in the contribution of each set of pairs. Equivalently, the logarithm must be additive, justifying the form of Eq. (3.118). Now, in order to find the proper ansatz for $p_A(x,k,t)$, we recognise that the string (3.119) simply counts the parity of the number of fermions within the interval (j,j'). Therefore, using the same notation of Section 3.2.1 for the auxiliary fermions $f_j^{x,k}$, we pose

$$p_A(x,k,t) = \left| \left\langle \prod_{i=1}^{2n} \left[1 - 2(f_i^{x,k})^\dagger f_i^{x,k} \right]_{x+\mathbf{v}_i^k t \in A} \right\rangle \right| , \tag{3.120}$$

where in the product only those fermions which semiclassically belong to the interval $x + \mathbf{v}_i^k t \in A$ must be considered. The expectation value is taken on the auxiliary Hilbert space as in Section 3.2.1. The time evolution of the order parameter itself may be accessed from Eq. (3.118) using the cluster decomposition principle, obtaining

$$\langle \sigma_j^x \sigma_{j'}^x \rangle \simeq \langle \sigma_j^x \rangle \langle \sigma_{j'}^x \rangle , \qquad |j - j'| \gg 1 . \tag{3.121}$$

Under the further assumption that $\langle \sigma_j^x \rangle$ is translational invariant in the scaling limit (as it is the case here), we therefore obtain a quasiparticle prediction for the one point function. This observation, besides providing an additional result, also helps a posteriori to understand the regime of applicability of the quasiparticle ansatz. Indeed, from Eq. (3.120) $|p_A(x,k,t)| \leq 1$ (it is a product of terms that are all smaller than 1). Therefore, the r.h.s. of Eq. (3.118) is surely negative (or at most zero), implying an exponentially decaying $|\langle \sigma_j^x \rangle|$, which cannot be correct if the order parameter is zero in the initial state.

We close this section mentioning that by the repeated use of the Wick Theorem, $p_A(x,k,t)$ can be efficiently formulated in terms of a determinant of a correlation function of the fermions. Assume that the fermions $f_{i_j}^{x,k}$ for a set of indexes i_j, $j \in \{1,...,n'\}$ are those belonging to A. Then, we consider a $2n' \times 2n'$ antisymmetric matrix $\mathcal{A}$ defined as

$$\mathcal{A}_{2(j-1)+1,2(j'-1)+1} = \begin{cases} \left\langle \left(f_{i_j}^{x,k} - (f_{i_j}^{x,k})^\dagger \right) \left(f_{i_{j'}}^{x,k} - (f_{i_{j'}}^{x,k})^\dagger \right) \right\rangle & j \neq j' \\ 0 & j = j' \end{cases} \tag{3.122}$$

$$\mathcal{A}_{2j,2j'} = \begin{cases} \left\langle \left(f_{i_j}^{x,k} + (f_{i_j}^{x,k})^\dagger \right) \left(f_{i_{j'}}^{x,k} + (f_{i_{j'}}^{x,k})^\dagger \right) \right\rangle & j \neq j' \\ 0 & j = j' \end{cases} \tag{3.123}$$

$$\mathcal{A}_{2(j-1)+1,2j'} = -\mathcal{A}_{2j',2(j-1)+1} = \left\langle \left(f_{i_j}^{x,k} - (f_{i_j}^{x,k})^\dagger \right) \right) \left(f_{i_{j'}}^{x,k} + (f_{i_{j'}}^{x,k})^\dagger \right) \Big\rangle . \tag{3.124}$$

In terms of the matrix $\mathcal{A}$, it holds (see [6, 107, 143])

$$p_A(x,k,t) = \sqrt{\det \mathcal{A}} . \tag{3.125}$$

We tested our ansatz against exact numerical calculations for quenches in the inhomogeneous Ising chain. We found that for all quenches within the ferromagnetic phase, our quasiparticle prediction perfectly reproduces the numerical data in the space-time scaling limit $t, \ell \to \infty$ with t/ℓ fixed. Two representative cases are shown in Fig. 3.8. It is evident that by increasing ℓ the numerical data approach the prediction, although finite size correction are clearly visible at small ℓ, but these are much smaller than those for the entanglement entropy. It is clear from the result that even for the two-point function of the order parameter, the "light-cone" spreading of correlations persists in the presence of correlated quasi-particles. We also checked that for other quenches (i.e. from and to the paramagnetic phase) the conjecture does not work, as expected. Finally, to be exhaustive, we remind the reader that the quasiparticle prediction is correct for quenches to the critical point from the ordered phase, but not for quenches originating from the

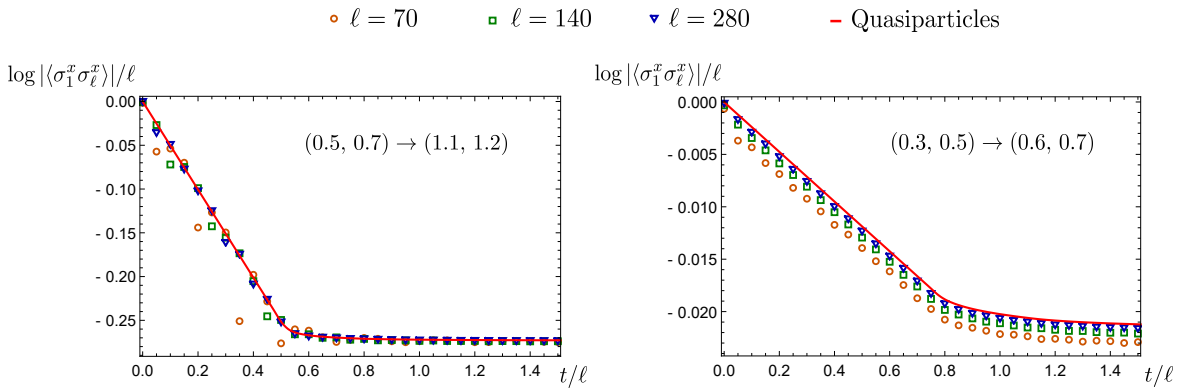

Figure 3.8: *Evolution of the two-point correlator for various quenches $\{h_i^{t<0}\}_{i=1}^n \to \{h_i\}_{i=1}^n$ in the inhomogeneous Ising model. We test the time evolution of the two-point correlator of the order parameter against the quasiparticle ansatz for increasing separation ℓ. It is evident that increasing ℓ the numerical data quickly approach the quasiparticle ansatz. The initial exponential decay is due to the evolution of the one-point function of the order parameter since, on that time scale, we have $\langle\sigma_1^x\sigma_\ell^x\rangle \simeq \langle\sigma_1^x\rangle\langle\sigma_\ell^x\rangle$. At late times, saturation to the steady state value is observed. Figure taken from Ref. [6].*

critical point [107, 143].

3.2.5 Concluding remarks

In this section we generalized the semiclassical quasiparticle picture for the spreading of entanglement and correlations to global quantum quenches with multiple species of quasiparticles that show momentum-pair correlations in the initial state. The main new physical result (compared to the standard uncorrelated case) is that the information encoded in the mode populations $\vartheta_i(k)$ of the single species and their velocities $v_i(k)$ are not enough to determine the time evolution of the entanglement entropy and correlations. We show that among the systems displaying this phenomenology for the quasiparticles, a remarkable example is the Ising chain with a periodically-modulated transverse field, which is easily mappable to a free fermionic theory. We then use this model to test our predictions for entanglement and correlations against exact numerical calculations, finding perfect agreement in the scaling regime.

A simple and straightforward generalization of our results concerns the case when the initial state is inhomogeneous on a large scale so to be describable by the generalised hydrodynamics approach (see Section 3.4). For example, we have in mind the joining of two different thermal states or groundstates of different Hamiltonians producing correlated quasiparticles. In this case, it is very simple to merge the results of the present paper with those of Ref. [176]. The spatial variation of the entanglement entropy may be properly captured by a term that locally is given by Eq. (3.86).

Another inhomogeneous setup in which several correlated pairs can be produced is that of moving defects (see Section 4.1), where an external localised perturbation is dragged at constant velocity in an otherwise homogeneous free lattice system. The moving impurity can be regarded as a source of quasiparticles and the propagation of entanglement could fall within our frame, again supplemented with the generalized hydrodynamics.

A simple generalization of our results is the time evolution of Rényi entanglement entropies that for free models just requires a minor variation of the form of the kernel (3.86), see for example the discussion in [356].

Finally, a more difficult open problem concerns the spreading of entanglement in interacting integrable models. For these models there are almost always multiple species of quasiparticles (they are bound states of the lightest species), but known integrable initial states do not have

correlations between them and the general evolution of the entanglement entropy has been understood in [139–141] (for the Rényi entropies see [356–358] while for inhomogeneous systems see [177]). This lack of correlations in solvable initial states has been sometimes related to the integrability of the quench problem itself [359, 360]. Yet, it would be very interesting to understand whether, at least in in some models, it is possible to have correlated quasiparticles which would require the generalization of our approach to interacting integrable systems.

3.3 Quenches from bosonic Gaussian initial states to the Tonks Girardeau limit: stationary states and effects of a confining potential

Despite the several achievements in driving out-of-equilibrium integrable models, analytic results on actual quench protocols (apart from free theories) have been extracted only at the price of tremendous efforts and for restricted classes of observables and initial states [104, 113, 114, 121, 360–366].

In between the complexity of quenching a truly interacting integrable model and the simplicity of a free model lies a special interaction quench in the Lieb Liniger model (1.1). For arbitrary values of κ the model is a truly interacting integrable model, however in two special limits the dynamics is that of free particles: at $\kappa = 0$ the model reduces to free bosons, while in the $\kappa = +\infty$ limit known as Tonks Girardeau gas (TG) the bosons behave as *free* but impenetrable particles [144–149] that are equivalent to *free fermions* by means of a Jordan Wigner transformation. In contrast with many other quenches among free theories, the modes at $\kappa = 0$ and $\kappa = +\infty$ are not connected through a simple linear relation.

This quench protocol has already been successfully addressed in the literature choosing as initial state the homogeneous non-interacting ground state (i.e. the Bose-Einstein condensate) and analytical expressions for the steady state correlators were obtained [150]. Subsequently, these results have been generalized to include a hard wall trap [151] and later an harmonic potential [152]. The presence of simple analytical results for an experimental relevant quench protocol is surely appealing, however the mentioned works concern a rather peculiar initial state. This choice has some flaws, such as *i)* the space independence of the correlation functions on in the initial state (apart from that induced by the trap) and *ii)* the strong dependence on the trap shape [151, 152] which makes difficult a proper definition of the thermodynamic limit.

In view of these observations, is natural to look at other initial states which retain a more physical behavior, but are still simple enough to allow for an analytical analysis: a good compromise are *gaussian* (in terms of the free bosons) initial states, e.g. free thermal states.

In particular, Section 3.3.1 provides the necessary results to solve the quench protocol in the homogeneous case, while the correlation functions in the steady state are instead studied in Section 3.3.2. Then, in Section 3.3.3 we include the effects of a thermodynamic large trap. We show how in the thermodynamic limit (that is necessary for the system to exhibit relaxation) a semiclassical time evolution naturally emerges and permits to consider traps of arbitrary shapes.

3.3.1 Quench set up

In the infinite repulsive regime, the Lieb Liniger gas (1.1) can be described as a free model of hard-core bosons $\Phi(x)$

$$H = \int \mathrm{d}x \frac{\partial_x \Phi^\dagger(x) \partial_x \Phi(x)}{2m}, \qquad \kappa = +\infty\,. \tag{3.126}$$

The infinite repulsive term prevents the possibility of having two particles in the same position [150] and this can be achieved through a definition of the hard-core bosonic fields $\Phi(x)$, obtained

projecting the standard bosonic fields $\psi(x)$ on the subspace with at most one particle in position x

$$\Phi(x) = P_x \psi(x) P_x \,. \tag{3.127}$$

Above, $P_x = |0_x\rangle\langle 0_x| + |1_x\rangle\langle 1_x|$ is the projector on the subspace with no more than a particle in position x. Actually, a correct definition of the hard-core bosons requires a proper lattice regularization (see Ref. [7, 150] for further details): in order to consider directly the continuum limit it is convenient to introduce the fermionic field $\Psi(x)$ through a Jordan-Wigner transformation

$$\Psi(x) = \exp\left(i\pi \int^x \mathrm{d}z\, \Phi^\dagger(z)\Phi(z)\right) \Phi(x)\,. \tag{3.128}$$

While the hard-core bosons need a lattice regularization, on the fermionic fields the continuum limit can be taken and standard commutation rules $\{\Psi(x), \Psi^\dagger(y)\} = \delta(x-y)$ are recovered. The strong-interacting Hamiltonian becoming thus quadratic in terms of those fermionic fields.

Both models, namely the non-interacting and the strong-interacting, are therefore related via a non-local transformation which nevertheless makes a well-established connection. Whenever we need to pass from one theory to the other, e.g. via a quench protocol, the problem reduces to compute the multipoint correlators of the post-quench fields in terms of the pre-quench ones. This dictionary is provided by the underling regularized hard-core bosons, whose normal ordered correlation functions can be computed as if the hard core bosons were canonical bosonic operators (see Ref. [7, 150]). For example, the fermionic multipoint correlation function can be expressed in terms of bosonic fields as

$$\langle \Psi^\dagger(y_1)\dots\Psi^\dagger(y_l)\Psi(x_l)\dots\Psi(x_1)\rangle = \langle : \psi^\dagger(y_1)\dots\psi^\dagger(y_l)e^{-2\int_{\mathcal{D}}\mathrm{d}z\, n(z)}\psi(x_l)\dots\psi(x_1) : \rangle,$$

where, without loss of generality, we assumed $y_1 < \dots < y_l$ and $x_1 < \dots < x_l$, $n(z) \equiv \psi^\dagger(z)\psi(z)$ being the density operator, and the integration domain $\mathcal{D}$ is defined via

$$\int_{\mathcal{D}} \mathrm{d}z\, n(z) = \int_{-\infty}^{\infty} \mathrm{d}z\, n(z)(1 - e^{i\pi\sum_{j=1}^{l}\chi_j(z)})/2\,, \tag{3.129}$$

where $\chi_j(z)$ is the characteristic function of the interval (y_j, x_j). The same expression can be used to compute the bosonic correlators starting from the fermionic ones, provided in Eq. (3.129) the bosons are replaced with fermions and vice versa. A rigorous derivation of this relation requires a lattice regularization similarly to what has been done in Ref. [150] and we leave these considerations to Ref. [7, 150].

In general, considering an homogeneous quench from the free bosons towards the Tonks Girardeau gas, the fermions evolve as free fields, therefore the system exhibits *gaussification* [332, 333, 367], i.e. all the fermionic multipoint connected correlators vanish apart from the two point correlator. Assuming translational invariance, the two point correlator is conserved by the time evolution and it is the only information of the initial state that survives in the steady state.

Therefore, the homogeneous quench problem is reduced to computing the expectation value of the two point correlator on the pre-quench state through Eq. (3.129): handling this expression for arbitrary pre-quench states appears as an hopeless task, since even in the computation of the fermionic two point correlator the whole set of multipoint bosonic correlators is required, as it is clear from the power expansion of the exponential in Eq. (3.129). Nevertheless, some special classes of states allow for a brute force computation of Eq. (3.129), i.e. the already studied BEC case [150] and the gaussian ensembles that we are going to analyze.

Notice that, being the steady state gaussian in terms of the fermionic fields, the bosonic correlators can be obtained solving the inverse problem with respect that analyzed so far. Thus, we discuss the computation of fermionic correlators from a gaussian bosonic ensemble: the calculations in the other direction are completely analogous. Evaluating Eq. (3.129) on a gaussian

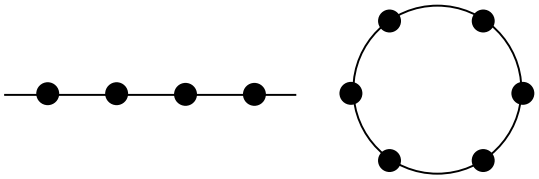

Figure 3.9: *Feynman diagram representation of Eq. (3.132-3.133): black dots represent the density operators $n(z)$. The Wick theorem contracts the fields pairwise: since the density contains two fields $n(z) = \psi^\dagger(z)\psi(z)$ there are two departing legs from each black dot. In Eq. (3.132) external legs are present in association with the fields $\psi^\dagger(y)$ and $\psi(x)$ (Left), while in the diagrams of Eq. (3.133) external legs are absent (Right). Figure taken from Ref. [7].*

ensemble amounts to an extensive use of the Wick theorem, however the calculations are greatly simplified replacing Eq. (3.129) with an expression in terms of the *connected correlators*

$$\langle \Psi^\dagger(y)\Psi(x)\rangle = \langle : \psi^\dagger(y) e^{-2\int_{\mathcal{D}} \mathrm{d}z\, n(z)} \psi(x) : \rangle = \langle : \psi^\dagger(y) e^{-2\int_{\mathcal{D}} \mathrm{d}z\, n(z)} \psi(x) : \rangle_{\mathrm{c}} \langle : e^{-2\int_{\mathcal{D}} \mathrm{d}z\, n(z)} : \rangle \,, \tag{3.130}$$

where $\langle ... \rangle_{\mathrm{c}}$ is the connected expectation value. It must be stressed that the connected part is constructed considering the particle density $n(z)$ as an unique operator and not as a composite one $n(z) = \psi^\dagger(z)\psi(z)$. The derivation of (3.130) is a simple exercise best understood through an analogy with standard Feynman diagrams where $e^{-2\int_{\mathcal{D}} dz\, n(z)}$ plays the role of the "action". In the computation of correlation functions the expectation value of the action factorizes and we are left with the sum of connected diagrams, i.e. (3.130). Besides, $\langle : e^{-2\int_{\mathcal{D}} dz\, n(z)} : \rangle$ can written in terms of connected correlators thanks to the cumulant expansion

$$\langle : e^{-2\int_{\mathcal{D}} \mathrm{d}z\, n(z)} : \rangle = e^{\sum_{j=1}^{\infty} \frac{(-2)^j}{j!} \int_{\mathcal{D}} \mathrm{d}^j z\, \langle : n(z_1) ... n(z_j) : \rangle_c} \,. \tag{3.131}$$

The computation of the connected correlators on a gaussian ensemble is straightforward (see Fig. 3.9) and we reach the following expressions (where $\mathcal{C}(y,x) = \langle \psi^\dagger(y)\psi(x)\rangle$)

$$\langle : \psi^\dagger(y) e^{-2\int_{\mathcal{D}} \mathrm{d}z\, n(z)} \psi(x) : \rangle_{\mathrm{c}} = \sum_{j=0}^{\infty} (-2)^j \int_{\mathcal{D}} \mathrm{d}^j z \prod_{l=0}^{j} \mathcal{C}(z_{l+1}, z_l) \tag{3.132}$$

and

$$\langle : e^{-2\int_{\mathcal{D}} \mathrm{d}z\, n(z)} : \rangle = e^{\sum_{j=1}^{\infty} \frac{(-2)^j}{j} \int_{\mathcal{D}} \mathrm{d}^j z \prod_{l=1}^{j} \mathcal{C}(z_{l+1}, z_l)} \,, \tag{3.133}$$

where in the first expression $z_{j+1} = y$ and $z_0 = x$, while in the second expression $z_{j+1} = z_1$. Eq. (3.216-2.125) are readily resummed in compact expressions once we define $\mathcal{C}_{\mathcal{D}}$ as the linear operator obtained restricting the correlator $\mathcal{C}$ on the domain $\mathcal{D}$, i.e. $\mathcal{C}_{\mathcal{D}}(s,t) = \mathcal{C}(s,t)$ and $s,t \in \mathcal{D}$.

$$\langle : \psi^\dagger(y) e^{-2\int_{\mathcal{D}} \mathrm{d}z\, n(z)} \psi(x) : \rangle_{\mathrm{c}} = \left(\frac{\mathcal{C}_{\mathcal{D}}}{1 + 2\mathcal{C}_{\mathcal{D}}} \right)(y,x) \,, \qquad \langle : e^{-2\int_{\mathcal{D}} \mathrm{d}z\, n(z)} : \rangle_{\mathrm{c}} = \det_{\mathcal{D}} (1 + 2\mathcal{C}_{\mathcal{D}})^{-1} \,. \tag{3.134}$$

The analysis of multipoint correlators is straightforward, leading to the general expression

$$\langle \Psi^\dagger(y_1) \dots \Psi^\dagger(y_l) \Psi(x_l) \dots \Psi(x_1) \rangle = \frac{1}{\det_{\mathcal{D}}(1 + 2\mathcal{C}_{\mathcal{D}})} \sum_{P} \prod_{j=1}^{l} \left(\frac{\mathcal{C}_{\mathcal{D}}}{1 + 2\mathcal{C}_{\mathcal{D}}} \right)(y_j, x_{P(j)}) \,,$$

where the sum runs over all the permutations P.

Computing bosonic correlators in the assumption of a gaussian ensemble in the fermionic

fields leads to similar expressions, with the introduction of extra minus signs due to the fermionic Wick Theorem

$$\langle \psi^\dagger(y_1)\dots\psi^\dagger(y_l)\psi(x_l)\dots\psi(x_1)\rangle = \det_{\mathcal{D}}(1-2\mathcal{F}_{\mathcal{D}})\sum_P \mathrm{sign}(P)\prod_{j=1}^{l}\left(\frac{\mathcal{F}_{\mathcal{D}}}{1-2\mathcal{F}_{\mathcal{D}}}\right)(y_j,x_{P(j)})\,, \quad (3.135)$$

where now $\mathcal{F}_{\mathcal{D}}$ is the fermionic two point correlator restricted to the domain $\mathcal{D}$. Fredholm-like expressions for the bosonic correlators based on a gaussian fermionic ensemble were already known [53, 150, 151, 368], but with the inverse formula Eq. (3.135) it is now possible to determine the initial conditions of the free (in terms of the fermions) evolution.

3.3.2 Homogeneous quenches in the Tonks gas phase

As first application of the derived expressions we consider the quench protocol in the homogeneous case towards the Tonks gas. For the sake of concreteness, we often refer to the free thermal ensemble as the pre-quench state

$$\mathcal{C}(x,y) = \int \frac{\mathrm{d}k}{2\pi}\frac{e^{ik(x-y)}}{e^{\beta\left(\frac{k^2}{2m}-\mu\right)}-1}\,, \quad (3.136)$$

where the chemical potential μ is fixed requiring $\mathcal{C}(x,x) = n$, with n the particle density. The steady state information is completely encoded in the initial two point fermionic correlator, that is conserved through the time evolution. While the numerical evaluation of Eq. (3.135) can be easily implemented, its analytical solution can be obtained only in very special cases, since the presence of the finite domain $\mathcal{D}$ prevents the possibility of diagonalizing the operators in the Fourier space. However, Eq. (3.135) is still feasible of proper analytical approximations in several regimes.

1. **Short distances**

   In the short distance regime or in the small density limit, a satisfactory approximation of Eq. (3.135) can be obtained from the series expansion in terms of $\mathcal{C}_{\mathcal{D}}$. For example, assuming low density and that the two point bosonic correlators decays fast enough to ensure the convergence of the integrals in Eq. (3.216-2.125) for infinite domain $\mathcal{D}$, we can readily write

   $$\langle \Psi^\dagger(y)\Psi(x)\rangle = \mathcal{C}(y,x)e^{-2|x-y|\left(n+\mathcal{O}(n^2)\right)} + \mathcal{O}(n^2)\ . \quad (3.137)$$

2. **Small temperatures**

   When the two point correlator is approximately constant $\mathcal{C}(x,y) \simeq \mathcal{C}(x,x) = n$ over the whole domain $\mathcal{D}$. This is an important case, since this condition is met in the zero temperature limit, at fixed density, of the free thermal ensemble: in the low temperature limit $\mathcal{C}(x,y) \simeq ne^{-\alpha|x-y|}$ with $\alpha = m(n\beta)^{-1}$. Thus in the small temperature limit α approaches zero and $\mathcal{C}$ is approximatively constant on an increasing range of distances. In this limit the following two point fermionic correlator is immediately derived

   $$\langle \Psi^\dagger(y)\Psi(x)\rangle = \frac{n}{(1+2n|x-y|)^2}\,. \quad (3.138)$$

   This correlator greatly differs from the findings in Ref. [150] for the BEC case, where the decaying has been found to be purely exponential rather than algebraic. The two results are not in contradiction, since the condensation of one dimensional systems is realized only exactly at zero temperature, thus the zero temperature limit of the thermal ensemble does not reproduce the BEC state.

3. **Large distances**

When the distance of the two fermionic operators in the two point correlator far exceeds the typical decay length of the bosonic correlator $\mathcal{C}$, we can extract the asymptotics of the two point fermionic correlator. We start considering the string contribution

$$\det_{\mathcal{D}}(1+2\mathcal{C}_{\mathcal{D}})^{-1} = e^{-\int_x^y \mathrm{d}z[\log(1+2\mathcal{C}_{\mathcal{D}})](z,z)}\,, \tag{3.139}$$

where we already specialized the domain $\mathcal{D}=(x,y)$. In the limit of a very large interval, most of the contribution to the integral comes from coordinates far from the edges of the domain. Thus, in first approximation, we can compute $[\log(1+2\mathcal{C}_{\mathcal{D}})](z,z)$ as if the domain $\mathcal{D}$ were the whole real axis and diagonalize the operator in the Fourier space. This approximation gives the extensive part of the integral

$$\det_{\mathcal{D}}(1+2\mathcal{C}_{\mathcal{D}})^{-1} = e^{-|x-y|\int \frac{\mathrm{d}k}{2\pi}\log\left[1+2\tilde{\mathcal{C}}(k)\right]+\mathcal{O}\left(|x-y|^0\right)}\,, \tag{3.140}$$

where $\tilde{\mathcal{C}}(k)$ is the Fourier transform of the two point bosonic correlator. The same approximation can be justified on the whole two point fermionic correlator, being reliable only in the asymptotic regime

$$\langle\Psi^\dagger(y)\Psi(x)\rangle \propto e^{-|x-y|\int \frac{\mathrm{d}k}{2\pi}\log\left[1+2\tilde{\mathcal{C}}(k)\right]}\int\frac{\mathrm{d}k}{2\pi}e^{ik(x-y)}\frac{\tilde{\mathcal{C}}(k)}{1+2\tilde{\mathcal{C}}(k)}\,.$$

In the case of the thermal ensemble, we have

$$\langle\Psi^\dagger(y)\Psi(x)\rangle \propto e^{-\xi|x-y|}\left(\frac{e^{-\lambda|x-y|}}{\lambda}+\text{c.c.}\right)\,, \tag{3.141}$$

where the parameters ξ and λ are

$$\begin{aligned}\xi &= \int\frac{\mathrm{d}k}{2\pi}\log\coth\left[\frac{\beta}{2}\left(\frac{k^2}{2m}-\mu\right)\right]\,, \\ \lambda &= \sqrt{m}\left(\sqrt{|\mu|+\sqrt{\mu^2+\frac{\pi^2}{\beta^2}}}+i\sqrt{-|\mu|+\sqrt{\mu^2+\frac{\pi^2}{\beta^2}}}\right)\,.\end{aligned} \tag{3.142}$$

The analysis of the asymptotes displays an oscillating behavior due to the imaginary part of λ, however in view of our crude approximations only the overall exponential decay $\langle\Psi^\dagger(y)\Psi(x)\rangle \propto e^{-(\xi+\Re(\lambda))|x-y|}$ is expected to be reliable. In Fig. 3.10 we plot the numerical computation of the stationary two point fermionic correlator after a quench from a thermal bosonic ensemble (3.136) and compare it with our analytical predictions. As already stated before, we only report the pure exponential decay. Notwithstanding, we checked the predicted period $2\pi/\Im(\lambda)$ against the numerical results and, quite remarkably, we found a very good agreement. However, the asymptotic expansion does not give a correct prediction for the oscillations' phase.

We also analyze the momentum density distribution $\tilde{n}(k) = \int dz\, \mathrm{e}^{-ikz}\langle\Psi^\dagger(z)\Psi(0)\rangle$, wich turns out to be very different from the fermionic momentum distribution at thermal equilibrium. In general, for any finite temperature, the momentum density distribution is an analytic function for all momenta. Only in the zero temperature limit, the algebraic decay of the fermionic two-point function affects the short-distance behavior of the momentum distribution which reads $\tilde{n}(k)\simeq 1-\pi|k|/4n$ (for $\beta\to\infty$). On the contrary, the large momentum behavior $\tilde{n}(k)\simeq 8n^2/k^2$

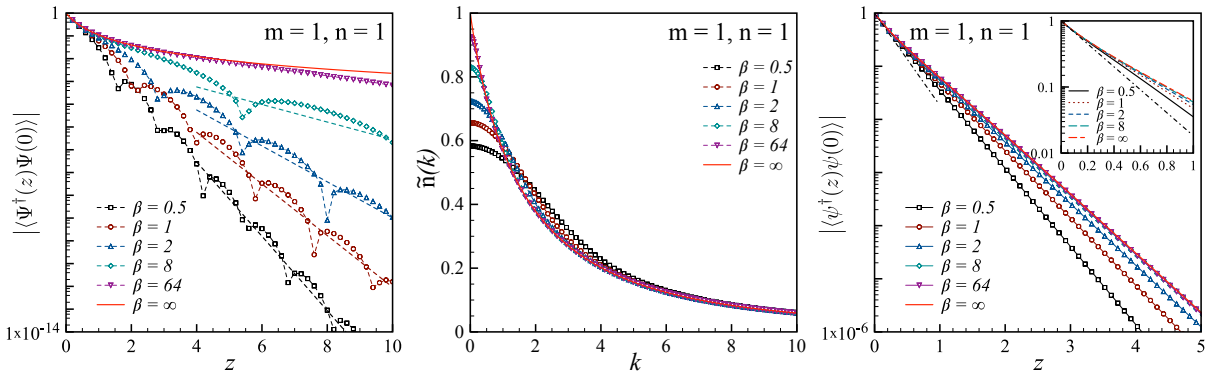

Figure 3.10: *(Left) Stationary fermionic two-point correlation function after an interaction quench ($\kappa = 0 \to \kappa = +\infty$) of a Bose gas initially prepared in a thermal state with inverse temperature β. Symbols are the numerical evaluation of Eq. (3.135) with initial bosonic correlator given by (3.136). In the limit of zero temperature, the correlation function approaches the analytic result (3.138) (full red line). However, for any finite temperature, the large-distance exponential decay is captured by the asymptotic expansion (3.141) (dashed lines). (Center) Stationary momentum density distribution obtained by Fourier transform $\langle \Psi^\dagger(z)\Psi(0)\rangle$. (Right) Stationary bosonic two-point correlation function $\langle \psi^\dagger(z)\psi(0)\rangle$ obtained by numerical evaluation of Eq. (3.135) with initial fermionic correlator given by $\langle \Psi^\dagger(z)\Psi(0)\rangle$. Notice the large distance exponential decay. Nevertheless, such decay is not exponential for all distances. Indeed, by comparing the correlator with the exact exponential decay which matches the short distance expansion, namely $ne^{-4n^2|x|}$ (dot-dashed black line), one reveals an appreciable discrepancy (see the inset for a zoom on the short distances). Figure taken from Ref. [7].*

it turns out to be independent of the temperature, being fixed by the non analyticity of the fermionic correlator $\langle \Psi^\dagger(z)\Psi(0)\rangle \simeq n - 4n^2|z|$ in $z = 0$. Let us point out that such non-analytic behavior in the fermionic two point function is somehow *universal* since it only depends on the properties of the initial bosonic correlator in the vicinity of $z = 0$, namely $\mathcal{C}(x,x) = n$ and $\partial_x \mathcal{C}(x,y)|_{y=x} = -\partial_y \mathcal{C}(x,y)|_{y=x} = 0$.

Finally, using the steady-state of the two-point fermionic correlation function, we can numerically evaluate the stationary bosonic correlators $\langle \psi^\dagger(z)\psi(0)\rangle$ via Eq. (3.135). The Bose gas in the steady state is fully characterized by a two-point function which exhibits a nearly exact exponential decay for all temperatures, even for $\beta = \infty$, even tough the stationary fermionic two-point function decays algebraically. Actually, the exponential decay of the bosonic correlator in the steady state can be argued by mean of the symmetric analysis performed to extract the asymptotic decay of the two-point fermionic correlator. Interestingly, for all temperatures, we can easily extract the short distance behaviour of the bosonic two-point function which, in particular, coincides with the fermionic one, i.e. $\langle \psi^\dagger(z)\psi(0)\rangle \simeq \langle \Psi^\dagger(0)\Psi(0)\rangle + \partial_z \langle \Psi^\dagger(z)\Psi(0)\rangle|_0 z = n - 4n^2|z|$. Lastly, we remark that even though the asymptotics behavior of the two point fermionic correlator does not suffice to determine the decay of an arbitrary bosonic correlator because of the presence of the string, it is the case when the string is absent. This is realized, for example, in the density-density correlator, being the density equivalently expressed in terms either with the fermions or with the bosons.

$$\langle n(x,t)n(y,t)\rangle_{\text{steady state}} = n^2 - |\langle \Psi^\dagger(x)\Psi(y)\rangle|^2 \tag{3.143}$$

Thus, the density-density correlator (connected part) decays twice as fast as the two point fermionic correlator (3.141) and it can be computed exactly in the zero temperature limit (3.138).

3.3.3 Quenching in a thermodynamic trap

We can now generalize the previous calculations to the more physical situation in which a confining potential is present and replace the Hamiltonian (1.1) with

$$H \to H + \int \mathrm{d}x \; V(x)\psi^\dagger(x)\psi(x), \tag{3.144}$$

where $V(x)$ is a trapping potential. Differently from the homogeneous case, the two point fermionic correlator exhibits now a non trivial time evolution. In presence of the trap, the discrete spectrum prevents the relaxation to a steady state, that can be recovered only in a proper thermodynamic limit: for this reason, we introduce a thermodynamic length-scale L. Parametrizing the confining potential as $V(x) = U(xL^{-1})$, where U is a smooth function kept fixed in the thermodynamic limit, the eigenvalues approach a continuum distribution when $L \to \infty$. While considering the limit of large trap, we must also rescale the number of particles consistently and keep constant the total density $n = L^{-1}\int dz\; \mathcal{C}(z,z)$. The thermodynamic limit hugely simplifies the forthcoming calculations and permits to consider a generic trap. First of all, in the thermodynamic limit the thermal initial state is described by the Local Density Approximation [156, 369–371] (LDA). In fact, the two point correlator decays on a typical scale (finite for any non zero temperature) much smaller than the thermodynamic length characterizing the variation of V. It is convenient to change variables in the two point bosonic correlator $\mathcal{C}(y,x) \to C(s,X)$, defining $s = y - x$ and $X = (x+y)/2L$. In the LDA approximation we have

$$C(s,X) = \int \frac{\mathrm{d}k}{2\pi} \frac{e^{iks}}{e^{\beta\left(\frac{k^2}{2m} + v(X) - \mu\right)} - 1} \; . \tag{3.145}$$

As it is clear from the general expression (3.135), the LDA on the bosonic correlators implies LDA for the fermionic correlators as well, i.e. $\mathcal{F}(x,y) \to F(s,X)$. Following the time evolution after the quench, we can clearly distinguish two time scales.

On a non-thermodynamic time scale, the system behaves as if it was locally homogeneous, therefore it exhibits gaussification of the correlators on the same time scale of the homogeneous system. In this first phase, the two point correlator does not evolve: even though the ensemble is gaussian, the steady state has not been reached yet.

Relaxation can be realized only on a time scale sufficient for the system to explore the whole trap, thus times $t \propto L$ must be considered. The two point correlator evolves under the Schrödinger equation, that in terms of the rescaled variables reads

$$i\partial_t F_t = \left\{ \frac{\partial_s \partial_X}{Lm} - \left[U\left(X + \frac{s}{2L}\right) - U\left(X - \frac{s}{2L}\right)\right] \right\} F_t \, . \tag{3.146}$$

For any finite time t, in the limit $L \to \infty$ the two point correlator does not evolve. However, rewriting the differential equation in terms of the rescaled time $\tau = t/L$ and Taylor expanding the potential U, we get a non trivial time evolution

$$i\partial_\tau F_\tau = \left[\frac{\partial_s \partial_X}{m} - sU'(X) \right] F_\tau \tag{3.147}$$

where we assumed $\tau \ll L$ (i.e. $t \ll L^2$). The above equation is associated with a classical evolution for the two point correlator. This is unveiled in terms of the well known Wigner distribution [372–374], that amounts to a partial Fourier transform of the correlator

$$\vartheta_\tau(k,X) = \int \mathrm{d}s \, e^{-iks} F_\tau(s,X) \, . \tag{3.148}$$

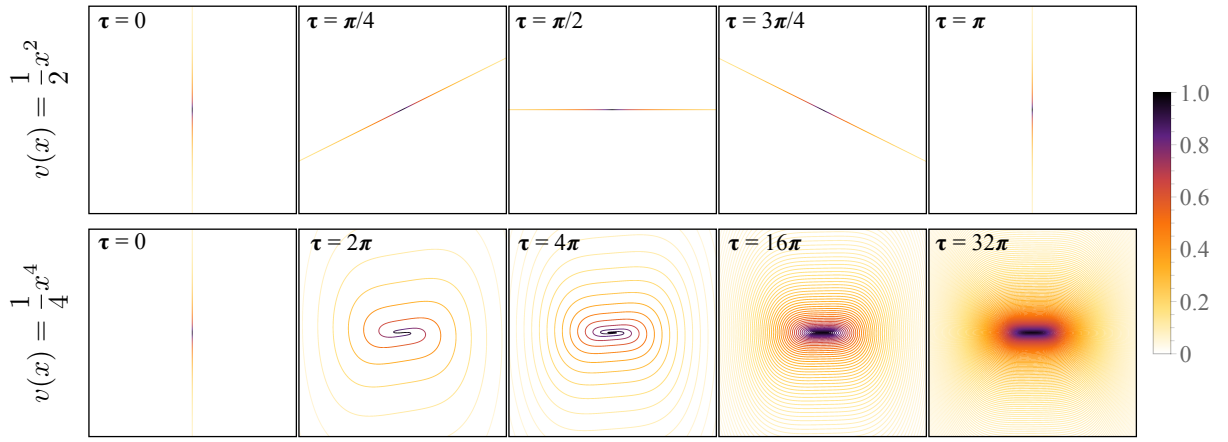

Figure 3.11: *Color density plot of the Wigner distribution $\vartheta_\tau(k, X)$ vs $(k, X) \in [-4, 4] \times [-8, 8]$, for different times τ and two representative traps (here $m = 1$ and $n = 1$). The system is initially prepared at zero temperature with $\vartheta_0(k, X)$ given by Eq. (3.152). In the harmonic case each phase-space trajectory is characterized by the same period thus preserving the shape of the initial Wigner distribution whose support simply rotates in time. In the anharmonic case, the typical dynamical period depends on the initial energy, being equal to $T(k_0) \simeq \int_0^{X^*} \mathrm{d}X / \sqrt{k_0^2 - 2mV(X)}$ (with $X^* > 0$ being the solution of $V(X^*) = k_0^2/2m$), and the δ-support of the Wigner distribution folds over time. For large times, it tends to cover the entire phase plane. Figure taken from Ref. [7].*

In this new notation, Eq. (3.147) can be written in the form of a classical Liouville equation in terms of X and its conjugated momentum k

$$\partial_\tau \vartheta_\tau + \{\vartheta_\tau, \mathcal{H}\}_{X,k} = 0\,, \tag{3.149}$$

where $\{a, b\}_{X,k} = \partial_X a \partial_k b - \partial_k a \partial_X b$ are the classical Poisson brackets and $\mathcal{H}$ is the classical Hamiltonian $\mathcal{H} = k^2/2m + U(q)$. In fact, the thermodynamic limit we are considering is equivalent to a semiclassical limit on the time evolution of the Wigner distribution (see e.g. Ref. [153–156] for semiclassical approaches). The notation $\vartheta_\tau(k, X)$ has been chosen on purpose: indeed, $\vartheta_{\tau=0}(k, X)$, as a function of k, is simply the LDA approximation of the fermionic excitation density at initial time. For $\tau > 0$, it evolves as if it was the density distribution of a collection of classical non interacting particles, whose dynamic is ruled by the classical Hamiltonian $\mathcal{H}$. In the next section, we will see how this picture is generalized to truly interacting integrable systems. If the frequency of the solution of the classical equation of motion does not have a trivial dependence on the energy, the correlator in the coordinate space reaches a steady state thanks to the dephasing between the different energy shells. The steady state is of course described in terms of the energy density of the initial Wigner distribution

$$\lim_{\tau\to\infty} F_\tau(s, X) = \int \frac{\mathrm{d}k}{2\pi} e^{iks} \Omega\left(\frac{k^2}{2m} + U(X)\right)\,, \tag{3.150}$$

where the energy density is defined as

$$\Omega(E) = \frac{\int \mathrm{d}k\mathrm{d}X\, \delta\left(\frac{k^2}{2m} + U(x) - E\right) \vartheta_0(k, X)}{\int \mathrm{d}k\mathrm{d}X\, \delta\left(\frac{k^2}{2m} + U(X) - E\right)}\,. \tag{3.151}$$

It is possible to show that the above classical approximation coincides with the quantum-mechanical diagonal ensemble constructed on the modes of the trap, as it should be (see Ref.

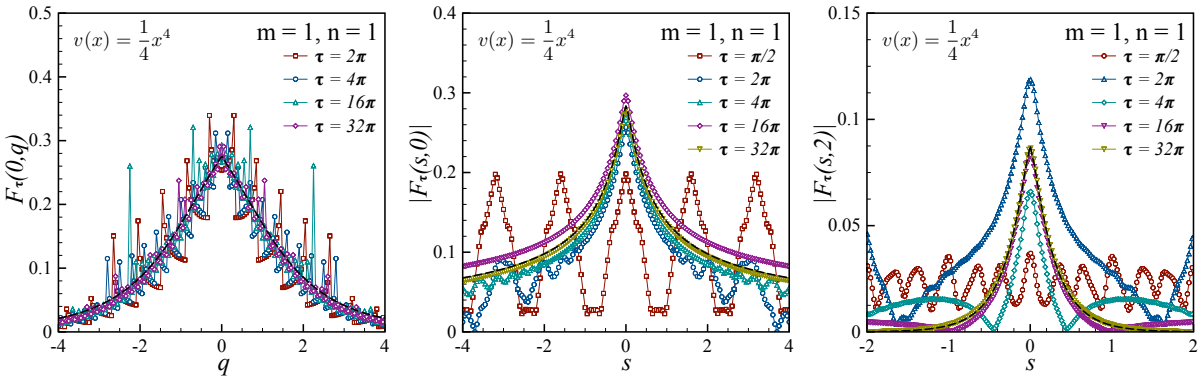

Figure 3.12: *Zero temperature two-point correlation function for different times after an interaction quench in the anharmonic trap. In the large time limit the correlator approaches the steady-state prediction of Eq. (3.150) (black dashed lines). Figure taken from Ref. [7]*

[7]). As we said, relaxation is caused by the dephasing between the different classical trajectories. While this is the common scenario for a generic trap, this is no longer true in the parabolic case: being isochronous, dephasing is absent and the two point correlator exhibits revivals. Amusingly, notice that for a parabolic potential Eq. (3.146) coincides with Eq. (3.147) without taking the thermodynamic limit, thus the Wigner distribution evolves classically even for finite harmonic traps.

As an example, we explicitly analyze the zero temperature limit. In this limit the LDA of the initial fermionic two-point correlation function reduces to

$$F_0(s, X) = \delta(X) \frac{n}{(1 + 2n|s|)^2} \,. \tag{3.152}$$

In Fig. 3.11 we plot the Wigner distribution at different times τ, and for two representative confining potentials, namely $U(x) = x^2/2$ and $U(x) = x^4/4$ (where, in the following, we fixed $m = 1$ and $n = 1$). In the harmonic case, the Wigner distribution exhibits a trivial periodic dynamics and the particle density never reaches a stationary profile.

On the contrary, in the anharmonic case, the excitation density approaches a continuos distribution; the system therefore relaxes to the stationary state whose correlation function is given by Eq. (3.150).

In Fig 3.12 we compare the steady-state predictions with the correlation function evaluated numerically, through a classical evolution of the initial root density, in the presence of the anharmonic confining potential $U(x) = x^4/4$. In particular, we plot the particle density vs X as well as the two-point correlator as a function of $s = y - x$ for fixed $X = 0$ and $X = 2$. As expected, for large time the numerical data approaches the stationary profiles.

3.3.4 Concluding remarks

In this section we studied the equilibration mechanism of 1D Bose gases in the Tonks-Girardeau limit starting with initial states that are gaussian in the bosonic fields, in the homogeneous case as well as the general inhomogeneous case of an arbitrary confining trap. Despite the noninteracting (in terms of the fermions) dynamics, this problem is nontrivial due to the nonlocal nature of the Jordan-Wigner transformation which links the bosonic and fermionic fields. By solving the problem of extracting fermionic correlations from the bosonic ones in a Gaussian state and vice versa, we derived exact closed formulas for the steady state correlations and analysed them both numerically and analytically in several asymptotic limits.

When a confining potential is considered, the relaxation of local observables can be attained only in a proper thermodynamic limit, where the local density approximation is applicable. In this limit, the evolution is separated on two time scales: initially the system behaves as if it was homogeneous with a subsequent gaussianification. Thereafter, the particles explore the whole trap on a thermodynamic time scale with an emergent semiclassical evolution for the two point fermionic correlator, in terms of which all the expectation values of local observables are determined.

3.4 Generalized Hydrodynamics and its application to classical field theories

In the previous section we saw the natural emergence of an hydrodynamic (semiclassical) description in the Tonks Girardeau gas (i.e. a free theory), where the system can be locally described by a GGE, the evolution of the latter interpreted as the phase-space density of a set of free particles. Generalizing this picture to truly integrable models has been out of reach until the recent works presented in Ref. [159, 160] paved the way to the Generalized Hydrodynamics: after a short recap of these concepts (see Section 3.4.1), in this section we present the work of Ref. [8] where we transposed these results into the classical realm.

Focussing on the classical Sinh-Gordon model, we confirmed that GHD can indeed be applied to classical fields, thus further suggesting its large universality. We explicitly compare GHD predictions with Metropolis simulations of classically fluctuating initial states evolved deterministically with the field's equations of motion. We study both the partitioning protocol (or domain wall initial condition), where two halves are initialized in different homogeneous GGEs and suddenly joined at one point, and Euler-scale dynamical correlation functions in homogeneous thermal states. Our study provided in particular the first numerical tests for the recent GHD constructions of Euler-scale correlation functions in integrable models [174, 175]. In particular, we provided numerical evidence for the necessity for fluid-cell averaging in the Euler scaling limit of correlation functions.

The theory of Gibbs states of classical integrable fields has already been developed in [375–378], and it is easy to extend it to GGEs. Interestingly, it takes a very similar form to that of the quantum TBA. The exact form of GGEs, and therefore of GHD, depends on the precise type of modes admitted by the integrable model. Indeed, in Section 2.1.2, dealing with fermions caused the appearance of a fermionic entropy term in the TBA (see Eq. (2.22) and (2.24)) which naturally lead to a Fermi distribution (2.26). Likewise, it has been observed that classical gases are associated to Boltzmann-type free energy functions [174].

In classical integrable field theories, it is observed [375–378] that many models admit two types of modes: solitonic modes and "radiative modes", both of which are involved in (generalized) thermalization processes. Solitons have clear particle-like behaviour, giving GHD modes with Boltzmann-like free energy function, like classical gases. By contrast, radiative modes do not display any obvious quasi-particle character in their dynamics, yet, as we will verify, in the GHD they can be accounted for by the same quasi-particle GHD equations, with the appropriate free energy function for radiative modes. Properly taking in account radiative modes is crucial for the correctness of the hydrodynamic description. Indeed, in this section we only study radiative modes, as the classical Sinh-Gordon model does not contain soliton modes.

The radiative free energy function is reminiscent of that of the classical prediction for blackbody radiation. Because of the "UV catastrophe", radiative modes make averages of fields containing high enough derivatives to diverge. This is characteristic of the roughness of (generalized) thermally fluctuating classical fields. We will verify that the GHD equations nevertheless describe correctly the averages of observables that are finite, such as the vertex operators which

are accessible through the classical version of the Smirnov-Negro result discussed in Section 2.2.1.

3.4.1 Summary of Generalized Hydrodynamics

The lack of homogeneity breaks most of the standard structures at the core of many-body integrability, such as the inverse scattering method. Nevertheless, these standard structures may be used in conjunction with the idea of emergence of hydrodynamics. With weak, large-scale inhomogeneity and non-stationarity, one describes a many-body state in terms of fluid cells: mesoscopic regions which are assumed homogeneous, stationary and very large compared with microscopic scales, where entropy is maximized.

The limit where this description becomes exact is often referred to as the "Euler scale". This is the scaling limit whereby parameters characterizing the state are taken to vary in space on an infinitely large scale, observables are at space-time points growing with this scale and appropriately averaged over fluid cells, and correlations are likewise scaled. See for instance [379]. Various microscopic distances are expected to control the approximate validity of the limiting behavior in real situations, including the inter-particle distance and the scattering length; however there is, as of yet, no general and rigorous theoretical understanding for the emergence of hydrodynamics in deterministic systems. Let us assume the dynamics is governed by an integrable homogeneous Hamiltonian, however the state is initialized in an inhomogeneous set up such that the inhomogeneity is sufficiently weak. Following [159, 160], we derive the emergence of hydrodynamic equations from two hypothesis

1. In the limit of weak inhomogeneity, the system can be described as if it was homogeneous, then the time/space dependence is recovered promoting the GGE to be space/time dependent.

2. GGEs at different times/spaces can be connected imposing the infinite set of conservation laws. Let $\mathcal{Q}_i = \int \mathrm{d}x\, \mathfrak{q}_i(x)$ be the charge and $\mathcal{J}_i = \int \mathrm{d}x\, \mathfrak{j}_i(x)$ the associated current, then along the time evolution it holds true

$$\partial_t \mathfrak{q}_i(t,x) + \partial_x \mathfrak{j}_i(t,x) = 0\,. \tag{3.153}$$

For the sake of simplicity, let us assume the existence of an unique excitation species and thus the GGE is fully determined by a root density $\rho(\theta)$: we promote the GGE to have weak space-time dependence, thus $\rho(\theta) \to \rho_{t,x}(\theta)$. Then, assuming the validity of the first of the two points above we write

$$\langle \mathfrak{q}_i(t,x)\rangle \simeq \langle \mathfrak{q}_i(t,x)\rangle_{\rho_{t,x}(\theta)} = \int \mathrm{d}\theta\, q_i(\theta)\rho_{t,x}(\theta)\,, \tag{3.154}$$

where with $\langle ...\rangle_{\rho_{t,x}(\theta)}$ we meant the expectation value over an homogeneous GGE having $\rho_{t,x}(\theta)$ as root density. The pivotal point in the result of Ref. [159, 160] was the expectation value of the current on arbitrary GGEs, which was previously unknown

$$\langle \mathfrak{j}_i(t,x)\rangle \simeq \langle \mathfrak{j}_i(t,x)\rangle_{\rho_{t,x}(\theta)} = \int \mathrm{d}\theta\, q_i(\theta) v^{\mathrm{eff}}_{t,x}(\theta)\rho_{t,x}(\theta)\,, \tag{3.155}$$

where the effective velocity is defined as per

$$v^{\mathrm{eff}}_{t,x}(\theta) = \frac{\partial_\theta E^{\mathrm{dr}}(\theta)}{\partial_\theta p^{\mathrm{dr}}(\theta)}\,. \tag{3.156}$$

Above, $E(\theta)$ and $p(\theta)$ are, respectively, the single particle energy and momentum eigenvalues. The space-time dependence is induced by the dressing operation (defined in Section 2.1.2),

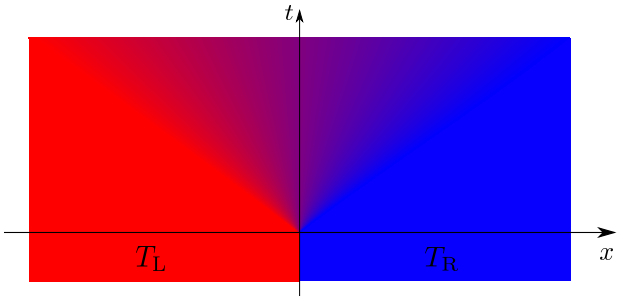

Figure 3.13: *Pictorial representation of the partitioning protocol. The system is initialized in two different halves, for example two thermal states at different temperatures T_L and T_R. At time $t > 0$ the system is let free to evolve and a perturbation spreads from the junction in a lightcone fashion, with the formation of non trivial currents. This is particularly evident in those systems which possess a maximum velocity in the propagation of information, as per relativistic systems or lattice models.*

which depends on the inhomogeneous root density. The physical interpretation of Eq. (3.155) is the following: the current is caused by propagating excitations, thus its expression is given by the charge carried by each particle q_i times the flux $v^{\rm eff}\rho$. $v^{\rm eff}$ is readily recognized to be the, suitably dressed, group velocity: indeed, in free models the group velocity is simply defined as $\partial_\theta E(\theta)/\partial_\theta p(\theta)$. However, due to the interaction, the single particle dispersion law is dressed by the effect of the other excitations, as we explained in Section 2.1.2. This is probably best appreciated in the molecular dynamic implementation [161], where GHD emerges in a gas of classical pointwise particles, which experience a time delay whenever they scatter with each others. In the framework of relativistic models, Eq. (3.155) can be proven [159].

Consider now the charge/current conservation (3.153), take the expectation value and use the approximation (3.154) and (3.155)

$$\int \mathrm{d}\theta\, q_i(\theta)\partial_t\rho_{t,x}(\theta) + \int \mathrm{d}\theta\, q_i(\theta)\partial_x\left[v^{\rm eff}_{t,x}(\theta)\rho_{t,x}(\theta)\right] = 0\,. \tag{3.157}$$

This equation is supposed to hold for any (quasi-)local charge: invoking the completeness of such a set, we are lead to the hydrodynamic equation

$$\partial_t\rho_{t,x}(\theta) + \partial_x\left[v^{\rm eff}_{t,x}(\theta)\rho_{t,x}(\theta)\right] = 0\,. \tag{3.158}$$

This is the main result of Ref. [159, 160], which found tons of applications and generalizations [161–180]. The interpretation is clear: on an Eulerian scale, the system can be described by mean of a collection of particles with phase-space density ρ, moving with an effective velocity $v^{\rm eff}_{t,x}(\theta)$. Hereafter, we quickly discuss two applications of GHD, then move to analyze in detail classical field theories.

A natural application: the partitioning protocol

Here we briefly discuss one of the most natural applications of GHD, namely the partitioning protocol. In this case, the infinite system is initialized in two different halves [380–385] each described by a given GGE, e.g. two thermal ensembles at different temperatures, and at time $t = 0$ let be free to evolve. We pose the origin of the space axis at the junction, in such a way the halves originally meet at $x = 0$. Indeed, this was the first application of GHD presented in the original papers [159, 160], and then has been repetitively examined in the hydrodynamic context [164, 167, 173, 176, 181, 386].

The sudden attachment of two different halves is absolutely not of weak variation and the initial condition does not fall into the paradigm of GHD. However, as time passes, the inhomogeneity is smeared more and more, the signal propagating in a ligthcone fashion from the junction (see Fig. 3.13): this is particularly clear in presence of a maximum velocity for the excitations, as it happens in relativistic models. At late times, we eventually enter in the hydrodynamic regime where Eq. (3.158) can be applied. Furthermore, the absence of any natural length scale in the system makes natural to look for scaling solutions, i.e. $\rho_{t,x}(\theta)$ is not an independent function of space and time, but only depends on their ratio $\zeta = x/t$. Conventionally, ζ is called "ray" and the inhomogeneous GGE with a ray dependence has been called Local Quasi Stationary State (LQSS) [160]. Instead, the restriction to the junction (i.e. the LQSS at $\zeta = 0$) is known as Non Equilibrium Steady State (NESS). In order to find the LQSS solution it is useful to reformulate Eq. (3.158) in an equivalent equation for the filling [159, 160]

$$\partial_t \vartheta_{t,x}(\theta) + v^{\text{eff}}_{t,x}(\theta)\partial_x \vartheta_{t,x}(\theta) = 0\,. \tag{3.159}$$

Showing the equivalence between Eq. (3.159) and Eq. (3.158) amounts to a simple manipulation of the integral equations defining the dressing, together with the fact that $2\pi\rho_t = \partial_\theta p^{\text{dr}}$. Looking for the mentioned ray-dependent solutions, together with the boundary condition that at $\zeta = \pm\infty$ the filling reduces to that of the initial left/right GGE, is found

$$\vartheta_{t,x}(\theta) = \Theta(v^{\text{eff}}_{t,x}(\theta) - \zeta)\vartheta_{\text{L}}(\theta) + \Theta(\zeta - v^{\text{eff}}_{t,x}(\theta))\vartheta_{\text{R}}(\theta)\,. \tag{3.160}$$

Above, Θ is the Heaviside theta function and $\vartheta_{\text{L}}, \vartheta_{\text{R}}$ are, respectively, the filling describing the left and right reservoirs. The solution Eq. (3.160) is implicit, since v^{eff} depends on the ray through the dressing, however an iterative numerical solution has been experienced to quickly converge. Firstly, Eq. (3.160) is solved ignoring the dressing in v^{eff}, then the obtained solution of the filling is used to compute v^{eff}, which is then updated with the new solution of the filling and so on, until convergence is attained. Lastly, ray-dependent profiles of local observables are computed in the local density approximation, namely as if they were computed on a homogeneous GGE having the GHD solution as root density. We will be back to the partitioning protocol while discussing the classical Sinh-Gordon, but we first consider correlation functions in the hydrodynamic regime.

Correlation functions on a hydrodynamic scale

Generalized Hydrodynamics resides on a local density approximation: on a hydrodynamic scale, different spatial points are uncorrelated and this allows to consider expectation values as if they were computed on homogeneous GGEs. However, quite surprisingly, hydrodynamics can give information even on correlation functions [174, 175]. Let us address a very simple, stationary situation: consider an homogeneous thermal state with inverse temperature β, which is easily solved through the TBA presented in Section 2.1.2. We consider a thermal ensemble for simplicity, but what it follows is easily generalized to arbitrary GGEs. Then, from the partition function $\mathcal{Z} = \text{Tr}[e^{-\beta H}]$ we can easily get the expectation value of the Hamiltonian, as well as all the connected correlators. Let $\mathcal{F} = \log \mathcal{Z}$ be the free energy, then

$$\mathcal{F} = \sum_{j=1}^{\infty} \frac{(-\beta)^j}{j!} \langle H^j \rangle_c\,. \tag{3.161}$$

The connected correlators $\langle H^j \rangle_c$ are defined subtracting from a given correlator all the possible "partitionings" in smaller correlation functions we can perform. For example, $\langle H^2 \rangle_{\text{c}} = \langle H^2 \rangle - (\langle H \rangle)^2$. Now, let us recall the equations defining the TBA, however we slightly generalize them in view of future applications to classical fields. We assume there exists an effective energy $\varepsilon(\theta)$

satisfying a non-linear integral equation in the same spirit of (2.25)

$$\varepsilon(\theta) = \beta E(\theta) - \int_{-\infty}^{\infty} \frac{\mathrm{d}\mu}{2\pi} \varphi(\theta,\mu) F(\varepsilon(\mu)) \,, \tag{3.162}$$

where the kernel is symmetric $\varphi(\theta,\mu) = \varphi(\mu,\theta)$. Notice that, if we pose $F(\varepsilon) = \log(1+e^{-\varepsilon})$ and $\varphi(\theta,\mu) = \varphi(\theta-\mu)$ we exactly recover Eq. (2.25). We also assume that the same function enters in the partition function, thus Eq. (2.28) is generalized to

$$\mathcal{F} = \lim_{L\to\infty} L^{-1} \log \mathcal{Z} = \int \frac{\mathrm{d}\theta}{2\pi} \partial_\theta p(\theta) F(\varepsilon(\theta)) \,. \tag{3.163}$$

Again, with the choice $F(\varepsilon) = \log(1+e^{-\varepsilon})$ we recover Eq. (2.28). Now, we *define* the filling as $\vartheta = -\partial_\varepsilon F(\varepsilon)$ and $\rho_t = 2\pi \partial_\theta p^{\mathrm{dr}}$, where $\partial_\theta p^{\mathrm{dr}}$ satisfies the same dressing equation Eq. (2.34). Lastly, we *define* $\rho(\theta)$ as per $\rho(\theta) = \vartheta(\theta)\rho_t(\theta)$. Then, with these definitions it is easy to prove that, consistently with the sought expectation value of local charges (2.27), we have

$$\langle H \rangle = -\partial_\beta \mathcal{F} = L \int \mathrm{d}\theta E(\theta) \rho(\theta) \,. \tag{3.164}$$

Considering partition functions of arbitrary GGEs (i.e. replacing $\beta E(\theta)$ with the proper source term in Eq. (3.162)), we get consistently that the expectation value of arbitrary charges, obtained deriving the partition function, coincides with the integral of the root density weighted with the proper single-particle eigenvalue.

Taking a double derivative of the free energy we access the connected correlation functions: manipulating the integral equation is not hard to arrive at

$$\langle H^2 \rangle_{\mathrm{c}} = L \int \mathrm{d}\theta \, \rho_t(\theta) E^{\mathrm{dr}^*}(\theta) \partial_\varepsilon^2 F(\varepsilon(\theta)) E^{\mathrm{dr}^*}(\theta) \,. \tag{3.165}$$

Above, the dressing operation $(..)^{\mathrm{dr}^*}$ is defined, for an arbitrary function $q(\theta)$, through the following integral equation

$$q^{\mathrm{dr}^*}(\theta) = q(\theta) + \int \frac{\mathrm{d}\mu}{2\pi} \varphi(\theta,\mu) \vartheta(\mu) q^{\mathrm{dr}^*}(\mu) \,. \tag{3.166}$$

Notice that this new dressing operation is closely related to the dressing defined in Section 2.1.2, namely Eq. (2.34). Indeed, we have $\partial_\theta q^{\mathrm{dr}} = (\partial_\theta q)^{\mathrm{dr}^*}$. The generalization of Eq. (3.165) to arbitrary charges is not hard

$$\langle \mathcal{Q}_i \mathcal{Q}_j \rangle_{\mathrm{c}} = L \int \mathrm{d}\theta \, \rho_t(\theta) q_i^{\mathrm{dr}^*}(\theta) \partial_\varepsilon^2 F(\varepsilon(\theta)) q_j^{\mathrm{dr}^*}(\theta) \,. \tag{3.167}$$

This result, among others, was presented for the first time in Ref. [174]. Since the charges are conserved, the equal time correlator trivially coincides with the two times correlator

$$\langle \mathcal{Q}_i(t) \mathcal{Q}_j(0) \rangle_{\mathrm{c}} = \langle \mathcal{Q}_i(0) \mathcal{Q}_j(0) \rangle_{\mathrm{c}} = L \int \mathrm{d}\theta \, \rho_t(\theta) q_i^{\mathrm{dr}^*}(\theta) \partial_\varepsilon^2 F(\varepsilon(\theta)) q_j^{\mathrm{dr}^*}(\theta) \,. \tag{3.168}$$

The story gets far more interesting (and also much more complicated) if we ask for correlation functions of charge densities, namely $\langle \mathfrak{q}_i(t,x) \mathfrak{q}_j(t',x') \rangle_{\mathrm{c}}$: is there a way to generalize the previous calculations to obtain such a result? The answer is affirmative, and this is the main achievement of Ref. [174, 175]: here we will not repeat those calculations and simply report the needed results, but nevertheless we want to convey the main ideas. In the GHD spirit, let us consider an arbitrary inhomogeneous GGE: instead of using an inhomogeneous root density, we can equivalently parametrize it in terms of some inhomogeneous Lagrange multipliers in

Eq. (3.162)

$$\varepsilon(t,x,\theta) = \sum_i \lambda_j(t,x) q_j(\theta) - \int_{-\infty}^{\infty} \frac{\mathrm{d}\mu}{2\pi} \varphi(\theta,\mu) F(\varepsilon(t,x,\mu)) \,. \tag{3.169}$$

Assuming $\lambda_j(t,x)$ are only weakly inhomogeneous, we can think about these TBA equations as associated with an inhomogeneous partition function

$$\mathcal{Z}(t) = \mathrm{Tr}\left[e^{-\sum_j \int \mathrm{d}x \lambda_j(t,x) \mathfrak{q}_j(x)} \right] . \tag{3.170}$$

Of course, computing the free energy and deriving it with respect to $\lambda_i(t,x)$ gives us $\langle \mathfrak{q}_i(t,x) \rangle$. Similarly, if we could have access to the partition function (and thus the free energy) at time t', identified by the inhomogeneous Lagrange multipliers $\{\lambda_i(t',x')\}$, suitable derivatives will lead us to the expectation values at time t'. The crucial point is to relate $\mathcal{Z}(t)$ with $\mathcal{Z}(t')$: as a matter of fact, if the sets $\{\lambda_i(t,x)\}$ and $\{\lambda_i(t',x')\}$ identify two GGEs such that one is the solution of the GHD equation having the other such as initial condition, then $\mathcal{Z}(t) = \mathcal{Z}(t')$ [1][172].

Thus, we could get the two point connected correlator as

$$\langle \mathfrak{q}_i(t,x) \mathfrak{q}_j(t',x') \rangle_{\mathrm{c}} \simeq \frac{\delta^2 \mathcal{Z}(t)}{\delta\lambda_i(t,x)\delta\lambda_j(t',x')} = \frac{\delta^2 \mathcal{Z}(t')}{\delta\lambda_i(t,x)\delta\lambda_j(t',x')} \tag{3.171}$$

The equality is expected to hold true whenever the large time and distance limits are considered. Furthermore, averaging on fluid cells in needed: as a matter of fact, GHD can resolve only weak variations, thus it cannot capture any strong oscillating component of $\langle \mathfrak{q}_i(t,x) \mathfrak{q}_j(t',x') \rangle_{\mathrm{c}}$, if present. The need of averaging over fluid cells was firstly pointed out in Ref. [175], while the project ended in our paper Ref. [8] was ongoing. Indeed, in the numerical simulations of Ref. [8] we testified the need of such an averaging procedure, which has been furthermore analytically confirmed in a free-field limit.

Therefore, hereafter, when we write a correlation function on eulerian scale we implicitly assume that the charge density (and later more general local observables) are replaced with the average on fluid cells

$$\mathfrak{q}_i(t,x) \to \frac{\int_{\mathcal{N}(t,x)} \mathrm{d}y \mathrm{d}\tau \, \mathfrak{q}_i(\tau,y)}{\int_{\mathcal{N}(t,x)} \mathrm{d}y \mathrm{d}\tau} \,. \tag{3.172}$$

Above, $\mathcal{N}(t,x)$ is a region centered around the space-time point (t,x). Since there is not a rigorous understanding of the precise conditions needed for the emergence of hydrodynamics, also a precise characterization of the domain $\mathcal{N}(t,x)$ is not available. In general, we expect different shapes of the domain $\mathcal{N}(t,x)$ to give the same result, provided it is chosen much larger than the typical microscopic length scales, but of course much smaller than the hydrodynamic scale on which the correlator varies. Pragmatically, when dealing with specific examples, we will specify which kind of fluid cell averaging has been experienced to make the numerical data to agree with the hydrodynamic prediction.

We will not present the long, non trivial computation (for which the reader can refer to Ref. [175]), but before quoting the result we want to discuss a further step. Indeed, correlators on an Eulerian scale can be computed not only for charges densities, but in principle also for arbitrary local operators.

The funding idea is that of the hydrodynamic projections [387] (see also Ref. [175]). Let us consider two local observables $\mathcal{O}(t,x)$ and $\mathcal{O}'(t',x')$, our aim is computing $\langle \mathcal{O}(t,x)\mathcal{O}'(t',x') \rangle_{\mathrm{c}}$ on an Eulerian scale. The idea is that correlation functions on large distances receive contributions only from the conserved charges. We can then suggestively "expand" the observable in terms of

[1] Actually, this is true if the free energy can be written in the form $\mathcal{F} = \int \mathrm{d}x \mathrm{d}\theta \, \partial_\theta p^{\mathrm{dr}} \tilde{F}(\vartheta)$, but this is the case both in the fermionic TBA (Section 2.1.2) and in the forthcoming classical case.

the (quasi-)local charges centered at the same point

$$\mathcal{O}(t,x) \simeq \sum_j \alpha_j \mathfrak{q}_j(t,x) + \dots \tag{3.173}$$

The coefficients of the expansion are fixed "projecting" on the charges $\mathcal{Q}_j$, i.e. imposing

$$\langle \mathcal{Q}_{j'} \mathcal{O}(t,x) \rangle_{\mathrm{c}} = \sum_j \alpha_j \langle \mathcal{Q}_{j'} \mathfrak{q}_j(t,x) \rangle_{\mathrm{c}} \,. \tag{3.174}$$

If the expectation values $\langle \mathcal{Q}_{j'} \mathcal{O}(t,x) \rangle_{\mathrm{c}}$ are known, we could solve for the coefficients α_j. Subsequently, the eulerian scale connected correlator $\langle \mathcal{O}(t,x)\mathcal{O}'(t',x') \rangle_{\mathrm{c}}$ is posed to be

$$\langle \mathcal{O}(t,x)\mathcal{O}'(t',x') \rangle_{\mathrm{c}} = \sum_{j,j'} \alpha_j \alpha'_{j'} \langle \mathfrak{q}_j(t,x) \mathfrak{q}_{j'}(t',x') \rangle_{\mathrm{c}} \,. \tag{3.175}$$

Above, α'_j are the coefficients of the expansion of $\mathcal{O}'$. We will not try to further justify or making rigorous the ideas we conveyed (for which the reader can refer to the original papers Ref. [174, 175]) and simply quote the general result for local observables, from which the charge-charge correlator follows as a special case.

Let us imagine that the expectation value of $\mathcal{O}$ is known for an arbitrary GGE fixed by a TBA equation such as (3.162), but in which we allow for a generic source term $\beta E(\theta) \to \omega(\theta)$. Then we take the variation with respect to the source, which can always be rewritten as

$$-\delta \langle \mathcal{O}(x) \rangle = \int \mathrm{d}\theta \, \delta\omega^{\mathrm{dr}^*}(\theta) \rho_t(\theta) f(\theta) V^{\mathcal{O}}(\theta) \tag{3.176}$$

where the above equation *defines* the quantity $V^{\mathcal{O}}(\theta)$ and

$$f(\theta) = -\frac{\partial_\varepsilon^2 F(\varepsilon(\theta))}{\partial_\varepsilon F(\varepsilon(\theta))} \,. \tag{3.177}$$

Notice that if we specialize to TBA sources in the form $\omega(\theta) = \sum_j \lambda_j q_j(\theta)$ and set $\delta\omega(\theta) = \partial_{\lambda_j}\omega(\theta)$, then $-\delta\langle\mathcal{O}\rangle = \langle \mathcal{Q}_j \mathcal{O}(x) \rangle$. Thus, Eq. (3.176) is nothing else the generalization of the hydrodynamic projection to infinitely many charges. Then, the two point correlation function specialized on an homogeneous GGE in background (generalizations to inhomogeneous GGEs are possible [175]) is

$$\langle \mathcal{O}(t,x)\mathcal{O}'(0,0) \rangle_{\mathrm{c}} = \int \mathrm{d}\theta \, \delta(x - v^{\mathrm{eff}}(\theta) t) \, \rho_t(\theta) f(\theta) V^{\mathcal{O}}(\theta) V^{\mathcal{O}'}(\theta) \,. \tag{3.178}$$

The interpretation is clear: the correlation is carried by those excitations which travel from one local operator to the other, i.e. moving with velocity $v^{\mathrm{eff}} = x/t$. Indeed, $t\langle \mathcal{O}(t,x)\mathcal{O}'(0,0) \rangle_{\mathrm{c}}$ is a pure function of the ray $\zeta = x/t$

$$t\langle \mathcal{O}(t,\zeta t)\mathcal{O}'(0,0) \rangle_{\mathrm{c}} = \int \mathrm{d}\theta \, \delta(\zeta - v^{\mathrm{eff}}(\theta)) \, \rho_t(\theta) f(\theta) V^{\mathcal{O}}(\theta) V^{\mathcal{O}'}(\theta) \,. \tag{3.179}$$

3.4.2 The classical Sinh Gordon model: TBA and GHD

As a proof of concept of using GHD to study classical integrable field theories, we study the Sinh Gordon model. In its classical version, the Sinh Gordon model does not have particle-like excitations, but rather radiative modes. The absence of a clear particle-like interpretation makes the construction of the TBA and then GHD somewhat less intuitive, see for example Ref. [182, 378] for a derivation of the Bethe Equations directly from the inverse scattering method.

However, dealing with the Sinh Gordon model, we can take advantage from the fact that the quantum version is remarkably well controlled: in Ref. [159] the GHD of the quantum Sinh Gordon model has been studied and, in particular, the expectation value of the current Eq. (3.155) rigorously proven. Therefore, a very natural way to access the classical Sinh Gordon model passes through a semiclassical limit of its quantum version: this path has been followed in Ref. [182], when the semiclassical limit of the TBA (and GGEs) and LeClair-Mussardo expansion has been performed. This gave access, in principle, to study homogeneous quenches in the classical Sinh Gordon and to compute one point functions on the steady state, through a semiclassical version of the LeClair-Mussardo expansion.

Here, we recover and extend such a program providing the semiclassical limit of the whole GHD, together with the Negro-Smirnov formula of Section 2.2.1. In particular, the resulting semiclassical Negro-Smirnov formula (which is a new result by us in the classical realm) allows for a much more efficient computation of local observables compared with the LeClair-Mussardo expansion, together with a derivation of the Eulerian scale correlation functions.

An advantage of dealing with a classical theory, as compared with a quantum model, is the relative simplicity of testing it through numerical simulations. This is especially true for continuous models, where the DMRG methods [115] are not efficient. Therefore, classical models constitute an important numerical benchmark for the validity of GHD. As a byproduct, we also provide a numerical test of the classical Smirnov-Negro formula, whose quantum counterpart had never been numerically checked.

Differently from the content of Chapter 2, where we were interested in the non relativistic limit of the Sinh Gordon and the notation was chosen consequently, here we work in natural units and set the speed of light to one $c = 1$. Therefore, along this section, the ShG model will be ruled by an action in this form

$$\mathcal{S}_{\text{ShG}} = \int \mathrm{d}x\mathrm{d}t \frac{1}{2}\partial_\mu\phi\partial^\mu\phi - \frac{m^2}{g^2}(\cosh(g\phi) - 1)\,. \tag{3.180}$$

The observables in which we are mostly interested in are the canonical stress energy tensor $T_{\mu\nu}$ (below, $\mathcal{L}$ is the Lagrangian density and $\eta_{\mu\nu}$ the Minkowski two-dimensional metric)

$$T_{\mu\nu} = -\eta_{\mu\nu}\mathcal{L} + \partial_\mu\phi\frac{\delta\mathcal{L}}{\delta\partial^\nu\phi}, \qquad T^\mu_{\ \mu} = 2\frac{m^2}{g^2}(\cosh(g\phi) - 1)\,, \tag{3.181}$$

as well as the vertex operators $e^{kg\phi}$, with k integer. The expectation value of the latter will be accessed through the Smirnov-Negro formula.

The TBA and GHD of the classical Sinh Gordon

We now quickly recap the TBA associated with the classical Sinh Gordon, present the classical GHD and the expectation value of the observables of interest. All the results can be recovered by mean of a suitable semiclassical limit of the known quantum expressions: here we do not report the derivation, which is left to Appendix 3.A, but simply state the results. In terms of the effective energy, the TBA of the classical Sinh Gordon is expressed as

$$\varepsilon(\theta) = w(\theta) - \mathcal{P}\int \frac{\mathrm{d}\mu}{2\pi}\frac{g^2}{4}\frac{1}{\sinh(\theta-\mu)}\partial_\mu \log\varepsilon(\mu)\,. \tag{3.182}$$

Above, $w(\theta)$ is the source term of the GGE (e.g. if we choose $\omega(\theta) = \beta E(\theta)$ we describe the usual thermal ensemble) and $\mathcal{P}$ stands for the principal value prescription in handling the singularity. In the perspective of the general TBA equation (3.162), if we set $\varphi(\theta,\mu) = \frac{g^2}{4}\mathcal{P}\frac{1}{\sinh(\theta-\mu)}\partial_\mu$ and

$F(\varepsilon) = \log\varepsilon$ we recover the TBA equations of the classical Sinh Gordon). Therefore, in the ShG model the resulting filling function is $\vartheta(\theta) = 1/\varepsilon(\theta)$.

In Ref. [182], Eq. (3.182) is derived both through the inverse scattering method and the semi-classical limit of the quantum TBA[2] (see also Appendix 3.A).

In general, local conserved charges can be organised into irreducible representations of the 1+1-dimensional Lorentz group, and, as is often done, these can be combined into parity-odd and parity-even charges. In the Sinh-Gordon model, all odd spins arise, but no even spins. In the following we concentrate on the parity-even charges, which we denote $\mathcal{Q}_n$ for $n \in \mathcal{N}$ odd. These have one particle eigenvalues $q_n(\theta)$ given by

$$q_n(\theta) = m^n \cosh(n\theta). \tag{3.183}$$

In particular, the Hamiltonian is $\mathcal{Q}_1 = H = \int \mathrm{d}x\, T^{00}(x)$. Thus, classical expectation values on GGEs with only local parity-even conserved quantities are described through the path integral

$$\langle \mathcal{O} \rangle = \frac{1}{\mathcal{Z}} \int \mathcal{D}\phi\mathcal{D}\Pi\ \mathcal{O}[\phi,\Pi] \exp\Big[- \sum_{n\in\mathbb{N}\text{ odd}} \beta_n \mathcal{Q}_n[\phi,\Pi] \Big], \tag{3.184}$$

where Π is the conjugate momentum $\Pi = \partial_t\phi$. The resulting source term in the TBA (3.182) is then

$$w(\theta) = \sum_{n\in\mathbb{N}\text{ odd}} \beta_n q_n(\theta). \tag{3.185}$$

Although quasi-local charges are not fully worked out in the Sinh-Gordon model, we expect they largely extend the space of allowed functions $w(\theta)$. Generically, the states emerging from the GHD time evolution belong to such an extended space. Note that the Lagrangian density is invariant under simultaneous scaling

$$(x,t,m,\Phi,g) \mapsto (\lambda x, \lambda t, \lambda^{-1}m, \lambda\Phi, \lambda^{-1}g), \tag{3.186}$$

while it gains a factor λ^{-2} under $(x,t,m) \mapsto (\lambda x, \lambda t, \lambda^{-1}m)$. Hence, from the latter, the GGE state is invariant under

$$(x,t,m,g,\{\beta_n\}) \mapsto (\lambda x, \lambda t, \lambda^{-1}m, g, \{\lambda^n\beta_n\}), \tag{3.187}$$

while from the former (and the explicit form of higher conserved densities, see Appendix 3.B.2), it is invariant under

$$(x,t,m,g,\{\beta_n\}) \mapsto (\lambda x, \lambda t, \lambda^{-1}m, \lambda^{-1}g, \{\lambda^{n-2}\beta_n\}). \tag{3.188}$$

As a consequence, in situations that only depend on the ratio x/t (as in the partitioning protocol and in the study of correlation functions in homogeneous states, considered below), the invariant ratios characterizing the strength of the interaction are

$$\frac{g^2}{\beta_n m^n}, \quad n \in \mathbb{N}. \tag{3.189}$$

In particular, the effective interaction strength is larger at large temperatures. This was expected, since at low temperature the field configurations explore only the bottom of the potential energy, where a quadratic approximation is reliable and the field behaves as if it was free.

[2] A typo of an overall minus sign in the kernel occurred in [182].

The Black Body catastrophe and UV finite quantities

It is well known that thermal states in classical electromagnetism suffer from UV catastrophes, intimately connected to Planck's original idea of quantizing oscillation modes in order to explain the black body radiation spectrum. The same problem appears in thermal ensembles and GGEs of other field theories such as the Sinh-Gordon model. The problem is that in such states fields can be very "rough". For instance, a GGE involving local conserved charges only up to some finite spin does not regularize the field enough to guarantee the existence of averages of its large-order derivatives. In the TBA formulae, this is clearly seen as a divergence of averages of conserved densities of high enough spin, which occurs at large rapidities due to radiative modes. Indeed, recalling the expressions of the filling $\vartheta(\theta) = 1/\varepsilon(\theta)$ and of the root density $2\pi\rho(\theta) = (\partial_\theta p(\theta))^{\mathrm{dr}^*}\vartheta(\theta)$, we get that at large rapidities (at large rapidities the dressing can be ignored) $\rho(\theta) \simeq e^{|\theta|}/w(\theta) \simeq e^{(1-n)|\theta|}$, where n is the maximum spin of the charges appearing in the source term. Consequently, the expectation value $\langle \mathcal{Q}_j \rangle$ is UV divergent whenever $j \geq n-1$. Nevertheless, it is a simple matter to see from the TBA formulae that the right combination of energy density and momentum current is finite: this is the trace of the stress-energy tensor $T^\mu_{\ \mu}$, which does not contain field derivatives, and it is finite on thermal state as well as GGEs based on higher-spin local charges. Clearly, averages of higher-spin densities and currents become finite as we increase the spin of the conserved charges involved in the GGE.

The energy density and current, $T^{00}(x)$ and $T^{10}(x)$ respectively, have GGEs expectation values given by

$$\langle T^{00}(x)\rangle = \int \mathrm{d}\theta\, m\cosh\theta\,\rho(\theta)\,, \qquad \langle T^{10}(x)\rangle = \int \mathrm{d}\theta\, m\cosh\theta\, v^{\mathrm{eff}}(\theta)\rho(\theta)\,. \tag{3.190}$$

Similar expressions hold for T^{01} and T^{11} replacing the energy eigenvalue $m\cosh\theta$ with the momentum one $m\sinh\theta$. In particular, the expectation value of $T^\mu_{\ \mu} = T^{00} - T^{11}$ is

$$\langle T^\mu_{\ \mu}\rangle = m\int \frac{\mathrm{d}\theta}{2\pi}\rho(\theta)\left(\cosh\theta - v^{\mathrm{eff}}(\theta)\sinh\theta\right)\,. \tag{3.191}$$

Clearly, $\langle T^\mu_{\ \mu}\rangle$ is UV finite on thermal states, as it must be being field derivatives absent in its expression (3.181). As already pointed out, other observables which are UV finite on thermal states are the vertexes operators $e^{kg\phi}$: their expectation value can be either accessed through the semiclassical limit of the LeClair-Mussardo expansion [182], but this provides a small excitation-density description unsuited for the present purpose, either through the semiclassical limit of the Smirnov Negro formula. The derivation of the latter is left for Appendix 3.A, the result is

$$\frac{\langle e^{(k+1)g\phi}\rangle}{\langle e^{kg\phi}\rangle} = 1 + (2k+1)\frac{g^2}{4\pi}\int \mathrm{d}\theta\; e^\theta \vartheta(\theta) p^k_{\mathrm{cl}}(\theta)\,, \tag{3.192}$$

where

$$p^k_{\mathrm{cl}}(\theta) = e^{-\theta} + \frac{g^2}{4}\mathcal{P}\int \frac{\mathrm{d}\gamma}{2\pi}\frac{1}{\sinh(\theta-\gamma)}\left(2k - \partial_\gamma\right)\left(\vartheta(\gamma)p^k_{\mathrm{cl}}(\gamma)\right)\,. \tag{3.193}$$

As in the quantum case, taking k to be an integer (and using the fact that $\langle e^{kg\phi}\rangle = 1$ if $k = 0$), we obtain explicit recursive formulas for $\langle e^{kg\phi}\rangle$.

The partitioning protocol

We now study the classical Sinh-Gordon model in the partitioning protocol. We recall that this is the protocol where the initial state is formed of two homogeneous field distributions, one for the left half $x < 0$ and the other for the right half $x > 0$ of space. This setup is useful to study as

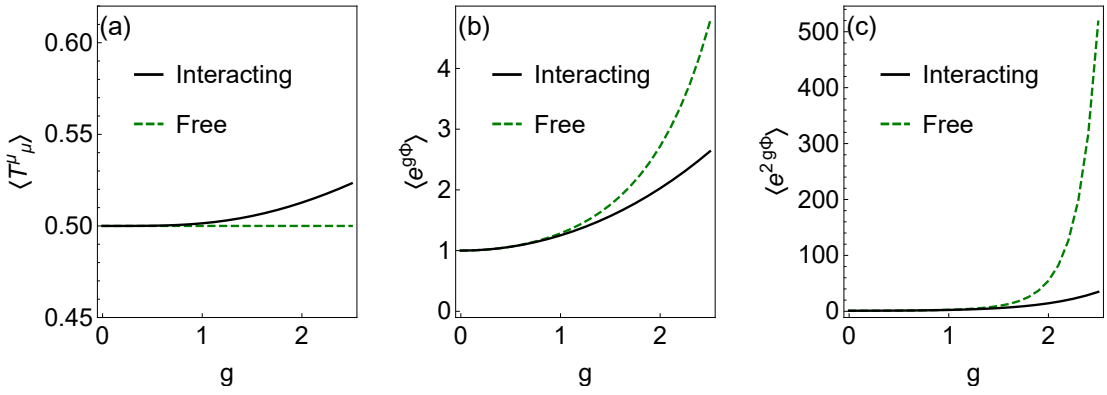

Figure 3.14: *Analytical expectation values of the trace of the stress energy tensor and of vertex operators in a homogeneous thermal ensemble at inverse temperature β are compared with the free model. By scaling* (3.187), (3.188)*, we may choose $\beta = m = 1$ and vary g. First panel on the left: the traces of the stress energy tensor for the interacting and free cases are compared. Second and third panel: the same is done for vertex operators. Note that passing from the interacting to the free theory, the trace of the stress energy tensor changes as function of the field. The difference between interacting and free is enhanced when comparing expectation values of fixed functions of the fields. Figure taken from Ref. [8].*

it generates truly non-equilibrium states, with nonzero currents and nontrivial profiles in space-time, yet it is simple enough so that GHD provides easily workable expressions. It is also the setup which is expected to be most accurately described by the hydrodynamic approximation, as at long times, profiles smooth out, making Euler hydrodynamics more applicable. Thus this setup gives the best playground for verifications of GHD non-equilibrium predictions.

For simplicity, we consider ensembles with nonzero (generalized) temperatures β_i for the Hamiltonian $H = \mathcal{Q}_1$ and for the first nontrivial (spin-3) parity-even local conserved charge $\mathcal{Q}_3$ only. In the partitioning protocol, one needs to specify the boundary or continuity conditions of the fields at $x = 0$. In particular, smoothness of the field at the boundary must be ensured in order to avoid producing shocks in the initial conditions of the protocol. Therefore, we do not initialize the system in two independent halves, but rather consider an unique system with a Boltzman weight

$$\exp\left[-\int \mathrm{d}x \sum_j (\beta_j^{\mathrm{L}}\Theta(-x) + \beta_j^{\mathrm{R}}\Theta(x))\mathfrak{q}_j(x)\right] . \tag{3.194}$$

where of course $\mathfrak{q}_j(x)$ is the density of the associated conserved charge $\mathcal{Q}_j = \int \mathrm{d}x\, \mathfrak{q}_j(x)$. This choice has been made also in view of the discretization needed to numerically simulate the partitioning protocol (see Appendix 3.B).

In order to illustrate the effect of the interaction and determine the values of g which significantly affect the averages, in Fig. 3.14 we plot the analytical thermal averages of the stress energy tensor and of the vertex operators both in the interacting and the free ($g = 0$) purely thermal Gibbs ensemble at the same temperature β^{-1}. This indicates that $g^2/(\beta m) \approx 2$ is well into the strongly interacting regime. We then compare the analytic predictions with direct numerical simulations of the above out-of-equilibrium protocol, see Appendix 3.B for details of the numerical methods. In particular, we consider three cases of the partitioning protocol:

I. The purely thermal case, where both sides are at different temperatures ($\beta_1^L \neq \beta_1^R$ and $\beta_3^L = \beta_3^R = 0$, Figs. 3.15 and 3.16).

II. The partitioning including differently coupled $\mathcal{Q}_3$ charges, but with equal temperatures ($\beta_1^L = \beta_1^R \neq 0$ and $\beta_3^L \neq \beta_3^R = 0$, Fig. 3.17).

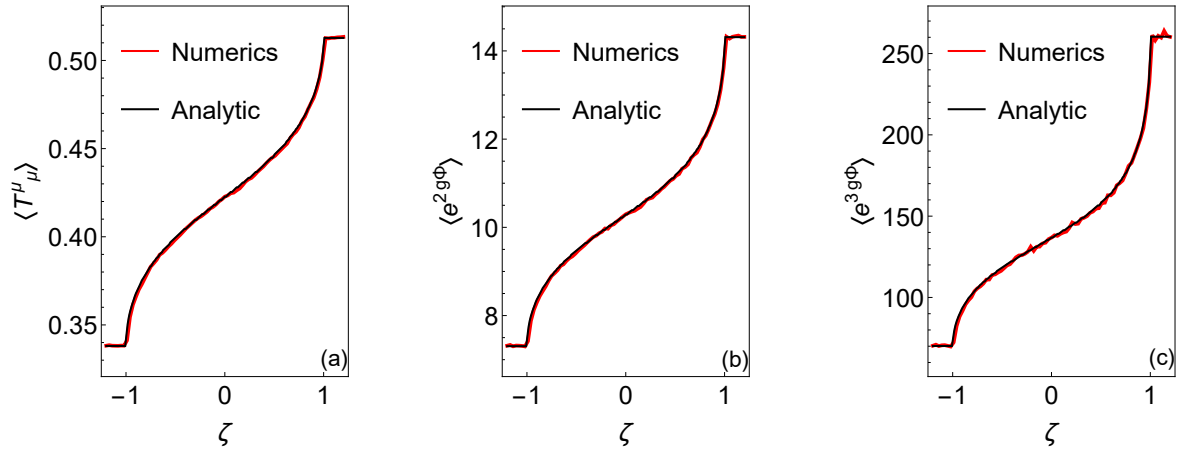

Figure 3.15: *Case I. Profiles of the trace of the stress energy tensor (a) and of the first vertex operators, (b) and (c), as functions of the ray $\zeta = x/t$ for a two-temperature partitioning protocol. Parameters: $m = 1$, $g = 2$, $a = 0.05$ inverse temperatures of the initial ensembles $\beta_1^L = 1.5$ and $\beta_1^R = 1$, the number of samples of the Metropolis is 84000. An additional average along the ray from $t = 50$ up to $t = 75$ smears out the statistical oscillations. In terms of the dimensionless coupling $g^2/m\beta$, we are in the strongly interacting regime (see Fig. 3.14). Figure taken from Ref. [8].*

III. The partitioning where both H and $\mathcal{Q}_3$ are differently coupled ($\beta_1^L \neq \beta_1^R$ and $\beta_3^L \neq \beta_3^R = 0$, Fig. 3.18), choosing the energy densities to be equal in the left and right reservoirs.

As explained above, in the purely thermal case (case I), because of the UV catastrophe, the expectation values of energy and momentum densities (as well as all the individual local charge densities and currents) are divergent. Hence in this case we do not have access to the non-equilibrium energy current. However, the averages of the trace of the stress-energy tensor T^{μ}_{μ} and of the vertex operators $e^{kg\phi}$ are finite, as these do not contain field derivatives. Thus in the thermal case we focus on these observables (Fig. 3.15). In the cases II and III, which include the charge $\mathcal{Q}_3$, we study the energy density and current independently. Interestingly, we find that a non-equilibrium energy current is generated in case II (Fig. 3.17). That is, the $\mathcal{Q}_3$ charge produces an imbalance in energy densities, hence a current develops. Having access to a UV finite non-equilibrium energy current is an important reason for considering the inclusion of $\mathcal{Q}_3$. In the case III, we study the case where the energy densities are equal on the left and right

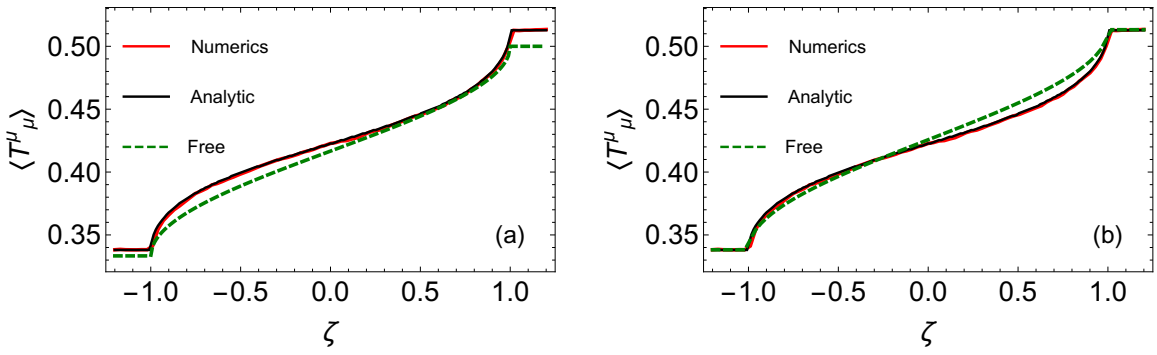

Figure 3.16: *The profile of the trace of the stress energy tensor already reported in Fig. 3.15, both analytic and numerical, with the same parameters used in Fig. 3.15 are compared against the expectation values in the free theory with (a) identical parameters and (b) β_1^L and β_1^R chosen so that the asymptotic values agree with the interacting theory. Figure taken from Ref. [8].*

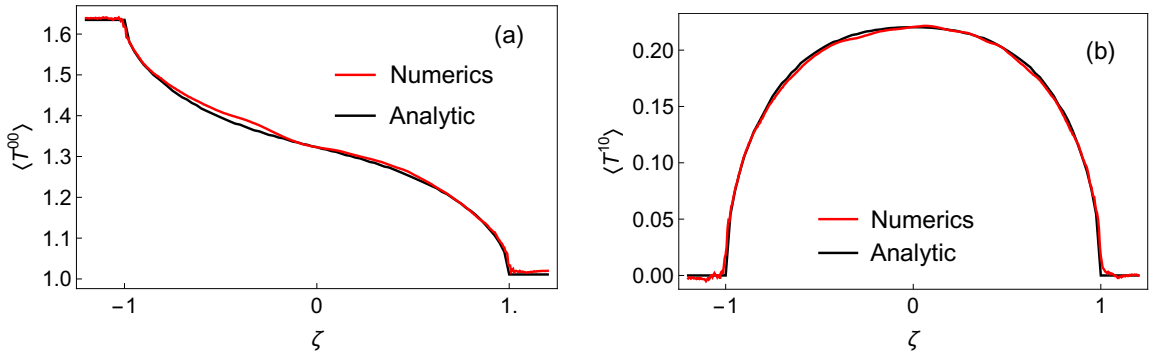

Figure 3.17: *Case II. Profiles of $\langle T^{00}(\zeta)\rangle$ (a) and $\langle T^{10}(\zeta)\rangle$ (b) are numerically computed and compared with the GHD predictions. The numerical results are obtained by averaging over the range $10 \leq t \leq 16$. The parameters are $m = 1$, $g = 1$, $\beta_1^L = \beta_1^R = 1$ with the coupling to the higher-spin charge varying, $\beta_3^L = 1/2$, $\beta_3^R = 1$ and the lattice spacing in the light-cone discretization is $a = 0.1$. Figure taken from Ref. [8].*

reservoirs, yet the coupling to H and $\mathcal{Q}_3$ are not balanced. This emphasizes the effects of the higher conserved charge: an energy current is generated even though the energy densities are balanced in the reservoirs, with a nontrivial profile developing (Fig. 3.18).

The results of the comparison between GHD analytical predictions and numerical simulations in the thermal case (case I) are presented in Figs. 3.15. We find excellent agreement. Measuring the difference between the numerical and analytical values by the relative $L(1)$ distance

$$R = \frac{\int |v^{\text{num}}(\zeta) - v^{\text{ana}}(\zeta)| d\zeta}{\int |v^{\text{ana}}(\zeta)| d\zeta} \tag{3.195}$$

(where v^{num} is the numerical data and v^{ana} is the analytical value), we obtain $R = 2.1 \times 10^{-3}$, 3.1×10^{-3} and 7.1×10^{-3} in the cases of Figs. 3.15a, 3.15b and 3.15c respectively. It must be stressed that, despite various checks in known limiting cases [90, 91, 222], the formula for the vertex operators (3.192-3.193) had never been numerically verified before. Fig. 3.15 constitutes both a verification of the validity of generalized hydrodynamics for the Sinh-Gordon model *and* a numerical verification of the classical limit of the vertex operator ansatz.

Our data is precise enough to show a clear departure from the free theory result. For comparison, Fig. 3.16 shows the numerical and hydrodynamic curves for the trace of the stress-energy tensor, as well as the curve for the same quantity obtained analytically in the free case ($g = 0$)

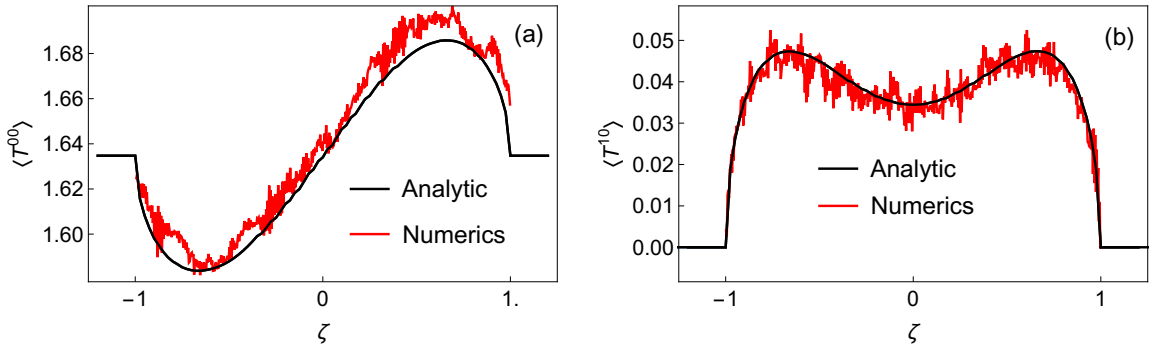

Figure 3.18: *Case III. Profiles of $\langle T^{00}(\zeta)\rangle$ (a) and $\langle T^{10}(\zeta)\rangle$ (b) are numerically computed and compared with the GHD predictions at $t = 25$. The parameters are $m = 1$, $g = 1$, $\beta_1^L = 1$, $\beta_3^L = 1/2$ and $\beta_1^R = 1/2$, $\beta_3^R = 0.609608$ and the lattice spacing in the light-cone discretization is $a = 0.1$. Figure taken from Ref. [8].*

for two different sets of free parameters. In the first case (a), we use the same values of β_1^L and β_2^L as in the interacting model, which clearly gives different values of the equilibrium expectation values for $\zeta < -1$ and $\zeta > 1$. We observe a relative $L(1)$ distance $R = 1.5 \times 10^{-2}$ (obtained by replacing v^{num} by v^{free} in (3.195)), thus about one order of magnitude larger compared with distance between numerics and hydrodynamic prediction reported above.

In the second case (b), we take the values of β_1^L and β_2^L in the free model so that the equilibrium expectation values for $\zeta < -1$ and $\zeta > 1$ agree with those of the interacting model, so $\beta_1^L = 1.47842$ and $\beta_1^R = 0.974279$. We still see a clear difference between the free and interacting models and observe a relative $L(1)$ distance $R = 1.3 \times 10^{-2}$, smaller than in case (a) but still an order of magnitude larger compared with distance between numerics and hydrodynamic prediction reported above.

In Fig. 3.17 we make the comparison for the energy density and energy current in the case II, including the charge H_3. Again, very good agreement is found with the measure of error being $R = 5.0 \times 10^{-3}$ and 1.0×10^{-2} for the charge and the current respectively.

In Fig. 3.18, we consider an example of case III, with $\beta_1^L \neq \beta_1^R$ and $\beta_3^L \neq \beta_3^R$ but chosen so that the expectation value of the energy density is the same in the two different ensembles. This does not mean that there is no net energy flow - the distribution of energy amongst particles of different speeds is different, and in this example there is a net flow of energy through $x = 0$ at late times. The relative error between the analytic and numerical results is larger in this case because the changes in energy density and the magnitude of the current are an order of magnitude smaller than case II, so the effects of the statistical error and the convergence to the scaling form appear larger on the graph, but they are the same absolute size as those in case II.

Both case II and case III confirm that GHD describes correctly the non-equilibrium energy current emerging from the partitioning protocol.

Euler scale correlation functions

We revert now to two-point dynamical correlation functions in homogeneous, stationary states (GGEs) of the Sinh-Gordon model. For simplicity we consider correlations in homogeneous thermal ensembles. Equation (3.178) gives a prediction for the behavior of the connected two-point correlators of local observables at the Euler scale: at long times and large distances, after fluid-cell averaging. Such expressions in integrable systems were never been tested before our work [8].

Again, from the numerical perspective, we take a finite volume on which the system is taken periodic, and analyze correlation functions at times long enough in order to reach the Euler scale, yet small enough in order to avoid finite-volume effects.

We note that the UV catastrophe still prevents us from computing correlation functions of arbitrary charges and currents. However one can check from the TBA formulae that a certain number of stress-energy tensor correlation functions do stay finite, such as $\langle T^{\nu\rho}(x,t)T^{\mu}_{\mu}(0,0)\rangle^c$ and the difference $\langle T^{01}(x,t)T^{01}(0,0)\rangle^c - \langle T^{11}(t,x)T^{11}(0,0)\rangle^c$, and similarly correlation functions involving vertex operators are finite. In the following we focus on two correlation functions: the trace two-point function $\langle T^{\mu}_{\mu}(t,x)T^{\nu}_{\nu}(0,0)\rangle^{\text{c}}$, and the symmetrized vertex operator two-point function $\langle \cosh(2g\phi(t,x)\cosh(2g\phi(0,0))\rangle^{\text{c}}$, because these offer the best chance of numerical precision. We first remark that, without fluid-cell averaging, one may expect persisting oscillations, of the order of the hydrodynamic value itself, at large space-time variables (t,x). Such oscillations are beyond the validity of the hydrodynamics, which becomes predictive only when fluid cell averages are considered, and can be analytically observed in the free-field limit $g = 0$ (see Ref. [8]). In Fig. 3.19, motivated by the hydrodynamic result (3.179), we study the scaled correlation functions

$$t\langle T^{\mu}_{\mu}(t,\zeta t)T^{\nu}_{\nu}(0,0)\rangle^{\text{c}}\,, \qquad t\langle \cosh(2g\phi(t,\zeta t))\cosh(2g\phi(0,0))\rangle^{\text{c}} \tag{3.196}$$

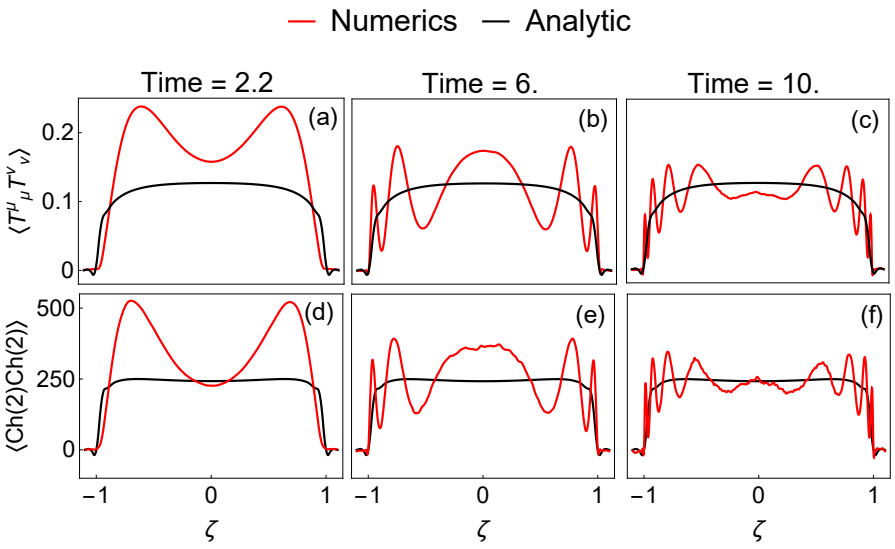

Figure 3.19: *Correlators* (3.196)*, upper panel (a-c) concerns the trace of the stress energy tensor, and lower panel (d-f) the correlation function of* $\cosh(2g\phi)$ *(here and below, we use* $\langle Ch(2)Ch(2)\rangle$ *as a shorthand notation for the axis label), are plotted at different times. Oscillations around the analytic prediction from hydrodynamics are present, although we are unable to conclude if they are asymptotically persisting (with an* $O(1)$ *amplitude) or not. Parameters:* $m = 1$*,* $g = 2$*, inverse temperature* $\beta = 1$*, the number of samples in the Metropolis is 340000, translational invariance of the system is used as further averaging procedure (500 lattice sites, lattice spacing 0.05). Ripples in the red lines are due to Metropolis noise, enhanced at late times due to the factor of* t *in front of the correlation function. Figure taken from Ref. [8].*

as a function of the ray ζ for different times t. Relatively large oscillations do arise at all times we were able to reach, although it is inconclusive whether these actually persist asymptotically.

In order to integrate out these oscillations most efficiently, we study the time-averaged and space-integrated scaled correlation functions. These averaging play the role of the fluid-cell integration, as a matter of fact the numerical data are experienced to collapse on the hydrodynamic result. More specifically, given two local observables $\mathcal{O}$ and $\mathcal{O}'$ we studied

$$\lim_{t\to\infty}\int\frac{\mathrm{d}\tau}{t}\tau\langle\mathcal{O}(\tau,\zeta\tau)\mathcal{O}'(0,0)\rangle^{\mathrm{c}}=\int\mathrm{d}\theta\,\delta(\zeta-v^{\mathrm{eff}}(\theta))\,\rho_t(\theta)f(\theta)V^{\mathcal{O}}(\theta)V^{\mathcal{O}'}(\theta)\tag{3.197}$$

and

$$\lim_{t\to\infty}\int\mathrm{d}x\,\langle\mathcal{O}(t,x)\mathcal{O}'(0,0)\rangle^{\mathrm{c}}=\int\mathrm{d}\theta\,\rho_t(\theta)f(\theta)V^{\mathcal{O}}(\theta)V^{\mathcal{O}'}(\theta)\tag{3.198}$$

We have numerically observed, and analytically calculated in the free case (see Ref.[8]), that it is not necessary, after the time averaging in Eq. (3.197), to perform any mesoscopic space averaging in order to recover the Euler-scale hydrodynamic result: the large time limit as in (3.197) indeed exists and gives the right-hand side.

On the other hand, space integrations are obtained as (3.198). In this case, we have analytically observed at the free-field point (see Ref. [8]) that, for certain observables, the mesoscopic time averaging in (3.198) is indeed *necessary* in order to recover the predicted hydrodynamic result. That is, at least for correlators in the generic form $\langle e^{kg\phi}e^{k'g\phi}\rangle$, undamped time-oscillating terms survive the space integration, but are canceled by a subsequent fluid-cell time average. In the interacting case, again our numerics does not allow us to reach unambiguous conclusions, although we observe long lived oscillations of the space integrated correlators around the GHD prediction within the numerically accessible time scale. It turns out, however, that

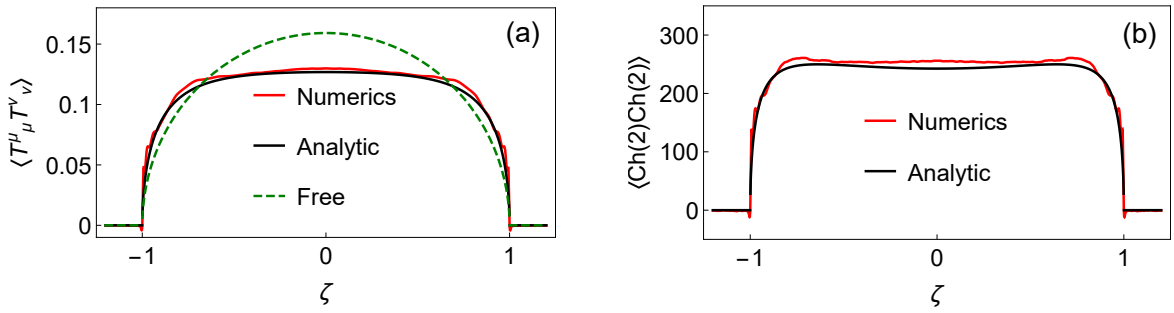

Figure 3.20: *The predictions (black curves) for the time average of two-point functions of (a) the trace of the stress-energy tensor,* (3.199)*, and (b) the analogue formula for the vertex operators are compared to the numerical simulation (red curves). In the case (a) the free result (see Ref. [8]) (dotted curve) is plotted for comparison. In order to improve the convergence, short times are avoided: the time average is taken in the interval* $[t_0, t]$*, rather than* $[0, t]$ *as in eq.* (3.199)*, with* $t_0 = 5$ *and* $t = 20$*. The same parameters as those of Fig. 3.19 are used. Figure taken from Ref. [8].*

mesoscopic time averaging is not necessary for the correlation functions $\langle T^\mu_\mu(t,x)T^\nu_\nu(0,0)\rangle^{\rm c}$ and $\langle\cosh(2g\phi(t,x)\cosh(2g\phi(0,0))\rangle^{\rm c}$ that we have chosen; this is seen analytically in the free case [8] and numerically observed in the interacting case, and simplifies our numerical checks.

From the expectation value of the charges and current the necessary $V^{\mathcal{O}}$ auxiliary functions (3.176) appearing in the correlators are easily obtained. This leads to the following expressions for the correlation functions of the trace of the stress-energy tensor

$$\lim_{t\to\infty}\int_0^t \frac{{\rm d}\tau}{t}\,\tau\langle T^\mu_\mu(\tau,\zeta\tau)T^\nu_\nu(0,0)\rangle^{\rm c} = m^2\frac{\rho(\theta)\vartheta(\theta)}{|\partial_\theta v^{\rm eff}(\theta)|}\Big[\cosh^{\rm dr^*}(\theta)\Big(1-\big(v^{\rm eff}(\theta)\big)^2\Big)\Big]^2\Big|_{v^{\rm eff}(\theta)=\zeta}, \tag{3.199}$$

while space integration gives

$$\lim_{t\to\infty}\int {\rm d}x\,\langle T^\mu_\mu(t,x)T^\nu_\nu(0,0)\rangle^{\rm c} = m^2\int {\rm d}\theta\,\rho(\theta)\vartheta(\theta)\Big[\cosh^{\rm dr^*}(\theta)\Big(1-\big(v^{\rm eff}(\theta)\big)^2\Big)\Big]^2. \tag{3.200}$$

For what it concerns the vertex operators, the hydrodynamic projection functions $V^{e^{kg\phi}}$ are

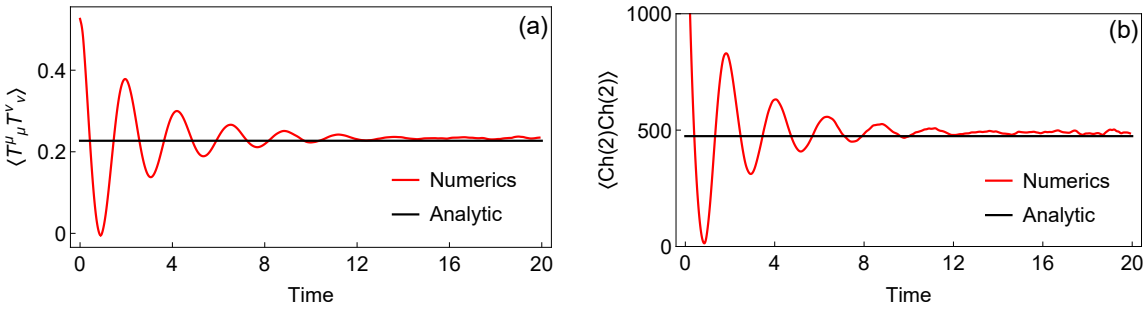

Figure 3.21: *The predictions (black curves) for the space integral of two-point functions of (a) the trace of the stress-energy tensor* (3.200)*, and (b) the analogue expression for the vertex operators, are compared to the numerical simulation (red curves) as functions of time. At large times, the oscillating ripples are due to the Metropolis noise and are observed to reduce on increasing the number of samples. The same parameters* m, β, g *as those of Fig. 3.19 are used. Figure taken from Ref. [8].*

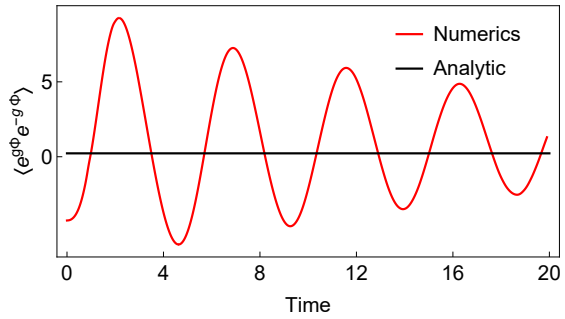

Figure 3.22: $\int \mathrm{d}x \, \langle e^{g\phi(x,t)} e^{-g\phi(0,0)} \rangle_{\mathrm{c}}$ *is numerically computed (red curve) and compared with the constant predicted by hydrodynamics (black curve). Compared with the correlators of* $\cosh(g\phi)$ *(proportional to the trace of the stress-energy tensor analysed in Fig. 3.21), strong oscillations around the GHD prediction on the accessible time scale are observed. The same parameters as those of Fig. 3.21 are used. Figure taken from Ref. [8].*

calculated from the one point expectation value as per (3.176), taking advantage of the Negro-Smirnov result (3.192). We show in Appendix 3.A that the function $V^{e^{kg\phi}} = V^{e^{-kg\phi}} = V^k(\theta)$ is given by

$$V^{k+1}(\theta) = \frac{g^2}{4\pi} \mathcal{V}^{k+1} \sum_{l=0}^{k} \frac{\mathcal{V}^l}{\mathcal{V}^{l+1}} (2l+1) \vartheta(\theta) \frac{p_{\mathrm{cl}}^l(\theta) d^l(\theta)}{\rho(\theta)} \tag{3.201}$$

where $\mathcal{V}^k = \langle e^{kg\phi} \rangle$, and where d^l is the solution of the following linear integral equation:

$$d^l(\theta) = e^\theta + \frac{g^2}{4} \mathcal{P} \int \frac{\mathrm{d}\gamma}{2\pi \sinh(\theta - \gamma)} \left(-2l - \partial_\gamma\right) \left(\vartheta(\gamma) d^l(\gamma)\right) . \tag{3.202}$$

Then one directly applies (3.197) and (3.198).

In Figs. 3.20 and 3.21 the time-averaged and space-integrated correlators, respectively, are considered. We see very good agreement between the numerical simulation and the hydrodynamic prediction. In Fig. 3.22 we study space-integrated correlation functions of vertex operator without symmetrizing. In this case, as discussed above, we observe long-lived oscillations around the hydrodynamic value.

3.4.3 Concluding remarks

In this section we addressed the Generalized Hydrodynamics, i.e. an hydrodynamic description of integrable models where the infinitely many (quasi-)local conserved charges are properly taken in account. After a short introduction mainly based on Ref. [159, 160, 174, 175], we revert to study the hydrodynamics of the classical Sinh-Gordon model. In the setups we studied, the initial state is distributed according to (generalized) Gibbs ensembles, and this distribution is deterministically evolved following the classical field equation. We studied both one-point averages in the non-equilibrium partitioning protocol, and dynamical two-point functions in homogeneous states. We compared predictions from GHD with results from a direct numerical simulation of the protocol. We found excellent agreement in all the cases we studied.

This gives direct evidence that GHD, first developed in the context of quantum chains and quantum field theory and later observed to be applicable to classical integrable soliton-like gases as well, is also applicable to classical field theories, thus further confirming its wide applicability. Because of the UV catastrophe of classical field theory, not all local observables have finite averages in thermal states or GGEs. Nevertheless, we verified that for those whose averages are finite, GHD predictions are correct.

The TBA formulation of GGEs in classical field theory generically involves two types of modes: solitonic modes and radiative modes. The latter are responsible for the UV catastrophe of classical fields. Similarly, the GHD of classical integrable field theory is that for a gas of solitons and radiation. Solitonic modes have a natural classical-particle interpretation, and the part of GHD related to such modes is indeed identical to the GHD of classical soliton gases. Radiative modes, on the other hand, do not have a clear particle interpretation, and were never studied within GHD before. Nevertheless the quasi-particle formulation of GHD still holds, with the appropriate radiative free energy function. In the classical Sinh-Gordon model, only radiative modes occur, hence our results give a verification of GHD in this new sector of the theory. The results of Ref. [8] on which this section is pivoted, also constitute the first direct verification of the recent GHD correlation function formula. Crucially, we analyzed not only conserved fields – specifically the trace of the stress-energy tensor, which is UV finite – but also vertex operators, local fields which are not part of conservation laws. GHD two-point functions for such fields involve the hydrodynamic projection theory, and our results confirm its validity. In addition, our results also provide the first numerical verification of GGE one-point functions formulae for vertex operators recently proposed by Negro and Smirnov, albeit in the classical realm.

In our study of correlation functions, we observed that GHD predictions are valid up to oscillations which may not subside at large times. We have observed this explicitly in the free-field case, where in certain cases, oscillations both in space and time, of the same order as that of the hydrodynamic predictions, persist indefinitely (see Ref. [8]). For certain observables, appropriate fluid cell averaging appears to be essential in order to recover the Euler-scale correlation predictions from hydrodynamics.

It would be interesting to analyze the approach, at large times, to the GHD predictions. In Ref. [8] have explicitly evaluated (and numerically verified) large-time power-law correction terms in the free-field case, but preliminary numerics suggest that in the interacting case, some correction terms are instead exponential. It would also be interesting to extend this analysis to the non-relativistic limit of the sinh-Gordon model, namely the well known nonlinear Schrödinger equation, and to other models, such as the sine-Gordon model, which possesses solitonic modes, and the classical Toda chain.

3.A Semi-classical limit of the Sinh-Gordon model

Even though the (generalized) TBA for classical models can be directly accessed by mean of the inverse scattering approach [376], the rather technical derivation appears to be more cumbersome compared with the quantum counterpart, which probably is more familiar to the reader. This appendix provides a self-consistent derivation of the TBA and hydrodynamics for the classical Sinh-Gordon, regarding the latter as the classical limit of its quantum version. Concerning the TBA, such a route was already considered in Ref. [182], together with the classical limit of the LeClair-Mussardo formula leading to a small excitation-density expansion for one-point functions. Here we resume such a program extending the derivation to the whole hydrodynamics, then we present a close expression for the expectation values of vertex operators obtained through the semi-classical limit of the Negro-Smirnov ansatz. While in agreement with the LeClair-Mussardo formula, this last result is not constrained to small excitation densities and is feasible to be applied to arbitrary GGEs.

Let us recall the TBA equation for the quantum Sinh Gordon model

$$\varepsilon_{\mathrm{q}}(\theta) = w(\theta) - \int \frac{\mathrm{d}\gamma}{2\pi}\, \varphi_{\mathrm{q}}(\theta-\gamma) \log\left(1+e^{-\varepsilon_{\mathrm{q}}(\gamma)}\right) , \tag{3.203}$$

where we explicitly use the subscript "q" as a remind we are dealing now with the *quantum* model; in the absence of any subscript we will refer to classical quantities. Differently from Ref. [182], along the semi-classical limit procedure we will use the fermionic formulation of the quantum ShG rather than the bosonic one: even though the two descriptions are equivalent [214], the quantum hydrodynamics is formulated in the fermionic basis making the latter a preferred choice. Referring to the parameter choice of the (quantum) Lagrangian (3.180), the quantum kernel $\varphi_{\rm q}$ is

$$\varphi_{\rm q}(\theta) = \frac{2\sin\pi\alpha}{\sinh^2\theta + \sin^2\pi\alpha}, \qquad \alpha = \frac{g^2}{8\pi + g^2}\,. \tag{3.204}$$

As already pointed out in [182], the semi-classical limit of the ShG model can be obtained through a combination of a small coupling and high temperature limit. More precisely we consider the rescaling (we reintroduce the Planck constant $\hbar$)

$$w(\theta) \to \hbar w(\theta), \qquad g \to \sqrt{\hbar} g, \qquad \mathcal{O}[\phi] \to \mathcal{O}[\sqrt{\hbar}\phi]\,, \tag{3.205}$$

with $\mathcal{O}$ a generic observable functional of the field and $w(\theta)$ the source term in the TBA (3.203). Then, in the $\hbar \to 0$ limit, the quantum expectation value reduces to the expectation value of the classical observable $\mathcal{O}[\phi]$ on a GGE having $w(\theta)$ as a source term. Such a claim is easily checked in the simplest case of a thermal state: using the path integral representation of the quantum expectation value we have

$$\langle \mathcal{O}[\sqrt{\hbar}\phi]\rangle_{\rm q}^{\hbar\beta} = \frac{1}{\mathcal{Z}} \int \mathcal{D}\phi\, \mathcal{O}[\sqrt{\hbar}\phi]\, e^{-\int_0^{\hbar\beta} {\rm d}\tau \int {\rm d}x \frac{1}{2}\partial_\mu\phi\partial^\mu\phi + \frac{m^2}{g^2\hbar}(\cosh(\sqrt{\hbar}g\phi)-1)}\,, \tag{3.206}$$

where the euclidean time τ runs on a ring of length $\hbar\beta$. In the high temperature limit the integral over the compact dimension can be approximated with the integrand at $\tau = 0$ times the length of the ring. In the same limit the measure collapses to $\mathcal{D}\phi\,\mathcal{D}\partial_\tau\phi$ where the fields are now restricted to $\tau = 0$.

$$\langle \mathcal{O}(\sqrt{\hbar}\phi)\rangle_{\rm q}^{\hbar\beta} \simeq \frac{1}{\mathcal{Z}} \int \mathcal{D}\phi\, \mathcal{D}\partial_\tau\phi\;\; \mathcal{O}(\sqrt{\hbar}\phi)\, e^{-\hbar\beta \int {\rm d}x \frac{1}{2}\partial_\mu\phi\partial^\mu\phi + \frac{m^2}{g^2\hbar}(\cosh(\sqrt{\hbar}g\phi)-1)}\,, \tag{3.207}$$

A final change of variable in the path integral $\phi \to \phi/\sqrt{\hbar}$ makes explicit the appearance of the classical expectation value of the observable $\mathcal{O}$ on a classical thermal ensemble of inverse temperature β. A similar reasoning can be extended to more general GGEs as well to the dynamics, confirming (3.205) as the correct scaling to obtain the desired semi-classical limit. In the small coupling limit, the physical mass of the quantum model reduces to the bare mass of the classical action. Concerning the TBA equation (3.203), a finite integral equation in the $\hbar \to 0$ limit is obtained provided we redefine $\varepsilon_{\rm q}(\theta) = \log\varepsilon(\theta) + \log\hbar$, with ε the classical effective energy (this rescaling differs from that of [182], where the *bosonic* rather than the *fermionic* quantum effective energy is used). Through straightforward manipulations, at the leading order in $\hbar$ the following integral equation is obtained

$$\varepsilon(\theta) = \omega(\theta) + \frac{g^2}{4}\lim_{\hbar\to 0}\int \frac{d\theta'}{2\pi}\frac{\cosh(\theta-\theta')}{\sinh^2(\theta-\theta') + (\hbar g^2/8)^2}\left(\log\varepsilon(\theta') - \log\varepsilon(\theta)\right)\,. \tag{3.208}$$

The last step involves an integration by parts that leads to the final $\hbar-$independent integral equation

$$\varepsilon(\theta) = \omega(\theta) - \frac{g^2}{4}\mathcal{P}\int \frac{{\rm d}\gamma}{2\pi}\frac{1}{\sinh(\theta-\gamma)}\partial_\gamma \log\varepsilon(\gamma)\,, \tag{3.209}$$

where $\mathcal{P}$ stands for the principal value prescription, natural emerging passing from (3.208) to (3.209): this is the sought-after TBA equation for the classical ShG (3.182). We should warn the reader about a difference in the sign in front of the integral between the above expression and the same reported in Ref. [182], where a typo must have occurred. This concludes the pure TBA calculation, but the map extends to the whole hydrodynamic. Through calculations close to those that provided the classical TBA, it is possible to show that the quantum dressing operation (3.166) (here specialized to the ShG case)

$$q_{\mathrm{q}}^{\mathrm{dr}^*}(\theta) = q(\theta) + \int \frac{\mathrm{d}\gamma}{2\pi}\, \varphi_{\mathrm{q}}(\theta-\gamma)\vartheta_{\mathrm{q}}(\gamma) q_{\mathrm{q}}^{\mathrm{dr}^*}(\gamma) \tag{3.210}$$

reduces to the sought definition of the classical dressing

$$q^{\mathrm{dr}^*}(\theta) = q(\theta) - \frac{g^2}{4}\mathcal{P}\int \frac{\mathrm{d}\gamma}{2\pi}\frac{1}{\sinh(\theta-\gamma)}\partial_\gamma[\vartheta(\gamma) q^{\mathrm{dr}^*}(\gamma)]\,, \tag{3.211}$$

provided we set $q_{\mathrm{q}}^{\mathrm{dr}^*}(\theta) = \hbar^{-1}\vartheta(\theta) q^{\mathrm{dr}^*}(\theta)$ while taking the $\hbar \to 0$ limit. In particular, this implies that the effective velocity of the quantum model converges, in the semi-classical limit, to the definition of the effective velocity in the classical case. Finally, from the definition of the occupation function $\vartheta(\theta)$ in the classical $\vartheta = 1/\varepsilon$ and quantum cases $\vartheta_{\mathrm{q}} = (e^{\varepsilon_{\mathrm{q}}}+1)^{-1}$ and the rescaling of the effective energies we have, at the leading order in $\hbar$, $\vartheta_{\mathrm{q}}(\theta) = 1 - \hbar/\vartheta(\theta) + \dots$. Replacing this last piece of information in the quantum version of the GHD (3.159) we readily find that the same equation holds true on the classical objects as well. Alternatively, we could have noticed that in the semi-classical limit the expectation values of the quantum conserved charges and their currents go, respectively, to the classical expectation values of charges and currents (apart from an overall and inessential $\hbar$ factor) and derive hydrodynamics imposing charge-current conservation from scratch.

The expectation value of the vertex operators and eulerian correlation functions

This part is devoted to the derivation of the equations (3.192-3.193) and the expressions (3.201) for the hydrodynamic projections of vertex operators, through the semi-classical limit of the Negro-Smirvon formula presented in Section 2.2.1. Let us recall the Negro-Smirnov formula for the sake of convenience

$$\frac{\langle e^{(k+1)g\phi}\rangle_{\mathrm{q}}}{\langle e^{kg\phi}\rangle_{\mathrm{q}}} = 1 + \frac{2\sin(\pi\alpha(2k+1))}{\pi}\int \mathrm{d}\theta\, \frac{e^\theta}{1+e^{\varepsilon_{\mathrm{q}}(\theta)}} p_{\mathrm{q}}^k(\theta)\,, \tag{3.212}$$

with

$$p_{\mathrm{q}}^k(\theta) = e^{-\theta} + \int \mathrm{d}\gamma \frac{1}{1+e^{\varepsilon_{\mathrm{q}}(\mu)}}\chi_k(\theta-\gamma) p_{\mathrm{q}}^k(\gamma) \tag{3.213}$$

$$\chi_k(\theta) = \frac{i}{2\pi}\left(\frac{e^{-i2k\alpha\pi}}{\sinh(\theta+i\pi\alpha)} - \frac{e^{i2k\alpha\pi}}{\sinh(\theta-i\pi\alpha)}\right). \tag{3.214}$$

As it is evident from the rescaling (3.205), the quantum expectation value of the vertex operators goes, in the semi-classical limit, directly to the classical expectation value of the latter (the rescaling of the coupling g and of the field in the observable cancel each others). Thus the classical limit of the r.h.s. of (3.212) will directly produce the ratio of the expectation values of the vertex operators in the classical theory. The first step to take the limit is to consider χ_k up to first order in $\hbar$. Using that α after the rescaling is first order in $\hbar$, we eventually need (in the distribution

sense)

$$\frac{1}{\sinh(\theta-\gamma-i\pi\alpha)} = i\pi\delta(\theta-\gamma) + \mathcal{P}\frac{1}{\sinh(\theta-\gamma)} + \pi\alpha\left(\pi\delta(\theta-\gamma)\partial_\theta - i\mathcal{P}\frac{1}{\sinh(\theta-\gamma)}\partial_\gamma\right) + \mathcal{O}(\alpha^2)\,. \quad (3.215)$$

In order to get a finite expression in the $\hbar \to 0$ limit, we define the classical $p^k_{\rm cl}$ function as $p^k_{\rm q}(\theta) = \hbar^{-1}\vartheta(\theta)p^k_{\rm cl}(\theta)$. Using this definition and (3.215) is a matter of a few straightforward passages to obtain the finite classical integral equations (3.192-3.193).

Armed with the classical Negro-Smirnov formula, we can now extract the hydrodynamic projection (3.176)

$$-\delta\mathcal{V}^k = \int \mathrm{d}\theta\,\rho(\theta)\vartheta(\theta)V^k(\theta)\delta w^{\mathrm{dr}^*}(\theta)\,, \quad (3.216)$$

where for simplicity $\mathcal{V}^k = \langle e^{kg\phi}\rangle$. Varying both sides of eq. (3.192) with respect to the TBA source term $w(\theta)$, we readily obtain the recurrence relation

$$\frac{\delta\mathcal{V}^{k+1}}{\mathcal{V}^{k+1}} = \frac{\delta\mathcal{V}^k}{\mathcal{V}^k} + \frac{\mathcal{V}^k}{\mathcal{V}^{k+1}}(2k+1)\frac{g^2}{4\pi}\int \mathrm{d}\theta\; e^\theta\delta(\vartheta(\theta)p^k_{\rm cl}(\theta))\,. \quad (3.217)$$

That has the obvious solution

$$\frac{\delta\mathcal{V}^{k+1}}{\mathcal{V}^{k+1}} = \sum_{l=0}^{k}\frac{\mathcal{V}^l}{\mathcal{V}^{l+1}}(2l+1)\frac{g^2}{4\pi}\int \mathrm{d}\theta\; e^\theta\delta(\vartheta(\theta)p^l_{\rm cl}(\theta))\,. \quad (3.218)$$

$\delta(\vartheta p^l_{\rm cl})$ can now be extracted from the integral equation (3.193). To carry on the calculation, it is convenient to introduce an operatorial representation of the integration kernel. In particular, we define the linear operators $\hat\vartheta$ and $\hat\varphi_l$ as it follows:

$$(\hat\vartheta\tau)(\theta) = \vartheta(\theta)\tau(\theta), \qquad (\hat\varphi_l\tau)(\theta) = \int \mathrm{d}\gamma\,\frac{g^2}{4}\frac{1}{\sinh(\theta-\gamma)}\big(\partial_\gamma - 2l\big)\tau(\gamma)\,, \quad (3.219)$$

for any given test function $\tau(\theta)$. In this language, the linear equation satisfied by $p^l_{\rm cl}$ (3.193) is written as

$$p^l_{\rm cl} = e^- - \frac{1}{2\pi}\hat\varphi_l\hat\vartheta p^l_{\rm cl}\,, \quad (3.220)$$

where we introduce $(e^-)(\theta) = e^{-\theta}$. The formal solution is immediately written

$$\hat\vartheta p^l_{\rm cl} = (\hat\vartheta^{-1} + \frac{1}{2\pi}\hat\varphi_l)^{-1}e^-\,, \quad (3.221)$$

and the variation with respect to $w(\theta)$ is easily performed, using the fact that $\vartheta(\theta) = 1/\varepsilon(\theta)$ and the TBA equations (3.182)

$$\delta(\hat\vartheta p^l_{\rm cl}) = -(\hat\vartheta^{-1} + \frac{1}{2\pi}\hat\varphi_l)^{-1}\hat\vartheta p^l_{\rm cl}(\delta w)^{\mathrm{dr}^*}\,. \quad (3.222)$$

As last technical step, we consider the integral appearing in eq. (3.218)

$$\int \mathrm{d}\theta\, e^\theta\delta(\vartheta(\theta)p^l_{\rm cl}(\theta)) = -\int \mathrm{d}\theta\mathrm{d}\gamma\, e^\theta(\hat\vartheta^{-1} + \frac{1}{2\pi}\hat\varphi_l)^{-1}_{(\theta,\gamma)}\vartheta(\gamma)p^l_{\rm cl}(\gamma)\delta w^{\mathrm{dr}^*}(\gamma)\,, \quad (3.223)$$

where we made explicit the convolution underlying the action of the operator. We define the auxiliary functions $d^l(\theta)$ as

$$\vartheta(\gamma)d^l(\gamma) = \int \mathrm{d}\theta\; e^\theta (\hat{\vartheta}^{-1} + \frac{1}{2\pi}\hat{\varphi}_l)^{-1}_{(\theta,\gamma)}\,. \tag{3.224}$$

Using the symmetry $(\hat{\vartheta}^{-1} + \frac{1}{2\pi}\hat{\varphi}_l)^{-1}_{(\theta,\gamma)} = (\hat{\vartheta}^{-1} + \frac{1}{2\pi}\hat{\varphi}_{-l})^{-1}_{(\gamma,\theta)}$ it is immediate to see that d^l satisfies the linear integral equation

$$d^l(\theta) = e^\theta + \frac{g^2}{4}\mathcal{P}\int \frac{\mathrm{d}\gamma}{2\pi}\frac{1}{\sinh(\theta-\gamma)}\left(-2l - \partial_\gamma\right)\left(\vartheta(\gamma)d^l(\gamma)\right)\,, \tag{3.225}$$

i.e. eq. (3.202) of Section 3.4.2. Using d^l in eq. (3.223), plugging the latter in (3.218) and finally comparing it with eq. (3.216), we finally get the desired result

$$V^{k+1}(\theta) = \frac{g^2}{4\pi}\mathcal{V}^{k+1}\sum_{l=0}^{k}\frac{\mathcal{V}^l}{\mathcal{V}^{l+1}}(2l+1)\vartheta(\theta)\frac{p^l_{\mathrm{cl}}(\theta)d^l(\theta)}{\rho(\theta)}\,, \tag{3.226}$$

i.e. eq. (3.201) of Section 3.4.2.

3.B Numerical Methods for the classical Sinh Gordon model

This Appendix contains a short summary of the numerical methods we used to find the results for the Sinh Gordon model presented in Section 3.4.2. In Section 3.B.1 we consider the numerical solution of the TBA and hydrodynamics, while in Section 3.B.2 we present the numerical simulation of the model from first principles.

3.B.1 Numerical solution of TBA and hydrodynamics

Both in the partitioning protocol and for the correlation functions, the first step is solving the TBA equation (3.182), which is more difficult compared with the more familiar quantum case. The main difficulties reside in *i)* the singular kernel and *ii)* the lack of convergence of (3.182) under a natural iterative approximation scheme, in contrast with the familiar quantum case. The first issue is overcome with a careful discretization of the integral equation, while the second issue is avoided using the a Newton-Raphson method. Consider the integral equation (3.182) where we set $m = g = 1$ for simplicity and specialize it to the thermal case $\omega(\theta) = \beta\cosh\theta$ (the needed generalizations are trivial). Actually, it is convenient to parametrize the effective energy as

$$\varepsilon(\theta) = \beta\cosh\theta\, e^{\chi(\theta)}\,. \tag{3.227}$$

This ensures the UV behaviour $\lim_{\theta\to\pm\infty}\chi(\theta) = 0$. In terms of the new variable eq. (3.182) can be written as

$$e^{\chi(\theta)} - 1 + f(\theta) + \frac{1}{4\beta\cosh\theta}\mathcal{P}\int_{-\infty}^{\infty}\frac{\mathrm{d}\gamma}{2\pi}\frac{1}{\sinh(\theta-\gamma)}\partial_\gamma\chi(\gamma) = 0\,, \tag{3.228}$$

where the principal value prescription is enforced and $f(\theta)$ is defined as

$$f(\theta) = \frac{1}{4\beta\cosh\theta}\mathcal{P}\int_{-\infty}^{\infty}\frac{\mathrm{d}\gamma}{2\pi}\frac{\tanh\gamma}{\sinh(\theta-\gamma)}\,. \tag{3.229}$$

In order to solve for $\chi(\theta)$ we symmetrically discretize the set of rapidities $\theta_i = \Delta\,(i - 1/2)$ with $i \in \{-N+1, -N, ..., N\}$. The linear operator defined through the integral is discretized as it

follows. Defining $t(\theta) = \partial_\theta \chi(\theta)$ we pose

$$\int_{-\infty}^{\infty} \mathrm{d}\gamma \frac{t(\gamma)}{\sinh(\theta_i - \gamma)} \simeq \sum_{j=-N+1}^{N} \int_{\theta_j - \Delta/2}^{\theta_j + \Delta/2} \mathrm{d}\gamma \frac{\sum_{a=0}^{2l} A_i^a[t](\gamma - \theta_j)^{2a}}{\sinh(\theta_i - \gamma)}\,, \tag{3.230}$$

where in each interval centred in θ_j we replace $t(\theta)$ with a symmetrical interpolation of the $(2l)^{\text{th}}$ order $t(\theta) = \sum_{a=0}^{2l} A_j^a[t](\theta - \theta_j)^a$. The $A_j^a[t]$ coefficients are linear in $t(\theta)$ and are solution of

$$\sum_{a=0}^{2l} A_i^a[t](b\Delta)^a = t(\theta_{i+b}), \qquad b \in \{-l, -l+1, ..., l-1, l\}\,. \tag{3.231}$$

The last step in the discretization procedure estimates $t(\theta) = \partial_\theta \chi(\theta)$ through a finite difference scheme of the $(2d)^{\text{th}}$ order, obtained solving for the first derivative the following system

$$\chi(\theta_{i+a}) = \sum_{s=0}^{2d} \frac{(a\Delta)^s}{s!} \partial_\theta^a \chi\Big|_{\theta=\theta_i}, \qquad a \in \{-d, ..., d\} \tag{3.232}$$

Combining together eq. (3.230-3.231-3.232) we obtain the desired discretization of the TBA equation (3.228)

$$e^{\chi(\theta_i)} - 1 + f(\theta_i) + \frac{1}{4\beta \cosh\theta_i} \sum_{j=-N+1}^{N} \omega_{i,j}\, \chi(\theta_j) = 0\,. \tag{3.233}$$

The coefficients $f(\theta_i)$ and the matrix $\omega_{i,j}$ are numerically computed once and for all evaluating the needed integrals, then the non-linear equation obtained this way is solved for the discrete set $\chi(\theta_i)$ through the iterative Newton-Raphson method. The algorithm is observed to have fast convergence properties using as starting point the non-interacting solution, i.e. $\chi = 0$. For $\beta \sim \mathcal{O}(1)$, with $N = 800$, $\Delta = 0.0175$ and $l = d = 3$, the TBA equation (3.228) is solved within an error $\sim 10^{-8}$. Once the needed TBA solutions are obtained the remaining passages follow smoothly: the linear dressing equations, which involve the same singular kernel of the TBA, are discretized again following eq. (3.230-3.231-3.232) and then solved through a matrix inversion. The nonlinear equation defining the solution of the partitioning protocol (3.160) is solved by simple iteration, displaying fast convergence.

3.B.2 Direct numerical simulation from first principles

The formal definition of the averages we want to compute is given by the path integral (3.184). We compute numerical values for these averages by the Metropolis-Hasting algorithm applied to a discretisation of the Sinh-Gordon field theory on a lattice. This algorithm generates a sequence of N field configurations $\mathcal{C}_i$ (at time $t = 0$) such that the statistical average is approximated by the average of the values on the configurations

$$\langle \mathcal{O} \rangle \simeq \frac{1}{N} \sum_{\mathcal{C}_i} \mathcal{O}(\mathcal{C}_i)\,, \tag{3.234}$$

where we use the equations of motion to find the value of $\phi(t, x)$ from the initial configuration $\mathcal{C}$, if needed to calculate the value of $\mathcal{O}$.

For various reasons (outlined below) we have chosen an integrable discretisation of the Sinh-Gordon field theory on a light-cone lattice. We have used the description of Hirota's integrable discretization of the Sine-Gordon model given by Orfanidis in [388] and analytically continued this to obtain the discrete Sinh-Gordon model.

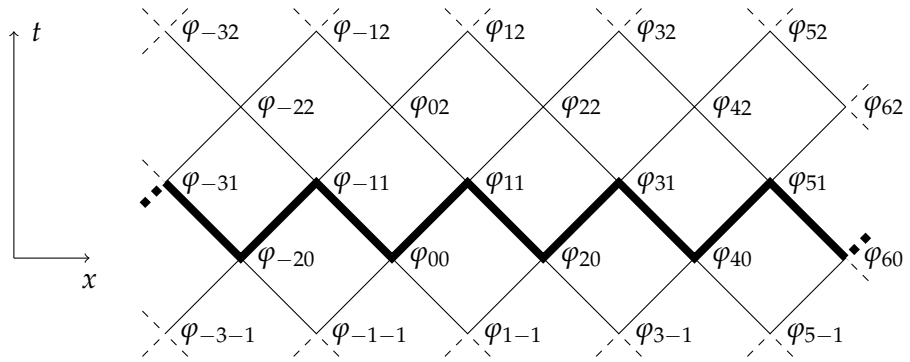

Figure 3.23: *The light-cone lattice and the field φ_{ij}*

The discrete model lives on a light-cone lattice, as shown in figure 3.23. We use the variable $\varphi = \exp(g\phi/2)$, and denote the lattice variables by $\varphi_{ij} \equiv \varphi(aj, ai)$ (the i index is referred to space, j to time: notice the reverted order in φ_{ij}, which makes the present convention on the order of the coordinates (t, x) with that used in Ref. [8], which was the opposite) where a is the lattice spacing as this simplifies the evolution equations and conserved quantities.

The time evolution is

$$\varphi_{i,j+1} = \frac{1}{\varphi_{i,j-1}} \left(\frac{\varphi_{i-1,j}\varphi_{i+1,j} + \lambda}{1 + \lambda\varphi_{i-1,j}\varphi_{i+1,j}} \right) , \quad \lambda = \frac{a^2 m^2}{4} . \tag{3.235}$$

We fully specify the field at each lattice point if we give the values $\{\varphi_{2i,0}, \varphi_{2i+1,1}\}$ on the thick zig-zag line in Fig. 3.23, so a configuration $\mathcal{C}$ for us is the set of values $\{\varphi_{2i,0}, \varphi_{2i+1,1}\}$ and this is the data used in the Metropolis algorithm to find a thermal or GGE ensemble.

One starts by assigning values randomly to an initial configuration$\{\varphi_{2i,0}, \varphi_{2i+1,1}\}_0$. Given a configuration $\{\varphi_{2i,0}, \varphi_{2i+1,1}\}_n$ we consider a new configuration obtained by picking a site, choosing a new value of the field at that site (through a suitable random process) and accepting or rejecting the new value according to the Metropolis algorithm. The resulting set of values is the new configuration $\{\varphi_{2i,0}, \varphi_{2i+1,1}\}_{n+1}$. This is then repeated, running through all the sites in the lattice in turn. One has to tune the process of choosing a new field value to maximise the rate at which the sequence of field configurations sample the total configuration space. The successive field configurations will be correlated, so that one has to discard an initial number which are correlated with the initial random configuration; after that, one collects a total number N of samples, with N large enough for the numerical approximation (3.234) to converge. The details of the Metropolis-Hasting algorithm are left to the original references [183, 184].

There were several reasons for choosing this integrable discretisation, the principle one being that for many quantities we need to evolve the field configurations in time. We found that the errors introduced by a non-integrable discretisation of the Sinh-Gordon model required a very small time step in the numerical time evolution, much smaller than the spatial separation in the discretised model as was also found in [182]. With an integrable discretisation we could use the same size step in the two directions (technically in both light-cone directions) which meant that the time-evolution was not only up to 100 times faster but had intrinsically smaller errors.

These evolution equations are integrable with an infinite set of conserved quantities as shown in [388], the simplest of which are the light-cone components of the momentum,

$$\mathcal{P}_{\pm} = (2a) \sum_{i \in 2\mathbb{Z}} \mathcal{P}_{\pm,i} , \tag{3.236}$$

$$\mathcal{P}_{\pm,i} = \frac{1}{a^2 g^2} \left(\frac{\varphi_{i,0}}{\varphi_{i\pm1,1}} + \frac{\varphi_{i\pm1,1}}{\varphi_{i,0}} - 2 \right) + \frac{\lambda}{a^2 g^2} \left(\varphi_{i,0}\varphi_{i\mp1,1} + \frac{1}{\varphi_{i\mp1,1}\varphi_{i,0}} - 2 \right) . \tag{3.237}$$

The energy and momentum are given by

$$H = \mathcal{P}_+ + \mathcal{P}_- \ , \quad P = \mathcal{P}_+ - \mathcal{P}_- \ . \tag{3.238}$$

The next simplest conserved charges $Q_{\pm 3}$ have spin ± 3, which are given in the continuum as space integrals of two conserved currents. These can easily be constructed explicitly in light-cone coordinates $x^{\pm} = t \pm x$ as, for example,

$$Q_{\pm 3} = \int (T_{\pm 4} + T_{\pm 2}) \mathrm{d}x \ , \quad \partial_{\pm} T_{\pm 2} + \partial_{\mp} T_{\pm 4} = 0 \ , \tag{3.239}$$

$$T_{\pm 4} = (\partial_{\pm}^2 \phi)^2 + \frac{g^2}{4} (\partial_{\pm} \phi)^4 \ , \quad T_{\pm 2} = \frac{m^2}{4} (\partial_{\pm} \phi)^2 \cosh(g\phi) \tag{3.240}$$

Note that these expressions are only defined up to the addition of total derivatives.

One can likewise define exactly conserved lattice conserved charges which have these as their continuum limit. There is a construction given in [388], but we will instead use the identification (after a change of variables) of the continuation of Orfanidis' equations with the integrable equations of type $\mathrm{H3}_{\delta=0}$ in the classification of Adler et al. [389] and use the simpler expression given by Rasin and Hydon in table 2 of [390]. After the required change of variables and using the evolution equation to express the conserved quantities (originally defined on a light cone) in terms of the field values on the initial zig-zag line we find

$$\mathcal{I}_{\pm 3} = (2a) \sum_{i \in 2\mathbb{Z}} \mathcal{I}_{\pm 3, i} \tag{3.241}$$

$$\begin{aligned} \mathcal{I}_{\pm 3, i} = \frac{1}{a^4 g^2} \Big(& \log[\varphi_{i \pm 2,0} \varphi_{i+1,1} \varphi_{i,0} \varphi_{i-1,1}] + 2 \log[2(1+\lambda)] \\ & - 2 \log \left[\varphi_{i \pm 2,0} \varphi_{i,0} + \varphi_{i+1,1} \varphi_{i-1,1} + \lambda (1 + \varphi_{i \pm 2,0} \varphi_{i,0} \varphi_{i+1,1} \varphi_{i-1,1}) \right] \Big) \end{aligned} \tag{3.242}$$

There are both conserved by the evolution equation but are not finite in the $a \to 0$ limit. The simplest combination which gives the expected form $m^3 \cosh(3\theta)$ in the continuum limit is

$$\mathcal{Q}_3 = 4(\mathcal{I}_{+3} + \mathcal{I}_{-3} + \frac{1}{a^2} H) \ . \tag{3.243}$$

The thermal and GGE ensembles are then constructed using the expressions (3.238) and (3.243) for H and $\mathcal{Q}_3$. For the homogeneous case, the lattice Hamiltonian was simply given by

$$\beta_1 H_1 + \beta_3 \mathcal{Q}_3 \ , \tag{3.244}$$

and we chose periodic boundary conditions for the lattice variables, so that if there are n sites then $\varphi_{1,j} = \varphi_{n+1,j}$. For the partitioning protocol chose a periodic lattice of length $2n$ where the lattice Hamiltonian was

$$\sum_{i=1}^{n} (\beta_1^L \cdot (\mathcal{P}_{+i} + \mathcal{P}_{-i}) + \beta_3^L \cdot 4(\mathcal{I}_{+3,i} + \mathcal{I}_{-3,i} + \frac{1}{a^2} (\mathcal{P}_{+i} + \mathcal{P}_{-i}))) \tag{3.245}$$

$$+ \sum_{i=n+1}^{2n} (\beta_1^R \cdot (\mathcal{P}_{+i} + \mathcal{P}_{-i}) + \beta_3^R \cdot 4(\mathcal{I}_{+3,i} + \mathcal{I}_{-3,i} + \frac{1}{a^2} (\mathcal{P}_{+i} + \mathcal{P}_{-i}))) \ . \tag{3.246}$$

This meant that the two halves of the periodic lattice were joined while in equilibrium in their separate GGE "heat baths" at $t = 0$, before being allowed to evolve freely for $t > 0$. This meant that there was a small, smooth, transition zone around the junctions of the two separate baths, but this does not seem to have had a big effect on the long time behaviour. We had considered

preparing the two halves each in their own heat bath and then joining them at $t = 0$, but the discontinuity in the fields and their derivatives created a "spike" of energy at the junction which then persisted for long times.

It is straightforward to include higher charges in the lattice Hamiltonian. The lattice equations of motion (in their $H3_{\delta=0}$ formulation) have been investigated extensively and several constructions of infinite series of conserved quantities are known, see [391, 392]. The terms in the conserved charges depend on increasing numbers of lattice variables: H depends on only two nearest neighbour sites, $\mathcal{Q}_3$ on four neighbouring sites, and $\mathcal{Q}_{2n+1}$ on $2n+2$ neighbouring sites. In terms of the numerical evaluation, this means a small increase in the computational time to evaluate the Hamiltonian but the main effect is the suppression of spatial variation through the coupling to higher powers of the derivative which mean that the standard Metropolis algorithm takes much longer to converge. Serious numerical work including $\mathcal{Q}_5$ or higher might need a more sophisticated algorithm for updating the configurations than the simple one outlined here.

Chapter 4

Impurity-induced out-of-equilibrium protocols

This last chapter is dedicated to out-of-equilibrium physics induced by the activation of defects in otherwise homogeneous integrable models. Hereafter, we will call defect (or impurity) a localized perturbation of an otherwise homogeneous hamiltonian H_0

$$H_0 \to H = H_0 + \int \mathrm{d}x\, U(t,x)\,, \tag{4.1}$$

with $U(t,x)$ having finite support and in principle function of time. Above, we have in mind a continuous system, but we will consider lattice models as well.

The activation of a defect in an otherwise thermodynamic large system could seem a rather innocent operation at first sight, but this is not absolutely the case, especially in integrable systems. For example, in Ref. [185] a local quench in the quantum Ising model in transverse field has been considered: in the homogeneous Ising model, at time $t = 0$ the hopping term at one site has been suddenly removed

$$H_0 = -\frac{1}{2}\sum_{j=1}^{N}\left[\sigma_j^x\sigma_{j+1}^x + h_j\sigma_j^z\right] \;\to\; H = H_0 + \frac{1}{2}\sigma_0^x\sigma_1^x\,. \tag{4.2}$$

Adding such an innocent defect cuts the chain in two halves, making impossible any communication between the halves $j < 0$ and $j > 0$. Consequently, at $t > 0$ the formation of a Local Quasi Stationary State was observed (see also Section 3.4): in the spirit of GHD, a perturbation of the initial state spread from the defect in a lightcone fashion, being locally described by an inhomogeneous GGE function of the ray $\zeta = j/t$.

From the quasiparticle viewpoint, the LQSS is simply understood: before activating the defect, the initial state is simply an "homogeneous gas" of ballistically propagating excitations. Cutting in two halves the spin chain, from the point of view of the excitations, can be seen as introducing an hard wall on which the excitations bounce back: the LQSS is then due to the quasiparticles scattered by the defect (see Ref. [185]). Albeit in the quench (4.2) the Hamiltonian is free and thus integrable even after the defect activation, the emergence of a LQSS is expected in interacting integrable models as well, even in the case where the defect destroys integrability. Indeed, far from the defect the Hamiltonian is locally integrable and GHD can be applied: from the perspective of the hydrodynamic equations in presence of a defect, we should solve Eq. (3.158) with proper boundary conditions where the impurity is placed.

This chapter presents two topics concerning out-of-equilibrium protocols induced by localized defects, in particular

1. In Section 4.1 we present the content of Ref. [9, 10], in collaboration with A. De Luca, where we analyzed the activation of moving impurities. In particular, we choose $U(t,x) = U(x-vt)$ in Eq. (4.1), thus the impurity moves at constant velocity v. Several models have a finite maximum velocity in the propagation of information, e.g. systems with relativistic invariance or living on a lattice [187], and thus a natural question is probing this bound through a moving impurity. How does the system react? Is a LQSS formed? In particular,

what does it happen if the defect moves faster than the maximum velocity of excitations? These are the main questions investigated in Section 4.1. More specifically, we analyze the case of free models, in particular a chain of hopping fermions and the Ising model in transverse field: we testify the emergence of a LQSS with absolutely non trivial dependence on the defect's velocity. The problem is framed in a suitable scattering theory, which can be exactly solved in specific cases, finding perfect agreement with numerical simulations. The friction force exerted by the medium on the impurity is also discussed.

2. In Section 4.2 we rather address integrability-breaking issues: the defect is at rest $U(t,x) = U(x)$ and it is chosen to spoil integrability. Within the context of homogeneous quenches, weak integrability-breaking terms have been framed in the "prethermalization" paradigm [188–205]: initially the system behaves as if it was integrable and apparently flows towards a GGE constructed on the intergable part of the Hamiltonian. However, then the integrability-breaking perturbation kicks in, causing a slow drift towards a thermal state: this happens regardless the strength of the perturbation, which thus has non-perturbative effects on the late time dynamics. The same question can be posed in the impurity case: an LQSS will be produced and we could wonder how the root density leaving the defect looks like. As a matter of fact, based on the fact that integrability is broken and inspired by what we know about the prethermalization in homogeneous systems, we could imagine that any finite subsystem encompassing the impurity will eventually reach a thermal state, regardless the strength of the impurity. If this reasoning was correct, then the excitations leaving the defect should be thermally distributed. Surprisingly, preliminary numerical results show that this naive conclusion is not correct [210]. In this Section we point out the perturbative nature of weak integrability-breaking impurities, which at late times are experienced to have mere perturbative effects on the emergent LQSS, thus preventing the local thermalization of the impurity region. Explicit calculations are performed in the simplified case where the bulk theory is free, while the defect interacting, but we also provide heuristic arguments in favor of our claim, which apply to the interacting case as well.

4.1 Late time dynamics induced by moving defects

Lattice models, due to the famous Lieb Robinson bound [187], have a finite maximum velocity $v_M < \infty$ for the information spreading: the presence of such a bound makes intriguing to consider moving defects and their late time effect on the system. As we already commented, an emergent LQSS is generally expected: the first step in order to sharpen our insight is surely constituted by free models, which allow for an exact, but non trivial, analysis. Indeed numerical simulations immediately point out the LQSS creation (see Fig. 4.1). While moving impurities have been considered in different contexts (see for example Ref. [393–398]), the investigation of the LQSS has been addressed for the first time in our works Ref. [9, 10], where, respectively, a system of hopping fermions and the Ising model in transverse field were analyzed. Along this section, we will consider at the same time both models

$$H_0^f = \sum_j -\frac{1}{2}\left(d_j^\dagger d_{j+1} + d_{j+1}^\dagger d_j\right) \;\to\; H^f = H_0^f + \sum_j V(j-vt) d_j^\dagger d_j \,. \tag{4.3}$$

$$H_0^I = -\frac{1}{2}\sum_j \left(\hat{\sigma}_j^x \hat{\sigma}_{j+1}^x + h\hat{\sigma}_j^z\right) \to\; H^I = H_0^I - \frac{1}{2}\sum_j V(j-vt)\hat{\sigma}_j^z \,, \tag{4.4}$$

In particular, after a Jordan-Wigner transformation, the Ising Hamiltonian can be written in terms of free fermions

$$H_0^I = \sum_j -\frac{1}{2}\left(d_j^\dagger d_{j+1}^\dagger + d_j^\dagger d_{j+1} + \text{h.c.}\right) + h d_j^\dagger d_j \;\to\; H^I = H_0^I + \sum_j V(j-vt) d_j^\dagger d_j \,. \tag{4.5}$$

Above, d_j are the fermionic operators $\{d_j, d_l^\dagger\} = \delta_{j,l}$, while $\hat{\sigma}_j^{x,y,z}$ the standard Pauli matrices. Before the defect activation, we assume the state to be initialized in a GGE of the homogeneous Hamiltonian. In the hopping fermion case (4.3) the defect is chosen as a perturbation in the chemical potential, while in the Ising model (4.4) we locally change the magnetic field. We assume $V(x)$ to be a fast decaying function centered around zero: most of our discussion can be carried out without further assumptions on its form. Lately, we will present some exact solutions of the emergent LQSS for certain defects. For the seek of simplicity, we unify the notation for the two models (thus, we mostly follow Ref. [10]). In both cases, the homogeneous Hamiltonian can be diagonalized in the Fourier space, with an additional Bogoliubov rotation if needed: for the seek of simplicity, let us organize the fermions in a two dimensional vector ψ_j as

$$\psi_j = \begin{pmatrix} d_j \\ d_j^\dagger \end{pmatrix} = \int_{-\pi}^{\pi} \frac{\mathrm{d}k}{\sqrt{2\pi}} e^{ikj} \begin{pmatrix} \cos\gamma_k & i\sin\gamma_k \\ i\sin\gamma_k & \cos\gamma_k \end{pmatrix} \begin{pmatrix} \eta(k) \\ \eta^\dagger(-k) \end{pmatrix} . \tag{4.6}$$

A suitable choice of the Bogoliubov angle puts the homogeneous Hamiltonian in diagonal form

$$H_0 = \int_{-\pi}^{\pi} \mathrm{d}k\, E(k) \eta^\dagger(k)\eta(k) + \text{const.} \tag{4.7}$$

For what it concerns the hopping fermions (4.3), the conservation of the number of particles imposes a trivial Bogoliubov rotation

$$E_f(k) = -\cos(k)\,, \qquad \gamma_k^f = 0 \tag{4.8}$$

while in the Ising model we need

$$E_I(k) = \sqrt{(\cos k - h)^2 + \sin^2 k}\,, \qquad \tan\gamma_k^I = \frac{E_I(k) + \cos k - h}{\sin k}\,. \tag{4.9}$$

The velocity of the excitations is, as usual, the group velocity $v(k) = \partial_k E(k)$. A GGE of the homogeneous Hamiltonian in terms of the modes is expressed as

$$\hat{\rho}_{\text{GGE}} = \frac{1}{\mathcal{Z}} \exp\left[-\int_{-\pi}^{\pi} \mathrm{d}k \log(2\pi\vartheta^{-1}(k) - 1)\eta(k)\eta^\dagger(k)\right] . \tag{4.10}$$

with ϑ the excitation density $\langle \eta^\dagger(k)\eta(q)\rangle = \delta(k-q)\vartheta(k)$. These states are translationally invariant and diagonal in the eigenmodes of the Hamiltonian in absence of the impurity, therefore the non-trivial time evolution will be entirely caused by the defect. Note that the modes $\eta(k)$ and the fermions d_j are linked by a linear transformation, therefore a Gaussian state in terms of the modes translates into a Gaussian state in the real-space field operators. In other words, any correlator of the d_j operators is determined in terms of $\langle \psi_j \psi_{j'}^\dagger \rangle$, which in our notation is a 2×2 matrix

$$\langle \psi_j \psi_{j'}^\dagger \rangle = \begin{pmatrix} \langle d_j d_{j'}^\dagger \rangle & \langle d_j d_{j'} \rangle \\ \langle d_j^\dagger d_j^\dagger \rangle & \langle d_j^\dagger d_{j'} \rangle \end{pmatrix} . \tag{4.11}$$

With the actual choice of parameters, in the hopping fermion system we have set to one the maximum velocity $v_{\text{M}}^f = 1$, while in the Ising model $v_{\text{M}}^I = \min(1, h)$. Since v_{M} plays the same

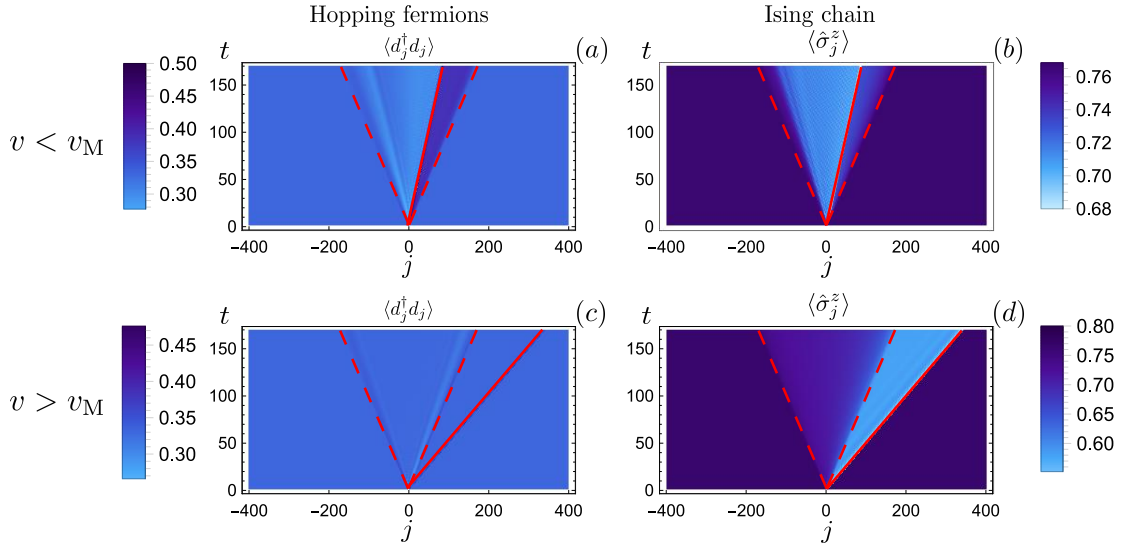

Figure 4.1: *Profiles of local observables induced by moving defects in the hopping fermions model (a, c) and Ising chain (b, d). In the first model we considered the fermionic density $\langle d_j^\dagger d_j \rangle$, while in the second case the local magnetization $\langle \hat{\sigma}_j^z \rangle$. The defect is chosen as a delta function $V(x) = c\delta(x)$ in each case (see also Section 4.1.2) and moves at subluminal velocity in Subfigures (a) and (b), while it is superluminal in Subfigures (c) and (d). Dashed red lines enclose the ligtcone propagating with velocity v_M from the initial position of the defect, while the continuous red line is the trajectory of the impurity. Notice the absence of superluminal LQSS in the hopping fermion case (c): the small ripples are a transient effect that is smeared out as times grows. Parameter used: in each plot the initial state is the ground state, in the hopping fermion case the Fermi momentum is chosen $k_f = \pi/3$, in the Ising model the background field is $h = 1.15$. In each case $v_M = 1$. Subfigures (a) and (b): $v = 0.5$ and defect's strength $c = 0.5$. Subfigures (c) and (d): $v = 2$ and $c = 2$.*

role that the velocity of light has in the information spreading in relativistic systems, from now on we will refer to fast defects $v > v_M$ as superluminal, while slow defects $v < v_M$ will be called subluminal.

Our strategy to understand the emergent LQSS is to frame the protocol in a suitable scattering theory: free quasiparticles start infinitely far from the defect, scatter with the moving impurity and finally leave the defect, contributing to the emergent LQSS. It turns out that the scattering data strongly depend on v. Indeed, in the case of a defect at rest $v = 0$, an incoming quasiparticle has only two possibilities: either passes through conserving the initial momentum, or bounces back with opposite momentum. The story is completely different if we allow for $v \neq 0$: as $v \to 0^+$ infinitely scattering channels open up (indeed, the presence of several channels cause a visible interference, see Appendix 4.A). Their number diminishes as v is increased, until the treshold $v > v_M$ is overcome. Here, the two cases Eq. (4.3) and (4.4) must be separately discussed.

In particular, these models have a crucial difference with great consequences on the superluminal regime. Indeed, Eq. (4.3) possesses an $U(1)$ symmetry, associated with the conservation of the number of fermions, which is not spoiled by the impurity. Thus, the defect acts as a moving scattering potential, but could not create or destroy quasiparticles. Instead, this is not the case of the Ising model (4.4).

In the superluminal case, the scattering theory underling the LQSS of the Ising model possesses only two scattering channels: one where an excitation is trivially transmitted, the other where the quasiparticle is destroyed and a hole is produced. In particular, this second possibility is responsible of the non trivial LQSS. Instead, in the $U(1)$ invariant case only the trivial scattering survives: superluminal defects in the hopping fermions case (4.3) do not produce an

LQSS, regardless the shape and strength of the potential V (see again Fig. 4.1). This section is organized as it follows: in Section 4.1.1 we gather all the technicalities needed to frame the LQSS formation in a scattering framework. The solution of both models require the same techniques and can be considered at once: we express the emergent LQSS in terms of the scattering data and its general features are discussed, with particular emphasis on the superluminal case. Section 4.1.2 is instead dedicated to provide exact solutions of the scattering problem in two opposite regimes: a very narrow defect, mimicked with a Dirac δ, and an extremely smooth impurity. In the first case the quantum mechanical problem is solved exactly, in the second case we revert to a semiclassical approximation which becomes exact for smooth defects: LQSS predictions are tested against numerical simulations, finding perfect agreement.

4.1.1 The moving defect and the scattering problem

Following the proposed out-of-equilibrium protocol, at time $t = 0$, we activate the moving defect. Thus, for $t > 0$ the dynamics is encoded in the Heisenberg equations of motion, which are linear in the fermionic field ψ. In the hopping fermion case (4.3) (f) and in the Ising model (4.4) (I) we respectively have

$$i\partial_t \psi_j = -\frac{\sigma^z}{2}\psi_{j-1} - \frac{\sigma^z}{2}\psi_{j+1} + V(j-vt)\sigma^z\psi_j\,, \qquad (f) \tag{4.12}$$

$$i\partial_t \psi_j = \frac{(i\sigma^y - \sigma^z)}{2}\psi_{j-1} - \frac{(i\sigma^y + \sigma^z)}{2}\psi_{j+1} + \big(h + V(j-vt)\big)\sigma^z\psi_j\,. \qquad (I) \tag{4.13}$$

Their linearity preserves the gaussianity of the ensemble along the whole time evolution, therefore only the two point correlators (4.11) are needed to completely describe the state. Note that we employ the notation of Pauli matrices without the "hat" to clarify that they act on the two components of ψ_j, rather than on the many-body Hilbert space as in Eq. (4.4). The explicit time dependence in the equation of motion introduced by the defect prevents a straightforward solution. On the other hand, time-dependent perturbation theory is not suited to study late-time dynamics. Our strategy is then to perform a change of reference frame which poses the defect at rest: in this way, any time dependence is removed from the equations of motion. Of course, the discreteness of the underlying lattice, compared with the continuous shift of the moving defect, obstructs such a transformation.

In order to overcome this issue, we firstly map the discrete problem in a continuous one, where such a change of reference system is possible. There, the late-time dynamics can be solved in terms of a scattering theory and the final solution is then pulled back to the original lattice.

Change of reference frame: mapping the discrete in the continuum

The formal solution of the equation of motion Eq. (4.12) and (4.13) can be expressed in terms of the Green function $G_{j,j'}(t)$, a 2×2 matrix, as

$$\psi_j(t) = \sum_{j'} G_{j,j'}(t)\psi_{j'}\,. \tag{4.14}$$

The Green function satisfies the differential equation

$$i\partial_t G_{j,j'}(t) = -\frac{\sigma^z}{2}G_{j-1,j'}(t) - \frac{\sigma^z}{2}G_{j+1,j'}(t) + V(j-vt)\sigma^z G_{j,j'}(t)\,, \qquad (f) \tag{4.15}$$

$$i\partial_t G_{j,j'}(t) = \frac{(i\sigma^y - \sigma^z)}{2}G_{j-1,j'}(t) - \frac{(i\sigma^y + \sigma^z)}{2}G_{j+1,j'}(t) + \big(h + V(j-vt)\big)\sigma^z G_{j,j'}(t)\,, \quad (I) \tag{4.16}$$

together with the initial condition $G_{j,j'}(0) = \delta_{j,j'}\mathbb{1}$.

The anticipated mapping to a continuous system can be achieved defining a closely-related *continuous* Green function $\mathcal{G}_{x,x'}(t)$. Hereafter, x and x' are continuous real variables and $\mathcal{G}_{x,x'}(t)$ is defined as the unique solution of

$$i\partial_t \mathcal{G}_{x,x'}(t) = -\frac{\sigma^z}{2}\mathcal{G}_{x-1,x'}(t) - \frac{\sigma^z}{2}\mathcal{G}_{x+1,x'}(t) + V(x-vt)\sigma^z\mathcal{G}_{x,x'}(t)\,, \qquad (f) \quad (4.17)$$

$$i\partial_t \mathcal{G}_{x,x'}(t) = \frac{(i\sigma^y - \sigma^z)}{2}\mathcal{G}_{x-1,x'}(t) - \frac{(i\sigma^y + \sigma^z)}{2}\mathcal{G}_{x+1,x'}(t) + \big(h + V(x-vt)\big)\sigma^z\mathcal{G}_{x,x'}(t)\,, \quad (I) \quad (4.18)$$

with the initial condition $\mathcal{G}_{x,x'}(0) = \delta(x-x')\mathbb{1}$. Given that Eq. (4.17) and (4.18) are nothing else than, respectively, Eq. (4.15) and (4.16) in which discrete coordinates are promoted to continuous ones, G and $\mathcal{G}$ are not surprisingly related. More specifically, since Eq. (4.17) and (4.18) couple together only points that differ of an integer distance, we can rewrite

$$\mathcal{G}_{x,x'}(t) = 2\pi\delta(e^{i2\pi(x-x')} - 1)g_{x,x'}(t)\,. \qquad (4.19)$$

Using the continuous equation of motion, $g_{x,x'}(t)$ for integer x, x' is shown to satisfy the same differential equation and initial conditions as $G_{j,j'}(t)$. Therefore, we can identify $G_{j,j'}(t) = g_{j,j'}(t)$ and work directly with the continuous variables.

Moreover, being the initial state most easily expressed in the momentum space, it is convenient to take a Fourier transform with respect to the second coordinate. Then, one observes that the Dirac δ in Eq. (4.19) transforms the Fourier integral in a Fourier series. In practice, we arrive at

$$\tilde{\mathcal{G}}_{j,k}(t) = \int \mathrm{d}x\, e^{-ikx}\mathcal{G}_{j,x}(t) = \sum_{j'} e^{-ikj'} g_{j,j'}(t) = \tilde{G}_{j,k}(t) \qquad (4.20)$$

where we explicitly used $G_{j,j'}(t) = g_{j,j'}(t)$, with the "tilda" superscript we indicate the Fourier transform and Fourier series of $\mathcal{G}$ and G respectively. We remark that since the Green function $\mathcal{G}$ is defined on a continuous space, its Fourier components run over the entire real axis. On the contrary, the Green function G is defined on a lattice and thus its Fourier transform is naturally embedded in a Brillouin zone. However, Eq. (4.19) makes the l.h.s. of Eq. (4.20) periodic in the momentum space, as it should be for Eq. (4.20) to hold true.

The advantage of dealing with a continuous system is that we can now perform a change of coordinates. Defining $\mathcal{G}^{(v)}_{x,x'}(t) = \mathcal{G}_{x+vt,x'}(t)$, we obtain a time-independent equation of motion

$$i\partial_t \mathcal{G}^{(v)}_{x,x'}(t) = iv\partial_x \mathcal{G}^{(v)}_{x,x'}(t) + \frac{-\sigma^z}{2}\mathcal{G}^{(v)}_{x-1,x'}(t) - \frac{\sigma^z}{2}\mathcal{G}^{(v)}_{x+1,x'}(t) + V(x)\sigma^z\mathcal{G}^{(v)}_{x,x'}(t)\,, \qquad (f) \quad (4.21)$$

$$i\partial_t \mathcal{G}^{(v)}_{x,x'}(t) = iv\partial_x \mathcal{G}^{(v)}_{x,x'}(t) + \frac{(i\sigma^y - \sigma^z)}{2}\mathcal{G}^{(v)}_{x-1,x'}(t) - \frac{(i\sigma^y + \sigma^z)}{2}\mathcal{G}^{(v)}_{x+1,x'}(t) + \big(h + V(x)\big)\sigma^z\mathcal{G}^{(v)}_{x,x'}(t)\,, \quad (I) \quad (4.22)$$

but which now explicitly involves the defect's velocity v. Eq. (4.21) and (4.22) can be interpreted as a single-particle Schröedinger equations, which can be solved in terms of their eigenfuctions. The set of eigenfunctions will depend on the specific choice of $V(x)$; however in the hypothesis of a localized defect, the problem is most easily addressed in the framework of a scattering theory.

The emerging LQSS as a scattering process

The equations of motion of the Green function Eq. (4.21) and (4.22) are most easily solved in terms of the eigenfunctions, i.e.

$$\mathcal{G}^{(v)}_{x,x'} = \sum_{a=1,2} \int \frac{dk}{2\pi} e^{-iE^a(k)t} \phi_{k,a}(x) \phi^\dagger_{k,a}(x') \,, \tag{4.23}$$

where $\phi_{k,a}$ constitute a complete set of two dimensional vectors satisfying the time-independent version of the Schröedinger equation (4.21-4.22)

$$E^a(k)\phi_{k,a}(x) = (\mathfrak{H}_0 \phi_{k,a})(x) + \sigma^z V(x) \phi_{k,a}(x) \,. \tag{4.24}$$

Above, in the linear operator $\mathfrak{H}_0$ we collected the homogeneous part of the equation (with the caveat of replacing $\mathfrak{H}_0$ with the hopping fermion or Ising homogeneous part), while the inhomogeneous term due to the defect is written explicitly. The notation $\phi_{k,a}$ has been chosen in the perspective of the scattering theory we are going to develop. We stress that $\phi_{k,a}(x)$ is a two dimensional vector, not a quantum operator: in this framework $\phi_{k,a}(x)\phi^\dagger_{k,a}(x')$ represents a 2×2 matrix, similarly to the notation of Eq. (4.11). The eigenfunctions satisfy the orthonormality and completeness relations

$$\int \mathrm{d}x \, \phi^\dagger_{k,a}(x) \phi_{q,b}(x) = \delta(k-q)\delta_{a,b} \,, \qquad \delta(x-x')\mathbb{1} = \sum_{a=1,2} \int \mathrm{d}k \, \phi_{k,a}(x) \phi^\dagger_{k,a}(x') \,. \tag{4.25}$$

Taking advantage of the fact that $V(x)$ is a localized impurity, we can describe the $\phi_{k,a}$ eigenfunctions in a scattering theory framework, in particular they must satisfy the Lippmann-Schwinger equation [399] having as source terms the eigenfunctions of the homogeneous problem. With the definition

$$u_{k,1} = \begin{pmatrix} \cos\gamma_k \\ i \sin\gamma_k \end{pmatrix} \,, \quad u_{k,2} = \begin{pmatrix} i\sin\gamma_k \\ \cos\gamma_k \end{pmatrix} \tag{4.26}$$

The Lippmann-Schwinger equation is simply

$$\phi_{k,a}(x) = \frac{e^{ikx}}{\sqrt{2\pi}} u_{k,a} + \int \mathrm{d}x' \left[\frac{1}{E^a(k) - H_0 + i0^+} \right]_{x,x'} V(x') \sigma_z \phi_{k,a}(x') \,. \tag{4.27}$$

Above, $e^{ikx}u_{k,a}$ are the eigenfunctions of the homogeneous problem. The energies E^a are obtained shifting the energy at rest in the hopping fermion and Ising models, giving respectively

$$E^1_{f/I}(k) = E_{f/I} - vk \,, \quad E^2_{f/I}(k) = -E_{f/I}(k) - vk \,. \tag{4.28}$$

We can recognize $E^1(k)$ as the energy of excitations $E(k)$ with an additional shifting $-vk$ due to the change of reference frame. Similarly, $E^2(k)$ represents the energy of a hole in the moving frame.

As we will see, the LQSS is completely determined by the behavior of the eigenfunctions in the scattering region, i.e. far away from the defect. From Eq. (4.27), the large distance expansion is immediately recovered retaining only the singularities in the kernel

$$\phi_{k,a}(x) \simeq \frac{1}{\sqrt{2\pi}} \Bigg(\Theta(-xv^a(k)) e^{ikx} u_{k,a} + \sum_b \int \mathrm{d}q \, e^{iqx} \times \\ \delta(E^b(q) - E^a(k)) \Theta(xv^b(q)) |v^b(q)| S_{b,a}(q,k) u_{q,b} \Bigg) \,, \tag{4.29}$$

where $\Theta(x)$, as usual, indicates the Heaviside Step function. This equation admits a simple interpretation: the step functions $\Theta(x)$ in Eq. (4.29) discern between incoming/outgoing states; the second term describes the scattering of a mode (k,a) into a mode (q,b): this is allowed only if the energy is conserved $E^b(q) = E^a(k)$ and it is mediated by the scattering amplitude $S_{b,a}(q,k)$. We remark that the number of solutions to $E^b(q) = E^a(k)$ is always finite for $v \neq 0$.

In Eq. (4.29), $v^a(k)$ represents the velocity of the excitation computed in the moving reference frame, defined as $v^a(k) = \partial_k E^a(k)$. In particular, from Eq. (4.29), it follows

$$v^1(k) = v(k) - v \qquad v^2(k) = -v(k) - v\,, \tag{4.30}$$

where we recall $v(k) = \partial_k E(k)$. The scattering amplitudes can be formally expressed in the form

$$S_{b,a}(q,k) = \begin{cases} 1 + \int \mathrm{d}x\, e^{-ikx} V(x) u^\dagger_{k,a} \sigma^z \phi_{k,a}(x) & (k,a) = (q,b) \\ \int \mathrm{d}x\, e^{-iqx} V(x) u^\dagger_{q,b} \sigma^z \phi_{k,a}(x) & (k,a) \neq (q,b) \end{cases} \tag{4.31}$$

This expression is not yet a solution for the scattering amplitudes, as it depends on the unknown eigenfunctions $\phi_{k,a}$ in the region where the defect is placed. However, we can already draw some general conclusions.

Indeed, the scattering wavefunctions are not arbitrary, but they must satisfy the constraints Eq. (4.25). These relations can be translated in *sum rules* that the scattering amplitudes must obey and are enough to determine the structure of the local GGE.

We leave the derivation of the sum rules, as well as the determination of the LQSS in terms of the scattering data to Appendix 4.A, while hereafter we simply report the results. A local observable relaxes to a ray-dependent GGE: it is convenient to consider the rays in the moving reference frame, which in the laboratory coordinates are simply defined as $\zeta = j/t - v$. The ray-dependent excitation density $\vartheta_\zeta(k)$, which ultimately uniquely identifies the GGE through Eq. (4.10), can be written as

$$\vartheta_\zeta(k) = \Big[\Theta(-\zeta v^1(k)) + \Theta(\zeta v^1(k))\Theta(|\zeta| - |v^1(k)|)\Big]\vartheta(k) + \Theta(\zeta v^1(k))\Theta(|v^1(k)| - |\zeta|)\vartheta_{\mathrm{scat}}(k)\,. \tag{4.32}$$

where $\vartheta(k)$ is the initial excitation density (4.10). The function $\vartheta_{\mathrm{scat}}(k)$ is the excitation density propagating from the defect and, in terms of the scattering data, it reads

$$\vartheta_{\mathrm{scat}}(k) = \sum_{n=-\infty}^{\infty} \sum_{a=1,2} \int_{-\pi}^{\pi} \mathrm{d}q \left[\delta(E^a(q) - E^1(k+2\pi n))|v^1(k+2\pi n)||S_{1,a}(k+2\pi n, q)|^2 \vartheta^a(q)\right]. \tag{4.33}$$

with the convention $\vartheta^1(q) = \vartheta(q)$ and $\vartheta^2(q) = 1 - \vartheta(q)$. Despite deriving Eq. (4.32) and (4.33) requires some rather technical steps, their meaning is readily explained on a physical ground.

At fixed momentum k, Eq. (4.32) simply describes the progressive replacement of the pre-quench excitation density with the one emerging from the scattering event. Indeed, let us suppose that k is such that $v^1(k) > 0$ and fix a large time t. Then, all the points on the left of the defect ($\zeta t < 0$) have not yet scattered on the defect; similarly, the points $\zeta t > v^1(k)t$ have not yet been reached by the excitations emitted by the scattering on the defect. Therefore, the excitation density is unaffected and $\vartheta_\zeta(k) = \vartheta(k)$ in these regions. Instead, for $0 < \zeta < v^1(k)$, the excitation density is replaced by the one produced by the scattering events, i.e $\vartheta_\zeta(k) = \vartheta_{\mathrm{scat}}(k)$.

As it is clear from Eq. (4.33), $\vartheta_{\mathrm{scat}}(k)$ receives contributions from excitations ($a = 1$, associated with $\vartheta(q)$) and holes ($a = 2$, associated with $1 - \vartheta(q)$), weighted with the proper squared scattering amplitudes. Finally, the sum over the integers in Eq. (4.33) accounts for the folding of momenta in the first Brillouin zone while coming back from the continuous to the discrete model. Overall, we have framed the quantum problem in a simple scattering picture, being the

details of the defect completely encoded in the scattering amplitudes.

The emerging LQSS and the friction force

The creation of a LQSS due to the traveling impurity is associated with an energy cost. This is particularly clear when the system is initialized in the ground state, where any non trivial effect is due to the creation of new excitations by the defect, which ultimately heats the system. Reverting this point of view, we can equivalently say that the system exerts a friction force on the moving impurity.

The general issue of studying the emergence of friction forces on heavy impurities embedded in quantum thermodynamic baths has been extensively studied (see e.g. [400] for a review), with several experimental implications. For example, in actual experiments heavy impurities are ultimately slowed down because of the recoil due to the scattering events (see e.g. Ref. [47]).

In our setup, the defect is considered as an external field and therefore it does not have a dynamics on its own, nevertheless this can be regarded as the zeroth order approximation of an heavy impurity, which is only slightly affected by each scattering event. The instantaneous dissipated power is naturally defined as the derivative of the instantaneous energy of the system $P(t) = \partial_t \mathcal{E}(t) = \partial_t \langle H(t) \rangle$ where $H(t)$ is the full time dependent Hamiltonian after the defect activation. From the dissipated power, we can readily define the friction force as $F = -P/v$.

However, the instantaneous dissipated power is affected by the microscopic dynamics around the defect, a region which lays beyond any scattering approximation. A physical quantity which has a well-defined stationary regime is the time average of the dissipated power

$$\bar{P} = -\bar{F}v = \lim_{\tau\to\infty} \frac{1}{\tau} \int_0^\tau \mathrm{d}t\, P(t) = \lim_{\tau\to\infty} \frac{\mathcal{E}(\tau) - \mathcal{E}(0)}{\tau}\,, \tag{4.34}$$

which can be readily computed from the LQSS. Indeed, computing $\bar{P}$ only requires the total energy $\mathcal{E}(\tau)$ at a given large time and, in the $\tau \to \infty$ limit, any (finite) region around the defect can be entirely neglected. Therefore, Eq. (4.34) can be computed simply looking at the system at large distances from the defect, where *i)* the LQSS (4.32) is valid and *ii)* the Hamiltonian reduces to the homogeneous one, where the defect is absent. In view of these considerations, computing $\mathcal{E}(\tau)$ amounts to locally consider the energy density using as excitation density that of the local LQSS, then integrate on the whole space. This immediately leads to the simple expression

$$\bar{P} = \int \mathrm{d}\zeta \int_{-\pi}^{\pi} \frac{\mathrm{d}k}{2\pi} E(k)[\vartheta_\zeta(k) - \vartheta(k)]\,. \tag{4.35}$$

Being $\vartheta_\zeta(k) = \vartheta(k)$ for ζ outside of the LQSS, the mean power is of course finite. Using the expression of ϑ_ζ Eq. (4.32), the mean power is completely written in terms of the density of scattered momenta

$$\bar{P} = \int_{-\pi}^{\pi} \frac{\mathrm{d}k}{2\pi} E(k)|v^1(k)|[\vartheta_{\mathrm{scat}}(k) - \vartheta(k)]\,, \tag{4.36}$$

which ultimately depends on the scattering data through Eq. (4.33).

General features of the LQSS: lack of superluminal LQSS in the hopping fermion case

Equations (4.32) and (4.33) fully characterize the emergent LQSS, encoding the details of the defect only in the scattering amplitudes. Even though, the specific values of the scattering amplitudes are eventually needed in order for Eq. (4.33) to be predictive (see Section 4.1.2), we can nevertheless sketch the qualitative behavior of the LQSS based only on kinematics. Thereafter, we discuss how the scattering features change for defect's velocities ranging from $v = 0$ up to $v > v_{\mathrm{M}}$.

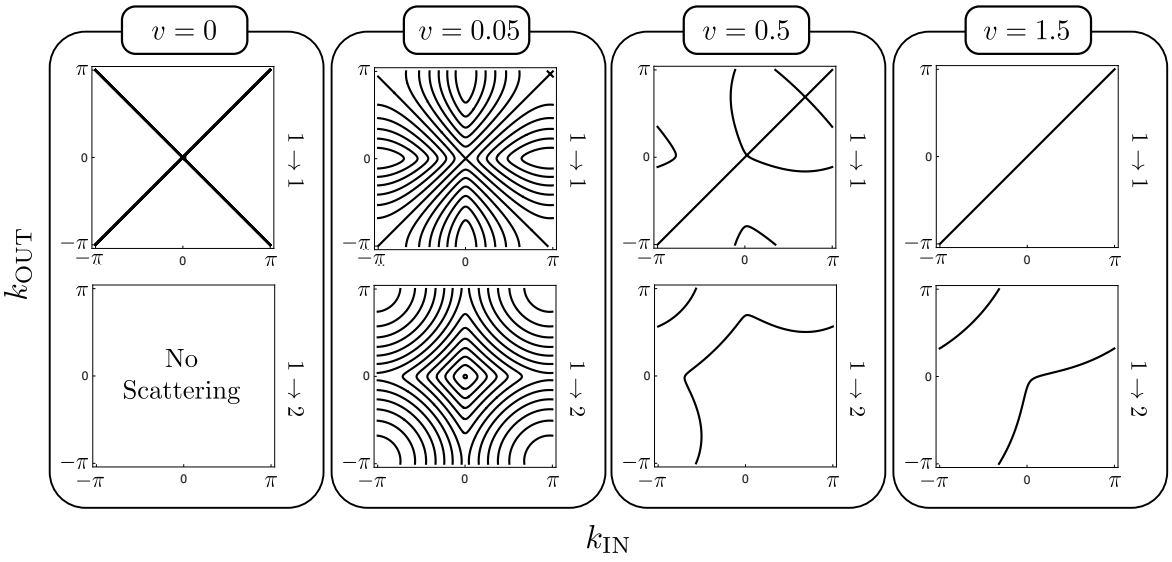

Figure 4.2: *Dynamically accessible scattering channels* $1 \to 1$ *and* $1 \to 2$ *(see text for notation) in the Ising model, analogue qualitative features hold true in the hopping fermion case. The scattering channels are identified as the solutions of Eq.* (4.37) *which are ultimately pulled back to the first Brillouin zone. The magnetic field is set* $h = 1.15$*, thus* $v_M = 1$*. Figure taken from Ref. [10].*

Consider at first a static defect ($v = 0$): in this case the complicated detour of mapping the discrete model in the continuous one is clearly superfluous and we must recover the simple solution we would have obtained from a direct analysis of the lattice problem. This is readily understood looking at the scattering processes in (4.33), which are allowed by the energy conservation

$$E^1(k_{\mathrm{IN}}) = E^a(k_{\mathrm{OUT}}) \,, \quad a = 1, 2 \,. \tag{4.37}$$

Note that, for the time being, we treat k as ranging on the whole real axis and only at the end fold it to the Brillouin zone. A graphical representation of the possible scattering channels is reported in Fig. 4.2 and hereafter explained.

For $v = 0$, as it is clear from Eq. (4.28) we simply have $E^1(k) = E(k)$ and $E^2(k) = -E(k)$. This immediately prevents any solution in the form $E^1(k) = E^2(q)$ (this because $E(k) > 0$): a hole can never be scattered into an excitation. Instead, the equation $E^1(k) = E^1(q)$ has infinitely many solutions because of the periodicity of $E(k)$, but once they are folded back to the Brillouin zone they reduce to only two possibilities $\pm k$. Therefore, for a static defect, an excitation is either transmitted or reflected with opposite momentum, as it should be.

As soon as we move to $v > 0$, the scattering picture becomes more involved. The equation $E^1(k) = E^1(q)$ has now only a finite number (divergent in the limit $v \to 0$) of solutions, but these zeros are no longer equivalent once folded back in the Brillouin zone. Furthermore, scattering of holes into excitations is also possible, since $E^1(k) = E^2(q)$ has non-trivial solutions. The number of possible scattering channels decreases as v grows until $v = v_M$: after this threshold, the equation $E^1(k) = E^1(q)$ possesses the unique solution $k = q$. Also the crossed channel $E^1(k) = E^1(q)$ has one (and only one) solution (see Fig. 4.2).

This concludes what it can be learn from the kinematics of the scattering theory, but we should now consider the dynamics as well: while scattering channels could be kinematically accessible, the scattering matrix connecting the two could be zero, thus forbidding the scattering to actually take place. Indeed, this explains the striking difference in the superluminal behavior of the hopping fermions, when compared with the Ising model. The $U(1)$ symmetry of H^f (4.3) conserves the number of particles: this implies that the scattering amplitudes are such that

$S_{1,2} = S_{2,1} = 0$. Therefore, in the superluminal case only the trivial scattering $(1,k) \to (1,k)$ is possible and, because of the sum rules (see Appendix 4.A) we have $|S_{1,1}(k,k)| = 1$ and Eq. (4.32) trivializes $\vartheta_\zeta(k) = \vartheta(k)$. This holds true regardless the actual shape of the defect $V(x)$: in the hopping fermion case (4.3) no superluminal LQSS can be produced.

The same reasoning does not apply to the Ising model (4.4): in this case there is not any symmetry preventing the scattering of holes into excitations (and the other way), thus superluminal defects allow for two scattering channels with the consequent formation of the LQSS.

A superluminal LQSS has clear differences from the subluminal counterpart. They become manifest looking closely at the ray dependence encoded in Eq. (4.32): for $v < v_M$ the combination of Heaviside Theta functions provides a non trivial ray dependence to ϑ_ζ (with a discontinuity in $\zeta = 0$) which ultimately ensures a non trivial profile of local observables. On the contrary, in the case $v > v_M$ we have $\min_k |v^1(k)| = |v - v_M|$, as it is clear from its very definition Eq. (4.30) and this ensures a ζ-independent excitation density $\vartheta_\zeta(k)$ as long as $|\zeta| \leq |v - v_M|$. Considering a local observable $\mathcal{O}_j$ back in the laboratory frame, this guarantees the formation of a tail beyond the defect whose size grows as $t|v - v_M|$ where $\langle \mathcal{O}_j \rangle$ is translationally invariant. Aside of the general discussion, in the next section we provide the explicit and exact scattering data in the case of an extremely narrow and smooth defect respectively, then benchmark our LQSS prediction against numerical simulations.

4.1.2 Exact scattering data: narrow and smooth defects

Scattering data for extremely narrow defects

There exists one peculiar defect for which the scattering data Eq. (4.31) can be computed exactly, i.e. the limit of an extremely narrow impurity described by a $\delta-$function

$$V(x) = c\delta(x)\,. \tag{4.38}$$

Before presenting the derivation, some additional comments are due: in Eq. (4.38) the $\delta-$function is a genuine *Dirac delta function*. Of course, as long as a static defect on a lattice is considered, Eq. (4.38) is not well-defined: while pinching a lattice site gives a singularity, placing the delta in between two lattice sites will leave the system completely unaffected. However, the inconsistency disappears as soon as a moving defect is considered: for $v \neq 0$, Eq. (4.38) describes a "kick" traveling along the lattice, impulsively acting on the system whenever the $\delta-$support meets a lattice site.

We now present the exact solution. If we directly approach Eq. (4.27), formally replacing $V(x) = c\delta(x)$ we would naively reach

$$\phi_{k,a}(x) \stackrel{?}{=} \frac{e^{ikx}}{\sqrt{2\pi}} u_{k,a} + \mathcal{K}(x) c\sigma_z \phi_{k,a}(0)\,, \tag{4.39}$$

where we pose $\mathcal{K}(x - x') = [E - H_0 + i0^+]^{-1}(x, x')$. Despite the appealing simplicity, the above equation is *not correct*. In the replacement of the $\delta-$function in the integral, it is implicit the continuity of the kernel, but this is not absolutely the case as $\mathcal{K}(0^+) \neq \mathcal{K}(0^-)$. This implies $\phi_{k,a}(0^+) \neq \phi_{k,a}(0^-)$ and it is therefore unclear how to properly interpret (4.39). A careful way to proceed is to employ directly the Lippman-Schwinger equation

$$\phi_{k,a}(x) = \frac{e^{ikx}}{\sqrt{2\pi}} u_{k,a} + \frac{1}{\sqrt{2\pi}} \mathcal{K}_{k,a}(x) W_{k,a}\,, \tag{4.40}$$

with $W_{k,a}$ a two dimensional vector coming from the (still) unknown regularization of the δ function. Eq. (4.40) on its own is of course not a solution, being both $\phi_{k,a}$ and $W_{k,a}$ unknown,

but we can provide an additional constraint from a direct analysis of the Schröedinger equation (4.24). Indeed, the singularity of the Dirac-δ must be balanced by the same singularity in the derivative of the wavefunction. Matching the most singular parts we deduce

$$iv\partial_x \phi_{k,a}(x) + c\delta(x)\sigma^z \phi_{k,a}(x) = 0\,, \quad x \to 0\,. \tag{4.41}$$

This is immediately translated in a jump discontinuity in $\phi_{k,a}$ around $x = 0$

$$\phi_{k,a}(0^+) = e^{i\frac{c}{v}\sigma^z}\phi_{k,a}(0^-)\,. \tag{4.42}$$

Combining Eq. (4.40) with the knowledge of the discontinuity, we can solve for $W_{k,a}$ in terms of the (still unknown) limits of the kernel $\mathcal{K}_{k,a}(0^\pm)$.

$$W_{k,a} = \left[e^{i\frac{c}{v}\sigma^z}\mathcal{K}_{k,a}(0^-) - \mathcal{K}_{k,a}(0^+)\right]^{-1}(1 - e^{i\frac{c}{v}\sigma^z})u_{k,a}\,. \tag{4.43}$$

The scattering amplitudes are now accessible through Eq. (4.31) with the regularization

$$\int \mathrm{d}x\, e^{-iqx} u^\dagger_{q,b}\sigma_z V(x)\phi_{k,a}(x) \to u^\dagger_{q,b} W_{k,a}\,. \tag{4.44}$$

The last ingredient we need is $\mathcal{K}_{k,a}(0^\pm)$, the latter being computed from its very definition. The calculations are somewhat lengthy but straightforward (see Ref. [9]), leading to

$$\mathcal{K}_{k,a}(0^\pm) = \pm\frac{i}{2v} + \sum_{b=1,2}\mathcal{P}\int\frac{\mathrm{d}q}{2\pi}\frac{u_{q,b}\,u^\dagger_{q,b}}{E^a(k) - E^b(q)} + \sum_{b=1,2}\int_{-\infty}^{\infty}\mathrm{d}q\,\delta(E^a(k) - E^b(q))\frac{u_{q,b}\,u^\dagger_{q,b}}{2i}\,, \tag{4.45}$$

where $\mathcal{P}$ means the singular points must be regularized via principal values.

In Fig. 4.3, the analytical results for the LQSS of a $\delta-$like impurity are compared with the numerical data, finding excellent agreement. In particular, in the hopping fermions case we focused on the local particle density $d^\dagger_j d_j$, while in the Ising chain we considered the magnetization along the z axis in the Ising model, directly associated with the fermionic density $\hat{\sigma}^z_j = 1 - 2d^\dagger_j d_j$. It is worth stressing the presence of the already anticipated plateau in the superluminal defect in the Ising chain, while the superluminal LQSS is absent in the hopping fermions model.

After the LQSS, we now revert to the friction force: in Fig. 4.4(a) we compare the analytic prediction (4.36) against the numerics for a $\delta-$like defect in the Ising chain, plotting $\bar{P}$ as a function of the defect velocity. Interestingly, in the limit of a very fast defect all possible impurities share the same behavior, decaying as $\sim 1/v$ (of course, in the hopping fermions case we trivially get zero for any impurity). This can be readily seen solving the Lippman-Schwinger equation (4.27) in the limit of large v, by mean of a simple Born approximation (see Ref. [10]), which ultimately leads to

$$\bar{P} \simeq \frac{1}{v}\int\frac{\mathrm{d}k}{2\pi}E(k)\left|\int\mathrm{d}x V(x)u^\dagger_{k,1}\sigma_z u_{k,2}\right|^2(1 - 2\vartheta(k))\,. \tag{4.46}$$

Actually, very fast defects are ultimately close to the $\delta-$potential, since they instantaneously kick each lattice site much faster than the speed of the signal between different sites ($v \gg v_M$). In fact, all the defects at large velocities converge towards the same formula Eq. (4.46), which is ultimately the large velocity limit of a $\delta-$like defect, with effective strength $c = \int \mathrm{d}x\, V(x)$ (see Fig. 4.4(b)). In the hopping fermion case, we consistently get that Eq. (4.46) vanishes, since $u^\dagger_{k,1}\sigma_z u_{k,2} = 0$.

Eq. (4.46) must also be commented in view of the forthcoming semiclassical approximation, which predicts that also in the Ising model we exactly have $\bar{P} = 0$ as soon as the defect is

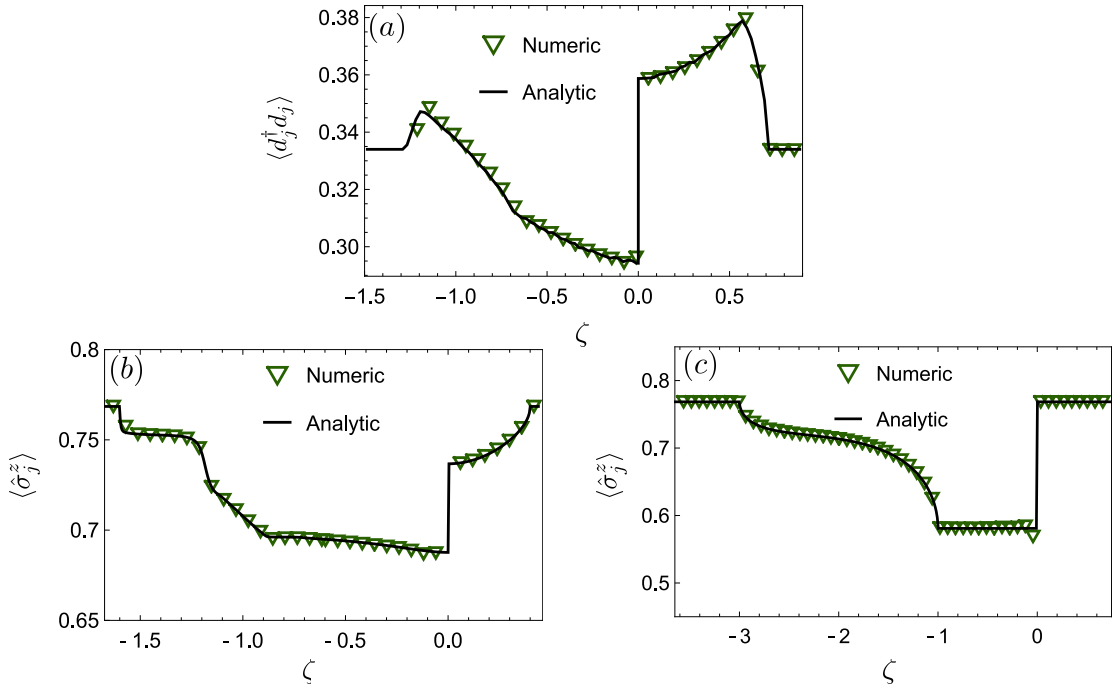

Figure 4.3: *Example of LQSS: the numerical profile of observables is tested against the LQSS prediction for a $\delta-$like potential $V(x) = c\delta(x)$. Above, $\zeta = j/t - v$ is the ray in the defect frame, which is then placed at $\zeta = 0$. Subfigure (a): in the hopping fermion case, we consider the fermionic density $\langle d_j^\dagger d_j \rangle$ for a subluminal defect moving at velocity $v = 0.3$, with the potential strength $c = 0.5$. The system is in the ground state with Fermi momentum $k_f = \pi/3$. Subfigures (b) and (c): in the Ising model, the local magnetization $\langle \hat{\sigma}^z \rangle$, trivially connected with the fermionic density $\hat{\sigma}_j^z = 1 - 2d_j^\dagger d_j$, is considered in the subluminal (Subfigure (b)) and superluminal (Subfigure (c)) cases. Notice the presence of the plateau in the superluminal case, accordingly with the discussion in the main text. In both cases, the light velocity is $v_M = 1$, the initial state is the ground state with magnetic field $h = 1.15$, in Subfigure (b) $v = 0.6$ and $c = 0.6$, in Subfigure (c) $c = 2$ $v = 2$. Data taken from Ref. [9, 10].*

superluminal, regardless its shape or the initial excitation density. There is no contradiction since the two results are valid in different regimes of approximation: the validity of the semiclassical approach requires weak inhomogeneities in space and time. Therefore, if we consider a defect of given shape and strength and move it at higher and higher velocities, we ultimately leave the semiclassic regime, eventually ensuring the validity of Eq. (4.46).

An opposite, interesting limit is of course $v \to 0$. We now consider the case of a $\delta-$like defect $V(x) = c\delta(j - vt)$: physically, a moving defect in this form locally kicks a single site with strength c/v at intervals $\Delta t = 1/v$. While a direct analytical or numerical evaluation of our formulas becomes cumbersome because of the presence of infinitely many scattering channels, we can forecast the $v \to 0$ limit of $\bar{F}$ based on simple physical arguments. As a matter of fact, as $v \to 0$, an infinite amount of time passes between two consecutive kicks and the system manages to relax back to the initial state. Thus, in first approximation, the dissipated power is simply $\bar{P} = -\Delta\mathcal{E}v$, with $\Delta\mathcal{E}$ the energy difference between the initial state and the state in which we act with the defect only once. Therefore, as $v \to 0$, we get $\bar{F} = -\Delta\mathcal{E}$, which is readily computed as (below, (f) refers to the hopping fermions and (I) to the Ising chain)

$$\Delta\mathcal{E}_f = \langle e^{i\frac{c}{v}d_j^\dagger d_j} H_0^f e^{-i\frac{c}{v}d_j^\dagger d_j} \rangle - \langle H_0^f \rangle = \frac{1}{2}\big\langle \big[(1 - e^{ic/v})d_j^\dagger d_{j+1} + (1 - e^{-ic/v})d_{j-1}^\dagger d_j + \text{h.c.}\big] \big\rangle\,, \quad (f) \tag{4.47}$$

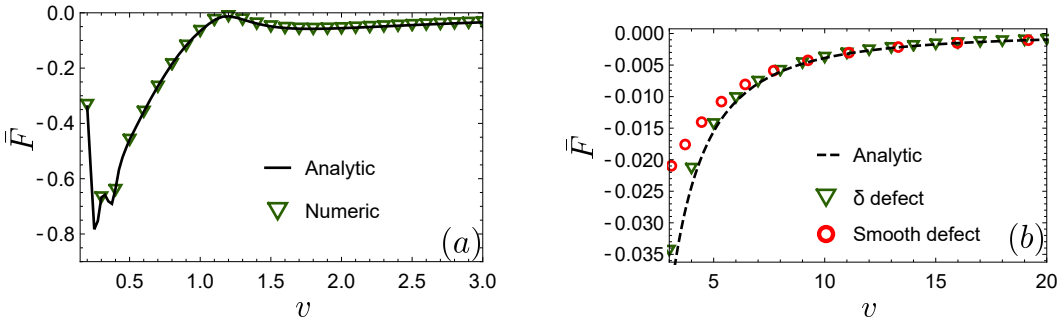

Figure 4.4: *The friction force is studied for the Ising model. Subfigure* (a)*: The mean friction force* $\bar{F}$ *is plotted as a function of the defect's velocity* v *for a* $\delta-$*like defect, showing excellent agreement between analytic and numerics. We considered velocities* $v > 0.2$*, since the increasing number of singularities in Eq.* (4.45) *makes difficult its practical evaluation for* $v \to 0$*. Parameters:* $h = 1.15$*,* $c = 1$*, the initial state is the ground state. Subfigure* (b)*: The numerical mean friction force* $\bar{F}$ *for large velocities in the case of a* $\delta-$*like and a smooth defect, their normalization has been chosen in such a way the share the same asymptotic decay Eq.* (4.46) *(dashed black line). Parameters:* $h = 1.15$*, the strength of the* $\delta-$*defect is set* $c = 1$*. The smooth defect is chosen as* $\delta h(x) = 0.56\, e^{-0.98\, x^2}$*. The system has been initialized in the ground state. Figure taken from Ref. [10].*

$$\Delta\mathcal{E}_I = \langle e^{-i\frac{c}{2v}\sigma_j^z} H_0^I e^{i\frac{c}{2v}\sigma_j^z}\rangle - \langle H_0^I\rangle = \frac{1}{2}\Big\langle \Big[(1-\cos(c/v))\sigma_j^x + \sin(c/v)\sigma_j^y\Big]\,(\sigma_{j+1}^x + \sigma_{j-1}^x)\Big\rangle\,, \quad (I) \tag{4.48}$$

Above, H_0 is the Hamiltonian in absence of the defect and the expectation value must be taken on the initial translational invariant state, thus the expression is independent on the actual choice of j. From the above, we clearly notice the non analyticity of the $v \to 0$ limit if c is kept constant, as we could have guessed from Eq. (4.43). In particular, $\bar{F}$ becomes zero each time $c/v = 0(\mathrm{mod}2\pi)$. A more sensible limit consists in sending $v \to 0$, but keeping c/v fixed: in this case, the instantaneous action of the defect on the lattice is kept constant as $v \to 0$ and the force tends to a constant value.

We end this section commenting on the non-monotonicity of the friction force. It is tempting to re-inject this force in the equation of motion of the impurity itself, thus investigating the dynamics of the system coupled impurity. In particular, if an external force $\mathcal{F}$ is acting on the impurity, we would predict a drift velocity v_d such that $\mathcal{F} + \bar{F}(v_d) = 0$. Of course, this result would require further investigation, as it strongly relies on the possibility for the system to reach an LQSS, which contrasts with the impurity being a dynamical object. A comparison with the behavior obtained in similar settings (see for instance [400, 401]) following a different methodology could be useful to define the range of validity of our approach.

The scattering problem in the semiclassical approximation

An opposite limit where quantitative results can be obtained is that of extremely smooth defects: in particular, similarly to what happened in the Tonks-Girardeau gas of Section 3.3, semiclassical approaches can be used for $V(x)$ of weak variations.

We can already anticipate that superluminal defects in the semiclassical regime do not produce any LQSS: as we previously discussed, superluminal LQSS are eventually due to the tunneling of a hole into an excitation, but such an event is classically forbidden and the defect becomes purely transmissive for $v > v_{\mathrm{M}}$.

The derivation of the semiclassical approximation of the Hamiltonian of the hopping fermions (4.3) is a straightforward generalization of what we did for the Tonks-Girardeau gas (see Ref.

[9]), while the more general case of the Ising model can be found in Ref. [10]. Here, we simply report and comment the result.

In the hypothesis of weak inhomogeneity in space and time, the state is pointwise described by a GGE whose local momentum dependent excitation density $\vartheta(k,x)$ evolves through the classical *Liouville Equation*

$$\partial_t \vartheta(k,x) + \{\vartheta(k,x), \mathcal{H}(k,x)\}_{x,k} = 0\,, \tag{4.49}$$

where $\{\ \}_{x,k}$ are the Poisson's brackets and $\mathcal{H}$ is the classical Hamiltonian, which is simply the energy of the mode in the local density approximation. In the hopping fermions and Ising chain we respectively have

$$\mathcal{H}_f(k,x) = -\cos k + V(x) \qquad \mathcal{H}_I(k,x) = \sqrt{(\cos k - h - V(x))^2 + \sin^2 k}\,. \tag{4.50}$$

Therefore, $\vartheta(k,x)$ behaves as a classical density of particles evolving through the Hamiltonian $\mathcal{H}$, i.e. obeying the equation of motion

$$\dot{k} = -\partial_x \mathcal{H}(k,x) \qquad \dot{x} = \partial_k \mathcal{H}(k,x)\,. \tag{4.51}$$

At the semiclassical level, the system is thus described by a classical gas of non interacting particles, moving in a background force where the defect is placed. In the classical picture the change of reference frame is most easily addressed, since in the semiclassical regime a coarse grain procedure is invoked and the lattice structure disappears (albeit it is still recognizable in the periodic $k-$dependence of $\mathcal{H}(k,x)$).

In the moving reference frame, where the defect is at rest, the scattering amplitudes are determined by the classical equation of motion: a particle with momentum k comes from infinity, scatters with the defect and then continues in a free motion with a new momentum. Being the classical equations fully deterministic, the scattering amplitude is non-zero only for a single scattering channel, determined by the equation of motion. Notice that, being excitations and holes decoupled at a classical level, a superluminal defect does not create any LQSS.

In the defect reference frame, the particles are governed by the following Hamiltonian

$$\mathcal{H}^{(v)}(k,x) = -vk + \mathcal{H}(k,x)\,. \tag{4.52}$$

Even though classical, an exact solution of the equation of motion can be challenging, but in the perspective of solving the scattering problem only the trajectories in the phase space (k,x), identified by the constant energy levels $\mathcal{H}^{(v)}(k,x) = \text{const}$, are needed. For any incoming momentum k_{IN} the proper outgoing momentum k_{OUT} is then readily found. This is particularly easy in the hopping fermions case, where the classical energy is a sum of a kinetic part (function of only the momentum k) and a potential part, function only of the position: in this case an analysis based on the classical *turning points* allows to a simple analytical determination of the classical scattering channels (see Ref. [9]). The classical expression of the LQSS is then obtained simply replacing in Eq. (4.32) ϑ_{scat} with the excitation density of the incoming momentum, i.e. assuming k_{IN} scatters in k_{OUT} we simply have $\vartheta_{\text{scat}}(k_{\text{OUT}}) = \vartheta(k_{\text{IN}})$.

So far, we focused on the LQSS, which is valid at long times and distances from the defect: a quantum mechanical description of what happens in proximity of the defect (and on top of it) requires a complete control over the eigenfunctions $\phi_{k,a}(x)$ (4.24), which is a difficult task. On the contrary, the semiclassical approximation allows for a simple analysis, especially in the superluminal case: superluminal defects do not produce LQSS (exactly in the hopping fermions, in the semiclassical approximation in the Ising chain), thus the non trivial profile on the top of the impurity is the only effect that persists at late times.

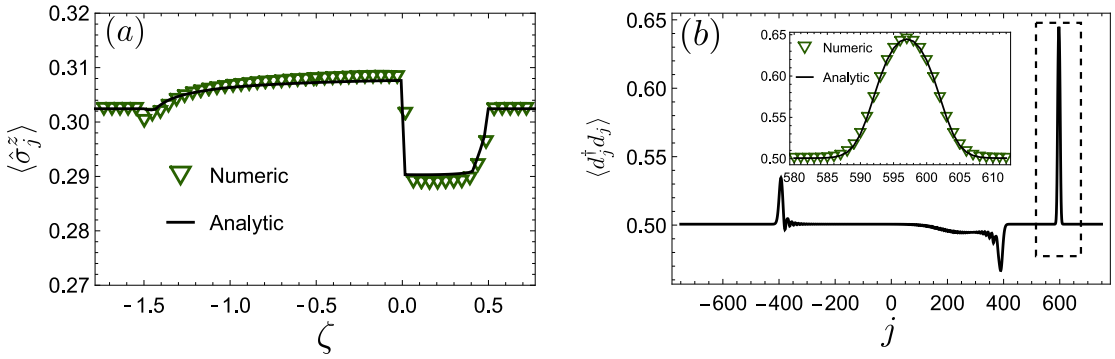

Figure 4.5: *Subfigure (a) the semiclassical LQSS is tested against the numerical data in the Ising model for a defect $V(x) = 0.5e^{0.02x^2}$ moving with velocity $v = 0.5$ and background magnetic field $h = 1.3$. $\zeta = j/t - v$ is the ray in the defect frame. The initial state is a thermal ensemble with inverse temperature $\beta = 0.5$ (in the semiclassical regime, the defect cannot create excitations on top of the vacuum, this is why we considered an excited state such as the Gibbs ensemble). Subfigure (b): in the hopping fermion case, the numerical fermionic density is tested against the semiclassical LQSS for a gaussian shaped repulsive potential $V(x) = e^{-\sigma x^2}$ with $\sigma = 0.04$, the initial ground state has Fermi momentum $k_f = \pi/2$. The impurity is superluminal $v = 1.5$. The profile is plotted in real space at time $t = 388$, the defect is placed in correspondence with the rightmost peak: the LQSS is indeed absent and the semiclassical prediction captures the density profile on the defect (inset). The corrections to the analytic prediction are a combined effect of* i) *the particles initially sat on the defect that have not yet managed to spread* ii) *the delay time experienced by the particles scattering on the defect. Both these effects are negligible at late time and in the scaling limit. Data taken from Ref. [9, 10].*

Thus, let us focus on the superluminal case: the excitation density, thanks to the Liouville equations (4.49), behaves as an incompressible fluid. Since in the superluminal case $v > v_{\rm M}$ the equation $\mathcal{H}^{(v)}(k, x) = \text{const.}$, for any fixed x, identifies an unique momentum, we can write the flux conservation

$$\mathrm{d}p_{k,x}\, \vartheta(p_{k,x}, x) = \mathrm{d}k\, \vartheta(k, +\infty)\,. \tag{4.53}$$

Above, we used that for $v > v_{\rm M}$, in the defect moving frame all particles move from the right to the left and define $p_{k,x}$ as the unique solution of

$$\mathcal{H}^{(v)}(p_{k,x}, x) = \mathcal{H}^{(v)}(k, +\infty)\,. \tag{4.54}$$

Our semiclassical analysis is tested against numerical data in Fig. 4.5, where we found perfect agreement.

4.1.3 Concluding remarks

In this section we analyzed a local quench, consisting in the sudden activation of a localized defect moving at velocity v in an otherwise homogeneous and thermodynamically large system. While we considered a system of hopping fermions and the Ising model as specific examples, the same techniques can be immediately extended to *arbitrary* quadratic models (fermionic or bosonic), or systems that can be mapped into this class.

Our main focus has been the late-time features far from the defect, which we investigated by exploring the formation of a Local Quasi Stationary State. We provided *exact* analytical results for an extremely narrow impurity and in the case of a smooth defect. Finally, we analyzed also the friction force exerted by the medium on the moving impurity. All our results have been tested against direct numerical simulations finding perfect agreement.

Moving impurities are the perfect benchmark to probe systems which possess a maximum velocity for the spreading of information, leading to the natural question whether or not the

excitations of the system can cope with a fast moving defect. We show how a superluminal defect in the hopping fermion chain cannot create a LQSS: this is due by the additional $U(1)$ symmetry associated with the conservation of particles. Such a symmetry is instead absent in the Ising model. Indeed, the latter manages to produce a LQSS even for superluminal defects, which nevertheless has rather characteristic features. The superluminal LQSS is flat (i.e., ray-independent) beyond the defect up to a ray $v - v_{\mathrm{M}}$ (v_{M} the maximum excitation velocity). A part from the Ising model, the creation of a LQSS with the mentioned features is expected in all the free models, among which the hopping fermion case constitutes a remarkable exception due to the presence of additional symmetries. It remains open the difficult question of studying moving impurities in truly *interacting* integrable models. Based on the experience gained so far, a superluminal LQSS is expected in general, even though the role of $U(1)$-symmetries in these cases would require further investigation. A fundamental difficulty is that, in most cases, defects break integrability: thus a scattering approach to connect the root densities on the two sides of the defect is only possible with some level of approximation.

A promising approach consists in considering smooth defects when Generalized Hydrodynamic (see in particular Ref. [171] for the inclusion of small force fields) can be applied. However, in the free case GHD reduces to the semiclassical approach, where no superluminal LQSS is observed: in this perspective, it is unclear whether GHD has any chance to capture the physics of superluminal LQSS.

Another interesting point left aside in our analysis concerns the entanglement properties of the moving defect: the impurity produces excitations which cause the entanglement spreading. How does the entanglement propagate? Entanglement and hydrodynamics have already been successfully merged in the partitioning protocol [176], but that fell into the standard "pair structure": since the moving defect allows for several scattering channels at once, quasiparticles should be correlated beyond the standard pair structure and we expect such a problem to be best addressed with the content of Section 3.2.

Finally, it is important to clarify how the behavior we observed is affected by perturbations which break integrability of the bulk Hamiltonian. In general, we do not expect ballistic transport, thus no LQSS (either subluminal or superluminal) should emerge. However, a maximum velocity of information will still be present. This ingredient can be at the root of interesting universal phenomena.

4.2 Lack of thermalization for integrability-breaking impurities

As we have stressed many times, integrable systems behave very differently from non integrable models when driven out of equilibrium. Despite the current experimental techniques allow for exceptional precision in realizing the desired interaction, there are always corrections which can induce non integrable terms: understanding the effect of integrability-breaking perturbations is of utmost importance, for experimentalists and theoreticians as well.

What will happen to a system driven out-of-equilibrium in presence of a weak non integrability? Concerning homogeneous out-of-equilibrium protocols, nowadays the effect of weak integrability-breaking terms has been framed in the "prethermalization" paradigm [188–205]. Local observables firstly experience an apparent relaxation towards a GGE state, built on the integrable part of the Hamiltonian, but then a slow drift towards a thermal ensemble is observed, as it has been experimentally confirmed [206–209]. Regardless the strength of the intergability-breaking term, the final relaxation to a thermal state always occurs. Many studies have been directed towards prethermalization in homogeneous quenches, however, to the best of our knowledge, the effect of localized integrability-breaking terms has not been systematically assessed so far. We consider at time $t < 0$ an integrable Hamiltonian H_0, the infinite system being initialized in a suitable homogeneous GGE, then for $t > 0$ a defect is suddenly activated (4.1): differently

from the previous section, the defect is at rest $U(t,x) = U(x)$ and it will be assumed to explicitly break integrability[1]. Although the impurity breaks the integrability of the system as a whole, far from the defect the system is locally subjected to an integrable Hamiltonian characterized by stable quasi-particle excitations. Therefore, in the spirit of GHD, far from the defect the system can be locally described by a LQSS.

From this semiclassical viewpoint, quasiparticles undergo non-elastic scattering events while crossing the defect's region, leading immediately to the natural central question of the present section: how does the density root of the quasiparticles emerging from the defect look like? At large times, a finite subsystem encompassing the defect will reach a stationary state: based on the insight gained in the homogeneous case, one could expect that, because of the broken integrability, a thermal ensemble is attained after a sufficiently long time. In this case, the quasiparticles emerging from the defect should be thermally distributed. However, preliminary numerical results go against this natural expectation [210].

In this section, presenting the work of Ref. [11], we study the thermalizing properties of integrability-breaking impurities. In contrast with the homogeneous case, we show how a weak integrability-breaking defect has poor mixing properties which ultimately prevent thermalization. We focus on a free theory in the bulk, but with an interacting defect: we build a perturbative expansion of the LQSS in the strength of the interaction, which is finite at any order. For technical reasons clarified later on, we focus on continuum models which are not suited for efficient numerical methods such as DMRG [115]. However, the same questions can be posed in classical models (see Section 3.4 for the discussion of GGE and GHD in classical models), which allow for a numerical benchmark. In the highly technically challenging situation where the bulk dynamics is a truly interacting integrable model, we expect the same general conclusions to hold true in view of the following heuristic argument.

Some heuristic considerations

It is widely accepted that standard time-dependent perturbation theory [399] is not suited to study the late-time physics of thermodynamically large homogeneous systems, making necessary to resort to other methods [188, 402]. This is due to energy degeneracies, which produce secular terms that grow unbounded in time: thermalization is intrinsically a non-perturbative effect. However, simple heuristic arguments point out the possible perturbative nature of the defect. In the spirit of GHD, we semiclassically regard the initial state as a gas of quasiparticles which, for $t > 0$, undergo inelastic scattering within the support of the integrability-breaking perturbation. In the case where the domain of the perturbation is the whole system, a given quasiparticle takes part in a growing number of inelastic scatterings. Despite any scattering event mildly affects the quasiparticle, as time grows more and more scattering pile up the global effect, causing the appearance of secular terms in the perturbation theory. The mechanism is different in the impurity case: a traveling quasiparticle can undergo inelastic processes only on the defect's support, where it typically spends a finite amount of time. Therefore, small inelastic scatterings cannot sum up to an appreciable contribution, suggesting the perturbative nature of the impurity.

4.2.1 A specific model

In order to test our ideas, we consider a chain of harmonic oscillators, namely the massive Klein Gordon model

$$H_0 = \int_{-\infty}^{\infty} \mathrm{d}x \; \frac{1}{2}\Big\{\Pi^2(x) + [\partial_x \phi(x)]^2 + m^2\phi^2(x)\Big\}\,, \tag{4.55}$$

[1] In the previous section, we always remained within gaussian models and the defect was quadratic as well, thus did not spoil integrability.

where $\Pi(x)$ and $\phi(x)$ are conjugated fields $[\phi(x),\Pi(y)] = i\delta(x-y)$. Being H_0 free, is of course also integrable. Generalizations to other free models, such as Galilean-invariant bosons and fermions (see Ref. [11]), are straightforward, but they will not be considered here.

The integrability-breaking potential is chosen as a function of $\phi(x)$, i.e. $U(x) = V(\phi(x))$ on a finite support $x \in [-\Delta,\Delta]$ and zero otherwise. H_0 is diagonalized in the Fourier space in terms of bosonic operators $[\eta(k),\eta^\dagger(q)] = \delta(k-q)$ [403] and the modes are readily interpreted as the quasiparticles with energy $E(k) = \sqrt{k^2+m^2}$ and velocity $v(k) = \partial_k E(k)$.

GGEs are simply gaussian ensembles in $\eta(k)$ [332, 367, 404, 405] (and thus in the field ϕ), with the root density being associated with the mode density $\langle \eta^\dagger(k)\eta(q)\rangle = \delta(k-p)\vartheta(k)$. Therefore, the two point function computed on a GGE, denoted as $\Gamma_{t-\tau}(x-y) = \langle \phi(t,x)\phi(\tau,y)\rangle_{\rm GGE}$, is (see also Eq. (3.18))

$$\Gamma_t(x) = \int_{-\infty}^{\infty} \frac{\mathrm{d}k}{2\pi} \frac{\cos(E(k)t-kx)}{E(k)} \vartheta(k) + \frac{\cos(kx)}{2E(k)} e^{-iE(k)t} \,. \tag{4.56}$$

At large times after the defect activation a LQSS is formed (see Section 4.1), described by a ray-dependent excitation density ϑ_ζ which we parametrize as

$$\vartheta_\zeta(k) = \vartheta(k) + \Theta(|v(k)|-|\zeta|)\Theta(v(k)\zeta)\delta\vartheta(k) \,. \tag{4.57}$$

Above, Θ is the Heaviside Theta function and $\zeta = x/t$. It must be stressed that $\delta\vartheta(k)$ describes the corrections to the initial $\vartheta(k)$ caused by the defect, but the quasiparticle density flowing out of the impurity is rather $\vartheta(k)+\delta\vartheta(k)$. A better parametrization to stress the scattered distribution would have been the one used in the previous section, namely Eq. (4.32): the correspondence with Eq. (4.57) is recovered posing $\vartheta_{\rm scat}(k) = \vartheta(k)+\delta\vartheta(k)$. The current notation is more convenient in view of the forthcoming analysis.

In order to point out the poor thermalization properties of the defect, we are going to show that $\delta\vartheta(k)$ can be made arbitrarily small, making the outgoing qusiparticles distribution $\vartheta_{\rm scat}(k)$ close to $\vartheta(k)$, which can be chosen to be far from thermal. In truly interacting integrable models, Eq. (4.57) needs to be modified through a suitable dressing (see Section 3.4), but in this case $\delta\vartheta(k)$ is much more difficult to be determined and it will not be considered here. It is convenient to proceed through the equation of motion in the Heisenberg picture

$$\partial_t^2\phi_t(x) = \begin{cases} \partial_x^2\phi(x) - m^2\phi(x) - :V'(\phi(x)): & x\in[-\Delta,\Delta] \\ \partial_x^2\phi(x) - m^2\phi(x) & x\notin[-\Delta,\Delta] \end{cases} , \tag{4.58}$$

which can be equivalently reformulated in an integral equation

$$\phi(t,x) = \psi(t,x) - \int_0^\infty \mathrm{d}\tau \int_{-\Delta}^{\Delta} \mathrm{d}y\, G_{t-\tau}(x-y) :V'(\phi(\tau,y)): \,. \tag{4.59}$$

Above, $\psi(t,x)$ is the field operator evolved in absence of interaction $\psi(t,x) = e^{itH_0}\phi(0,x)e^{-itH_0}$, V' is the derivative of V and G_τ the free retarded Green Function

$$G_\tau(x) = \Theta(t)\int_{-\infty}^{\infty} \frac{\mathrm{d}k}{2\pi} \frac{e^{ikx}}{E(k)} \sin(E(k)t) \,. \tag{4.60}$$

Normal ordering ": :" must be used to remove UV singularities [403] and it can be achieved inserting proper counterterms in the potential, or equivalently dropping the vacuum contribution in the normal ordered correlators. In this respect, $\langle : \psi(t,x)\psi(\tau,y) : \rangle$ is defined as per Eq. (4.56)

dropping the "$\cos(kx)e^{-iE(k)t}/(2E(k))$" term, i.e.

$$\langle : \psi(t,x)\psi(\tau,y) : \rangle = \int_{-\infty}^{\infty} \frac{\mathrm{d}k}{2\pi} \frac{\cos(E(k)(t-\tau) - k(x-y))}{E(k)} \vartheta(k) \,. \tag{4.61}$$

The emerging LQSS

In the physical assumption that the defect's region locally relaxes to a stationary state on a finite timescale, the emergent LQSS can be derived from Eq. (4.59) and $\delta\vartheta(k)$ (4.57) completely determined in terms of correlation functions in the defect region. The time needed to the defect in order to relax contributes only as a transient, thus ineffective in the LQSS limit. Before presenting the lengthy, albeit simple, derivation we summarize the results. We define two auxiliary functions $A_{x,x'}(t)$ and $F_{x,x'}(t)$ as it follows: firstly, we pose

$$A_{x,x'}(t) = \lim_{T\to\infty} \langle : V'(\phi(t+T,x)) :: V'(\phi(T,x')) : \rangle \,, \tag{4.62}$$

where the fields are computed within the defect support and the expectation values are taken with respect to the initial conditions. Provided the defect's support relaxes to a steady state, the above limit exists: we assume this reasonable fact to hold true. The second auxiliary function $F_{x,x'}(t)$ is defined through the following convolution

$$\lim_{T\to\infty} \langle : V'(\phi(t+T,y)) : \psi(T,x') \rangle = \int_{-\infty}^{\infty} \mathrm{d}\tau \int_{-\Delta}^{\Delta} \mathrm{d}y' \, \Gamma_{-\tau}(x'-y') F_{y,y'}(t-\tau) \,. \tag{4.63}$$

Above, ϕ is always supported on the defect, while no restriction is imposed on ψ: the physical assumptions which guarantee the correctness of Eq. (4.63) are the same supporting Eq. (4.62), but extra work is needed. We postpone the discussion of Eq. (4.63) to Appendix 4.B.1, while for the time being we take it for granted.

With these definitions, emergence of the LQSS at late times can be derived and $\delta\vartheta(k)$ computed as

$$\delta\vartheta(k) = \frac{\Re(\mathcal{A}_k) - (\vartheta(k)+1)\Im(\mathcal{F}_k^+) + \vartheta(k)\Im(\mathcal{F}_k^-)}{2E(k)|v(k)|} \,, \tag{4.64}$$

where $\Re$ and $\Im$ are the real and imaginary part respectively and

$$\mathcal{A}_k = \int_{-\infty}^{\infty} \mathrm{d}\tau \int_{-\Delta}^{\Delta} \mathrm{d}y\mathrm{d}y' \, \cos\big(k(y-y') - \tau E(k)\big) \, A_{y,y'}(\tau) \tag{4.65}$$

$$\mathcal{F}_k^{\pm} = \int_{-\infty}^{\infty} \mathrm{d}\tau \int_{-\Delta}^{\Delta} \mathrm{d}y\mathrm{d}y' \, e^{\pm i(k(y-y') - \tau E(k))} F_{y,y'}(\tau) \,. \tag{4.66}$$

This relation is unperturbative and, as we said, relies on the assumption that the correlators on the impurity reach a steady state at large times: in this case the large times behavior (i.e. the LQSS) will be completely determined in terms of the mentioned correlators. We are then left with the issue of computing $A_{x,x'}(t)$ and $F_{x,x'}(t)$, which will be approached in perturbation theory in Section 4.2.2. Now we derive these results.

Hereafter, we consider the two point correlator $\langle \phi(t,x)\phi(t',x') \rangle$ at large times and far from the defect, recognizing that it can be written as if the ensemble was homogeneous, but with a space-time dependent root density (4.64). For simplicity we consider the equaltime correlator $t = t'$, but the same analysis can be performed on $t \neq t'$, leading to the same conclusions. In principle, the gaussification of the multipoint correlators (i.e. the validity of the Wick theorem) must be checked: this can be done, but it requires further lengthy calculations closely related to

those presented in Ref. [332]. Using the exact integral equation (4.59) we can surely write

$$\langle\phi(t,x)\phi(t,x')\rangle = \left\langle \left(\psi(t,x) - \int_0^\infty \mathrm{d}\tau \int_{-\Delta}^{\Delta} \mathrm{d}y\, G_{t-\tau}(x-y) : V'(\phi(\tau,y)) : \right) \right.$$
$$\left. \left(\psi(t,x') - \int_0^\infty \mathrm{d}\tau \int_{-\Delta}^{\Delta} \mathrm{d}y'\, G_{t-\tau'}(x'-y') : V'(\phi(\tau',y')) : \right) \right\rangle \quad (4.67)$$

We expand the above and consider each term separately

$$\langle\phi(t,x)\phi(t,x')\rangle = \langle\psi(t,x)\psi(t,x')\rangle +$$
$$- \int_0^\infty \mathrm{d}\tau \int_{-\Delta}^{\Delta} \mathrm{d}y \left\{ G_{t-\tau}(x'-y)\langle\psi(t,x) : V'(\phi(\tau',y)) :\rangle + G_{t-\tau}(x-y)\langle : V'(\phi(\tau,y)) : \psi(t,x')\rangle \right\} +$$
$$+ \int_0^\infty \mathrm{d}\tau\mathrm{d}\tau' \int_{-\Delta}^{\Delta} \mathrm{d}y\mathrm{d}y'\, G_{t-\tau}(x-y)G_{t-\tau'}(x'-y')\langle : V'(\phi(\tau,y)) :: V'(\phi(\tau',y')) :\rangle \quad (4.68)$$

Consider now the last row: we assume that after a finite time the correlator $\langle : V'(\phi(\tau,y)) :: V'(\phi(\tau',y')) :\rangle$ has reached a steady state and define $A_{x,x'}(t)$ as per Eq. (4.62), which we ultimately replace in the above. Any integration over a finite time window contributes as a transient with respect to the infinite time limit.

As a further technical assumption, we require the correlators on the defect to decorrelate when separated by an infinite time $\lim_{|\tau|\to\infty} A_{x,x'}(\tau) = 0$ and we assume $A_{x,x'}(\tau)$ approaches zero fast enough in order to have an integrable Fourier transform.

Subsequently, we consider a large distance-time expansions: in this respect, it is useful to consider the asymptotics of the Green function (4.60) extracted by mean of a saddle point approximation

$$G_t(x) \simeq \frac{\Theta(t)}{2\pi E(k_\zeta)} \sqrt{\frac{2\pi}{t\partial_k v(k_\zeta)}} \sin\left(tE(k_\zeta) - k_\zeta x + \pi/4\right) + \mathcal{O}(t^{-1}) \quad (4.69)$$

Above, k_ζ is the solution of the equation $\zeta = x/t = v(k_\zeta)$ where we recall $v(k) = \partial_k E(k)$ is the group velocity. Using Eq. (4.69) and with some tedious, but straightforward, calculations we find

$$\int_0^\infty \mathrm{d}\tau\mathrm{d}\tau' \int_{-\Delta/2}^{\Delta/2} \mathrm{d}y\mathrm{d}y'\, G_{t-\tau}(x-y)G_{t-\tau'}(x'-y')\langle : V'(\phi(\tau,y)) :: V'(\phi(\tau',y')) :\rangle \simeq$$
$$\int_{-\infty}^{\infty} \frac{\mathrm{d}k}{2\pi} \frac{\Theta(\zeta v(k))\Theta(|v(k)| - |\zeta|)\delta\vartheta_A(k)}{E(k)} \cos\left(k(x-x')\right) , \quad (4.70)$$

where

$$\delta\vartheta_A(k) = \frac{\Re(\mathcal{A}_k)}{2E(k)|v(k)|} \quad (4.71)$$

with $\mathcal{A}_k$ given in Eq. (4.65). We can now consider the remaining terms in Eq. (4.68), i.e. the second row. Here, provided we assume the validity of Eq. (4.63) , we can repeat the same calculations using the large distance expansion of $\Gamma_t(x)$ (4.56)

$$\Gamma_t(x) \simeq \frac{1}{2\pi}\frac{1}{2E(k_\xi)} \sqrt{\frac{2\pi}{t\partial_k v(k_\zeta)}} \left(e^{-i(tE(k_\zeta)-k_\zeta x+\pi/4)}(\vartheta(k_\zeta)+1) + e^{i(tE(k_\zeta)-k_\zeta x+\pi/4)}\vartheta(k_\zeta)\right) \quad (4.72)$$

and find that the second row of Eq. (4.68) can be written in the same form of Eq. (4.70), provided we replace $\delta\vartheta_A \to \delta\vartheta_F$

$$\delta\vartheta_F(k) = \frac{-(\vartheta(k)+1)\Im(\mathcal{F}_k^+) + \vartheta(k)\Im(\mathcal{F}_k^-)}{2|v(k)|E(k)} \tag{4.73}$$

with $\mathcal{F}_k^\pm$ defined in Eq. (4.66). Summing all the contributions we readily recognize the two point correlator $\langle\phi(t,x)\phi(t,x')\rangle$ to acquire the LQSS form, i.e. it is locally described by Eq. (4.56) with a ray dependent excitation density (4.57), where $\delta\vartheta(k) = \delta\vartheta_A(k) + \delta\vartheta_F(k)$, which is the anticipated result Eq. (4.64).

4.2.2 The perturbation theory

In the previous section we saw how the emergent LQSS, can be fully determined in terms of the steady state of correlation functions on top of the impurity, which acts as a source for the LQSS.

As we anticipated, it turns out that, differently from weak homogeneous integrability-breaking terms, localized defects allow for a perturbation theory, even at infinite times. Along this section, is our intention to convey and comment the results, avoiding technicalities as much as we can and leaving the needed details to Appendix 4.B.

From now on, we focus on the simplest example of a $\delta-$like defect (i.e. in Eq. (4.59) replace $V' \to (2\Delta)^{-1}V'$ and take $\Delta \to 0$), but see Ref. [11] for the finite interval case.

Firstly, we will address an exactly solvable case, namely a gaussian defect: being the model quadratic, in principle we could determine the LQSS from a scattering theory similarly to what we did for the moving defects in Section 4.1. However, we address the gaussian impurity from a different perspective: beside being the starting point from which we develop the perturbation theory in the interacting case, it also clarifies some aspects of the heuristic argument previously presented. For what it concerns the interacting case, a systematic treatment of the perturbative orders is best addressed through Feynman diagrams. Here we limit ourselves to general comments and the first perturbative order, while a more systematic analysis can be found in Appendix 4.B.

The gaussian defect

Let us consider a gaussian repulsive $\delta-$supported defect $V(\phi) = \mu^2\phi^2/2$. In Eq. (4.59) we compute all the fields on the defect and obtain

$$\phi(t,0) = \psi(t,0) - \mu^2 \int_0^\infty \mathrm{d}\tau\, G_{t-\tau}(0)\phi(\tau,0)\,. \tag{4.74}$$

Since we are ultimately interested in the infinite time limit and assume relaxation on the top of the defect, we can extend the time-integration domain in the infinite past. Eq. (4.74) is then reformulated in the Fourier space through the definition

$$g(\omega) = \int_{-\infty}^\infty \mathrm{d}\tau e^{-i\omega\tau} G_\tau(0)\,, \qquad g(\omega) = \begin{cases} \frac{\mathrm{sgn}(\omega)}{2i\sqrt{\omega^2-m^2}} & |\omega| > m \\ \frac{1}{2\sqrt{m^2-\omega^2}} & |\omega| < m \end{cases} \tag{4.75}$$

Above, we used Eq. (4.60) to explicitly compute the Fourier transform. Eq. (4.74) in the Fourier space states

$$\Phi(\omega) = \Psi(\omega) - \mu^2 g(\omega)\Phi(\omega)\,, \tag{4.76}$$

where Φ, Ψ are the Fourier transforms of the fields $\phi(t,0)$ and $\psi(t,0)$ (we drop the spatial dependence, since in Eq. (4.74) only the fields at $x = 0$ are needed). In its simplicity, Eq. (4.76) has

a lot to teach: even though it can be easily solved

$$\Phi(\omega) = \frac{\Psi(\omega)}{1+\mu^2 g(\omega)}\,, \tag{4.77}$$

it is worth to blindly proceed through a recursive solution, as we would have done considering μ^2 in perturbation theory

$$\Phi(\omega) = \Psi(\omega) - \mu^2 g(\omega)\Psi(\omega) + [\mu^2 g(\omega)]^2\Psi(\omega) + ... \tag{4.78}$$

This series is ill defined, since $g(\omega)$ is singular when $\omega = |m|$ (despite Eq. (4.77) being regular): such a singularity encloses a clear physical meaning. Tracking back the singularity from Eq. (4.75) to the definition of the Green function (4.60), it is evident that the singularities are due to the modes with $k = 0$, which are such that $E(k=0) = m$ and $v(k=0) = 0$. Singularities in the frequency space are translated into secular terms when read in time: as we commented while presenting our "heuristic argument", secular terms are due to quasiparticles that keep on interacting as time goes further. In the defect's case, the only quasiparticles that can interact for arbitrary long times are those sat on the impurity, i.e. having zero velocity, thus explaining the singularities in Eq. (4.78). This point will be crucial in dealing with the truly interacting case.

The unperturbed field Ψ satisfies the Wick theorem and the two point function is computed on a GGE as per Eq. (4.56), leading to

$$\langle \Psi(\omega)\Psi(\omega')\rangle = 2\pi\delta(\omega+\omega')\gamma(\omega) \tag{4.79}$$

$$\gamma(\omega) = \int_{-\infty}^{\infty} \mathrm{d}t\, e^{-i\omega t}\Gamma_t(0) = \begin{cases} 0 & |\omega| < m \\ \frac{\vartheta\left(\sqrt{\omega^2-m^2}\right)+\vartheta\left(-\sqrt{\omega^2-m^2}\right)+2\Theta(-\omega)}{2\sqrt{\omega^2-m^2}} & |\omega| \geq m \end{cases}, \tag{4.80}$$

If normal ordering is required, is sufficient to drop the "$2\Theta(-\omega)$" term in the above expression. A straightforward use of Eq. (4.77) allows to compute $\mathcal{A}_k$ and $\mathcal{F}_k^{\pm}$ and subsequently $\delta\vartheta(k)$

$$\delta\vartheta(k) = \mu^4 \frac{\vartheta(-k)-\vartheta(k)}{4E^2(k)v^2(k)+\mu^4}\,. \tag{4.81}$$

The interacting defect

We now turn on the interaction choosing $V(\phi) = \mu^2\phi^2/2 + \lambda\delta V(\phi)$, δV being a truly interacting potential and λ a parameter to tune its strength. Being δV not quadratic, we are forced to left aside any exact solution and revert to perturbation theory, in this case is crucial to select the convenient exact solution on the top of which the perturbative series is constructed.

An expansion around the solution in absence of the defect, namely $\mu^2 = \lambda = 0$ is plagued with singularities, exactly as it happens in Eq. (4.78). Again, quasiparticles with zero velocity are responsible of the break down of the perturbative expansion.

However, if we rather expand around the solution $\mu^2 > 0$, $\lambda = 0$, we are adding a repulsive potential on the defect, with the consequence that no quasiparticles with zero velocity can remain on the top of it. The perturbative expansion around $\mu^2 > 0$, $\lambda = 0$ is no longer singular. For definiteness, we focus on the explicit case $\delta V(\phi) = \phi^4/4!$, where the analogue of Eq. (4.76) is

$$\Phi(\omega) = \Psi(\omega) - \mu^2 g(\omega)\Phi(\omega) - \frac{\lambda}{3!}g(\omega)\int \frac{\mathrm{d}^3\nu}{(2\pi)^2}\,\delta\Big(\omega - \sum_{i=1}^{3}\nu_i\Big) : \prod_{i=1}^{3}\Phi(\nu_i) : \tag{4.82}$$

and can be readily recast as

$$\Phi(\omega) = \frac{1}{1+\mu^2 g(\omega)}\Psi(\omega) - \frac{\lambda}{3!}\frac{g(\omega)}{1+\mu^2 g(\omega)}\int \frac{\mathrm{d}^3\nu}{(2\pi)^2}\,\delta\Big(\omega - \sum_{i=1}^{3}\nu_i\Big) : \prod_{i=1}^{3}\Phi(\nu_i) : \ . \tag{4.83}$$

A recursive solution of the above provides a $\lambda-$expansion around the solution $\mu^2 > 0$, $\lambda = 0$ (4.77). When compared with the perturbative expansion around $\mu^2 = 0$ (4.78), a recursive solution of Eq. (4.83) is no longer singular. Indeed, singularities in Eq. (4.78) are due to the Green function, as well as to the two point correlator Eq. (4.79,4.80): however, in the recursive solution of Eq. (4.83) the propagator $g(\omega)$ always appears in the combination $g(\omega)/(1+\mu^2 g(\omega))$, which is no longer singular for $\mu^2 > 0$. Similarly, the two point correlator $\gamma(\omega)$ (4.80) always appears as $\gamma(\omega)|1+\mu^2 g(\omega)|^{-2}$, which is not singular anymore. Therefore, the perturbative series remains finite at any order and secular terms are absent.

As we already commented, a systematic treatment of the perturbative expansion is best addressed through Feynman diagrams, whose discussion is left to Appendix 4.B: here we simply quote that the $\mathcal{O}(\lambda)$ result can be obtained replacing $\mu^2 \to \mu^2 + \lambda\alpha$ in Eq. (4.81), where

$$\alpha = \int_0^\infty \frac{\mathrm{d}k}{2\pi}\frac{2E(k)v^2(k)}{4v^2(k)+\mu^4}(\vartheta(k)+\vartheta(-k))\,. \tag{4.84}$$

Our choice of considering a continuum model can be finally motivated: lattice systems have a bounded dispersion law, which leads to self-trapping and to the formation of boundstates even in the case of repulsive potentials [406].

Semiclassically, it can be explained as it follows: imagine we turn on a repulsive potential of strength $U > 0$ in the defect region. A particle initially sat on the defect with momentum k, after the potential activation, will have a total energy $E(k) + U$, being $E(k)$ the kinetic energy. Due to energy conservation, the particle can leave the defect with a momentum k' only if $E(k) + U = E(k')$: however, if the kinetic energy is bounded and U is large enough there are not solutions to this equation. Therefore, despite the potential being repulsive, the particle is doomed to live within the defect region, thus forming a bound state. A more precise analysis through a specific example can be found in Ref. [11]. Bound states necessarily causes singularities in $g(\omega)/(1+\mu^2 g(\omega))$ that eventually plague the recursive solution of Eq. (4.83) (see Ref. [11]). We would have faced a similar issue in the continuum case considering an attractive potential $\mu^2 < 0$ rather than repulsive $\mu^2 > 0$.

A rightful question concerns the convergence of the perturbative expansion: indeed, albeit being the latter finite order by order, this does not suffice to establish the existence of a finite convergence radius. On the other hand, the physical motivations that broke perturbation theory in the homogeneous case are absent in the impurity case. Morevoer, in the analogue classical case discussed hereafter, the convergence of the perturbation theory can be proven (for the proof, see Ref. [11]). In view of these facts, we are confident for what it concerns the trustability of the expansion even in the quantum case.

The classical case and the numerical benchmark

So far, we have focused on a quantum model, but the Hamiltonian (4.55) can be also regarded as a classical object, functional of the classical fields ϕ and Π, similarly to what we have done in Section 3.4. Hereafter, we enlist the minor changes between the quantum and classical case, we attach a superscritp "cl" to distinguish the classical version of the previous quantities. The GGE correlator (4.56) retains the same form even in the classical case, provided we drop the "$\cos(kx)e^{-iE(k)t}/(2E(k))$" contribution, which in the quantum case was due to the non trivial

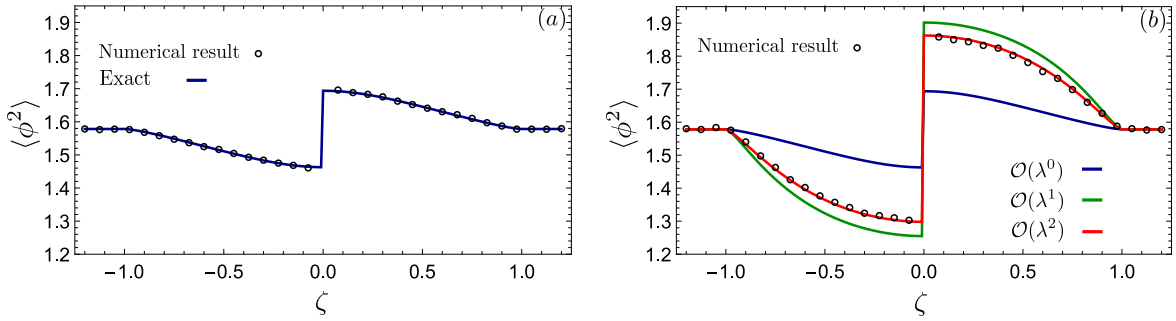

Figure 4.6: *Within the classical theory, the analytic prediction for the LQSS is tested against the numeric simulation for a $\delta-$supported defect $V(\phi) = \mu^2\phi^2/2 + \lambda\phi^4/4!$. In particular, the profile of $\langle\phi^2\rangle$ as function of the ray $\zeta = x/t$ is plotted. Subfigure (a): $\mu = 1$, $\lambda = 0$, the exact result (4.81) is available. Subfigure (b): $\mu = 1$, $\lambda = 3$, the first orders in the perturbative series are considered (details in Appendix 4.B.1). In both cases the initial GGE is chosen $\vartheta^{\rm cl}(k) = 1/\left[(\beta E(k) + \beta_2 k)(e^{r(|k|-c)} + 1)\right]$ with $\beta = 0.5$, $\beta_2 = 0.4$, $r = 2$, $c = 20$ and bulk mass $m = 1$. The state is a boosted thermal state (asymmetry in $k \to -k$ guarantees non trivial LQSS (4.81)) with an additional UV cut off to improve the numerical discretization (see also Appendix 4.C). Figure taken from Ref. [11].*

commutator of the modes. Thus we get

$$\Gamma_t^{\rm cl}(x) = \int_{-\infty}^{\infty} \frac{{\rm d}k}{2\pi} \frac{\cos(E(k)t - kx)}{E(k)} \vartheta^{\rm cl}(k)\,. \tag{4.85}$$

Above, $\vartheta^{\rm cl}$ is the classical filling. The Green function (4.60) and the equation of motion (4.59) do not change, but the normal ordering is now absent. The definitions of the $A_{x,x'}(t)$ and $F_{x,x'}(t)$ functions Eq. (4.62) and Eq. (4.63) remain the same (without normal ordering), while in the definition of $\delta\vartheta^{\rm cl}(k)$ Eq. (4.64) we must replace $\vartheta^{\rm cl}(k) + 1 \to \vartheta^{\rm cl}(k)$, thus

$$\delta\vartheta^{\rm cl}(k) = \frac{\Re(\mathcal{A}_k) - \vartheta^{\rm cl}(k)\Im(\mathcal{F}_k^+) + \vartheta^{\rm cl}(k)\Im(\mathcal{F}_k^-)}{2E(k)|v(k)|}\,. \tag{4.86}$$

Incidentally, the classical and quantum results for the gaussian defect (4.81) and the $\mathcal{O}(\lambda)$ order in the interacting case (4.84) coincide. As anticipated, the classical theory is suited for a numerical simulation: in Fig. 4.6 we test the gaussian impurity and the first two perturbative orders in the interacting case, finding excellent agreement. The analytical expression of the second perturbative order can be found in Appendix 4.B, for a discussion of the numerical methods see instead Appendix 4.C.

4.2.3 Concluding remarks

Along this section we considered the issue of suddenly activating an integrability-breaking localized perturbation, in an otherwise homogeneous integrable model. In contrast with the homogeneous case, which is intrinsically non-perturbative and eventually leads to thermalization, the localized impurity has less dramatic mixing properties being, at least in the example analyzed, relegated to perturbative effects. In the case where the bulk theory is free, our claim is supported by an order-by-order finite perturbative expansion constructed on top of a gaussian repulsive defect. Our analysis opens to several interesting directions.

First of all, non-perturbative effects are present in lattice systems, due to the phenomenon of self trapping: however, in view of our heuristic considerations, small integrability-breaking

defects are expected to do not lead to thermalization, as numerically observed in [210].

Properly including the effect of bound states in the analysis we presented is an urgent matter, since it would give access to study lattice systems. In particular, quantum lattice systems are of utmost importance for experiments and are suited for numerical benchmarks (DMRG).

Another interesting point concerns the defect's size, whose growth could lead to a crossover in its thermalizing properties. We can expect that as the defect support is increased, the behavior of the integrability-breaking region becomes much closer to a thermodynamic system, which should thermalize due to integrability breaking.

Another interesting setup to be analyzed is that of finite sizes: let us imagine that, instead of considering an infinite system, we focus on a finite ring of length L with periodic boundary conditions. Suddenly, we activate the defect and let the system to evolve. In the infinite system case, the excitations do not thermalize because they spend a finite amount of time on the defect, then flew away without undergoing further inelastic processes. However, when we consider the ring of finite length L, quasiparticles come back infinite times on the impurity, where they pile up inelastic effects. Does it sufficie to cause thermalization? For very large system sizes L, we expect the hydrodynamic approach to be correct and the problem could be studied by mean of a simple generalization of our findings. Finally, quantitative results in truly interacting integrable models are surely a compelling quest.

4.A Scattering theory for moving defects

This Appendix supports Section 4.1, in particular it is devoted to some technical details needed in the derivation of the LQSS formula Eq. (4.32). First of all, we enlist some useful symmetries. Using that in the fermionic field ψ_j the first component is the Hermitian conjugated of the second (and this is reflected on a symmetry of the Green function) leads us to the conclusion

$$E^a(k) = -E^{\bar{a}}(-k), \;\; v^a(k) = v^{\bar{a}}(-k), \;\; \sigma^x u_{k,a} = (u_{-k,\bar{a}})^* \tag{4.87}$$

with $a = 1$ or 2 and $\bar{a} = 2$ or 1 respectively. A similar symmetry holds for the wavefunctions $\phi_{k,a}$ which must ultimately obey

$$\phi_{k,a} = \sigma^x (\phi_{-k,\bar{a}})^* \tag{4.88}$$

and leads to an useful symmetry of the scattering amplitudes

$$S_{b,a}(q,k) = \left[S_{\bar{b},\bar{a}}(-q,-k) \right]^* . \tag{4.89}$$

Other important constraints obeyed by the scattering amplitudes are certain *sum rules* derived by the orthonormality and completeness of the eigenfunctions $\phi_{k,a}$. The two sum rules involve a sum over the incoming and outgoing momenta respectively

$$\delta(k-k')\delta_{a,a'} = \sum_{b=1,2} \int \mathrm{d}q \, \delta(E^a(k) - E^b(q)) \delta(E^a(k') - E^b(q)) [S_{a,b}(k,q)]^* S_{a',b}(k',q) |v^a(k)|^2 , \tag{4.90}$$

$$\delta(k-k')\delta_{a,a'} = \sum_{b=1,2} \int \mathrm{d}q \, \delta(E^a(k) - E^b(q)) \delta(E^{a'}(k') - E^b(q)) [S_{b,a}(q,k)]^* S_{b,a'}(q,k') \left| v^b(q) \right|^2 . \tag{4.91}$$

Which can be derived from the completness and orthonormality relations (4.25) respectively: indeed, the singular behavior of Eq. (4.25) is due to the asymptotic part of the wavefunction (4.29), thus imposing Eq.(4.25) is translated into constraints on the scattering amplitudes.

Even though not difficult, their derivation requires some lengthy manipulations and will not be reported, see however Ref. [9] for a derivation in the hopping fermions case.

With the help of the sum rules, the late-time behavior of the Green function can be extracted and from this the LQSS. Rather than considering the Green function in the coordinate space, it is more convenient to take a Fourier transform with respect to the second coordinate. In this way, the connection between the continuous and the lattice model is best displayed, as it is clear from Eq. (4.20). Applying the desired Fourier transform to the decomposition (4.23), we reduce ourselves to compute

$$\mathcal{G}'_{x,k} = \sum_{a=1,2} \int \frac{\mathrm{d}q}{2\pi} e^{-iE(q,a)t} \phi_{q,a}(x) \int \mathrm{d}x' \, \phi^\dagger_{q,a}(x') e^{ikx'} \tag{4.92}$$

and we focus on the limit of large times and far from the defect. In this assumption we can *i)* compute $\int \mathrm{d}x' \, \phi^\dagger_{q,a}(x') e^{ikx'}$ replacing the wavefunction with its approximation in the scattering region and *ii)* use the same approximation for $\phi_{q,a}(x)$ as well. In computing the scalar product we face the Fourier transform of the Heaviside theta

$$\int \mathrm{d}x' \, \phi^\dagger_{q,a}(x') e^{ikx'} \simeq \frac{1}{\sqrt{2\pi}} \left(\frac{i u^\dagger_{q,a}}{\mathrm{sgn}(-v^a(q))(k-q) + i0^+} + \right.$$
$$\left. \sum_{b=1,2} \int \mathrm{d}q' \, \frac{i\delta(E^a(q) - E^b(q'))\Theta(x v^b(q'))|v^b(q')| S^*_{b,a}(q',q)}{\mathrm{sgn}(v^b(q'))(k-q') + i0^+} u^\dagger_{q',b} \right), \tag{4.93}$$

where "sgn" is the sign function. This scalar product must now be used in (4.92): in the large time limit all the smooth contributions in k vanish, only the singular parts of the above scalar product matters. These singularities, combined with the oscillating exponentials in $\phi_{q,a}(x)$, contribute again as Fourier transforms of Heaviside Theta functions leading to the final result (in the same notation of Eq. (4.20))

$$\tilde{\mathcal{G}}_{x,k}(t) \simeq \sum_{a=1,2} \frac{e^{-iE^a(k)t}}{2\pi} \left[(\Theta(-\zeta v^a(k)) + \Theta(\zeta v^a(k))\Theta(|\zeta| - |v^a(k)|)) e^{ikx} u_{k,a} + \right.$$
$$\left. \sum_{b=1,2} \int \mathrm{d}q \, \delta(E^b(q) - E^a(k)) \theta(|v^b(q)| - |\zeta|) \Theta(\zeta v^b(q)) |v^b(q)| S_{b,a}(q,k) e^{iqx} u_{q,b} \right] u^\dagger_{k,a}, \tag{4.94}$$

valid in the large time limit, where ζ is the ray x/t in the defect reference frame. The sum rule (4.90) is crucial in the simplification of the squared scattering amplitudes that arise while evaluating Eq. (4.92). The asymptotic form of the Green function can now be used in the computation of the two point correlators and the large distance/time behavior extracted. It must be said that corrections to the scattering wavefunction (4.29) decay exponentially fast away from the defect and the Green function (4.94) is valid in the same regime, provided the long time limit has been taken. However, when the Green function is used in the two point correlators to derive the LQSS, a further long distance approximation must be invoked, in order to get rid of space-oscillating terms. With this caveat, recognizing in the two point correlator a local GGE with density root (4.32) is a matter of a long and tedious (but straightforward) computation, where the symmetries and the sum rules presented at the beginning of the Appendix play a fundamental role in simplifying many terms.

The oscillating terms discarded in the last passage we mentioned, thus coming from the interference of different scattering channels, can be quite slowly damped in the distance from the defect, nevertheless they vanishes in the LQSS limit. However, it must be said that while these

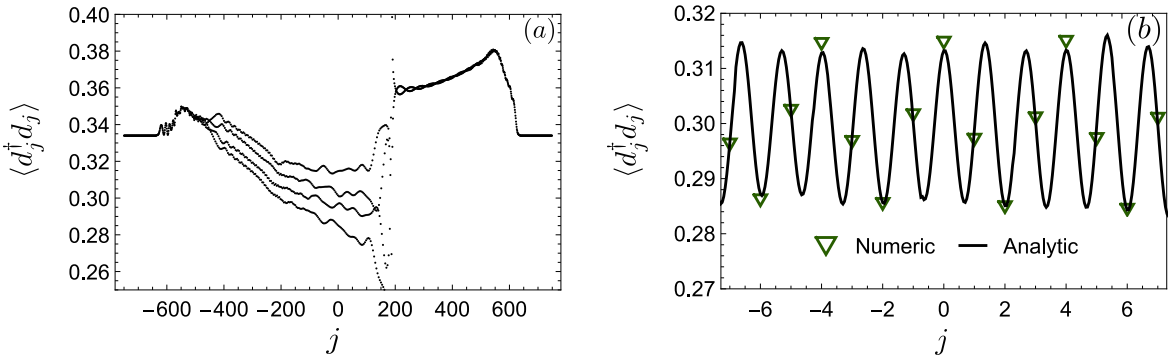

Figure 4.7: *Hopping fermions. Density profile generated by a delta-like potential $V(x) = c\delta(x)$ with $c = 0.5$, $v = 0.3$ and $k_f = \pi/3$ at time $t = 620$. Subfigure (a): the numerical result of the whole density profile is displayed, showing slow vanishing oscillations on the left of the defect (placed where the discontinuity occurs). Subfigure (b): the density profile is zoomed in a few-sites region around zero and the numerics is compared with the analytic prediction.*

oscillations are not captured by the LQSS, the scattering theory is still sufficient in describing them: using Eq. (4.94) to evaluate the two point function, but without discarding the oscillatory terms, we get good agreement (see Fig. 4.7).

4.B Feynman diagrams for Section 4.2

Feynman diagrams are a central tool in handling interacting systems: they constitute a remarkably compact way of representing a complicated perturbative expansion. Furthermore, partial resummations of the perturbative series are most easily carried out playing with the graphical representation, which sometimes gives access even to non-perturbative information. A detailed step-by-step discussion of the Feynman diagrams lays outside our current purposes, therefore we confidently assume the reader to be already familiar with the method (a complete discussion can be found in Ref. [403], as well as in several other textbooks) and outline the Feynman rules we need. Here we present two sets of Feynman rules: the first concerns the representation of the iterative solution of the equation of motion Eq. (4.59) as it stands. We already commented how such an expansion is plagued by singularities, but its formal representation allows for a justification of Eq. (4.63). Subsequently, we instead discuss the diagrammatic representation of the iterative solution of Eq. (4.83) (thus, we focus on the $\delta-$like potential), which allows a perturbative computation of the LQSS, i.e. the analytic prediction tested in Fig. 4.6.

4.B.1 Justification of Eq. (4.63)

We now consider the iterative solution of Eq. (4.59). Our ultimate goal is a Feynman-diagram representation of the correlation functions, which can be achieved in two subsequent steps

1. Represent through Feynman diagrams the iterative solution of the integral equation Eq. (4.59).

2. Compute the correlation functions taking as input the previous step.

Assume for simplicity $V(\phi) = \frac{\lambda}{n!}\phi^n$, generalizations to arbitrary Taylor expandable potentials will appear clear, thus $V'(\phi) = \frac{\lambda}{(n-1)!}\phi^{n-1}$. We represent each interaction by mean of a vertex with n departing legs. The Green function G is associated with a dashed line. The recursive solution of Eq. (4.59) is then represented through all the possible tree-like diagrams (i.e. no loops) constructed with the following rules

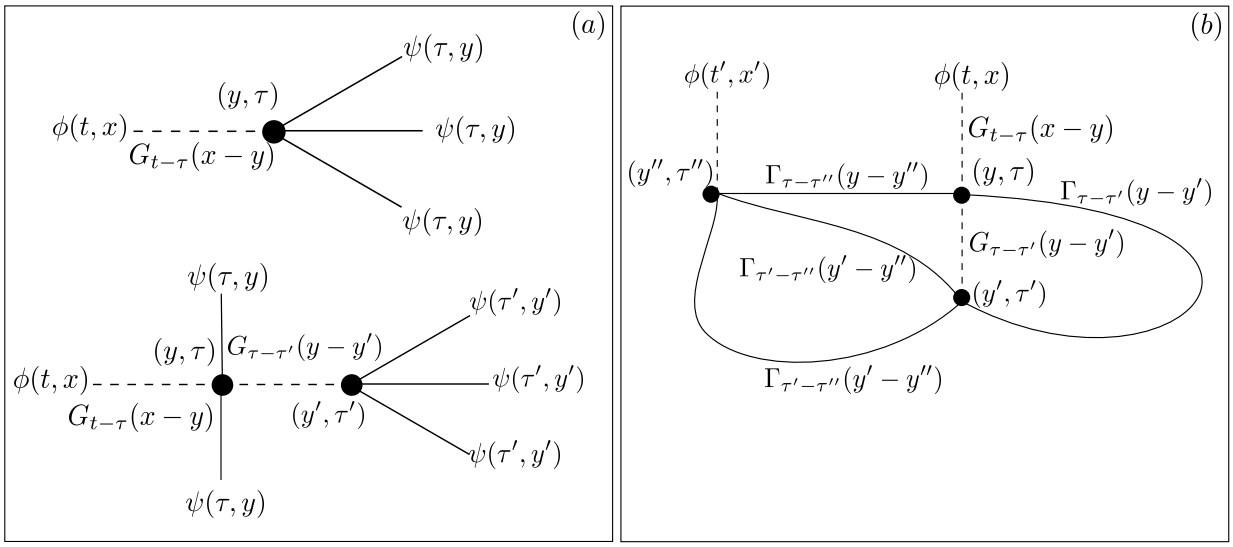

Figure 4.8: *(a) Tree level Feynman diagrams appearing in the recursive solution of Eq.* (4.59) *for* $V(\phi) = \lambda\phi^4/4!$*, (b) Feynman diagrams representing correlators: these are obtained joining together the external legs of the graphs representing the iterative solution of Eq.* (4.59)*. As an example, we construct a graph joining together the two diagrams of panel* (a)*. Figure taken from Ref. [11].*

- External legs are such that one (dashed) is associated with the desired solution $\phi(t,x)$, the others to the unperturbed solutions ψ computed at the time and position of the vertex to which they are attached.
- Internal legs are mediated by the dashed lines associated with the Green function that are thus attached to two vertexes. The coordinates appearing in G are those of the two vertexes.
- The $1/(n-1)!$ contribution of each vertex is (almost) canceled by the sum of several equivalent diagrams. In this perspective, each interaction vertex contributes simply as $-\lambda$.
- Each graph must be divided by an overall symmetry factor, which is equal to the number of permutations of legs which do not change the topology of the graph.
- After an integration of the space/time coordinates of the vertexes on the suitable domain, $\phi(t,x)$ is obtained summing over all the possible graphs.

An example is depicted in Fig. 4.8(a). From these Feynman diagrams we can now construct those of the correlation functions: consider for example the case of the two point correlator $\langle\phi(t,x)\phi(t',x')\rangle$, the generalization to multipoint correlators will appear trivial. Within a recursive solution of Eq. (4.59), correlators of $\phi(t,x)$ are obtained by mean of a repetitive use of the Wick theorem on the fields ψ. Therefore, the Feynman diagrams associated with the correlator can be constructed as it follows: choose one Feynman diagram in the representation of $\phi(t,x)$ and one concerning $\phi(t',x')$, then connect pairwise together all the possible external lines associated with the fields ψ. These new internal lines are associated with the correlator $\langle\psi\psi\rangle$, therefore with Γ (4.56). Γ must be evaluated at positions and times equal to the difference of the coordinates of the two vertexes which are connected by Γ. Normal ordering on Γ must be used if the line starts and ends at the same vertex. An example is depicted in Fig. 4.8(b). Finally, all the possible choices among the Feynman diagrams contributing to ϕ must be considered and connected together in all the possible ways: this generates all the Feynman diagrams associated with the correlator.

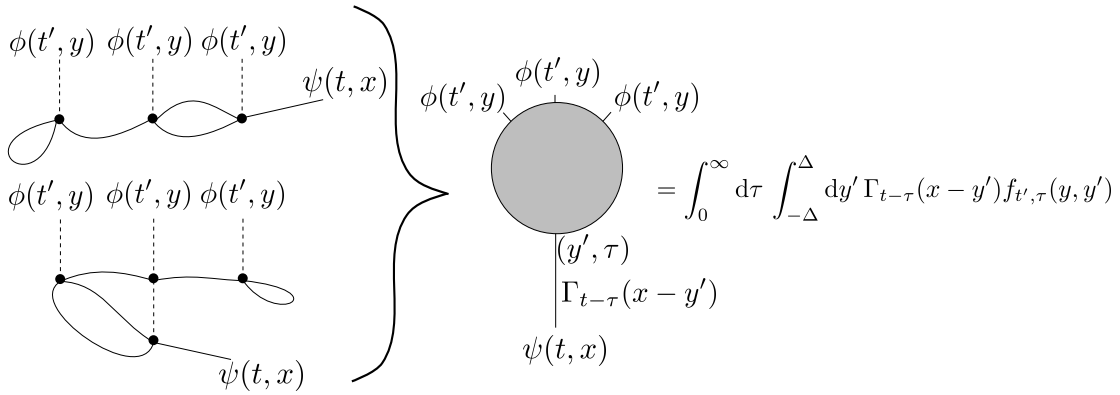

Figure 4.9: *Feynman diagrams representing $\langle : V'(\phi(t',y)) : \psi(t,x)\rangle$, where we used as an example $V'(\phi) = \lambda\phi^3/3!$. All the possible diagrams we can draw have the same structure, which is then promoted to be an exact identity. Figure taken from Ref. [11].*

In this respect, it is convenient to reconsider the symmetry factor as it follows: compute the contribution of the Feynman diagram of the single field ϕ ignoring the symmetry factors and, after the Feynman diagram of the correlator has been constructed, divide by the number of permutations of leg and vertexes which leave the diagram the same. Finally, the expansion of the correlator is obtained summing over all the distinct Feynman graphs.

We can now justify Eq. (4.63) at any order in the diagrammatic expansion: consider the diagrams for $\langle : V'(\phi(t',y)) : \psi(t,x)\rangle$, which are obtained expanding $: V'(\phi(t',y)) :$ and then contracting the resulting graphs with $\psi(t,x)$ (see Fig. 4.9). When the field $\psi(t,x)$ is contracted with a ψ field contained in the expansion of $: V'(\phi(t',y)) :$, the latter is always constrained on the defect support. Therefore, any Feynman diagram in the expansion of $\langle : V'(\phi(t',y)) : \psi(t,x)\rangle$ can be written in the following form, that we promote to be an identity of the correlator itself

$$\langle V'(\phi(t',y)) : \psi(t,x)\rangle = \int_0^\infty \mathrm{d}\tau \int_{-\Delta}^{\Delta} \mathrm{d}y' \, \Gamma_{t-\tau}(x-y') f_{t',\tau}(y,y') \,, \tag{4.95}$$

where the function $f_{t,\tau}(y,y')$ contains the contribution of all the Feynman diagrams. If we require the correlator to reach a stationary state on the defect, we are forced to impose *i)* $f_{t',\tau}(y,y')$ to become time translational invariant $f_{t',\tau}(y,y') = f_{t'+T,\tau+T}(y,y')$ and *ii)* decaying fast enough in $|t-\tau| \to \infty$ in such a way we can safely extend the time integration from $\tau \in [0,+\infty)$ to $\tau \in (-\infty,\infty)$. In this case, we are naturally lead to Eq. (4.63).

4.B.2 The perturbative analysis of the $\delta-$defect

We now analyze the perturbative LQSS of the $\delta-$like defect, more specifically we focus on the ϕ^4 interaction and then look at the recursive solution of Eq. (4.83), here reported for convenience

$$\Phi(\omega) = \frac{1}{1+\mu^2 g(\omega)} \Psi(\omega) - \frac{\lambda}{3!} \frac{g(\omega)}{1+\mu^2 g(\omega)} \int \frac{\mathrm{d}^3\nu}{(2\pi)^2} \, \delta\Big(\omega - \sum_{i=1}^{3} \nu_i\Big) : \prod_{i=1}^{3} \Phi(\nu_i) : \,. \tag{4.96}$$

In principle, we should now compute $\langle : V'(\phi(t,0)) :: V'(\phi(t',0)) :\rangle$ and $\langle : V'(\phi(t,0)) : \psi(t',0)\rangle$, then from these extract the functions A and F from their definitions Eq. (4.62,4.63). However, the needed Feynman diagrams are complicated even at the first orders. In this respect, it is more convenient to express the desired correlators in terms of simpler correlation functions, using the integral equation (4.59) (in which we extend the time integration domain up to $-\infty$,

being focuses on the late time behavior). We introduce the definitions

$$d(\omega) = \int_{-\infty}^{\infty} \mathrm{d}t\, e^{-i\omega(t-t')} \langle \phi(t,0)\psi(t',0)\rangle\,, \qquad c(\omega) = \int_{-\infty}^{\infty} \mathrm{d}t\, e^{-i\omega(t-t')} \langle \phi(t,0)\phi(t',0)\rangle\,. \quad (4.97)$$

In the long time limit, the system locally relaxes and the two point correlator acquires time translation invariance, thus the above expression is independent on the actual value of t'. With the definitions above, it is not hard to get the following identities (for example, the first one is obtained multiplying $\psi(t',0)$ to both sides of Eq. (4.59), taking the expectation value and then going in the Fourier space)

$$d(\pm E(k)) = \frac{\gamma(\pm E(k))}{1+\mu^2 g(\pm E(k))} - \frac{g(\pm E(k))}{1+\mu^2 g(\pm E(k))}\left[\gamma(\pm E(k))\mathcal{F}_k^{\pm} - \mu^2 d(\pm E(k))\right] \quad (4.98)$$

which leads to

$$\mathcal{F}_k^{\pm} = \frac{\gamma(\pm E(k)) - d(\pm E(k))}{g(\pm E(k))\gamma(\pm E(k))}\,. \quad (4.99)$$

With similar passages it can be found

$$\mathcal{A}_k = \frac{1}{2g(E(k))g(-E(k))}\Big[c(E(k)) + c(-E(k)) - \gamma(E(k)) - \gamma(-E(k)) + 2g(E(k))\gamma(E(k))\mathcal{F}_k^{+} + 2g(-E(k))\gamma(-E(k))\mathcal{F}_k^{-}\Big]\,. \quad (4.100)$$

We are thus left with the simpler problem of computing certain two point functions $c(\omega)$ and $d(\omega)$, then from these $\mathcal{A}_k$ and $\mathcal{F}_k^{\pm}$ easily follow. Notice that from the definitions of $c(\omega)$ and $d(\omega)$ Eq. (4.97) we clearly have

$$\langle \Phi(\omega)\Phi(\omega')\rangle = 2\pi\delta(\omega+\omega')c(\omega)\,, \qquad \langle \Phi(\omega)\Psi(\omega')\rangle = 2\pi\delta(\omega+\omega')d(\omega)\,. \quad (4.101)$$

The Feynman diagrams needed to describe the solution of Eq. (4.96) and the correlators can be constructed similarly to what we did in Section 4.B.1, however they are best described in the Fourier space. The rules are the following. The perturbative solution of $\Phi(\omega)$ is represented as tree-like Feynman diagrams. The interaction vertex is a dot with $4-$ departing legs (in the case of $\delta V(\phi) = \lambda/n!\phi^n$ we would have had n legs), which can be either dashed or continuum.

- One external leg is associated with Φ, the others to the fields Ψ. At this level, all the internal lines are dashed lines and are associated with the dressed Green function $\tilde{g}(\omega) = g(\omega)/(1+\mu^2 g(\omega))$. The external line associated with $\Phi(\omega)$ is a dashed line, while all the others are continuum lines.
- In order to construct the correlator $\langle \Phi(\omega)\Phi(\omega')\rangle$, draw together two of the diagrams described above and join pairwise all the continuum lines. When computing $\langle \Phi(\omega)\Psi(\omega')\rangle$, draw a Feynman diagram associated with $\Phi(\omega)$ and connect all the continuum lines except one, which remains an external leg associated with $\Psi(\omega')$.
- Each line carries its own frequency ν and it must have its own direction, along which ν flows. Continuous internal lines are associated with $\tilde{\gamma}(\nu) = \gamma(\nu)/|1+\mu^2 g(\nu)|^2$, while the external continuous line associated with $\Psi(\omega')$ contributes as $\gamma(\omega')/(1+\mu^2 g(\omega'))$.
- Each vertex carries a $-\lambda 2\pi\delta(\sum_i \pm_i \nu_i)$ factor, where ν_i are the frequencies flowing into the vertex. The sign $\pm_i$ is chosen $+$ if the frequency flows into the vertex, $-$ in the other case.

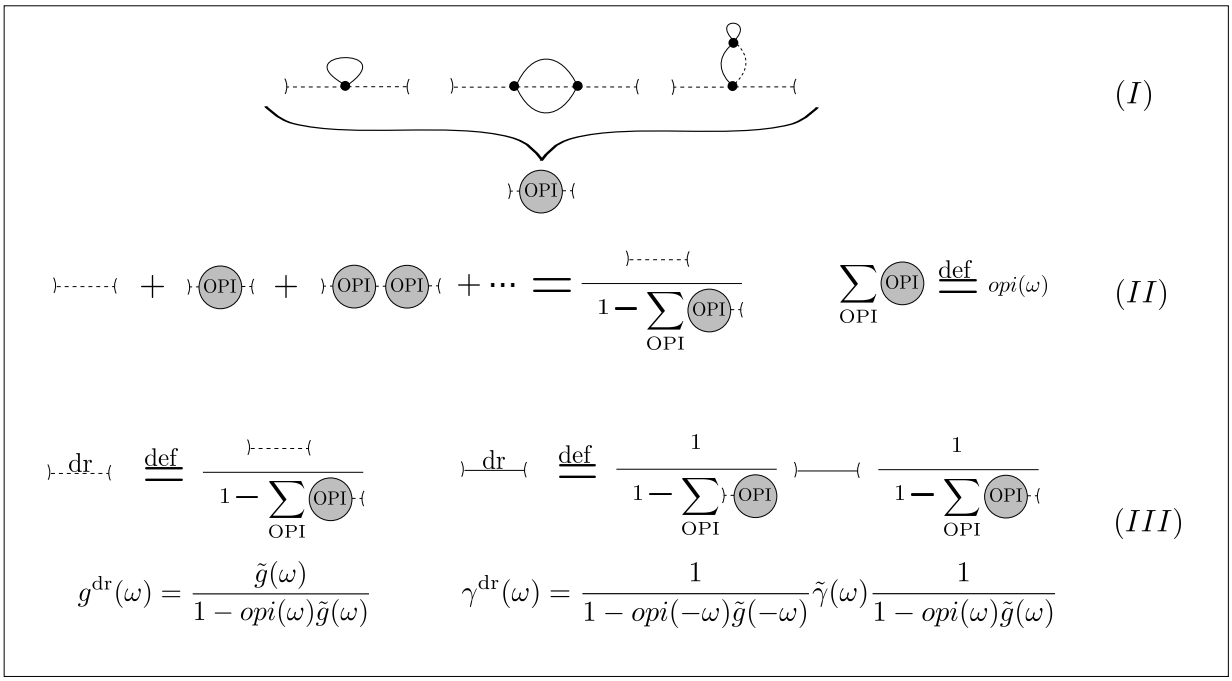

Figure 4.10: *A few examples of OPIs (I). Several graphs can be constructed attaching together OPIs and forming "chains" of arbitrary length (II): the contribution of these graphs can be easily resummed as a geometric series, which can be absorbed in a dressing of $\tilde{g}$ and $\tilde{\gamma}$ (III). Figure taken from Ref. [11].*

- Integrate over all frequencies ν_i of the graph, with a measure $\mathrm{d}\nu_i/(2\pi)$.
- Divide for the symmetry factor, i.e. the number of permutations of internal legs which leave the graph unchanged, and sum all the possible diagrams.

With these rules we can systematically compute the contribution up to the desired order in λ. We stress that each graph is constructed using as building blocks $\tilde{\gamma}(\nu)$ and $\tilde{g}(\nu)$, both of them being non singular and decaying as $\sim \nu^{-1}$ for large frequencies: once normal ordering has been considered, all the integrals are UV convergent. Thus, all the terms of the expansions are finite.

The formalism of Feynman diagrams can be even pushed further, performing partial resummations of the graphs.

In this respect, a key role is played by the one-particle irreducible (OPI) graphs. We borrow the same notation of high-energy physics and the reader can refer to Ref. [403] for a pedagogical and extensive discussion of diagrammatic techniques and OPI resummation. The OPIs in our case are defined as "blocks" such that they can be disconnected from the whole diagram cutting two dashed lines. Moreover, these blocks cannot be further disconnected cutting a single additional dashed line: a few examples are given in Fig. 4.10. Several graphs can be obtained composing together OPIs (Fig. 4.10): because of frequency conservation, the frequencies in the incoming and outgoing legs of an OPI must be the same. This enormously simplifies evaluating

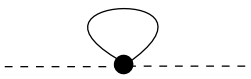

Figure 4.11: *The only $\mathcal{O}(\lambda)$ graph that can be drawn has a single interaction vertex, a loop and two departing legs. Above we represented the departing legs as dashed lines, but one of the two can also be chosen to be continuous. This is clearly an OPI graph. Figure taken from Ref. [11].*

the blocks constructed composing together several OPIs, whose sum is a simple geometric series and can be absorbed in a "dressing" of the dashed and continuous lines (see again Fig. 4.10). When computing Feynman diagrams, we can replace the continuum and dashed lines with their dressed counterparts: of course, in the "dressed" Feynman diagrams we should avoid any OPI, since their contribution has already been taken in account.

We can finally use the constructed machinery to compute the needed correlators, for the time being we focus on the $\mathcal{O}(\lambda)$ contribution. At this order, we can construct only one Feynman diagram (Fig. 4.11), which is clearly an OPI: using this graph in the dressing procedure, we get

$$\langle \Phi(\omega)\Phi(\omega')\rangle = 2\pi\delta(\omega+\omega')\frac{1}{1+\lambda\alpha\tilde{g}(-\omega)}\tilde{\gamma}(\omega)\frac{1}{1+\lambda\alpha\tilde{g}(\omega)} + \mathcal{O}(\lambda^2) \tag{4.102}$$

$$\langle \Phi(\omega)\Psi(\omega')\rangle = 2\pi\delta(\omega+\omega')\frac{1}{1+\lambda\alpha\tilde{g}(\omega)}\frac{1}{1+\mu^2 g(-\omega)}\gamma(\omega) + \mathcal{O}(\lambda^2) \tag{4.103}$$

The neglected graphs contribute as $\mathcal{O}(\lambda^2)$. The constant α comes from the loop (Fig. 4.11) (the prefactor $1/2$ is the symmetry factor)

$$\alpha = \frac{1}{2}\int_{-\infty}^{\infty}\frac{\mathrm{d}\omega}{2\pi} : \gamma^{\mathrm{dr}}(\omega) := \int_0^{\infty}\frac{\mathrm{d}k}{2\pi}\frac{2E(k)v^2(k)}{4v^2(k)+\mu^4}(\vartheta(k)+\vartheta(-k)) \tag{4.104}$$

With the double dots, we mean the normal ordering must be considered. Using now the relations (4.99), (4.100) and (4.101) we can compute $\mathcal{A}_k$ and $\mathcal{F}_k$, and finally $\delta\vartheta(k)$ through Eq. (4.64). This requires only simple algebraic manipulations and leads to the compact result

$$\delta\vartheta(k) = \frac{(\mu^2+\lambda\alpha)^2}{4E^2(k)v^2(k)+(\mu^2+\lambda\alpha)^2}\Big[\vartheta(-k)-\vartheta(k)\Big] + \mathcal{O}(\lambda^2) \tag{4.105}$$

which has the same form of the non-interacting case (4.81), provided we replace $\mu^2 \to \mu^2+\lambda\alpha$. Incidentally, the expression of the first order in the quantum and classical case coincide. Computing the next order in $\delta\vartheta$ is more cumbersome and involves several diagrams. For completeness, hereafter we report the result within the classical realm used in Fig. 4.6

$$c(\omega) = \gamma_{\mathrm{dr}}(\omega) + 2\Re\left[\frac{\lambda^2}{2}\gamma^{(1)}_{\mathrm{dr}}g^{(1)}_{\mathrm{dr}}(\omega)\left(I_1(\omega)+I_0I_3\right)\right] + \frac{\lambda^2}{6}I_2(\omega)|g_{\mathrm{dr}}(\omega)|^2 + \mathcal{O}(\lambda^3) \tag{4.106}$$

$$d(\omega) = \left[1+\frac{\lambda^2}{2}g^{(1)}_{\mathrm{dr}}(\omega)\left(I_1(\omega)+I_3I_0\right)\right]\frac{\gamma(\omega)}{1+(\mu^2+\alpha\lambda)g(\omega)} + \mathcal{O}(\lambda^3) \tag{4.107}$$

where the auxiliary functions are defined as:

$$g^{(1)}_{\mathrm{dr}}(\omega) = \frac{g(\omega)}{1+(\mu^2+\lambda\alpha)g(\omega)}, \qquad \gamma^{(1)}_{\mathrm{dr}}(\omega) = \left|\frac{1}{1+(\mu^2+\lambda\alpha)g(\omega)}\right|^2\gamma(\omega) \tag{4.108}$$

$$G^{(1)}_{\mathrm{dr}}(t) = \int_{-\infty}^{\infty}\frac{\mathrm{d}\omega}{2\pi}e^{i\omega t}g^{(1)}_{\mathrm{dr}}(\omega), \qquad \Gamma^{(1)}_{\mathrm{dr}}(t) = \int_{-\infty}^{\infty}\frac{\mathrm{d}\omega}{2\pi}e^{i\omega t}\gamma^{(1)}_{\mathrm{dr}}(\omega) \tag{4.109}$$

$$I_0 = \int_0^{\infty}\frac{\mathrm{d}k}{2\pi}2\Re\left[\gamma^{(1)}_{\mathrm{dr}}(E(k))|v(k)|g^{(1)}_{\mathrm{dr}}(E(k))\right], \qquad I_1(\omega) = \int_{-\infty}^{\infty}\mathrm{d}te^{-i\omega t}\left[\Gamma^{(1)}_{\mathrm{dr}}(t)\right]^2G^{(1)}_{\mathrm{dr}}(t) \tag{4.110}$$

$$I_2(\omega) = \int_{-\infty}^{\infty}\mathrm{d}te^{-i\omega t}\left[\Gamma^{(1)}_{\mathrm{dr}}(t)\right]^3, \qquad I_3 = \int_{-\infty}^{\infty}\frac{\mathrm{d}\omega}{2\pi}\gamma^{(1)}_{\mathrm{dr}}(\omega) \tag{4.111}$$

In order to obtain the result (4.106-4.107) we took advantage of the OPIs when possible.

4.C Numerical methods for Section 4.2

This section is dedicated to describe the numerical method used in Fig. 4.6 to simulate the classical defect. The classical theory is discretized as

$$\phi(x) \to \phi_j \qquad \Pi(x) \to \Pi_j\,, \tag{4.112}$$

a lattice space ℓ is introduced and the system is put in finite size $L = N\ell$, with N the number of lattice sites. We impose periodic boundary conditions. The evolution of the expectation value of a given observable $\langle \mathcal{O}_t \rangle$ is computed as it follows

1. A random initial condition ϕ_j, Π_j is chosen. The probability distribution is determined by the pre-quench GGE.
2. The initial condition is deterministically evolved and $\mathcal{O}_t$ computed for a single realization.
3. The previous steps are repeated for several realizations and $\langle \mathcal{O}_t \rangle$ is computed averaging on the initial conditions.

The main difficulty resides in a good approximation of the continuum model by mean of a lattice regularization. In principle, we could have discretized the problem in the real space replacing derivatives in the equation of motion with finite differences, then numerically solve the discrete model. However, after a preliminary numerical analysis, this approach seemed to lead to large errors caused by the finite lattice space, therefore we opted for a different method. For what it concerns the initial conditions, we use the mode expansion

$$\phi_j = \frac{1}{\sqrt{N\ell}} \sum_{n=0}^{N-1} \frac{\sqrt{\vartheta_{N,\ell}(n)}}{\sqrt{2E_{N,\ell}(n)}} \Big(e^{-i2\pi jn/N} \eta_n + \text{c.c.} \Big) \tag{4.113}$$

$$\Pi_j = \frac{1}{\sqrt{N\ell}} \sum_{n=0}^{N-1} \sqrt{\frac{E_{N,\ell}(n)\vartheta_{N,\ell}(n)}{2}} \Big(-ie^{-i2\pi jn/N} \eta_n + \text{c.c.} \Big) \tag{4.114}$$

where c.c. stands for the complex conjugated and

$$E_{N,\ell}(n) = \begin{cases} \sqrt{m^2 + [2\pi/(\ell N)]^2 n^2} \\ \\ \sqrt{m^2 + [2\pi/(\ell N)]^2 (N-n)^2} \end{cases}, \qquad \vartheta_{N,\ell}(n) = \begin{cases} \vartheta\big(2\pi n/(\ell N)\big) & n < N/2 \\ \\ \vartheta\big(2\pi(N-n)/(\ell N)\big) & n \geq N/2 \end{cases} \tag{4.115}$$

Above $\vartheta(k)$ is the excitation density of the GGE in the continuous model. The modes η_n are complex uncorrelated gaussian variables with variance $\langle |\eta_n|^2 \rangle = 1$, the probability distribution of the phase is flat. It is a simple exercise to compute the two point correlator and recover the continuum GGE-expectation values in the limit $N \to \infty$ and $\ell \to 0$

$$\langle \phi_j \phi_{j'} \rangle_{\text{GGE}} \xrightarrow{N\to\infty,\ell\to 0} \langle \phi(\ell j)\phi(\ell j') \rangle_{\text{GGE}}\,. \tag{4.116}$$

The same correspondence holds true for correlation functions involving the conjugated momentum. For what it concerns the time evolution, we used a "Trotterization" procedure discussed hereafter. We describe the algorithm in the case of a $\delta-$like defect which, in the discretized version, will act non trivially only on a lattice site which we choose to be $j = 0$. We assume $V'(\phi)$ can be written as

$$V'(\phi) = U^2(\phi)\phi\,, \tag{4.117}$$

with $U(\phi)$ real and positive, which is surely the case for $V(\phi) = \mu^2\phi^2/2 + \lambda\phi^4/4!$ ($\lambda > 0$), i.e. the potential we used as example. We discretize the time evolution in steps Δt and the method is accurate up to $\mathcal{O}(\Delta t^2)$.

The infinitesimal solution is carried out in two steps: in the first step we evolve the field as if the defect was absent, then we consider the effect of the impurity. Given the field configuration $\{\phi_j(t), \Pi_j(t)\}_j$ we construct the mode expansion similarly to (4.113, 4.114)

$$\phi_{j,t} = \frac{1}{\sqrt{N\ell}} \sum_{n=0}^{N-1} \frac{\sqrt{\vartheta_{N,\ell}(n)}}{\sqrt{2E_{N,\ell}(n)}} \left(e^{-i2\pi jn/N} \eta_n(t) + \text{c.c.} \right), \tag{4.118}$$

$$\Pi_{j,t} = \frac{1}{\sqrt{N\ell}} \sum_{n=0}^{N-1} \sqrt{\frac{E_{N,\ell}(n)\vartheta_{N,\ell}(n)}{2}} \left(-ie^{-i2\pi jn/N} \eta_n(t) + \text{c.c.} \right). \tag{4.119}$$

The modes $\eta_j(t)$ are *defined* by the above equation. Then, an intermediate field configuration $\phi'_{j,t}$, $\Pi'_{j,t}$ is constructed evolving the modes $\eta_n(t) \to e^{-i\Delta t E_{n,\ell}(j)} \eta_n(t)$

$$\phi_{j',t} = \frac{1}{\sqrt{N\ell}} \sum_{n=0}^{N-1} \frac{\sqrt{\vartheta_{N,\ell}(n)}}{\sqrt{2E_{N,\ell}(n)}} \left(e^{-i2\pi jn/N - i\Delta t E_{N,\ell}(n)} \eta_n(t) + \text{c.c.} \right) \tag{4.120}$$

and similarly for $\Pi'_{j,t}$. Then, we act with the defect: for $j \neq 0$ we set $\phi_{j,t+\Delta t} = \phi'_{j,t}$ and $\Pi_{j,t+\Delta t} = \Pi'_{j,t}$, while for $j = 0$

$$\Pi_{0,t+\Delta t} = -i\sqrt{\frac{U(\phi'_{0,t})}{2}}(z - z^*) \qquad \phi_{0,t+\Delta t} = \frac{1}{\sqrt{2U(\phi'_{0,t})}}(z + z^*) \tag{4.121}$$

where

$$z = e^{-i\Delta t U(\phi'_{0,t})} \sqrt{\frac{U(\phi'_{0,t})}{2}} \left(\phi'_{0,t} + \frac{i}{U(\phi'_{0,t})} \Pi'_{0,t} \right) \tag{4.122}$$

Going back and forth from the real and Fourier space is surely computationally expensive, however for what it concerns the time evolution the only information we need is the fields at $j = 0$, which can be computed with $\sim N$ steps from the knowledge of the Fourier modes. Therefore, implementing the algorithm in the Fourier space the time evolution can be carried up to time $t_{\max}$ in $\sim N t_{\max}/\Delta t$ steps. The most time-consuming operation is evaluating observables in real space for which the whole $\phi_{i,t}$ is needed: using a fast Fourier transform algorithm, we can pass from the Fourier space to the real one in $N \log N$ steps.

We now give further details on the simulation presented in Fig. 4.6 of the main text. In both panels of Fig. 4.6 we used $N = 2^{12}$ lattice sites with $\ell = 0.08$, which implies a system length $L \simeq 300$ and the time interval used for discretizing the evolution is $\Delta t = 0.005$. The observable in real space (chosen to be ϕ^2 in Fig. 4.6) is sampled at constant time steps $t_{\text{samples}} = 1$ until a maximum time $t_{\max} = 120$. This choice of $t_{\max}$ prevents any effect due to the boundary conditions. In both cases we considered roughly 16000 field realizations, which were sampled from a GGE with excitation density

$$\vartheta(k) = \frac{1}{\beta E(k) + \beta_2 k} \frac{1}{e^{r(|k|-c)} + 1} \tag{4.123}$$

with $\beta = 0.5$, $\beta_2 = 0.4$, $r = 2$, $c = 20$, the bulk mass $m = 1$. The choice $\vartheta(k)$, which is an honest GGE, is nothing else than a boosted thermal ensemble with an additional exponential cut off. A pure thermal-like GGE has poor UV convergency properties: the state cut off determined by the

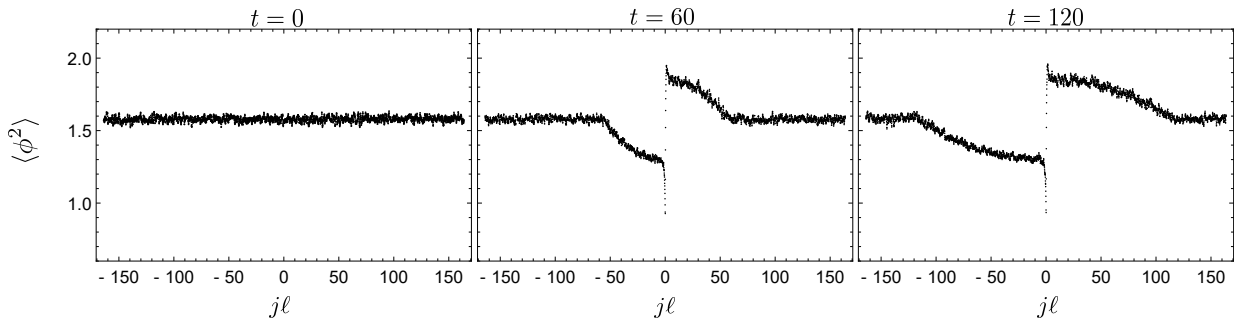

Figure 4.12: $\langle \phi^2 \rangle$ *profiles at different times, the parameters used in these plots are described in the text. For the seek of clarity, we take advantage of the periodic boundary conditions translating the defect in the middle of the system and placing it in zero. Figure taken from Ref. [11].*

parameter "c" has been added to further damp the effects of the UV cut off introduced by the lattice discretization $k \simeq \pi/\ell \simeq 40$. In Fig. 4.12 we plot screenshots at different times of the ϕ^2 profile (already averaged over the field realizations) in the interacting case $\mu = 1$, $\lambda = 3$. While the emerging profile is already clearly displayed, strong statistical fluctuations are still present: in order to further damp these oscillations, we rescaled the profiles as functions of the ray $j\ell/t$, averaging on the sampled times and finally obtaining the smooth profiles in Fig. 4.6.

Conclusions and outlook

The time to draw our conclusions has come. Since through the various sections we already provided step-by-step conclusions and outlooks of each original contribution, here we limit ourselves to more general considerations.

The work presented in this thesis has been pivoted on integrable models, mainly focusing on out-of-equilibrium protocols. As we stressed in the introduction and several times along the various chapters, integrable models are an outstanding theoretical laboratory (but, it must be stressed, with experimental realizations) to study strongly correlated many-body systems in an exact, non perturbative manner. Despite the promises of exact results, these are far from being trivially accessible: the machinery of non relativistic limits discussed in Chapter 2 showed to be a powerful and rather economic tool to assess galilean invariant systems, taking advantage of results derived in the relativistic realm.

For example, passing through the Sinh Gordon model, we solved the long-standing problem of deriving the whole set of one-point functions in the Lieb Liniger model, whose experimental relevance is hardly overestimated. The very natural further steps then go towards two directions, namely *i)* enlarging the variety of accessible galilean invariant models and *ii)* aiming to further more general results, e.g. two-point correlation functions.

Indeed, we show how with the method of non relativistic limits we can assess a whole plethora of interesting generalizations of the Lieb Liniger model, ranging from purely bosonic systems, to fermion-based models and mixtures of them. Even though the current comprehension of the needed relativistic models has not reached the same level of the Sinh Gordon model yet, new results could be soon achieved in this active research topic.

Chapter 3 was dedicated to various aspects of integrable models in out-of-equilibrium protocols, in particular to the emergent semiclassical description in terms of quasiparticles. At least two main directions urge to be further investigated, the first concerning the entanglement growth. We saw how the quasiparticle description is an extremely valuable tool in understanding the out-of-equilibrium behavior of such an important quantity: indeed, this is a very active research field (see Section 3.2 and references therein). So far, the focus has been mostly on quenches where the initial state has the so-called pair structure in terms of the post quench excitations, leading to a complete semiclassical interpretation of the entanglement growth. Instead, we provided and solved an example in a free model where the initial state possesses a more complicated structure, with the resulting entanglement entropy no longer describable in terms of purely-classical quantities, but requiring a true quantum description. So, it is natural to wonder what lays beyond the case we analyzed, both in the direction of further generalizing the initial state and of including true interactions in the integrable model.

The second direction of Chapter 3 which needs further investigations is that of the Generalized Hydrodynamics: several efforts have been dedicated to deepen our understanding of this new powerful tool, which found a lot of applications. In this perspective, pushing further the study of GHD in classical models can give several contributions, providing both a set of alternative theoretical tools and more efficient numerical benchmarks.

Finally, in Chapter 4 we considered out-of-equilibrium protocols induced by defects. It is remarkable how, in an integrable model, the presence of a perturbation concerning a finite part of the system can affect the latter on a thermodynamically large scale. In this chapter we touched two different aspects, each of them leaving room to new interesting questions.

At first, we were concerned with moving impurities: even though we focused into the integrable world, more specifically we worked in free models, the real main character of this part is the finite maximum velocity of the information spreading v_{M}. We unveiled the peculiar reaction that the system has to an impurity moving faster than the mentioned velocity, but such a question can be posed in non integrable systems as well. Probing v_{M} in completely generic and interacting models by mean of moving impurities is an intriguing setup, which could lead to new universal phenomena. Moreover, addressing higher dimensions is an interesting question as well, with the possibility of observing effects closely related to the Cherenkov radiation. The second topic we considered concerned the thermalization properties caused by non integrable defects: we unveiled a completely different mechanism compared with the well known prethermalization paradigm of the homogeneous case. In particular, we showed how a localized integrability-breaking perturbation does not suffice to cause "thermalization" (further comments in Section 4.2), provided it is weak enough. A whole set of questions arise, for example understanding the crossover between a localized weak perturbation (not thermalizing) and an homogeneous one (thermalizing) is of utmost importance. We expect that the study of integrability-breaking impurities can further sharpen our understanding in the processes behind thermalization (or lack of it).

Bibliography

[1] A. Bastianello, A. D. Luca, and G. Mussardo, Journal of Statistical Mechanics: Theory and Experiment **2016**, 123104 (2016).

[2] A. Bastianello, A. D. Luca, and G. Mussardo, Journal of Physics A: Mathematical and Theoretical **50**, 234002 (2017).

[3] A. Bastianello, L. Piroli, and P. Calabrese, Phys. Rev. Lett. **120**, 190601 (2018).

[4] A. Bastianello and L. Piroli, ArXiv e-prints, 1807.06869 (2018).

[5] A. Bastianello and S. Sotiriadis, Journal of Statistical Mechanics: Theory and Experiment **2017**, 023105 (2017).

[6] A. Bastianello and P. Calabrese, ArXiv e-prints, 1807.10176 (2018).

[7] A. Bastianello, M. Collura, and S. Sotiriadis, Phys. Rev. B **95**, 174303 (2017).

[8] A. Bastianello, B. Doyon, G. Watts, and T. Yoshimura, SciPost Phys. **4**, 45 (2018).

[9] A. Bastianello and A. De Luca, Phys. Rev. Lett. **120**, 060602 (2018).

[10] A. Bastianello and A. De Luca, Phys. Rev. B **98**, 064304 (2018).

[11] A. Bastianello, ArXiv e-prints, 1807.00625 (2018).

[12] A. Bastianello and S. Sotiriadis, Nuclear Physics B **909**, 1020 (2016).

[13] E. Fermi, P. Pasta, S. Ulam, and M. Tsingou, *Studies of the nonlinear problems*, tech. rep. (Los Alamos Scientific Lab., N. Mex., 1955).

[14] G. P. Berman and F. M. Izrailev, Chaos: An Interdisciplinary Journal of Nonlinear Science **15**, 015104 (2005).

[15] G. Gallavotti, *The fermi-pasta-ulam problem: a status report*, Vol. 728 (Springer, 2007).

[16] V. I. Arnol'd, *Mathematical methods of classical mechanics*, Vol. 60 (Springer Science & Business Media, 2013).

[17] N. J. Zabusky and M. D. Kruskal, Phys. Rev. Lett. **15**, 240 (1965).

[18] L. Faddeev and L. Takhtajan, *Hamiltonian methods in the theory of solitons* (Springer Science & Business Media, 2007).

[19] M. Onorato, L. Vozella, D. Proment, and Y. V. Lvov, Proceedings of the National Academy of Sciences **112**, 4208 (2015).

[20] J. v. Neumann, Zeitschrift für Physik **57**, 30 (1929).

[21] I. Bloch, J. Dalibard, and W. Zwerger, Rev. Mod. Phys. **80**, 885 (2008).

[22] M. H. Anderson, J. R. Ensher, M. R. Matthews, C. E. Wieman, and E. A. Cornell, Science **269**, 198 (1995).

[23] C. C. Bradley, C. A. Sackett, J. J. Tollett, and R. G. Hulet, Phys. Rev. Lett. **75**, 1687 (1995).

[24] K. B. Davis, M. O. Mewes, M. R. Andrews, N. J. van Druten, D. S. Durfee, D. M. Kurn, and W. Ketterle, Phys. Rev. Lett. **75**, 3969 (1995).

[25] M. Greiner, O. Mandel, T. W. Hänsch, and I. Bloch, Nature **419**, 51 (2002).

[26] H. T. C. Stoof, M. Houbiers, C. A. Sackett, and R. G. Hulet, Phys. Rev. Lett. **76**, 10 (1996).

[27] T. Kinoshita, T. Wenger, and D. S. Weiss, Science **305**, 1125 (2004).

[28] T. Kinoshita, T. Wenger, and D. S. Weiss, Phys. Rev. Lett. **95**, 190406 (2005).

[29] A. H. van Amerongen, J. J. P. van Es, P. Wicke, K. V. Kheruntsyan, and N. J. van Druten, Phys. Rev. Lett. **100**, 090402 (2008).

[30] N. Fabbri, M. Panfil, D. Clément, L. Fallani, M. Inguscio, C. Fort, and J.-S. Caux, Phys. Rev. A **91**, 043617 (2015).

[31] F. Meinert, M. Panfil, M. J. Mark, K. Lauber, J.-S. Caux, and H.-C. Nägerl, Phys. Rev. Lett. **115**, 085301 (2015).

[32] N. Fabbri, D. Clément, L. Fallani, C. Fort, and M. Inguscio, Phys. Rev. A **83**, 031604 (2011).

[33] A. Polkovnikov, K. Sengupta, A. Silva, and M. Vengalattore, Rev. Mod. Phys. **83**, 863 (2011).

[34] C. Gogolin and J. Eisert, Reports on Progress in Physics **79**, 056001 (2016).

[35] S. Hofferberth, I. Lesanovsky, B. Fischer, T. Schumm, and J. Schmiedmayer, Nature **449**, 324 (2007).

[36] L. Hackermüller, U. Schneider, M. Moreno-Cardoner, T. Kitagawa, T. Best, S. Will, E. Demler, E. Altman, I. Bloch, and B. Paredes, Science **327**, 1621 (2010).

[37] S. Trotzky, Y.-A. Chen, A. Flesch, I. P. McCulloch, U. Schollwöck, J. Eisert, and I. Bloch, Nature Physics **8**, Article, 325 (2012).

[38] M. Gring, M. Kuhnert, T. Langen, T. Kitagawa, B. Rauer, M. Schreitl, I. Mazets, D. A. Smith, E. Demler, and J. Schmiedmayer, Science **337**, 1318 (2012).

[39] M. Cheneau, P. Barmettler, D. Poletti, M. Endres, P. Schauß, T. Fukuhara, C. Gross, I. Bloch, C. Kollath, and S. Kuhr, Nature **481**, 484 (2012).

[40] T. Langen, R. Geiger, M. Kuhnert, B. Rauer, and J. Schmiedmayer, Nature Physics **9**, 640 (2013).

[41] F. Meinert, M. J. Mark, E. Kirilov, K. Lauber, P. Weinmann, A. J. Daley, and H.-C. Nägerl, Phys. Rev. Lett. **111**, 053003 (2013).

[42] J. P. Ronzheimer, M. Schreiber, S. Braun, S. S. Hodgman, S. Langer, I. P. McCulloch, F. Heidrich-Meisner, I. Bloch, and U. Schneider, Phys. Rev. Lett. **110**, 205301 (2013).

[43] L. Vidmar, J. P. Ronzheimer, M. Schreiber, S. Braun, S. S. Hodgman, S. Langer, F. Heidrich-Meisner, I. Bloch, and U. Schneider, Physical Review Letters **115**, 175301, 175301 (2015).

[44] I. Bloch, Nature Physics **1**, Review Article, 23 (2005).

[45] B. Paredes, A. Widera, V. Murg, O. Mandel, S. Fölling, I. Cirac, G. V. Shlyapnikov, T. W. Hänsch, and I. Bloch, Nature **429**, 277 (2004).

[46] R. Jördens, N. Strohmaier, K. Günter, H. Moritz, and T. Esslinger, Nature **455**, 204 (2008).

[47] S. Palzer, C. Zipkes, C. Sias, and M. Köhl, Phys. Rev. Lett. **103**, 150601 (2009).

[48] T. Fukuhara, A. Kantian, M. Endres, M. Cheneau, P. Schauß, S. Hild, D. Bellem, U. Schollwöck, T. Giamarchi, C. Gross, I. Bloch, and S. Kuhr, Nature Physics **9**, Article, 235 (2013).

[49] T. Kinoshita, T. Wenger, and D. S. Weiss, Nature **440**, 900 (2006).

[50] E. H. Lieb, Phys. Rev. **130**, 1616 (1963).

[51] E. H. Lieb and W. Liniger, Phys. Rev. **130**, 1605 (1963).

[52] J.-S. Caux and J. Mossel, Journal of Statistical Mechanics: Theory and Experiment **2011**, P02023 (2011).

[53] V. E. Korepin, N. M. Bogoliubov, and A. G. Izergin, *Quantum inverse scattering method and correlation functions*, Vol. 3 (Cambridge university press, 1997).

[54] S. Coleman and J. Mandula, Phys. Rev. **159**, 1251 (1967).

[55] F. D. M. Haldane, Phys. Rev. Lett. **47**, 1840 (1981).

[56] F. D. M. Haldane, Journal of Physics C: Solid State Physics **14**, 2585 (1981).

[57] M. Takahashi, *Thermodynamics of one-dimensional solvable models* (Cambridge University Press, 2005).

[58] W. Heisenberg, Zeitschrift für Physik **49**, 619 (1928).

[59] R. Orbach, Phys. Rev. **112**, 309 (1958).

[60] H. Bethe, Zeitschrift für Physik **71**, 205 (1931).

[61] F. A. Smirnov, *Form factors in completely integrable models of quantum field theory*, Vol. 14 (World Scientific, 1992).

[62] A. Arinshtein, V. Fateyev, and A. Zamolodchikov, Physics Letters B **87**, 389 (1979).

[63] A. Zamolodchikov, in *Integrable sys quantum field theory*, edited by M. Jimbo, T. Miwa, and A. Tsuchiya (Academic Press, San Diego, 1989), pp. 641–674.

[64] H. Braden, E. Corrigan, P. Dorey, and R. Sasaki, Nuclear Physics B **338**, 689 (1990).

[65] H. Braden, E. Corrigan, P. Dorey, and R. Sasaki, Nuclear Physics B **356**, 469 (1991).

[66] P. Christe and G. Mussardo, Nuclear Physics B **330**, 465 (1990).

[67] P. Christe and G. Mussardo, International Journal of Modern Physics A **05**, 4581 (1990).

[68] A. Fring, H. Liao, and D. Olive, Physics Letters B **266**, 82 (1991).

[69] G. Mussardo, Physics Reports **218**, 215 (1992).

[70] G. Mussardo, *Statistical field theory: an introduction to exactly solved models in statistical physics* (Oxford University Press, 2010).

[71] P. Dorey, ArXiv High Energy Physics - Theory e-prints, hep (1998).

[72] T. Oota, Nuclear Physics B **504**, 738 (1997).

[73] A. Fring, C. Korff, and B. Schulz, Nuclear Physics B **567**, 409 (2000).

[74] C. Destri, H. D. vega, and V. Fateev, Physics Letters B **256**, 173 (1991).

[75] G. Delius, M. Grisaru, and D. Zanon, Nuclear Physics B **382**, 365 (1992).

[76] G. Watts and R. A. Weston, Physics Letters B **289**, 61 (1992).

[77] M. Beccaria, Phys. Rev. D **53**, 3266 (1996).

[78] A. B. Zamolodchikov and A. B. Zamolodchikov, in *Yang-baxter equation in integrable systems* (World Scientific, 1990), pp. 82–120.

[79] R. Shankar and E. Witten, Phys. Rev. D **17**, 2134 (1978).

[80] K. Schoutens, Nuclear Physics B **344**, 665 (1990).

[81] C. Ahn, Nuclear Physics B **422**, 449 (1994).

[82] T. J. Hollowood and E. Mavrikis, Nuclear Physics B **484**, 631 (1997).

[83] A. B. Zamolodchikov and A. B. Zamolodchikov, Nuclear Physics B **133**, 525 (1978).

[84] E. Ogievetsky and P. Wiegmann, Physics Letters B **168**, 360 (1986).

[85] M. Kormos, G. Mussardo, and A. Trombettoni, Phys. Rev. Lett. **103**, 210404 (2009).

[86] M. Kormos, G. Mussardo, and A. Trombettoni, Phys. Rev. A **81**, 043606 (2010).

[87] A. LeClair and G. Mussardo, Nuclear Physics B **552**, 624 (1999).

[88] M. Kormos, Y.-Z. Chou, and A. Imambekov, Phys. Rev. Lett. **107**, 230405 (2011).

[89] B. Pozsgay, Journal of Statistical Mechanics: Theory and Experiment **2011**, P11017 (2011).

[90] S. Negro and F. Smirnov, Nuclear Physics B **875**, 166 (2013).

[91] S. Negro, International Journal of Modern Physics A **29**, 1450111 (2014).

[92] S. Hofferberth, I. Lesanovsky, T. Schumm, A. Imambekov, V. Gritsev, E. Demler, and J. Schmiedmayer, Nature Physics **4**, Article, 489 (2008).

[93] T. Kitagawa, S. Pielawa, A. Imambekov, J. Schmiedmayer, V. Gritsev, and E. Demler, Phys. Rev. Lett. **104**, 255302 (2010).

[94] T. Kitagawa, A. Imambekov, J. Schmiedmayer, and E. Demler, New Journal of Physics **13**, 073018 (2011).

[95] M. Arzamasovs and D. M. Gangardt, ArXiv e-prints, 1807.09381 (2018).

[96] P. Calabrese and J. Cardy, Journal of Statistical Mechanics: Theory and Experiment **2007**, P06008 (2007).

[97] P. Calabrese and J. Cardy, Phys. Rev. Lett. **96**, 136801 (2006).

[98] M. Rigol, V. Dunjko, V. Yurovsky, and M. Olshanii, Phys. Rev. Lett. **98**, 050405 (2007).

[99] F. H. L. Essler and M. Fagotti, Journal of Statistical Mechanics: Theory and Experiment **2016**, 064002 (2016).

[100] J.-S. Caux and F. H. L. Essler, Phys. Rev. Lett. **110**, 257203 (2013).

[101] B. Pozsgay, Journal of Statistical Mechanics: Theory and Experiment **2014**, P10045 (2014).

[102] F. H. L. Essler, S. Evangelisti, and M. Fagotti, Phys. Rev. Lett. **109**, 247206 (2012).

[103] J.-S. Caux and R. M. Konik, Phys. Rev. Lett. **109**, 175301 (2012).

[104] B. Pozsgay, Journal of Statistical Mechanics: Theory and Experiment **2013**, P07003 (2013).

[105] G. Mussardo, Phys. Rev. Lett. **111**, 100401 (2013).

[106] M. Rigol, Phys. Rev. Lett. **103**, 100403 (2009).

[107] P. Calabrese, F. H. L. Essler, and M. Fagotti, Phys. Rev. Lett. **106**, 227203 (2011).

[108] P. Calabrese, F. H. L. Essler, and M. Fagotti, Journal of Statistical Mechanics: Theory and Experiment **2012**, P07022 (2012).

[109] M. Fagotti and F. H. L. Essler, Phys. Rev. B **87**, 245107 (2013).

[110] P. Calabrese, F. H. L. Essler, and G. Mussardo, Journal of Statistical Mechanics: Theory and Experiment **2016**, 064001 (2016).

[111] B. Pozsgay, M. Mestyán, M. A. Werner, M. Kormos, G. Zaránd, and G. Takács, Phys. Rev. Lett. **113**, 117203 (2014).

[112] M. Mestyán, B. Pozsgay, G. Takács, and M. A. Werner, Journal of Statistical Mechanics: Theory and Experiment **2015**, P04001 (2015).

[113] J. De Nardis, B. Wouters, M. Brockmann, and J.-S. Caux, Phys. Rev. A **89**, 033601 (2014).

[114] B. Wouters, J. De Nardis, M. Brockmann, D. Fioretto, M. Rigol, and J.-S. Caux, Phys. Rev. Lett. **113**, 117202 (2014).

[115] U. Schollwöck, Rev. Mod. Phys. **77**, 259 (2005).

[116] J.-S. Caux, Journal of Statistical Mechanics: Theory and Experiment **2016**, 064006 (2016).

[117] E. Ilievski, M. Medenjak, and T. Prosen, Phys. Rev. Lett. **115**, 120601 (2015).

[118] E. Ilievski, J. De Nardis, B. Wouters, J.-S. Caux, F. H. L. Essler, and T. Prosen, Phys. Rev. Lett. **115**, 157201 (2015).

[119] E. Ilievski, M. Medenjak, T. Prosen, and L. Zadnik, Journal of Statistical Mechanics: Theory and Experiment **2016**, 064008 (2016).

[120] L. Piroli and E. Vernier, Journal of Statistical Mechanics: Theory and Experiment **2016**, 053106 (2016).

[121] L. Piroli, E. Vernier, and P. Calabrese, Phys. Rev. B **94**, 054313 (2016).

[122] E. Ilievski, E. Quinn, J. D. Nardis, and M. Brockmann, Journal of Statistical Mechanics: Theory and Experiment **2016**, 063101 (2016).

[123] F. H. L. Essler, G. Mussardo, and M. Panfil, Phys. Rev. A **91**, 051602 (2015).

[124] F. H. L. Essler, G. Mussardo, and M. Panfil, Journal of Statistical Mechanics: Theory and Experiment **2017**, 013103 (2017).

[125] S. Sotiriadis, Phys. Rev. A **94**, 031605 (2016).

[126] S. Weinberg, *The quantum theory of fields. vol. 1: foundations* (Cambridge University Press, 1995).

[127] E. Vernier and A. C. Cubero, Journal of Statistical Mechanics: Theory and Experiment **2017**, 023101 (2017).

[128] L. Amico, R. Fazio, A. Osterloh, and V. Vedral, Rev. Mod. Phys. **80**, 517 (2008).

[129] P. Calabrese, J. Cardy, and B. Doyon, Journal of Physics A: Mathematical and Theoretical **42**, 500301 (2009).

[130] N. Laflorencie, Physics Reports **646**, Quantum entanglement in condensed matter systems, 1 (2016).

[131] N. Schuch, M. M. Wolf, F. Verstraete, and J. I. Cirac, Phys. Rev. Lett. **100**, 030504 (2008).

[132] N. Schuch, M. M. Wolf, K. G. H. Vollbrecht, and J. I. Cirac, New Journal of Physics **10**, 033032 (2008).

[133] Á. Perales and G. Vidal, Phys. Rev. A **78**, 042337 (2008).

[134] P. Hauke, F. M. Cucchietti, L. Tagliacozzo, I. Deutsch, and M. Lewenstein, Reports on Progress in Physics **75**, 082401 (2012).

[135] J. Dubail, Journal of Physics A: Mathematical and Theoretical **50**, 234001 (2017).

[136] E. Leviatan, F. Pollmann, J. Bardarson, D. Huse, and E. Altman, ArXiv e-prints, 1702.08894 (2017).

[137] P. Calabrese and J. Cardy, Journal of Statistical Mechanics: Theory and Experiment **2005**, P04010 (2005).

[138] M. Fagotti and P. Calabrese, Phys. Rev. A **78**, 010306 (2008).

[139] V. Alba and P. Calabrese, Proceedings of the National Academy of Sciences **114**, 7947 (2017).

[140] V. Alba and P. Calabrese, SciPost Phys. **4**, 17 (2018).

[141] P. Calabrese, Physica A: Statistical Mechanics and its Applications **504**, Lecture Notes of the 14th International Summer School on Fundamental Problems in Statistical Physics, 31 (2018).

[142] B. Bertini, E. Tartaglia, and P. Calabrese, Journal of Statistical Mechanics: Theory and Experiment **2018**, 063104 (2018).

[143] P. Calabrese, F. H. L. Essler, and M. Fagotti, Journal of Statistical Mechanics: Theory and Experiment **2012**, P07016 (2012).

[144] M. RIGOL and A. MURAMATSU, Modern Physics Letters B **19**, 861 (2005).

[145] W. Xu and M. Rigol, Phys. Rev. A **95**, 033617 (2017).

[146] A. Minguzzi and D. M. Gangardt, Phys. Rev. Lett. **94**, 240404 (2005).

[147] F. Cartarius, E. Kawasaki, and A. Minguzzi, Phys. Rev. A **92**, 063605 (2015).

[148] A. del Campo and J. G. Muga, EPL (Europhysics Letters) **74**, 965 (2006).

[149] M. Á. García-March, T. Fogarty, S. Campbell, T. Busch, and M. Paternostro, New Journal of Physics **18**, 103035 (2016).

[150] M. Kormos, M. Collura, and P. Calabrese, Phys. Rev. A **89**, 013609 (2014).

[151] P. P. Mazza, M. Collura, M. Kormos, and P. Calabrese, Journal of Statistical Mechanics: Theory and Experiment **2014**, P11016 (2014).

[152] M. Collura, M. Kormos, and P. Calabrese, Phys. Rev. A **97**, 033609 (2018).

[153] E. Bettelheim and P. B. Wiegmann, Phys. Rev. B **84**, 085102 (2011).

[154] E. Bettelheim and L. Glazman, Phys. Rev. Lett. **109**, 260602 (2012).

[155] I. V. Protopopov, D. B. Gutman, P. Schmitteckert, and A. D. Mirlin, Phys. Rev. B **87**, 045112 (2013).

[156] P. Wendenbaum, M. Collura, and D. Karevski, Phys. Rev. A **87**, 023624 (2013).

[157] M. Kormos, SciPost Phys. **3**, 020 (2017).

[158] G. Perfetto and A. Gambassi, Phys. Rev. E **96**, 012138 (2017).

[159] O. A. Castro-Alvaredo, B. Doyon, and T. Yoshimura, Phys. Rev. X **6**, 041065 (2016).

[160] B. Bertini, M. Collura, J. De Nardis, and M. Fagotti, Phys. Rev. Lett. **117**, 207201 (2016).

[161] B. Doyon, T. Yoshimura, and J.-S. Caux, Phys. Rev. Lett. **120**, 045301 (2018).

[162] V. B. Bulchandani, R. Vasseur, C. Karrasch, and J. E. Moore, Phys. Rev. Lett. **119**, 220604 (2017).

[163] V. B. Bulchandani, R. Vasseur, C. Karrasch, and J. E. Moore, Phys. Rev. B **97**, 045407 (2018).

[164] L. Piroli, J. De Nardis, M. Collura, B. Bertini, and M. Fagotti, Phys. Rev. B **96**, 115124 (2017).

[165] B. Doyon, J. Dubail, R. Konik, and T. Yoshimura, Phys. Rev. Lett. **119**, 195301 (2017).

[166] E. Ilievski and J. De Nardis, Phys. Rev. B **96**, 081118 (2017).

[167] M. Collura, A. De Luca, and J. Viti, Phys. Rev. B **97**, 081111 (2018).

[168] L. Mazza, J. Viti, M. Carrega, D. Rossini, and A. De Luca, ArXiv e-prints, 1804.04476 (2018).

[169] B. Bertini, L. Piroli, and P. Calabrese, Phys. Rev. Lett. **120**, 176801 (2018).

[170] B. Bertini and L. Piroli, Journal of Statistical Mechanics: Theory and Experiment **2018**, 033104 (2018).

[171] B. Doyon and T. Yoshimura, SciPost Phys. **2**, 014 (2017).

[172] J.-S. Caux, B. Doyon, J. Dubail, R. Konik, and T. Yoshimura, ArXiv e-prints, 1711.00873 (2017).

[173] E. Ilievski and J. De Nardis, Phys. Rev. Lett. **119**, 020602 (2017).

[174] B. Doyon and H. Spohn, SciPost Phys. **3**, 039 (2017).

[175] B. Doyon, ArXiv e-prints, 1711.04568 (2017).

[176] B. Bertini, M. Fagotti, L. Piroli, and P. Calabrese, ArXiv e-prints, 1805.01884 (2018).

[177] V. Alba, Phys. Rev. B **97**, 245135 (2018).

[178] V. Alba, ArXiv e-prints, 1807.01800 (2018).

[179] M. Fagotti, Phys. Rev. B **96**, 220302 (2017).

[180] J. De Nardis, D. Bernard, and B. Doyon, ArXiv e-prints, 1807.02414 (2018).

[181] B. Doyon and H. Spohn, Journal of Statistical Mechanics: Theory and Experiment **2017**, 073210 (2017).

[182] A. D. Luca and G. Mussardo, Journal of Statistical Mechanics: Theory and Experiment **2016**, 064011 (2016).

[183] N. Metropolis, A. W. Rosenbluth, M. N. Rosenbluth, A. H. Teller, and E. Teller, The Journal of Chemical Physics **21**, 1087 (1953).

[184] W. K. Hastings, Biometrika **57**, 97 (1970).

[185] B. Bertini and M. Fagotti, Phys. Rev. Lett. **117**, 130402 (2016).

[186] M. Ljubotina, S. Sotiriadis, and T. Prosen, ArXiv e-prints, 1802.05697 (2018).

[187] E. H. Lieb and D. W. Robinson, Communications in Mathematical Physics **28**, 251 (1972).

[188] B. Bertini, F. H. L. Essler, S. Groha, and N. J. Robinson, Phys. Rev. B **94**, 245117 (2016).

[189] M. Moeckel and S. Kehrein, Phys. Rev. Lett. **100**, 175702 (2008).

[190] M. Moeckel and S. Kehrein, Annals of Physics **324**, 2146 (2009).

[191] A. Rosch, D. Rasch, B. Binz, and M. Vojta, Phys. Rev. Lett. **101**, 265301 (2008).

[192] M. Kollar, F. A. Wolf, and M. Eckstein, Phys. Rev. B **84**, 054304 (2011).

[193] M. van den Worm, B. C. Sawyer, J. J. Bollinger, and M. Kastner, New Journal of Physics **15**, 083007 (2013).

[194] M. Marcuzzi, J. Marino, A. Gambassi, and A. Silva, Phys. Rev. Lett. **111**, 197203 (2013).

[195] F. H. L. Essler, S. Kehrein, S. R. Manmana, and N. J. Robinson, Phys. Rev. B **89**, 165104 (2014).

[196] N. Nessi, A. Iucci, and M. A. Cazalilla, Phys. Rev. Lett. **113**, 210402 (2014).

[197] M. Fagotti, Journal of Statistical Mechanics: Theory and Experiment **2014**, P03016 (2014).

[198] G. P. Brandino, J.-S. Caux, and R. M. Konik, Phys. Rev. X **5**, 041043 (2015).

[199] B. Bertini and M. Fagotti, Journal of Statistical Mechanics: Theory and Experiment **2015**, P07012 (2015).

[200] C. Kollath, A. M. Läuchli, and E. Altman, Phys. Rev. Lett. **98**, 180601 (2007).

[201] M. Rigol, Phys. Rev. Lett. **103**, 100403 (2009).

[202] A. Mitra, Phys. Rev. B **87**, 205109 (2013).

[203] A. Chiocchetta, M. Tavora, A. Gambassi, and A. Mitra, Phys. Rev. B **91**, 220302 (2015).

[204] A. Chiocchetta, A. Gambassi, S. Diehl, and J. Marino, Phys. Rev. Lett. **118**, 135701 (2017).

[205] V. Alba and M. Fagotti, Phys. Rev. Lett. **119**, 010601 (2017).

[206] M. Gring, M. Kuhnert, T. Langen, T. Kitagawa, B. Rauer, M. Schreitl, I. Mazets, D. A. Smith, E. Demler, and J. Schmiedmayer, Science (2012) 10.1126/science.1224953.

[207] D. A. Smith, M. Gring, T. Langen, M. Kuhnert, B. Rauer, R. Geiger, T. Kitagawa, I. Mazets, E. Demler, and J. Schmiedmayer, New Journal of Physics **15**, 075011 (2013).

[208] T. Langen, M. Gring, M. Kuhnert, B. Rauer, R. Geiger, D. A. Smith, I. E. Mazets, and J. Schmiedmayer, The European Physical Journal Special Topics **217**, 43 (2013).

[209] Y. Tang, W. Kao, K.-Y. Li, S. Seo, K. Mallayya, M. Rigol, S. Gopalakrishnan, and B. L. Lev, Phys. Rev. X **8**, 021030 (2018).

[210] M. Fagotti, Journal of Physics A: Mathematical and Theoretical **50**, 034005 (2017).

[211] B. Sutherland, *Beautiful models: 70 years of exactly solved quantum many-body problems* (World Scientific Publishing Company, 2004).

[212] A. Koubek, G. Mussardo, and R. Tateo, International Journal of Modern Physics A **07**, 3435 (1992).

[213] R. J. Eden, P. V. Landshoff, D. I. Olive, and J. C. Polkinghorne, *The analytic s-matrix* (Cambridge University Press, 2002).

[214] M. Wadati, Journal of the Physical Society of Japan **54**, 3727 (1985).

[215] K. M. Watson, Phys. Rev. **95**, 228 (1954).

[216] D. Fioretto and G. Mussardo, New Journal of Physics **12**, 055015 (2010).

[217] H. Saleur, Nuclear Physics B **567**, 602 (2000).

[218] B. Pozsgay, Journal of Statistical Mechanics: Theory and Experiment **2011**, P01011 (2011).

[219] B. Pozsgay and I. Szécsényi, Journal of High Energy Physics **2018**, 170 (2018).

[220] A. Grauel, Physica A: Statistical Mechanics and its Applications **132**, 557 (1985).

[221] A. Koubek and G. Mussardo, Physics Letters B **311**, 193 (1993).

[222] B. Bertini, L. Piroli, and P. Calabrese, Journal of Statistical Mechanics: Theory and Experiment **2016**, 063102 (2016).

[223] B. Davies and V. E. Korepin, ArXiv e-prints, 1109.6604 (2011).

[224] A. B. Zamolodchikov, International Journal of Modern Physics A **10**, 1125 (1995).

[225] A. Fring, G. Mussardo, and P. Simonetti, Nuclear Physics B **393**, 413 (1993).

[226] and, Proceedings of the Royal Society of London A: Mathematical, Physical and Engineering Sciences **352**, 481 (1977).

[227] A. Fring, G. Mussardo, and P. Simonetti, Physics Letters B **307**, 83 (1993).

[228] V. Fateev, S. Lukyanov, A. Zamolodchikov, and A. Zamolodchikov, Nuclear Physics B **516**, 652 (1998).

[229] S. Ferrara, L. Girardello, and S. Sciuto, Physics Letters B **76**, 303 (1978).

[230] S. Sengupta and P. Majumdar, Phys. Rev. D **33**, 3138 (1986).

[231] D. J. Gross and A. Neveu, Phys. Rev. D **10**, 3235 (1974).

[232] A. B. Zamolodchikov and A. B. Zamolodchikov, Physics Letters B **72**, 481 (1978).

[233] C. Ahn, Nuclear Physics B **354**, 57 (1991).

[234] E. Witten, Phys. Rev. D **16**, 2991 (1977).

[235] C. N. Yang, Phys. Rev. Lett. **19**, 1312 (1967).

[236] B. Sutherland, Phys. Rev. Lett. **20**, 98 (1968).

[237] P. Calabrese, M. Kormos, and P. L. Doussal, EPL (Europhysics Letters) **107**, 10011 (2014).

[238] H. Grosse, E. Langmann, and C. Paufler, Journal of Physics A: Mathematical and General **37**, 4579 (2004).

[239] R. Sasaki and F. P. Zen, International Journal of Modern Physics A **08**, 115 (1993).

[240] A. M. Polyakov, Contemp. Concepts Phys. **3**, 1 (1987).

[241] E. Abdalla, M. C. B. Abdalla, and K. D. Rothe, *Non-perturbative methods in 2 dimensional quantum field theory* (World Scientific, 1991).

[242] C. K. Lai and C. N. Yang, Phys. Rev. A **3**, 393 (1971).

[243] C. K. Lai, Journal of Mathematical Physics **15**, 954 (1974).

[244] A. Imambekov and E. Demler, Phys. Rev. A **73**, 021602 (2006).

[245] A. Imambekov and E. Demler, Annals of Physics **321**, 2390 (2006).

[246] R. Haag, J. T. Lopuszanski, and M. Sohnius, Nucl. Phys. **B88**, [,257(1974)], 257 (1975).

[247] D. Friedan, Z. Qiu, and S. Shenker, Physics Letters B **151**, 37 (1985).

[248] Z. Qiu, Nuclear Physics B **270**, 205 (1986).

[249] A. B. Zamolodchikov, Sov. J. Nucl. Phys. **44**, 529 (1986).

[250] G. Mussardo, Nucl. Phys. **B779**, 101 (2007).

[251] M. F. Sohnius, Physics Reports **128**, 39 (1985).

[252] K. Hori and C. Vafa, arXiv preprint hep-th/0002222 (2000).

[253] S. J. Gates Jr, M. T. Grisaru, M. Rocek, and W. Siegel, ArXiv High Energy Physics - Theory e-prints, hep (2001).

[254] E. Witten and D. Olive, Physics Letters B **78**, 97 (1978).

[255] R. F. Dashen, B. Hasslacher, and A. Neveu, Phys. Rev. D **12**, 2443 (1975).

[256] H.-T. Fan, F.-C. Pu, and B.-H. Zhao, Nuclear Physics B **299**, 52 (1988).

[257] M. Jimbo and T. Miwa, *Algebraic analysis of solvable lattice models*, Vol. 85 (American Mathematical Soc., 1994).

[258] H. B. Thacker, Rev. Mod. Phys. **53**, 253 (1981).

[259] F. H. Essler, H. Frahm, F. Göhmann, A. Klümper, and V. E. Korepin, *The one-dimensional hubbard model* (Cambridge University Press, 2005).

[260] M. Jimbo, K. Miki, T. Miwa, and A. Nakayashiki, Physics Letters A **168**, 256 (1992).

[261] M. Jimbo and T. Miwa, Journal of Physics A: Mathematical and General **29**, 2923 (1996).

[262] J. M. Maillet and J. Sanchez de Santos, in Eprint arxiv:q-alg/9612012 (Dec. 1996).

[263] N. Kitanine, J. Maillet, and V. Terras, Nuclear Physics B **554**, 647 (1999).

[264] N. Kitanine, J. Maillet, N. Slavnov, and V. Terras, Nuclear Physics B **641**, 487 (2002).

[265] N. Kitanine, J. M. Maillet, N. A. Slavnov, and V. Terras, Journal of Physics A: Mathematical and General **35**, L753 (2002).

[266] N. Kitanine, J. Maillet, and V. Terras, Nuclear Physics B **567**, 554 (2000).

[267] H. E. Boos, F. Göhmann, A. Klümper, and J. Suzuki, Journal of Physics A: Mathematical and Theoretical **40**, 10699 (2007).

[268] H. E. Boos, F. Göhmann, A. Klümper, and J. Suzuki, Journal of Statistical Mechanics: Theory and Experiment **2006**, P04001 (2006).

[269] F. Göhmann, A. Klümper, and A. Seel, Journal of Physics A: Mathematical and General **38**, 1833 (2005).

[270] F. Göhmann, A. Klümper, and A. Seel, Journal of Physics A: Mathematical and General **37**, 7625 (2004).

[271] J.-S. Caux, R. Hagemans, and J. M. Maillet, Journal of Statistical Mechanics: Theory and Experiment **2005**, P09003 (2005).

[272] J.-S. Caux and J. M. Maillet, Phys. Rev. Lett. **95**, 077201 (2005).

[273] M. Jimbo, T. Miwa, and F. Smirnov, Journal of Physics A: Mathematical and Theoretical **42**, 304018 (2009).

[274] H. Boos, M. Jimbo, T. Miwa, F. Smirnov, and Y. Takeyama, Communications in Mathematical Physics **286**, 875 (2009).

[275] H. Boos, M. Jimbo, T. Miwa, F. Smirnov, and Y. Takeyama, Communications in Mathematical Physics **272**, 263 (2007).

[276] B. Aufgebauer and A. Klümper, Journal of Physics A: Mathematical and Theoretical **45**, 345203 (2012).

[277] J. Sato, B. Aufgebauer, H. Boos, F. Göhmann, A. Klümper, M. Takahashi, and C. Trippe, Phys. Rev. Lett. **106**, 257201 (2011).

[278] C. Trippe, F. Göhmann, and A. Klümper, The European Physical Journal B **73**, 253 (2010).

[279] M. Jimbo and T. Miwa, Phys. Rev. D **24**, 3169 (1981).

[280] M. Olshanii and V. Dunjko, Phys. Rev. Lett. **91**, 090401 (2003).

[281] D. M. Gangardt and G. V. Shlyapnikov, New Journal of Physics **5**, 79 (2003).

[282] D. M. Gangardt and G. V. Shlyapnikov, Phys. Rev. Lett. **90**, 010401 (2003).

[283] P. Calabrese and J.-S. Caux, Phys. Rev. Lett. **98**, 150403 (2007).

[284] J.-S. Caux, P. Calabrese, and N. A. Slavnov, Journal of Statistical Mechanics: Theory and Experiment **2007**, P01008 (2007).

[285] J.-S. Caux and P. Calabrese, Phys. Rev. A **74**, 031605 (2006).

[286] V. V. Cheianov, H. Smith, and M. B. Zvonarev, Phys. Rev. A **71**, 033610 (2005).

[287] V. V. Cheianov, H. Smith, and M. B. Zvonarev, Journal of Statistical Mechanics: Theory and Experiment **2006**, P08015 (2006).

[288] V. V. Cheianov, H. Smith, and M. B. Zvonarev, Phys. Rev. A **73**, 051604 (2006).

[289] B. Schmidt and M. Fleischhauer, Phys. Rev. A **75**, 021601 (2007).

[290] L. Piroli and P. Calabrese, Phys. Rev. A **94**, 053620 (2016).

[291] A. Minguzzi, P. Vignolo, and M. Tosi, Physics Letters A **294**, 222 (2002).

[292] K. V. Kheruntsyan, D. M. Gangardt, P. D. Drummond, and G. V. Shlyapnikov, Phys. Rev. Lett. **91**, 040403 (2003).

[293] A. G. Sykes, D. M. Gangardt, M. J. Davis, K. Viering, M. G. Raizen, and K. V. Kheruntsyan, Phys. Rev. Lett. **100**, 160406 (2008).

[294] M. Kulkarni and A. Lamacraft, Phys. Rev. A **88**, 021603 (2013).

[295] A. Klümper and O. I. Pâ ţu, Phys. Rev. A **90**, 053626 (2014).

[296] O. I. Pâ ţu and A. Klümper, Phys. Rev. A **88**, 033623 (2013).

[297] G. Lang, P. Vignolo, and A. Minguzzi, The European Physical Journal Special Topics **226**, 1583 (2017).

[298] P. Vignolo and A. Minguzzi, Phys. Rev. Lett. **110**, 020403 (2013).

[299] M. Panfil and J.-S. Caux, Phys. Rev. A **89**, 033605 (2014).

[300] E. Nandani, R. A. Römer, S. Tan, and X.-W. Guan, New Journal of Physics **18**, 055014 (2016).

[301] J. Armijo, T. Jacqmin, K. V. Kheruntsyan, and I. Bouchoule, Phys. Rev. Lett. **105**, 230402 (2010).

[302] T. Jacqmin, J. Armijo, T. Berrada, K. V. Kheruntsyan, and I. Bouchoule, Phys. Rev. Lett. **106**, 230405 (2011).

[303] E. Haller, M. Rabie, M. J. Mark, J. G. Danzl, R. Hart, K. Lauber, G. Pupillo, and H.-C. Nägerl, Phys. Rev. Lett. **107**, 230404 (2011).

[304] A. Lamacraft and P. Fendley, Phys. Rev. Lett. **100**, 165706 (2008).

[305] V. Gritsev, E. Altman, E. Demler, and A. Polkovnikov, Nature Physics **2**, Article, 705 (2006).

[306] R. W. Cherng and E. Demler, New Journal of Physics **9**, 7 (2007).

[307] Y. Shi and I. Klich, Journal of Statistical Mechanics: Theory and Experiment **2013**, P05001 (2013).

[308] R. Singh, J. H. Bardarson, and F. Pollmann, New Journal of Physics **18**, 023046 (2016).

[309] D. J. Luitz, N. Laflorencie, and F. Alet, Phys. Rev. B **91**, 081103 (2015).

[310] I. Lovas, B. Dóra, E. Demler, and G. Zaránd, Phys. Rev. A **95**, 053621 (2017).

[311] S. Humeniuk and H. P. Büchler, Phys. Rev. Lett. **119**, 236401 (2017).

[312] H. F. Song, C. Flindt, S. Rachel, I. Klich, and K. Le Hur, Phys. Rev. B **83**, 161408 (2011).

[313] H. F. Song, S. Rachel, C. Flindt, I. Klich, N. Laflorencie, and K. Le Hur, Phys. Rev. B **85**, 035409 (2012).

[314] P. Calabrese, M. Mintchev, and E. Vicari, EPL (Europhysics Letters) **98**, 20003 (2012).

[315] D. A. Ivanov and A. G. Abanov, Phys. Rev. E **87**, 022114 (2013).

[316] M. Moreno-Cardoner, J. F. Sherson, and G. D. Chiara, New Journal of Physics **18**, 103015 (2016).

[317] B. Gulyak, B. Melcher, and J. Wiersig, ArXiv e-prints, 1806.04403 (2018).

[318] R. Süsstrunk and D. A. Ivanov, EPL (Europhysics Letters) **100**, 60009 (2012).

[319] Y. D. van Nieuwkerk, J. Schmiedmayer, and F. H. L. Essler, ArXiv e-prints, 1806.02626 (2018).

[320] V. Eisler, Phys. Rev. Lett. **111**, 080402 (2013).

[321] V. Eisler and Z. Rácz, Phys. Rev. Lett. **110**, 060602 (2013).

[322] J.-M. Stéphan and F. Pollmann, Phys. Rev. B **95**, 035119 (2017).

[323] I. Klich, Journal of Statistical Mechanics: Theory and Experiment **2014**, P11006 (2014).

[324] K. Najafi and M. A. Rajabpour, Phys. Rev. B **96**, 235109 (2017).

[325] M. Collura, F. H. L. Essler, and S. Groha, Journal of Physics A: Mathematical and Theoretical **50**, 414002 (2017).

[326] S. Groha, F. H. L. Essler, and P. Calabrese, SciPost Phys. **4**, 43 (2018).

[327] A. Seel, T. Bhattacharyya, F. Göhmann, and A. Klümper, Journal of Statistical Mechanics: Theory and Experiment **2007**, P08030 (2007).

[328] B. Golzer and A. Holz, Journal of Physics A: Mathematical and General **20**, 3327 (1987).

[329] M. Jimbo, T. Miwa, and F. Smirnov, Nuclear Physics B **852**, 390 (2011).

[330] M. Jimbo, T. Miwa, and F. Smirnov, Letters in Mathematical Physics **96**, 325 (2011).

[331] M. Jimbo, T. Miwa, and F. Smirnov, ArXiv e-prints, 0912.0934 (2009).

[332] S. Sotiriadis and P. Calabrese, Journal of Statistical Mechanics: Theory and Experiment **2014**, P07024 (2014).

[333] S. Sotiriadis and G. Martelloni, Journal of Physics A: Mathematical and Theoretical **49**, 095002 (2016).

[334] F. W. Byron and R. W. Fuller, *Mathematics of classical and quantum physics* (Courier Corporation, 2012).

[335] S. Sotiriadis, G. Takacs, and G. Mussardo, Physics Letters B **734**, 52 (2014).

[336] J. M. Deutsch, H. Li, and A. Sharma, Phys. Rev. E **87**, 042135 (2013).

[337] M. Collura, M. Kormos, and P. Calabrese, Journal of Statistical Mechanics: Theory and Experiment **2014**, P01009 (2014).

[338] W. Beugeling, A. Andreanov, and M. Haque, Journal of Statistical Mechanics: Theory and Experiment **2015**, P02002 (2015).

[339] A. M. Kaufman, M. E. Tai, A. Lukin, M. Rispoli, R. Schittko, P. M. Preiss, and M. Greiner, Science **353**, 794 (2016).

[340] A. Nahum, J. Ruhman, S. Vijay, and J. Haah, Phys. Rev. X **7**, 031016 (2017).

[341] A. Nahum, S. Vijay, and J. Haah, Phys. Rev. X **8**, 021014 (2018).

[342] A. Nahum, J. Ruhman, and D. A. Huse, Phys. Rev. B **98**, 035118 (2018).

[343] Y. O. Nakagawa, M. Watanabe, H. Fujita, and S. Sugiura, Nature Communications **9**, 1635 (2018).

[344] H. Kim and D. A. Huse, Phys. Rev. Lett. **111**, 127205 (2013).

[345] A. J. Daley, H. Pichler, J. Schachenmayer, and P. Zoller, Phys. Rev. Lett. **109**, 020505 (2012).

[346] A. Elben, B. Vermersch, M. Dalmonte, J. I. Cirac, and P. Zoller, Phys. Rev. Lett. **120**, 050406 (2018).

[347] T. Brydges, A. Elben, P. Jurcevic, B. Vermersch, C. Maier, B. P. Lanyon, P. Zoller, R. Blatt, and C. F. Roos, ArXiv e-prints, 1806.05747 (2018).

[348] X. Cao, A. Tilloy, and A. De Luca, ArXiv e-prints, 1804.04638 (2018).

[349] L. Hackl, E. Bianchi, R. Modak, and M. Rigol, Phys. Rev. A **97**, 032321 (2018).

[350] E. Bianchi, L. Hackl, and N. Yokomizo, Journal of High Energy Physics **2018**, 25 (2018).

[351] M.-C. Chung and I. Peschel, Phys. Rev. B **64**, 064412 (2001).

[352] I. Peschel, Journal of Physics A: Mathematical and General **36**, L205 (2003).

[353] I. Peschel and V. Eisler, Journal of Physics A: Mathematical and Theoretical **42**, 504003 (2009).

[354] V. Gurarie, Journal of Statistical Mechanics: Theory and Experiment **2013**, P02014 (2013).

[355] L. Bucciantini, M. Kormos, and P. Calabrese, Journal of Physics A: Mathematical and Theoretical **47**, 175002 (2014).

[356] V. Alba and P. Calabrese, Phys. Rev. B **96**, 115421 (2017).

[357] V. Alba and P. Calabrese, Journal of Statistical Mechanics: Theory and Experiment **2017**, 113105 (2017).

[358] M. Mestyán, V. Alba, and P. Calabrese, ArXiv e-prints, 1806.00624 (2018).

[359] G. Delfino, Journal of Physics A: Mathematical and Theoretical **47**, 402001 (2014).

[360] L. Piroli, B. Pozsgay, and E. Vernier, Nuclear Physics B **925**, 362 (2017).

[361] M. Fagotti and F. H. L. Essler, Journal of Statistical Mechanics: Theory and Experiment **2013**, P07012 (2013).

[362] W. Liu and N. Andrei, Phys. Rev. Lett. **112**, 257204 (2014).

[363] J. D. Nardis and J.-S. Caux, Journal of Statistical Mechanics: Theory and Experiment **2014**, P12012 (2014).

[364] M. Fagotti, M. Collura, F. H. L. Essler, and P. Calabrese, Phys. Rev. B **89**, 125101 (2014).

[365] L. Piroli, E. Vernier, P. Calabrese, and M. Rigol, Phys. Rev. B **95**, 054308 (2017).

[366] M. Mestyán, B. Bertini, L. Piroli, and P. Calabrese, Journal of Statistical Mechanics: Theory and Experiment **2017**, 083103 (2017).

[367] M. Gluza, C. Krumnow, M. Friesdorf, C. Gogolin, and J. Eisert, Phys. Rev. Lett. **117**, 190602 (2016).

[368] A. Lenard, Journal of Mathematical Physics **7**, 1268 (1966).

[369] K. V. Kheruntsyan, D. M. Gangardt, P. D. Drummond, and G. V. Shlyapnikov, Phys. Rev. A **71**, 053615 (2005).

[370] R. Haussmann and W. Zwerger, Phys. Rev. A **78**, 063602 (2008).

[371] S. Bergkvist, P. Henelius, and A. Rosengren, Phys. Rev. A **70**, 053601 (2004).

[372] E. Wigner, Phys. Rev. **40**, 749 (1932).

[373] M. Hillery, R. O'Connell, M. Scully, and E. Wigner, Physics Reports **106**, 121 (1984).

[374] F. J. Narcowich, Physica A: Statistical Mechanics and its Applications **134**, 193 (1985).

[375] N.-N. Chen, M. D. Johnson, and M. Fowler, Phys. Rev. Lett. **56**, 904 (1986).

[376] J. Timonen, M. Stirland, D. J. Pilling, Y. Cheng, and R. K. Bullough, Phys. Rev. Lett. **56**, 2233 (1986).

[377] J. Timonen, R. K. Bullough, and D. J. Pilling, Phys. Rev. B **34**, 6525 (1986).

[378] R. K. Bullough, D. J. Pilling, and J. Timonen, Journal of Physics A: Mathematical and General **19**, L955 (1986).

[379] H. Spohn, *Large scale dynamics of interacting particles* (Springer Science & Business Media, 2012).

[380] H. Spohn and J. L. Lebowitz, Comm. Math. Phys. **54**, 97 (1977).

[381] Y. Ogata, Physical Review E **66**, 016135 (2002).

[382] W. H. Aschbacher and C.-A. Pillet, Journal of Statistical Physics **112**, 1153 (2003).

[383] D. Bernard and B. Doyon, Journal of Physics A: Mathematical and Theoretical **45**, 362001 (2012).

[384] D. Bernard and B. Doyon, Annales Henri Poincaré **16**, 113 (2015).

[385] D. Bernard and B. Doyon, Journal of Statistical Mechanics: Theory and Experiment **2016**, 064005 (2016).

[386] A. De Luca, M. Collura, and J. De Nardis, Phys. Rev. B **96**, 020403 (2017).

[387] H. Spohn, Journal of Statistical Physics **154**, 1191 (2014).

[388] S. J. Orfanidis, Phys. Rev. D **18**, 3822 (1978).

[389] V. Adler, A. Bobenko, and Y. Suris, Communications in Mathematical Physics **233**, 513 (2003).

[390] O. G. Rasin and P. E. Hydon, Journal of Physics A: Mathematical and Theoretical **40**, 12763 (2007).

[391] A. G. Rasin, Journal of Physics A: Mathematical and Theoretical **43**, 235201 (2010).

[392] P. Xenitidis, Journal of Physics A: Mathematical and Theoretical **44**, 435201 (2011).

[393] I. Hans, J. Stockhofe, and P. Schmelcher, Phys. Rev. A **92**, 013627 (2015).

[394] M. Cheng, V. Galitski, and S. Das Sarma, Phys. Rev. B **84**, 104529 (2011).

[395] T. Karzig, G. Refael, and F. von Oppen, Phys. Rev. X **3**, 041017 (2013).

[396] T. Karzig, A. Rahmani, F. von Oppen, and G. Refael, Phys. Rev. B **91**, 201404 (2015).

[397] G. E. Astrakharchik and L. P. Pitaevskii, Phys. Rev. A **70**, 013608 (2004).

[398] H. P. Büchler, V. B. Geshkenbein, and G. Blatter, Phys. Rev. Lett. **87**, 100403 (2001).

[399] J. J. Sakurai and E. D. Commins, *Modern quantum mechanics, revised edition*, 1995.

[400] A. Rosch, Advances in Physics **48**, 295 (1999).

[401] M. Schecter, D. Gangardt, and A. Kamenev, Annals of Physics **327**, 639 (2012).

[402] N. Nessi and A. Iucci, Journal of Physics: Conference Series **568**, 012013 (2014).

[403] M. E. Peskin, *An introduction to quantum field theory* (CRC Press, 2018).

[404] S. Sotiriadis and P. Calabrese, Journal of Statistical Mechanics: Theory and Experiment **2014**, P07024 (2014).

[405] S. Sotiriadis, Journal of Physics A: Mathematical and Theoretical **50**, 424004 (2017).

[406] C. Zener, Proceedings of the Royal Society of London A: Mathematical, Physical and Engineering Sciences **145**, 523 (1934).